

Simulation Of Large System Disturbances

A thesis submitted by

Dusko P. Nedic

to



the University of Manchester Institute for Science and Technology

for the Degree of

Doctor of Philosophy

Department of Electrical Engineering and Electronics

December 2003

Dedicated to my family: Maja and Luka

Declaration

No portion of the work referred to in this thesis has been submitted in support of an application for another degree or qualification in this or any other university or other institution of learning.

About the Author

Dusko P. Nedic was born in Sabac, Yugoslavia in 1968. He received his B.Sc degree from University of Novi Sad, Yugoslavia and his M.Sc degree from University of Belgrade of Yugoslavia. From 1994 to 1996 he worked at University of Novi Sad, Yugoslavia, Department of Electrical Engineering as a teaching assistant. In 1997 he joined Power Distribution Company “Elektrovojvodina”, where he first worked as a senior engineer on the technical information systems. In 1999 he became a senior engineer in the dispatcher centre of the company. In this centre he took part in control and operation of 110/35/20 kV power system. He joined UMIST in March 2003. He is currently working at UMIST as a research assistant on security of decarbonised electricity systems. His e-mail addresses are:

dusko.nedic@umist.ac.uk

maludu@ntlworld.com

Acknowledgements

The title page of this thesis lists only one name, but as the bibliography shows this subject has had many more authors. Naturally, none of the authors mentioned in the bibliography is responsible for what myself together with my supervisor have done with their ideas.

I would like to express my gratitude to all my teachers: Mrs Gordana Andric, Mr. Vlastimir Stoicevic, Dr. Radojica Pejovic and Mr. Slavoljub Marjanovic for their support, guidance and the most important their patience.

After my undergraduate studies at University of Novi Sad, Yugoslavia I was a bit reluctant to enter the academic world. The gratification of working with Prof. Victor Levi was very rewarding for me, he overturned my reluctance in an aspiration and help me make a solid basis for my further work in the power system field. I was very fortunate to have Prof. Levi at that stage of my career.

I would also like to express my gratitude to Prof. Daniel Kirschen, who was my supervisor during this PhD work. He has far exceeded the expectation of a great supervision and his support, encouragement and invaluable ideas were of great help since the first beginning of this PhD work. I am especially thankful to him for stopping all of my crazy ideas. His insights and thoughtful comments inspired me to deliver my best.

I am grateful to National Grid of sponsoring this PhD work and using its data. In particular, I am thankful to Dr. Keith Bell for his suggestions, critics and support over these three years. He was a kind of industrial supervisor many students would not like to have, which to be honest was my opinion at the very beginning. However, from today's perspective I believe that Keith is a prototype of the industrial supervisor who can be of great help in building the cooperation between academy and industry.

Finally, I wish to thank my family for their unlimited dedication, support and love throughout so many years. I am especially thankful to my wife, Maja Borota-Nedic for her unfailing support and patience during the many months, weekends, nights I worked on this thesis. My son Luka was always a source of inspiration and motivation but there surely were times that I could have done more for him.

Abstract

Large system disturbances are rare events, which often develop from a benign fault to a severe multiple outage causing serious problems to the power systems. Utilities employ various control measures to protect power systems from these catastrophic events. Utilities analyse events that have taken place and take appropriate actions to prevent similar occurrences. The entire response is therefore based on a principle that can be stated as “lesson learned, actions taken”. Due to disturbance rareness and the unique ways in which they develop, relatively small efforts have been made in predicting how such events unfold.

This thesis argues that the previous work on the analysis of these events can be used to develop a tool capable of simulating how such disturbances develop. Such simulation is certainly not able to create all possible disturbances that can hit a power system. However, it can help power system planners and operators consider dangerous event developments that are usually out of scope of most security plans. Moreover, it can help identify the most vulnerable power system component that should be inspected more frequently.

Such simulation requires models for various system phenomena such as: transient stability, frequency response, voltage stability and steady state conditions. These models have to be able to identify different system failures such as: transient instability, frequency collapse, and activation of underfrequency load shedding and voltage collapse. Apart from these failures there are a lot of contributing and external factors that have to be considered in such simulation. The analysis of recent system disturbances show that the most important contributing factors are failures in the protection system that remain hidden until they are exposed by abnormal system conditions. Considering these failures means that the protection system operations have to be appropriately modelled in the simulation.

To develop and connect all these models in a simulation procedure was the main challenge of this thesis. The searches for disturbances have to be restricted and focused on the most dangerous ones in order to avoid a combinatorial explosion. The test results obtained on a small system confirm that the simulation is able to create disturbances similar to disturbances that have occurred in real life. These results also pinpoint the most vulnerable areas in a power system. These areas contain power system components whose outages might cause dangerous disturbance developments.

Publications

The algorithms and models developed described in this thesis have also been described in the following conference papers and journal articles:

1. D.S. Kirschen, K.R.W. Bell, D.P. Nedic, D.Jayaweera, R. N. Allan, “Computing the Value of Security”, accepted for publication, IEE Proceedings on Generation, Transmission, and Distribution, 2003.
2. M A Rios, D S Kirschen, D Jayaweera, D P Nedic, R N Allan, “Value of Security: Modeling Time-Dependent Phenomena and Weather Conditions”, IEEE Transactions on Power Systems, Vol. 17, No. 3, August 2002, pp. 543-548.
3. D. S. Kirschen, D. P. Nedic, “Consideration of Hidden Failures in Security Analysis”, Power System Computation Conference, Sevilla, 2002.
4. D S Kirschen, K R W Bell, D P Nedic, D Jayaweera, R N Allan, “Computing the Value of Security”, in Proceedings of the Fifth International Conference on Power System Management and Control, London, April 2002.

Table of Contents

	<i>Page</i>
Declaration	<i>iv</i>
About the Author	<i>v</i>
Acknowledgements	<i>vi</i>
Abstract	<i>vii</i>
Publications	<i>viii</i>
Table of Contents	<i>ix</i>
List of Symbols	<i>xiii</i>
List of Figures	<i>xvi</i>
List of Tables	<i>xix</i>
CHAPTER 1 –Introduction	<i>1</i>
CHAPTER 2 – Large Systems Disturbances	<i>6</i>
2.1. Disturbance Perform	<i>7</i>
2.1.1. Disturbance Performance by Utility Characteristics	<i>9</i>
2.1.2. Disturbance Performance by Triggering Events	<i>10</i>
2.1.3. Summary of CIGRE Report	<i>11</i>
2.1.4. Cost of Disturbances	<i>12</i>
2.2. Analysis of Recent System Disturbances	<i>13</i>
2.2.1. UK Incidents	<i>16</i>
2.2.2. Incidents in France	<i>17</i>
2.2.3. Incidents in Scandinavia	<i>17</i>
2.2.4. Incidents in the Far East and Australia	<i>18</i>
2.2.5. US Incidents	<i>19</i>
2.3. A Typical Pattern of Disturbance Developmen	<i>23</i>
2.4. Power System in Emergencies – Definitions and Control Concepts	<i>26</i>
2.5. Measures to Minimise the Impact of Disturbances	<i>29</i>
2.5.1. Planning Measures	<i>29</i>
2.5.2. Operational Measures	<i>30</i>
2.5.3. Special Protection Schemes	<i>31</i>
2.6. Previous Work	<i>34</i>
2.7. A New Simulation of Large System Disturbances	<i>37</i>

CHAPTER 3 - Power System Failures	40
3.1. Dangerous System Failures	42
3.1.1. Transient Instability	42
3.1.2. Frequency Variations	44
3.1.2.1. <i>Frequency collapse</i>	46
3.1.2.2. <i>Underfrequency load shedding</i>	47
3.1.3. Voltage Collapse	49
3.1.4. System Separation	51
3.2. Contributory Factors	52
3.2.1. Failures in the Protection System	52
3.2.2. Line Outages	54
3.2.3. Switching Equipment Malfunction	55
CHAPTER 4 - Modelling of Failure Modes in the Simulation of Large System Disturbances	58
4.1. Transient Stability	59
4.1.1. Methods for Transient Stability Assessment	60
4.1.2. Complete Time Domain Model and Modelling Assumptions Used for the Classical Model	63
4.1.3. Direct Solution	65
4.1.4. Alternate Cycle Solution	69
4.2. Frequency control	70
4.2.1. A Complete Model for System Frequency Evaluation	70
4.2.1.1. <i>Network model</i>	71
4.2.1.2. <i>Dynamic models of turbo/hydro generators</i>	71
4.2.1.3. <i>Voltage regulator model</i>	74
4.2.1.4. <i>Hydraulic turbine and governing system model</i>	76
4.2.1.5. <i>Steam turbine and governing system model</i>	78
4.2.1.6. <i>A complete short- term dynamic model</i>	79
4.2.2. Fast Simplified Models for System Frequency Evaluation	80
4.2.2.1 <i>Dynamic model for evaluation of inertia centre frequency</i>	81
4.2.2.2 <i>Dynamic model for evaluation of system frequency</i>	81
4.3. Line Overloading	84

CHAPTER 5 - Hidden Failures In A Protection System	86
5.1. Definition and Modes of Hidden Failures	87
5.2. Protection of Transmission Lines	90
5.2.1. Directional Comparison Blocking Scheme	90
5.2.2. Directional Comparison Unblocking Scheme	92
5.2.3. Permissive Overreaching Transfer Trip Scheme	92
5.2.4. Permissive Underreaching Transfer Trip Scheme	93
5.2.5 Phase comparison relays	94
5.2.6. Back-Up Protection	96
5.2.7. Transformer Differential Relay	96
5.3. Generator Hidden Failures	97
5.3.1. Stator Phase – Fault Protection	100
5.3.2. Excitation System Control and Protective Devices	101
5.3.3. Inadvertent Energisation	103
5.4. Vulnerability Region	104
CHAPTER 6 - Search for Disturbances Based on the Distance to Voltage Collapse	106
6.1. Voltage Instability Mechanisms	108
6.2. Dynamic Versus Static Models	110
6.2.1. Dynamic Model	111
6.2.2. Static Model	115
6.2.1.1. <i>Modelling requirements for the static model</i>	119
6.3. Static Voltage Stability Indices	122
6.3.1. L Indicator	125
6.3.2. Eigenvalue Decomposition	128
6.3.3. Singular Values	131
6.3.4. Voltage Collapse Proximity Indicator	133
6.3.5. Branching Test Function	134
6.4. Test Results	140
6.4.1. Results for the System-Wide Indicators	140
6.4.2. Results for Node-Based Indices	145
CHAPTER 7 - Simulation of Large System Disturbances	149
7.1. Event Tree	150

7.2. Creation of an Event Tree	151
7.3. Simulation of Large System Disturbances	154
7.4. Simulation Outputs	158
7.4.1. Probability Calculation	159
7.4.2. Cost of Interruption Supply	160
7.4.3. Modelling of Load Shedding	161
7.4.4. Risk Calculation	163
CHAPTER 8 –Simulation Results	164
8.1. Simulation Results for the IEEE 39 Buses System	165
8.1.1. Vulnerability Region	165
8.1.2. Totals	166
8.1.3. Ranking and Vulnerability Areas	169
8.1.3. Risk and Costs versus Load Increase	172
8.1.5. Interesting Sequences	175
CHAPTER 9 – Conclusions	178
9.1. Recommendations for further research	180
References	182

List of Symbols

<i>Symbol</i>	<i>Description</i>
I	current
Z_{LN}	network impedance
V_R	voltage at receiving end
Z_{LD}	load impedance
P_R	transmitted active power
H_i	inertia constant
δ_i	the angle difference between the internal and terminal voltages
P_{Mi}	constant
P_{Gi}	electrical output
M_i	inertia constant of machine i
ω_i	angular frequency of machine i
D_i	damping coefficient of machine i
V_{Li}	voltage
I_{Li}	current
S_{Li}	complex power demand
P_{Li}	active load
Q_{Li}	reactive load
y_{Li}	equivalent shunt load admittance
g_{Li}	equivalent shunt load conductance
b_{Li}	equivalent shunt load susceptance
x_{di}	direct axis transient reactance
Y_{BUS}	post-fault network admittance matrix
I_m	injected currents
E_m	internal generator bus voltages
P_i	injected active power
Q_i	injected reactive power
V_i	magnitude of the i^{th} node voltage

δ	rotor angle
ω	angular system frequency
H_{SYS}	system inertia constant
D_{SYS}	system dumping coefficient
P_{MSYS}	total mechanical power of all the generators in the system
P_{GSYS}	total electrical power of all generators in the system
Δf	change in the system frequency
ΔP_{me}	change in the mechanical power output of the equivalent unit
ΔP_o	the active power mismatch at instant t_o
k_l	self-regulation coefficient of the total power system demand
P_{lo}	total active power load at t_o
T_e	inertia time constant of the equivalent generating unit
P_{ne}	rated active power of the equivalent unit
s_{ne}	governor control droop of the equivalent unit
T_{se}	servomotor relative time constant of the equivalent unit control system
ΔP_{me}^{\max}	maximum mechanical power output change
\mathbf{y}	vector of bus voltages
\mathbf{x}	short-term state vector
\mathbf{z}_c	continuous long-term state vector
\mathbf{z}_d	discrete long-term state vector
$\Delta \mathbf{P}$	vector of active power changes
$\Delta \mathbf{Q}$	vector of reactive power changes
\mathbf{J}	Jacobian matrix
$\Delta \theta$	vector of incremental angle changes
$\Delta \mathbf{V}$	vectors of incremental voltage changes
\mathbf{J}_R	reduced Jacobian matrix
n	total number of buses
\mathbf{I}^G	sub-vector of generators complex currents

V^G	sub-vectors of generators complex voltages
I^L	sub-vector of load complex currents
V^L	sub-vector of load complex voltages
H	hybrid matrix
α_L	set of all load buses
α_G	set of all generator buses
R	right eigenvector matrix
L	left eigenvector matrix
r_i	right eigenvector
l_i	left eigenvector
P_i^{SV}	participation vector
Ω_G	sets of all generator
Ω_L	sets of load buses
R_k	risk of any sequence k
C_k	cost of sequence k
P_k	probability of sequence k
R_{jk}	Risk associated with initial event j
α_j	set of all sequences triggered by the initial event j
TR	total risk

List of Figures

	<i>Page</i>
CHAPTER 2	
Figure 2.1.: Overall results of BES disturbances	8
Figure 2.2.: Results by utility characteristics	9
Figure 2.3.: Disturbance grouped by main causes	11
Figure 2.4.: Disturbance grouped by credible and non-credible contingencies	11
Figure 2.5.: June 2 nd disturbance, sequence and islands separations	21
Figure 2.6.: August 10 th disturbance, sequence and islands separations	22
Figure 2.7.: A typical disturbance development	25
Figure 2.8.: System states	26
Figure 2.9.: Emergency Control Concepts	28
Figure 2.10.: Probabilities of incorrect tripping of (a) lines (b) generator	36
CHAPTER 3	
Figure 3.1.: Equal area criterion (a) short clearing time (b) long clearing time	43
Figure 3.2.: Frequency variation during primary control	46
Figure 3.3.: Frequency collapse	47
Figure 3.4.: Underfrequency load shedding	48
Figure 3.5.: Characteristics of a simple radial system	51
Figure 3.6.: Representations of power system: (a) substation structure (b) switch level representation (c) branch node representation	55
Figure 3.7.: Busbar fault	56
CHAPTER 4	
Figure 4.1.: Structure of the complete power system model for transient stability analysis	64
Figure 4.2.: Terminal representation at internal nodes of generators	66
Figure 4.3.: Two axis turbo-generator model	72
Figure 4.4.: Two-axis hydro-generator model	73
Figure 4.5.: Type 1 excitation system representation for a continuously acting regulator and exciter	74
Figure 4.6.: Simplified voltage regulator block diagram	75

Figure 4.7.: Mechanical-hydraulic governor	76
Figure 4.8.: Mechanical-hydraulic governor system and turbine	77
Figure 4.9.: A simplified model of mechanical-hydraulic governing system and turbine	78
Figure 4.10.: Simplified model of steam turbine and its governing system	79
Figure 4.11.: Flowchart of the applied procedure during governor control	83
Figure 4.12.: Line overload modelling in the simulation procedure	85

CHAPTER 5

Figure 5.1.: Illustration of hidden failure modes	89
Figure 5.2.: Directional comparison blocking scheme a) One-line diagram b) Logic diagram	91
Figure 5.3.: Logic diagram of directional comparison unblocking scheme	92
Figure 5.4.: Permissive underreaching transfer trip scheme a) One-line diagram b) Logic diagram	93
Figure 5.5.: Permissive underreaching transfer trip scheme a) One-line diagram b) Logic diagram	94
Figure 5.6.: Basic principles of phase comparison scheme	95
Figure 5.7.: Logic diagram of phase comparison blocking scheme	95
Figure 5.8.: One line diagram of distance protection	96
Figure 5.9.: Percentage differential protection	97
Figure 5.10.: Typical protection for a direct-grounding generator	98
Figure 5.11.: Excitation system control and protective scheme	101
Figure 5.12.: Logic diagram for loss of excitation relay	103
Figure 5.13.: Logic diagram of inadvertent energisation	104
Figure 5.14.: A simple example of vulnerability region	105

CHAPTER 6

Figure 6.2.: OXL block model	114
Figure 6.3.: Generator Capability Limits	121
Figure 6.4.: Classification of Methods used for Static Voltage Stability Indices	123
Figure 6.5.: A simple two node system	126

Figure 6.6.: The L indicator for two node system	128
Figure 6.7.: The solvability boundary for two node system	130
Figure 6.8.: a)V-Q curve b)eigenvalues of \mathbf{J}_R for two node system	131
Figure 6.9.: The smallest singular value of \mathbf{J} for two node system	132
Figure 6.10.: VCPI characteristic for two node system	134
Figure 6.11.: Test function for two node system	139
Figure 6.12.: The system-wide indicators for the IEEE 14 node system	143
Figure 6.13.: The system-wide indicators for the NGC power system model	144
Figure 6.14.: Branch tracing for the IEEE 14 node system	144
Figure 6.15.: The test functions for $k = l = 12, 13$ and 14	146
Figure 6.16.: The VCPI indices for the IEEE 14 node system	146

CHAPTER 7

Figure 7.1.: Event tree	151
Figure 7.2.: (a) Depth first search (b) Breadth first search	152
Figure 7.3.: Depth search and <i>ONL</i> evolution for a simple example	154
Figure 7.4a.: The first stage of the simulation procedure	156
Figure 7.4b.: The second stage of the simulation procedure	157
Figure 7.5: Probability functions	160

CHAPTER 8

Figure 8.1.: The vulnerability region of line 1-2	166
Figure 8.2.: Simulation Totals	167
Figure 8.3.: Participation of different events in the simulated sequences	168
Figure 8.4.: Length of sequences	169
Figure 8.5.: Vulnerable areas	172
Figure 8.6.: Risk and Cost versus load increase	174
Figure 8.7.: Totals versus load increase	174
Figure 8.8.: Sequence length versus load increase	175
Figure 8.9.: Interesting sequence developments	177
Figure 8.10.: Length of sequences	179

List of Tables

	<i>Page</i>
CHAPTER 2	
Table 2.1 – World wide system incidents	14
Table 2.2 – System conditions and events in disturbance developments	15
Table 2.3 – Unit characteristics	29
CHAPTER 4	
Table 4.1 – Voltage regulator model symbols	75
Table 4.2 – MHC symbols	76
Table 4.3 – Symbols used in the steam turbine model	79
Table 4.4 –Equations and variables in short-term dynamic model	80
CHAPTER 6	
Table 6.1 – Power system components response	110
Table 6.2 – General Dynamic Model	113
Table 6.3 – Known and unknown variables in a power flow calculation	119
Table 6.4 – Methods, routines and libraries used for the calculation of system wide indicators	143
Table 6.5 – Node based indices for two different power system state	147
CHAPTER 7	
Table 7.1- Load Restoration Rates	161
Table 7.2 - VOLL as a function of the duration of interruption for different sectors	161
CHAPTER 8	
Table 8.1 – Ranking of initial contingencies	171
Table 8.2 – The simulation totals	178

1

Introduction

A genuine characteristic of human nature is to face and stand up to all threats that might have a catastrophic impact on the human life. Such threats have been emerged in many fields of the human life. In the power system field large system disturbances are becoming a serious threat today. These events are rare but might cause catastrophic consequences. Previous experience with large disturbances indicates that each of them is unique in terms of its sequence of events. Due to this rareness and uniqueness, power system planners and operators are often unable to predict such events, so let alone control them. That is why many times utilities are caught unaware by a large disturbance before they undertake appropriate preventive measures. Therefore, we first learn how it happened before we learn why it happens. This is a natural learning order, taking into account that for example we first learn calculus before we learn algebra. Accepting this natural learning order in case of large system disturbances can be very dangerous and costly. Therefore, the main motivation for this work was to inverse this learning order and first learn why before we learn how.

Such inverse learning order is feasible if instead of waiting for something to happen we have a simulation tool able to create sequences similar to some that happened before. The development of a new simulation procedure that can help planners and operators cope with these situations is a challenge and the main objective of the research described in this thesis. The main objectives of this simulation procedure are to increase the operator's confidence in his or her ability to evaluate situations under stress, to make and implement timely and correct

decisions, to improve the community's knowledge of the technical characteristics of the system under dynamic or degraded operating conditions and to improve knowledge of facilities for handling emergency situations.

Various surveys from all over the world show that these catastrophic events are not quite as rare as one might expect. These surveys are discussed in section 2.1. However, the collected surveys show that each disturbance has a unique development. A range of initial events, protection and human failures combined with severe weather condition might create dangerous sequences of events that are unlikely to be repeated. An analysis of such sequences in Europe and the North America is discussed in section 2.2. Although descriptions of actual disturbances indicate many and varied causes, it is possible to identify a pattern to the way in which many of the large scale disturbances of the past have developed. This pattern, originally proposed by U.G. Knight in [Kni01], is discussed in section 2.3. If power system planners and operators knew the pattern they would be able to suggest and implement emergency control actions to bring the system to a secure state. The objective of various emergency concepts discussed in section 2.4 is to implement actions as necessary to prevent the system from degenerating into an emergency state. However, if this is not possible, then power system operators have to take measures to minimise the disruption and restore normal conditions as quickly as possible. These measures are taken in the management, planning and operation of a power system to minimise the effects of disturbances on their viable operation. The measures are discussed in section 2.5. A lot of engineering and research work has been focused on large system disturbances. However, only a small portion of that work is devoted to help power system planners and operators increase their knowledge of the potential weaknesses of their own systems in terms of large system disturbances. A simulation able to predict unforeseen disturbance developments is a tool that power system planners and operators really need to cope with this threat. Developing such a simulation tool is a challenge and the main focus of this work. The first step regarding this challenge was done at Cornell University and Virginia Tech. This work identifies the main factors contributing to the spreading of disturbances and uses probabilistic simulations to create new disturbances. The work is discussed in section 2.6.

A power system can fail for a variety of reasons: instability, frequency collapse, voltage collapse, excessive load shedding, system islanding, or many others. The first section of Chapter 3 focuses on the most dangerous system failures, their causes and their developments. The collected surveys and analysis of recent system disturbances confirm that disturbances are often made worse by circuit outages caused by factors such as line overloads, protection system failures or switching equipment malfunctions. Such factors do not usually produce

serious consequences like the failures discussed in the first section, but they are seen as contributory factors in terms of spreading a disturbance over a network. An analysis of recent system failures has shown that hidden failures in the protection system play a key role in terms of escalating these disturbances. It was shown that line overloads can disconnect an entire transmission corridor, when the power system is already stressed. Analysis of switching equipment malfunctions suggests that it might be practical to replace the traditional branch-node representation of the power system used in this thesis to a more detail representation, where nodes are replaced by the complex substation structure.

In a perfect world, the simulation of large system disturbances would include detail mathematical models able to identify various system failures. These models can be dynamic or static depending on the nature of the failure. Using such models in a simulation of large system disturbances would require a significant amount of computing time. For the sake of simplicity and brevity complex mathematical models and methodological solutions are avoided in this work. Instead, the focus is placed on the connections between various models that can be used to analyse both dynamic and static phenomena. The dynamic models are discussed in Chapter 4, while the static related models are described in Chapter 6.

Chapter 4 is devoted to the dominant dynamic phenomena such as transient stability and power-frequency control. Second order motion differential equations for each generator were used to build a model for transient stability evaluation. This model and its methodological solution are discussed in the first section of Chapter 4. The objective of power-frequency control is to keep frequency variation caused by a power imbalance within the specified limits. Therefore, frequency response model have to be used to evaluate the power system frequency variations that could take place after a severe active power imbalance. To estimate frequency variations, a second order differential model has been used. This model is based on the motion equation of the equivalent system generator and the corresponding governing system. If the frequency variation due to a significant active power imbalance is sufficiently large, then it will trigger under-frequency load shedding, it might activate the underfrequency protection of generators, and a frequency collapse incident might take place. Using the frequency variation diagram these events can be identified.

At the beginning of Chapter 5 the most important contributory factors in disturbance development, namely hidden failures in the protection system, are defined. The first section of Chapter 5 distinguishes between hidden failures and all other failures in protection system. In sections 5.2 and 5.3 hidden failures in a transmission network and generation related protection schemes are analysed. If the protection system design is known in a troubled area

then a list of possible hidden failures can be predefined. In the last section of Chapter 5 the concept of vulnerability region is introduced. A vulnerability region is a set of electrical circuits, which can be unnecessarily tripped due to hidden failures.

Voltage stability and the analysis of the behaviour of power systems with respect to voltage have been two areas of intense research interest in power system engineering in recent years. The subjects are of considerable academic and industrial importance, especially for power systems where the power is transmitted over a long distance. Voltage stability is a dynamic phenomenon that can be analysed using static models [Cut91]. In this work, voltage stability is not considered directly like for example transient stability. Instead of using a detailed dynamic model to assess voltage stability, the power system is forced toward the voltage collapse using static voltage indices. For instance, if at a certain stage during the simulation process, more than one event from a vulnerability region can take place, the advantage will be given to the event whose occurrence leads the system closer to voltage instability. Therefore, the distance to voltage instability has been used as a measure of the importance of each particular event in a disturbance sequence. Knowing that the space of possible combinations of events in the sequences is vast, voltage stability is used to reduce the number of these combinations, focusing the simulation only on the most dangerous events in terms of voltage stability. Various voltage stability indicators have been developed as a measure of the distance to voltage collapse. These indicators have been extensively studied and a comparison is presented in Chapter 6.

A large system disturbance is a transition process in which one power system state leads to another due to component outages caused by different events and failures. This transition process can be described using an event tree. Thus, power system states in the transition process are denoted as the nodes of event tree, while the component outages in the transition process corresponds to the branches of the event tree. This representation is discussed in section 7.1.

Starting from the top node (base case) in the event tree, each sequence of events is uniquely determined using the branches and nodes between the top node and a leaf node in the sequence. In general two techniques can be used to create such event trees. The first one called depth-first technique creates nodes one by one in the subsequent layers until a sequence is completed. Therefore, this technique completes sequence one by one. On the other hand, a breadth-first technique generates all nodes in each layer, completing the event tree layer by

layer. Thus, all sequences are completed at the end of the creation process. These techniques are discussed in Section 7.2.

Finally, a detailed algorithm of the suggested simulation procedure is discussed in section 7.3. This algorithm links the models and concepts discussed in Chapter 4, Chapter 5 and Chapter 6. The analysis of the simulation outputs is given in the last section of Chapter 7.

Chapter 8 of this thesis presents the results obtained while testing the simulation on a small power system model.

The complete work is summarised in the last chapter. This chapter contains suggestions for further work on this topic.

2

Large System Disturbances

The term disturbance will be used frequently in this thesis. Knight in [Kni01] suggests that its connotation is usually of some quite serious incident, such as the tripping of a circuit due to a fault, occurring unexpectedly. A large system disturbance is however any disturbance that can seriously affect system integrity.

Large system disturbances are rare events but their consequences can be catastrophic. Therefore, today utility practice is to extend the security plans in order to pay more attention to such catastrophic events [CWG93]. Measures to minimise the risk and impact of such disturbances have been implemented by many utilities.

Disturbances have different severity, they are triggered by various events and they can strike even power systems that seem to be very secure. This is shown in a statistical analysis based on the collected surveys on disturbance performance for the period from 1972 to 1989. This analysis is discussed in 2.1. It measures the severity of disturbances and the influence of the system size, the nature of its limitation and the position within the large interconnection and correlates this information with the overall disturbance performance. Triggering events for the period from 1983 to 1989 are identified for more than 250 disturbances in this analysis.

This overall analysis does not reveal a typical pattern of disturbance development. However, analysis of individual disturbances has shown that it is possible to identify some common events. This analysis is given in 2.2. The weakness of this analysis is the lack of information about European disturbances. On the other hand detailed descriptions and analyses of recent

system disturbances in North America are gathered and made available by the North American Reliability Council.

Section 2.3 describes a typical pattern of disturbance development based on the analysis of individual disturbances carried out by Knight in [Kni01]

Power system security is the global framework used for this work on large system disturbances. Emergency control is a more specific area that deals with operation during large system disturbances. Its objective is to save the integrity of the system. The concepts of emergency control are discussed in section 2.4.

In order to minimise the risk and impact of large system disturbances, utilities develop and implement various measures. These measures are implemented through planning studies, operation and using special protection schemes, which are normally automatic control actions that are activated only during some abnormal system conditions. These measures are discussed in section 2.5.

Previous work on large system disturbances is divided into two groups. The first group focuses on the descriptions, statistical analysis and the summation of disturbances. On the other hand, the second group deals with the simulation of large system disturbances. A short summary of previous work is given in section 2.6.

In the last section of this chapter, the main objectives of the work presented in this thesis are discussed. The simulation of large system disturbances proposed in this thesis is compared with similar simulations proposed by other researchers active in this area.

2.1. Disturbance Performance

Several reports on disturbance performance have been published by CIGRE. These reports are based on two world-wide surveys carried out in 1983 and 1989. These surveys cover the system disturbances from 1972-1989. Respectively 168 and 198 utilities responded to these surveys. These utilities provided data covering 2206 years of utility experience. The results are published in [LeT92]. In these questionnaires large system disturbances were treated as events that cause wide spread load loss and one or more of the following [LeT92]:

- Loss of system stability,
- Cascading outages of transmission circuits,

- Abnormal ranges of frequency and/or voltages.

In order to classify each of the reported disturbances in terms of its severity a new measure of severity called *System Minute* (SM) is introduced. One *System Minute* is equivalent to an interruption of the total system load for 1 minute at the time of annual system peak. Severity is being defined as the unsupplied energy in an event (MW-Minutes) divided by the annual system peak load (MW) and measured in *System Minutes*. Each disturbance is assigned to a *Degree of Severity* in accordance to the following definitions [LeT92]:

- Degree 1 – an event with a severity from 1 to 9 SM.
- Degree 2 – an event with a severity from 10 to 99 SM.
- Degree 3 - an event with a severity from 100 to 999 SM.

The impact of several factors on disturbance performance was investigated in this report. These factors are based on utility characteristics and type of triggering events. The utility characteristics are system size, the system position within its interconnection and the nature of the phenomena limiting system operation. The impact of these factors is presented in section 2.1.1. The triggering events can be classified using two criteria: the nature of the events and their type in terms of security criteria. In terms of second criteria, a triggering event can belong to one of the following distinct classes: credible contingencies (foreseen by security criteria) or non-credible contingencies (beyond security criteria). The impact of triggering event classification is described in section 2.1.2.

The overall performance results are shown in Figure 2.1. It can be seen that on average, each utility experience a Degree 1 of severity disturbance every 2.6 (2206/835) years, a Degree 2 disturbance every 8.8 (2206/249) years and a Degree 3 of Severity disturbance every 81.7 (2206/27) years [LeT92].

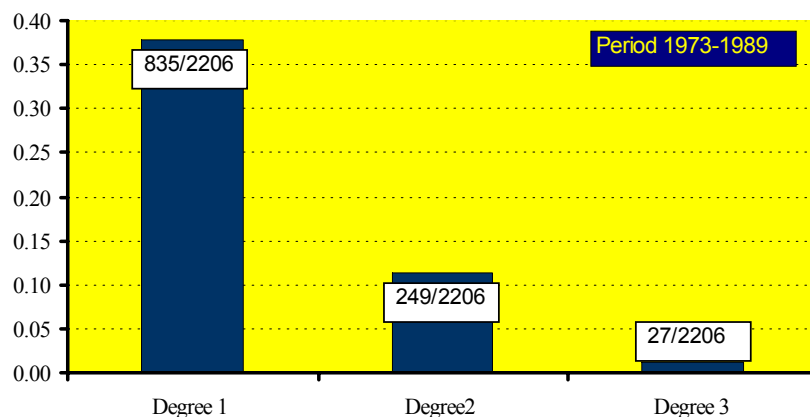


Figure 2.1.: Overall results of BES disturbances [LeT92]

2.1.1. Disturbance Performance by Utility Characteristics

The first classification of disturbances is based on different system characteristics. This classification is shown in Fig. 2.2. In the first classification all utilities are divided into two groups [LeT92]:

- a. Utilities that have thermal limitations and dispersed generation and load,
- b. Utilities that have stability limitations (voltage and transient) and localised centres of generation and load.

Stability limited systems have a significantly larger frequency of disturbances for all three *Degrees of Severity*.

The second classification is based on the position of the system in a large interconnection. The following groups were identified [LeT92]:

1. Utilities that are a part of a large interconnection but centrally located,
2. Utilities that are part of large interconnection but peripherally located and
3. Utilities that are not interconnected.

Figure 2.2 shows that isolated systems experience significantly more disturbances than peripherally and centrally located disturbances.

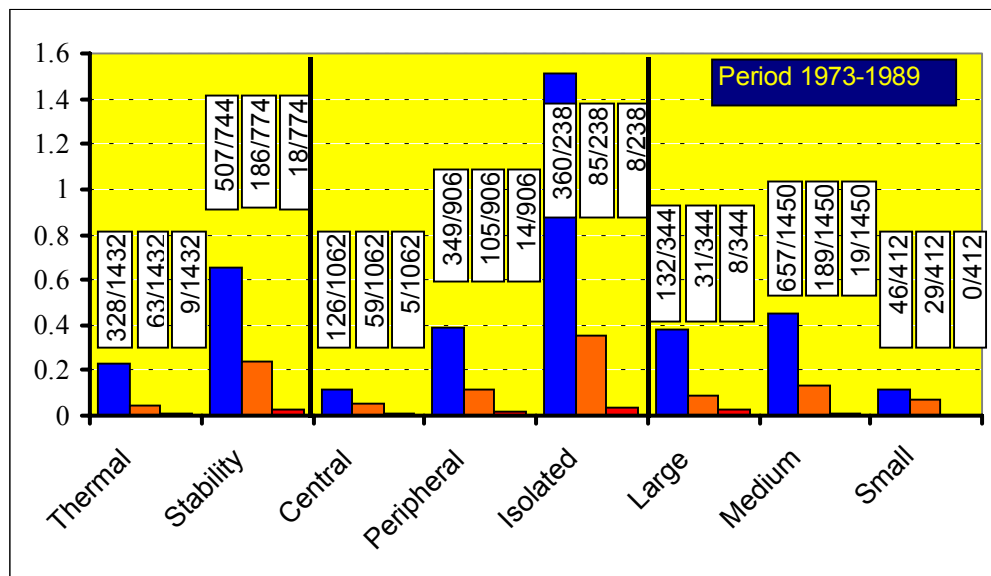


Figure 2.2.: Results by utility characteristics [LeT92]

The last classification is based on system size. The following groups of systems are identified using the system size criteria:

1. Large System – a system whose annual peak load is greater than 10 GW,
2. Medium System – a system whose annual peak is from 1 to 10 GW, and
3. Small System – a system whose annual peak is below 1 GW.

Figure 2.2 shows that small systems experience fewer disturbances for all three *Degrees of Severity*.

2.1.2. Disturbance Performance by Triggering Events

Only the second survey on disturbance performance carried out in 1989 contains information related to the nature of the triggering event and its type in terms of security plans. Triggering events are classified with respect to their nature as follows [LeT92]:

- faulty conventional protection and control equipment,
- faulty special protection equipment,
- solar magnetic disturbances,
- lightning,
- weather other than lightning,
- faulty high voltage equipment,
- personnel errors,
- other causes and
- unknown.

However, it is sometimes very difficult to determine the nature of the triggering event when a lot of factors are involved at the beginning of a disturbance. However, Figure 2.3 shows that various equipment failures triggered about 47% (128 out of 271) disturbances, 22% were triggered by lightning, other weather conditions and solar magnetic disturbances (33+27+1 out of 271) and 7% were the result of human errors.

These triggering events can be treated as contingency from the security point of view. In deterministic security analysis these contingencies are usually divided into two distinct groups: credible and non-credible. Knight in [Kni01] defines a credible contingency as a contingency or fault that has been foreseen in the planning and operation of the system. Specific measure can be taken against such a contingency in order to ensure that no serious consequences would follow its occurrence. However, a non-credible contingency is a contingency that is much less likely to occur and for which only general measures are taken. Figure 2.4 shows that 3 out of 4 disturbances were caused by non-credible contingencies.

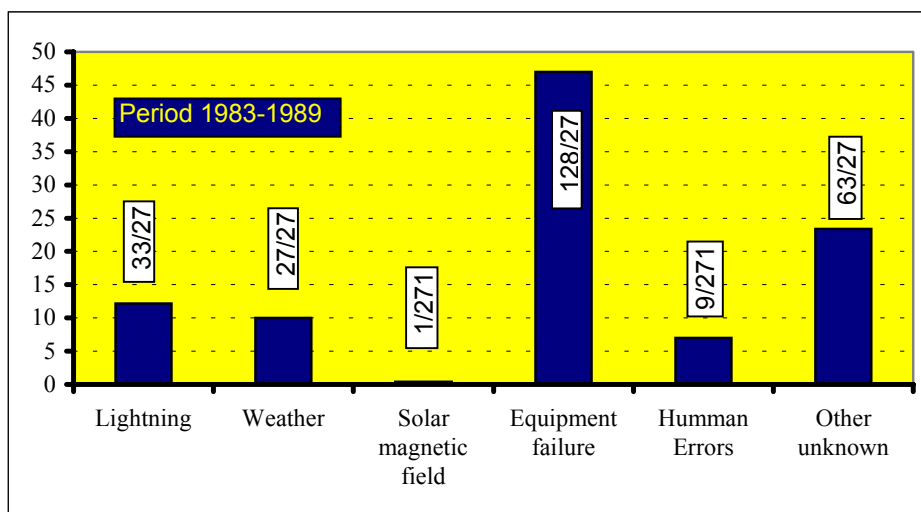


Figure 2.3.: Disturbance grouped by main causes [LeT92]

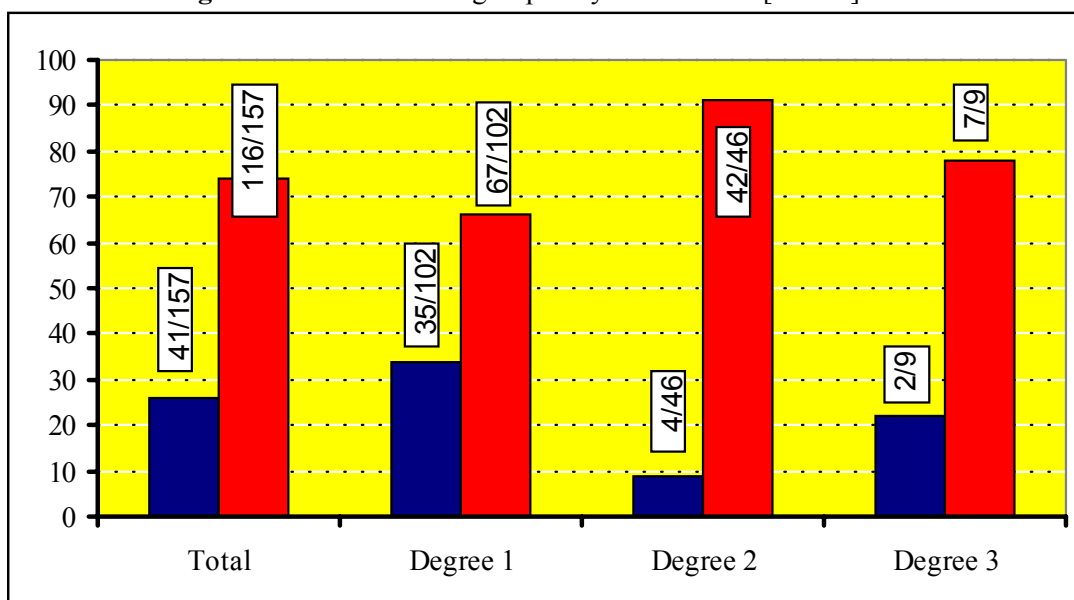


Figure 2.4.: Disturbance grouped by credible and non-credible contingencies [LeT92]

2.1.3. Summary of CIGRE Report

As far as this thesis is concerned, the most relevant conclusions of this CIGRE report are [LeT92]:

- On average between 1972 and 1989, each utility experienced one disturbance of *Severity Degree 1* every 2.6 years, one *Degree of Severity 2* disturbance every 8.8 years and one *Degree of Severity 3* disturbance every 81.7 years.

- Thermally limited system experience fewer disturbances than stability limited systems, while isolated systems experience a significantly larger number of disturbances than centrally and peripherally located system.
- Over 22% of disturbances were triggered by external factors such as lightning and weather conditions other than lightning. Over 47% of disturbances were caused by faulty equipment and 7% were caused by human error.
- Only about 25% of disturbances were caused by events that are foreseen in security plans.

2.1.4. Cost of Disturbances

A disturbance can cause damage to the economy and to the people either directly or indirectly. It is therefore not always possible to measure such damage in terms of costs. The costs of a disturbance were analysed by Knight in [Kni01]. His summary of world-wide disturbances shows that the costs can be significant:

- Greece 1983, \$6 millions cost to the economy
- Sweden, 1983, SWKr 200-300 millions,
- USA, 1997, \$310 millions, which is equal to 20% of net generation and transmission assets.
- Canada, CDN\$13.2 millions.

One of the very important factors after a disturbance is the restoration of satisfactory service. Alan and Billinton in [AIB00] confirm that several countries are already imposing financial penalties on suppliers who do not provide a satisfactory service. For instance in the UK the service must be restored within 24 hours after an interruption, otherwise a payment of 40£ to domestic customers and \$100 to non-domestic customers must be made on request with a further £20 for each subsequent 12h of non-restoration. In 1997/1998, because of incidents due to cold weather, a total of 15,353 standards payments and 30,791 extra payments were made which led to a total payment of £3,370,134. Norway operates a penalty system in which the 1997 compensation rates were 16 NOK/kWh of energy not supplied for long interruptions and 8 NOK of power interrupted for short interruptions [AIB00]. Experts in Japan calculated that the cost of a large disturbance could be higher than 100 years of standard security costs.

Kirschen in [Kir02] argues that a single blackout could easily cause the equivalent of ten to twenty years' worth of "normal" unavailability in one day. In monetary terms, the cost would be even higher. He further confirms that the massive disruptions caused by a large-scale disturbance cannot be represented appropriately by a factor called the "Value Of Lost Load" (VOLL). He gives a rough idea of the numbers involved, saying that, if the disturbance takes place in the morning, there would be virtually no economic activity for one day and that a substantial part of the next day would be devoted to cleaning up and the restoration of business and industrial processes. The economic cost of a one-day blackout could therefore be about 0.5% of GDP. In addition, social costs might include deaths and injuries attributable to the lack of electricity supply as well as the consequences of the acts of vandalism and civil disturbances that might arise [Kir02].

2.2. Analysis of Recent System Disturbances

The main problem faced at the beginning of this work was a lack of knowledge related to description of disturbances. A good description of a disturbance should include a detailed chronological list of events followed by a clear explanation of the conditions and factors that affected the disturbance and the main conclusions of the investigation. However, descriptions of disturbances are often limited to a precise chronological list of events but rarely provide sensible explanations. It was observed that utilities in North America generally have better descriptions of disturbances than European utilities. This observation was confirmed by the CIGRE report whose results are given in the previous section.

Knight in [Kni01] describes over 20 disturbances that have happened till 1999 world-wide. His work is extended in this thesis using the reviews of several US incidents done by the North American Reliability Council (NERC). The incidents analysed in this thesis are given in Table 2.1 and described in the following sections. The first column in Table 2.1 represents the area or country where the disturbance occurred, the second column is related to the time of occurrence, while the last column is an abbreviation that will be used when referring to any of these disturbances in this thesis.

Knight in [Kni01] summarises the system conditions and events that took place in recent system disturbances. These are discussed in Table 2.2. Table 2.2 is divided into three parts. The first part represents events (IDs from 1 to 6) that initiated the incidents. Power system conditions and events that took place between the initial fault and the system separation are

given in the second section (IDs from 7 to 21). The last part of Table 2.2 encompasses the system conditions and events that appeared after the system separation (IDs from 22 to 31) [Kni01].

Table 2.1: World wide system incidents

<i>Area/Country</i>	<i>Date</i>	<i>Abbreviation</i>
UK	1981, August	UK81
	1986, spring	UK86
	1987, autumn	UK87
France	1977, winter	Fr77
	1987, winter	Fr89
	1999, winter	Fr99
Scandinavia	1979	Nordel79
	1983	Nordel83
Far East and Australia	Japan 1987	Jap87
	Thailand 1985	Thai85
	Australia 1977	Au77
US	March 12, 1996	US120396
	April 16, 1996	US160496
	August 10, 1996	US100896
	July 2, 1996	US020796
	June 25, 1998	US250698
	June 10, 1999	US100699
	July 16, 1999	US160799
	August 13, 1999	US130899
August 18, 1999	US180899	

The focus of the incident analysis is on triggering events. However, events and conditions from Table 2.2 are used for the description of triggering sequences. Whenever it was possible geographically related details are avoided. The analysed incidents are given in the following sections.

Table 2.2: System conditions and events in disturbance developments [Kni01]

<i>IDs</i>	<i>Conditions and Events in the sequences</i>
1	Relatively simple fault
2	External fault
3	Multiple faults (without reclosing)
4	Malfunction of protective gear or signalling equipment causing loss of transmission
5	Loss of generation within station or transmission fault(s) between station and main network
6	Other
7	Malfunction of protection system
8	Instability of transmission system
9	Overload on transmission system
10	Sectioning of system into two parts
11	Major disconnection of load
12	Major loss of generation system
13	System stabilised
14	Significant imbalance between demand and generation in the whole system
15	System stabilised by demand disconnection or generation reduction
16	Excessive disconnection of demand
17	Insufficient or too slow disconnection of demand
18	Excessive reduction of generation
19	Failure of stations to hold required load rejection
20	System collapses or stabilises at much reduced level of demand
21	Disconnection of demand by under-frequency relays
22	System separation between sections
23	Demand and generation essentially balanced in island
24	Significant imbalance between demand and generation in Island
25	Island stabilised by demand disconnection or generation reduction
26	Excessive disconnection of demand
27	Insufficient or too slow disconnection of demand
28	Excessive reduction of generation
29	Failure of stations to hold required load rejection
30	Disconnection of demand by under-frequency relays
31	Island collapses at much reduced level of demand

2.2.1. UK Incidents

Three serious incidents occurred in the UK between 1981 and 1987. These incidents show the range of hazards that the system operator faces, even in a temperate climate.

Conditions at the time of the first incident in August 1981 (UK81) were consistent with the conditions foreseen during the operational planning work. However, the sagging of conductors caused flashovers to trees on three very important circuits between the south east and south-west. The south-west and a part of the south-east were then split from the rest of the system. A significant generation deficit was observed in this electrical island. On the other hand, generation and demand remained reasonably well balanced in the rest of the system. High power flows and a serious loss of generation were the consequences of these initial events and conditions. Local shedding by underfrequency relays, tap changer actions and manual actions reduced the local demand by 30%. The sequence of spread was: 1,1,9,12,21,24,(26,27) [Kni01]. The numbers in brackets are used to indicate the events which occurred when the network was split.

The second incident in the UK (UK86) can be described as a “near miss” because a major load area was close to voltage instability. The incident happened in the spring of 1986. The weather at the time of the incident was very bad with torrential rains and thunderstorms. Lightning strikes tripped circuits into a load area, leaving the remaining circuits heavily loaded. Voltages decreased rapidly over only a few minutes, which caused the shedding of 3% of the load through automatic undervoltage load shedding. The interaction of tap changers and the load shedding helped to avoid severe load disruption. The sequence of events was thus: 1,9,15. [Kni01]

In the third incident in the UK, which happened in the autumn of 1987 (UK87), very strong winds caused the outage of many circuits. About 16% of the total load was disconnected. During the most critical few minutes generation was lost at several stations, some because of transmission faults and some because of voltage and frequency variations at the generator terminals. A lot of faults occurred due to external (environmental) factors. Damage to local distribution systems was so extensive that distribution utilities were unable to restore supplies for many hours. The sequence of events was: 2,12,(2,...,2),11 [Kni01].

2.2.2. Incidents in France

The most severe disturbances in France, occurred during the winters of 1978, 1987 and 1999. In 1978 incident (Fr77) the system suffered from low voltages and very high power flows. The initial cause of disturbance was a significant number of 400 kV and 225 kV lines switched off due to overloads. These outages and a continuing increase in demand further deteriorated the situation and caused the disconnection of generating units. About 75% of the total load was disconnected. The sequence of spread was: 6,9,14,10,8,12, (26),(26),(26),(26) [Kni01].

The second disturbance happened in 1987 (Fr87) and was not as severe as the previous one. About 14% of the total load was disconnected. Very low temperatures were observed in the west of the country but the system conditions were reasonable. The initial cause of disturbance was a trip of five generating units, which further depressed the voltage and caused new generator outages. The sequence of events was: 5 (3), 2, 12 [Kni01].

The worst storms in recent history crossed France on Sunday 26th of December 1999 and overnight of 27th/28th (Fr99) [Mer00],[Kni01]. During these two storms, 38 out of 450 400 kV lines, 81 out of 1050 225 kV lines, and 406 out 4900 HV circuits were put out of operation. This led to the outage of 184 high voltage substations, while 5000 MW of demand was disconnected. The main cause of this major incident [Mer00] was the mechanical loading of lines caused by snow and ice.

2.2.3. Incidents in Scandinavia

Two large incidents were recorded in the Nordel system during the winters of 1979 and 1983. At that time the Nordel system consisted of several hundred generators ranging in size from windmills of 0.2 MW to nuclear units of 1100 MW. These were interconnected via the 400 kV transmission network.

The incident that occurred in 1979 (Nordel79) was initiated by the incorrect operation of a protective gear followed by an incorrect operation of a part of the protection system. These incorrect operations caused the instability of the system and the loss of a significant number of generating units. This led to a frequency deviation of 1.5 Hz and the activation of underfrequency load shedding. About 13% of the southern load and the entirety of the

northern load were disconnected. The sequence of disturbance spread was: 4,7,8,12 (24,26,27) [Kni01].

During the 1983 disturbance (Nordel83) a faulty isolator caused a busbar fault, opening an important interconnection and a few lower voltage connections. An incorrect protection operation further aggravated the situation. This produced other overloads and the voltages fell rapidly. The system separated into two sections. Instability caused the disconnection of major generating units and further excessive disconnection of demand (63% of total load). In this incident, like in the previous one, incorrect protection operations and line overloads played a key role. The sequence of events in this incident was: 6, 1, 7, 9, 10, 8,12 (26,32,33), (26,27) [Kni01].

2.2.4. Incidents in the Far East and Australia

The disturbances that hit Japan in 1987, Thailand in 1985 and Australia in 1977 are the most severe incidents that occurred in the Far East and Australia. The disturbance that happened in Japan in 1987 (Jap87) is one that has a very short sequence of events. The disturbance was initiated by a correct but unwanted operation of an impedance relay caused by low system voltages and high currents. This further caused a system split, triggered instability in the system and caused the loss of 21% of total demand. The sequence of events was: 6,10,8, 13 [Kni01].

During the incident in Thailand in 1985 (Thai85), 28% of load and 47% of generation was lost. The incident was initiated by an incorrect switchgear operation. A random fault and an incorrect protection system operation split the system into two sections, but produced a significant imbalance between demand and generation. This caused excessive disconnection of demand and further system splitting. The sequence of events was: 6,1,7,10,13,14,16,22,23 [Kni01].

The incident in Australia in 1977 (Au77) is an example of high impedance fault. System design and environment make some systems more prone to such faults. This was the case in the South East interconnection of Australia at the time of incident. The disturbance was initiated by the activation of an impedance relay in zone three that cleared a fault on a 330 kV line. The next event was an incorrect protection operation. Frequency fell to 48.7 Hz, which activated underfrequency load shedding and excessive disconnection of demand. After the

shedding, the system frequency rose to 50.35 Hz. Next, a 500 MW generator tripped because of the incorrect operation of the protection of the boiler. This caused the frequency to drop to 49 Hz. About 7% of the total demand was disconnected in order to restore nominal frequency. The sequence of events was: 1,7, 16, 17,5, 17, 23. [Kni01].

2.2.5. US Incidents

Some reviews of selected system disturbances in North America are available on the North American Electric Reliability Council web site [Nerc], [Nerc02a],[Nerc02b],[Nerc02c]. The worst disturbances occurred in 1996, 1998, 1999 and 2000. They are analysed in this section.

Transmission problems that occurred in Florida on March 12, 1996 (US120396) created an electrical island in west Florida and portions of central Florida, resulting in the loss of about 3440 MW of demand. This separation was the result of several events: planned and forced outages, unseasonably cool temperatures, and higher than normal electricity transfers from north and north-east Florida into west and west-central Florida. This resulted in overloads on the 115 kV and 230 kV lines. To reduce the loading the operators intentionally opened one of the 230 kV lines, which caused overloading of the second east-west 230 kV tie, which was beginning to overload. In order to decrease flows the operators started the peaking units and split intentionally one of the most affected buses. This action split the system into two islands. Unfortunately, it also caused serious overloads on two very important lines (more than 120%). Shortly afterwards these lines were tripped by the protection system. This further caused cascading outages due to overload. A very important generator producing 507 MW was removed from service due to low voltages. The loss of this generation reduced the frequency in one of the islands to 58.65 Hz. Underfrequency load shedding then took place. About 27% of the total demand in the island was disconnected (3440 MW). The sequence of events was: 6,10 (22), 9,9,12,30.

The second large incident happened on 16th April 1996 (US160496). A lot of generating substations insulators in the Southwestern Public Service Company (SPS) system were contaminated due to a combination of factors. An inspection of these substations showed that the washing of insulators using a high-pressure demineralised water washer was required. During the washing of one of these substations, several circuit breakers in the same substation were opened due to a fault on a 230 kV busbar. These breaker openings removed from service a generating unit that was producing 537 MW at that time. An incorrect operation of a Zone 3 distance relay removed another unit, while the voltage dip at the same substation initiated the

trip of the third unit. After a significant amount of generation was lost one 345 kV line, one 230 kV line and one 115 kV line were opened by the protection system due to overload. These outages caused the SPS system separation. After the separation frequency rapidly dropped and all three steps of underfrequency relays operated, shedding about 700 MW of demand. The sequence of events was: 6, 12, 7,9,10,24,30.

Severe disturbances happened in the Western System Co-ordinating Council (WSCC) system on the 2nd of July 1996 (US020796) and the 10 of August 1996 (US100896) [TaE97]. These disturbances attracted a huge amount of attention from many researchers and power system engineers. During the first incident 29 significant events were recorded, the system split into five islands and for less than one minute more than 2 millions customer were disconnected. The sequence of events and system islands are shown in Fig.2.5. The disturbance was initiated by a phase to ground fault (1), but an incorrect protection operation (2) aggravated severely the situation. A remedial action scheme removed two generating units (3) from service (about 1040 MW) and another incorrect protection system operation (4) removed the next 230 kV line. Due to low voltages and high currents another two 230 kV lines were opened by impedance relays (5). Shortly after, impedance relays opened four parallel 230 kV lines (6) due to extremely low voltages and high currents (900 Amps at about 212 kV). The next 230 kV line was removed from service by a Zone 2 distance relay (7), which separated the 230 kV path between the north-west and the central areas (see Fig 2.1). Two 500 kV line outages caused by an under-impedance switch into fault logic began the separation of the south-west from the north-west (8). Analysing the sequence of events, it appears that events (1) to (8) started a chain reaction of outages. The outages of 500 kV and 345 kV lines denoted as (9)-(19) in Fig .2.1. are caused mainly by impedance relays operations due to low voltages and high current. The outages from (20) to (29) are 345 kV and 230 kV line trips due to power out of step protection operations. The sequence of events was: 1,7,5,7,9,9.

The second large disturbance separated the system into four islands and resulted in a serious load reduction. The sequence of events is shown in Fig. 2.6. Fifty significant events were recorded, mainly outages of 500 kV lines and a few 345 kV lines. This time more than ten generating units were tripped due to extremely high reactive requirements. The first three 500 kV line outages were caused by flashover to a tree ((0)-(2)). Afterwards a 115 kV line was removed from service due to an incorrect protection operation (3). The conditions prior to the disturbance were marked by high summer temperatures and heavy export from the north-west to the south-west. Due to such conditions another flashover to a tree occurred on a 230 kV line. However, the same protection removed a generating unit (207 MW) (4), which caused

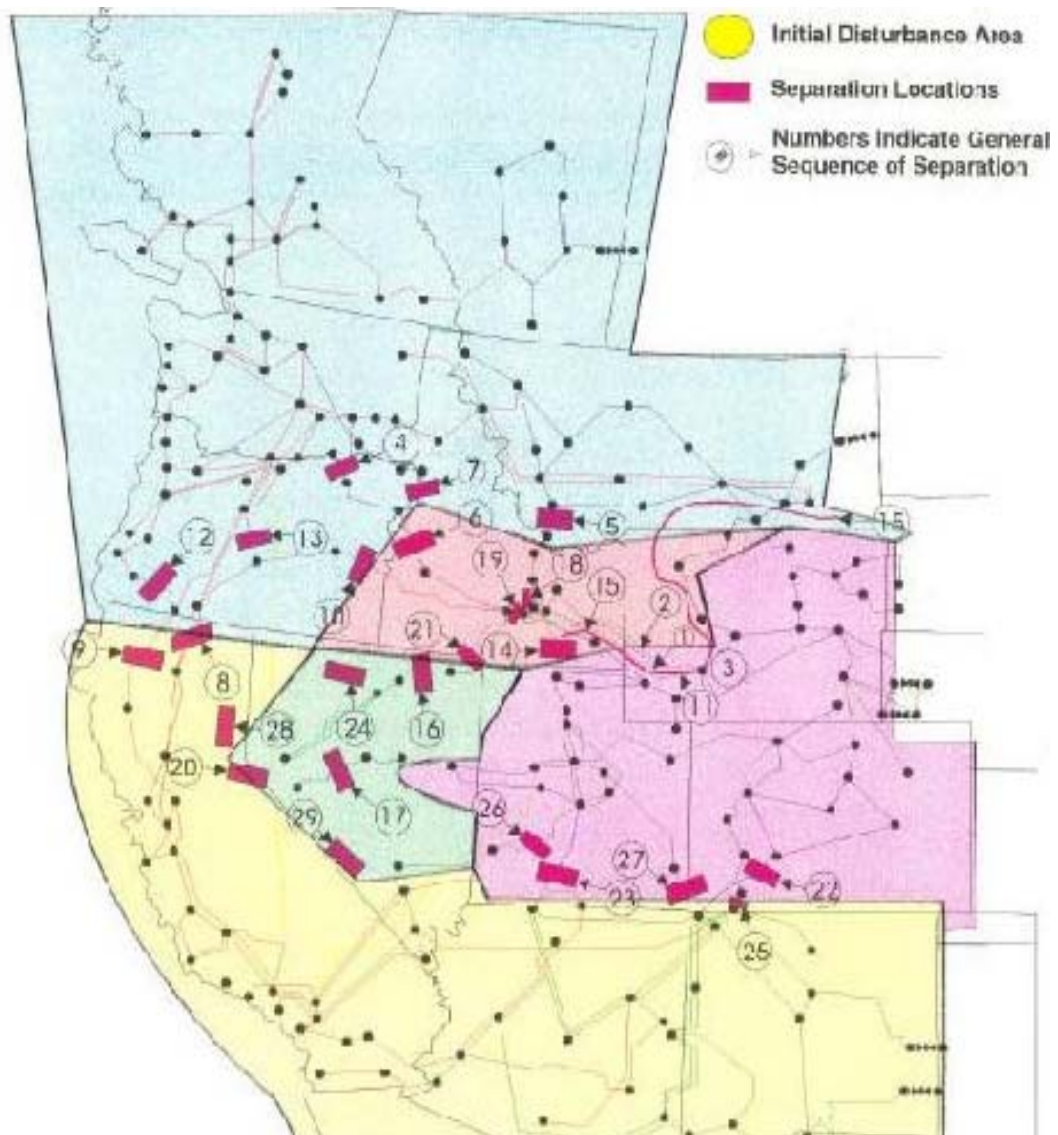


Figure 2.5.: June 2nd disturbance, sequence and islands separations [Nerc02a]

a relatively small increase in reactive generation at nearby generating units (480 MVar to 494 MVar). The system protection removed all these units shortly afterwards as a result of erroneous operations of a phase unbalance relay in generation excitors (5). Following the removal of these units, mild power oscillations began on the transmission system and started a chain reaction of outages. Frequency oscillations were between 58 and 61 Hz and underfrequency load shedding took place. In contrast to the previous WSCC system incident, this process was a few minutes longer, excluding the initial faults (0) and (1), which happened respectively two hours and one hour before. The events (1) to (5) are indicated as the main triggering events in [Nerc02a]. The sequence of events was: 3,7,1,5,7,14,21.

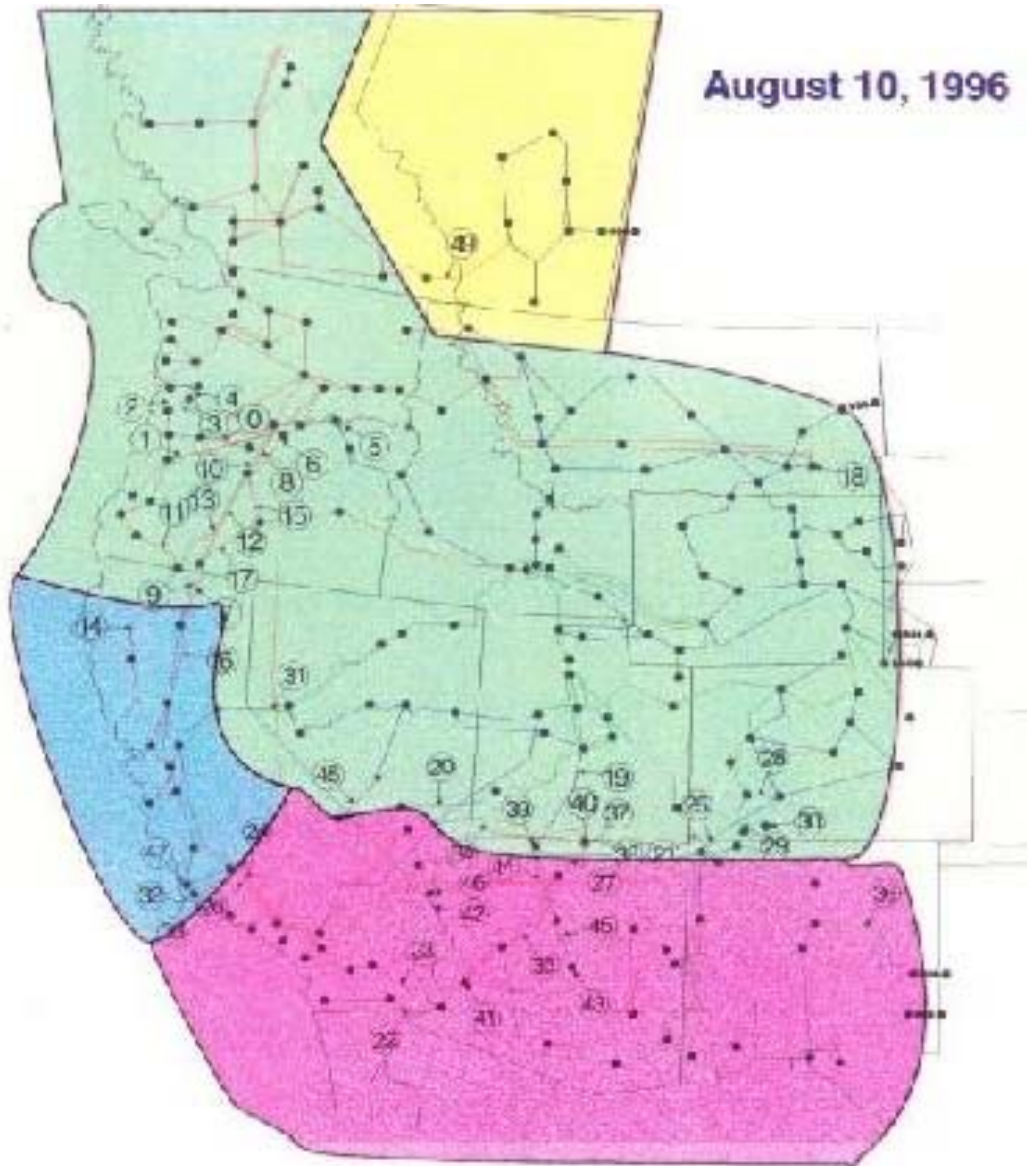


Figure 2.6.: August 10th disturbance, sequence and islands separations [Nerc02a]

Several incidents, which occurred during 1998 in North America are described in [Nerc02b]. The most severe was the incident that happened in the northwest Ontario on 25th of June, 1998 (US250698). The impact of disturbance was widespread, affecting a large area including several states. Three islands were formed and a part of Ontario system experienced a complete blackout. More than 60 transmission lines and 4GW of generation was removed from service leaving more than 150,000 customers (about 1GW) disconnected. The initial fault was a phase to ground fault on a 345 kV line. Another line (161 kV) was removed from service by the protection system and shortly after that another 345 kV line was struck by lightning. These outages triggered a chain reaction of new outages caused by protection

system operation due to low voltages and large overloads. The sequence of events was:3,1,9,10,24,26,31.

The four low voltage incidents (US100699, US160799, US130899, US180899) that occurred in North American Power System in 1999 demonstrate the need to accurately assess MVAR requirements and the ability of the system to provide them. Three problems are identified in an analysis of these incidents [Nerc02d]:

- system modelling studies did not have sufficient, and/or accurate data, or failed to take into account enough contingencies,
- customer demand (MW and especially MVAR) under hot weather conditions was underestimated, and
- the ability of generators to deliver reactive support during periods of peak demand was over estimated.

The first low voltage incident occurred on June 10th and 11th and resulted in very low voltages on the 138 kV network. These low voltages were caused by high temperatures combined with isolated facility outages, high power flows and a random fault followed by incorrect operation of protection breaker failure scheme. A review of the incidents indicates that the reactive power support to the 138 kV network from the 345 kV network was very weak, mainly because of very low EHV. The second low voltage incident happened on July 6th, in an area whose peak demand was 51.6 GW. Such peak demand was the forecast peak demand for the summer of the year 2004 for the area. An analysis of the incident shows that generator MVAR capability limits used by the real-time security assessment were not achievable under the ambient temperature on those dates. The third low voltage incident happened on August 13th was very similar to the first one, except that weak reactive support was dominantly caused by the outage of two big generating units (2x840 MW). Transmission Planning studies were blamed for the last low voltage incident happened in North America on August 18. It was shown that transmission planning studies had not predicted the low voltage conditions that occurred.

2.3. A Typical Pattern of Disturbance Development

To obtain a typical pattern of any process a detailed analysis based on statistical criteria is required. Such analysis deals with the various outcomes of the process. These outcomes are the result of changes caused by the various factors that can influence the development of a

process. Unfortunately, large system disturbances are very rare “processes”, whose development can be affected by a large number of factors.

Knight in [Kni01] suggests that it is possible to identify a general pattern to the way in which many of the large system disturbances of the past have developed. This pattern is shown in Fig. 2.7. A typical disturbance begins with random single or multiple faults that might expose some incorrect operation of secondary equipment. These faults can be more severe if they occur simultaneously with some compounding factors such as: errors in operational planning, errors in control, malfunction of protective gear and telecommunications failures. Such events can produce loss of transmission lines, load or generation. All of these might lead to an imbalance between load and generation in the whole system or a part of it.

There are several possible effects of sudden loss of transmission lines. The most severe first stage effects are: serious transmission overload, transient instability, system oscillations and voltage drops. The second stage effects that may develop from the first stage if the containment actions are insufficient or taken too slowly are:

- sequential tripping of overloaded circuits, system split and large imbalance between generation and demand,
- power system oscillations, impedance relay operations, tripping of generator units, system split, a serious imbalance between generation and demand,
- cumulative voltage decreases as tap changers operate, further voltage drop and current increases, generator hitting their capability limits and system approaching voltage collapse. This mechanism of voltage collapse will be further discussed in Chapter 6.

If a sudden load loss takes place the first stage effects are: system frequency rise, system voltage rise, transmission overload, transient instability, and system oscillations. The second stage effects that can result from the last three first stage effects are already described. The second stage effects for the system frequency rise and system voltage rise are respectively:

- too responsive governors might lead to oscillation of frequency with cumulative loss of generation and demand and possibly total loss of system.
- if the voltage rise can not be halted and is very severe, extensive faults/tripping of circuit due to impedance relay operation can result in a system collapse.

Loss of generation can produce the following first stage effects: system frequency falls, transmission overloads, transient instability, power system oscillations and system voltage drop. The possible second stage effects are already described for the last four effects. When

the frequency drops either an increase in generation or a load disconnection is required. A combination of excessive disconnection of load and too high gain with poor damping on governors can lead to a succession of under-frequency load shedding and over-frequency/generation reduction actions, culminating in a complete system collapse.

The first and second stage effects are shown in Fig. 2.7 for each sudden loss discussed above. The system or its separate parts should stabilise after a significant imbalance between demand and generation through the action of governors and load frequency control, disconnection of demand or less frequently disconnection of generation. All these actions intend to eliminate generation load imbalance and to restore the frequency to its nominal value. If, however, after these control actions an imbalance still exists, further adjustment of generation will be needed, which can lead to further load disconnection, loss of generation and collapse, which is shown in lower part of Fig. 2.7.

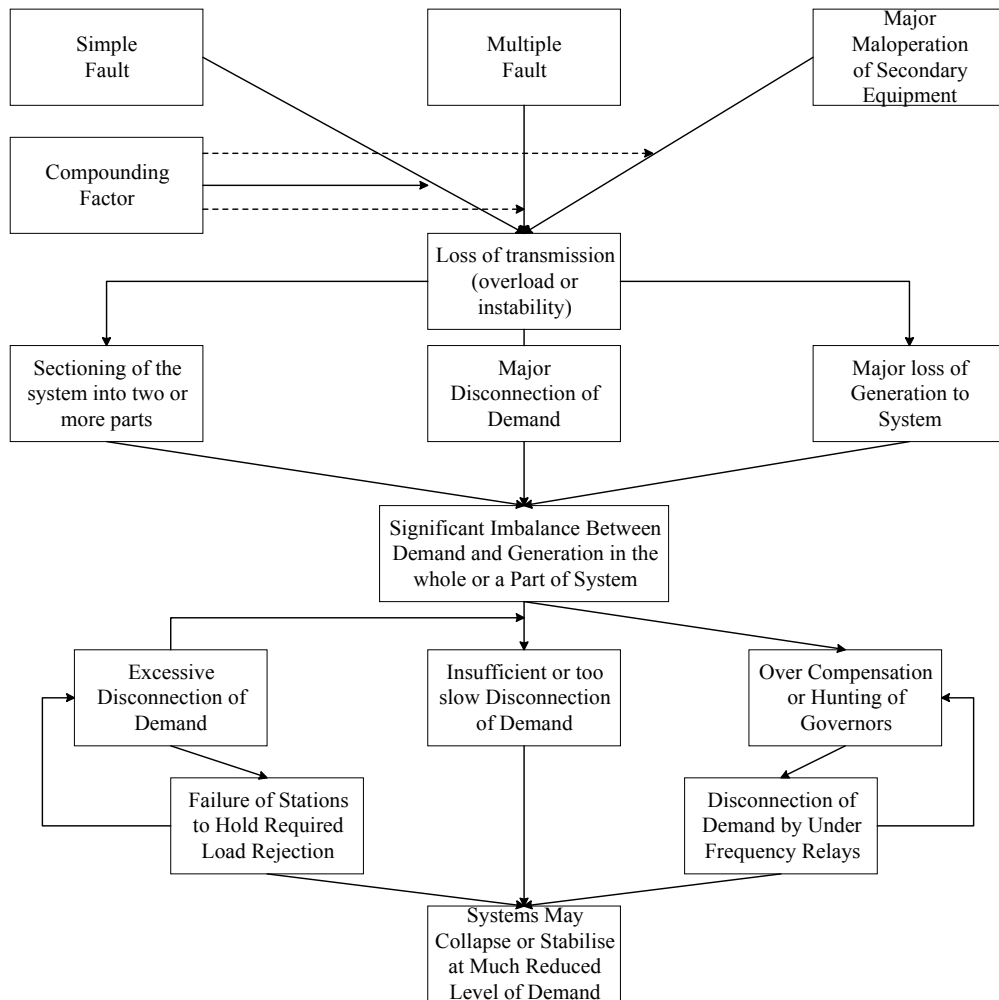


Figure 2.7.: A typical disturbance development [Kni01]

2.4. Power System in Emergencies – Definitions and Control Concepts

A power system can be in different system states. “System state” is a concise statement of the viability of the system in its current operating mode [Kni01]. There are various definition and transition diagrams of system state. The composite power system was classified into different operating states in [BiK92], [KhB92] to deal with different security considerations in system reliability assessment. A very similar transition diagram, but restricted to four operating states, is given in [Kni01] and is shown in Fig.2.8. The four states shown in this figure are interrelated by using credible contingencies (solid lines, single arrows), non-credible contingencies (dashed lines, single arrows) and restorative actions (double arrows). In the alert and emergency states action must be taken immediately to bring the system to an acceptable state (normal or normal alert). In the *emergency* state unacceptable loading, voltages or frequency already exists, while in the *alert* state some actions must be taken immediately in order to prevent the system from entering the emergency state. In standard security analysis, the majority of credible contingencies lead a power system to the *normal* (*alert*) state where rapid actions are not necessary, but must be taken to restore the system to the *normal* state. A credible contingency rarely brings a power system directly from the *normal* to the *alert* state.

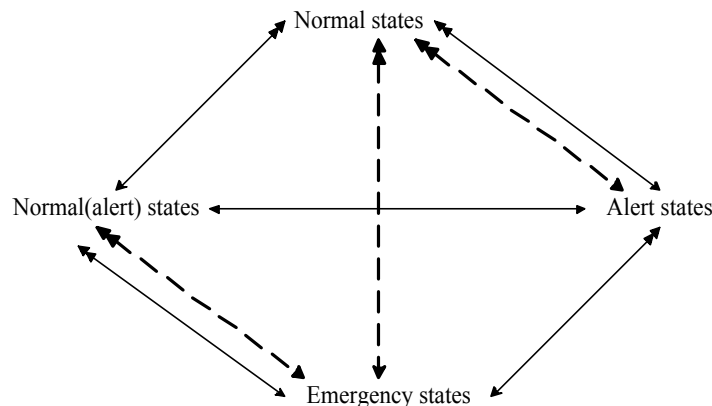


Figure 2.8.: System states [Kni01]

The disturbances analysed in Section 2.2 show that those incidents began with a disturbance capable of shifting a power system from a *normal* to an *emergency* state. A common feature of such disturbances is that they are extreme events that are unlikely to happen. Emergency control has an extremely difficult task to save the system integrity restoring one of *normal* states (see Fig. 2.8). The task is difficult because the control actions should be fast and carefully selected. These two requirements are contradictory because carefully selected control actions rely on detailed modelling and significant engineering effort. On the other

hand, fast decisions require both considerable experiences of similar situations or a simplified analysis.

A few emergency control concepts are suggested in [Kni01]. These concepts are shown in Fig. 2.9. The concepts are called:

- a. Pre-defined logic,
- b. Specific contingency based and
- c. Adaptive emergency control.

For the emergency control based on concepts a and c, actions are taken following an undefined contingency. These contingencies can be defined as a class, for instance, the sudden loss of the largest amount of generation possible, following a random fault. However, different utilities use different logic to define such contingencies. On the other hand, specific contingency based control (Fig. 2.9 b) is activated only in the event of a pre-defined contingency, for example the tripping of defined circuits in a part of the system with limited transmission connections [Kni01].

The first concept (Fig. 2.9a) is activated after an undefined contingency. Such contingency causes system effects that result in frequency, voltage or other important system changes. Pre-defined actions for containment are implemented to maintain as much as possible of the system in a viable operating state. Once they have saved everything that can be saved, power system operators should try to restore it to a normal operating state.

In the second concept (Fig. 2.9b), pre-defined containment actions are implemented immediately or after checks to confirm that actions are justified.

The last concept (Fig. 2.9c) is the most advanced concept based on adaptive control. Adaptive control actions are implemented in accordance with a set of measurements and completely rely on the operator. The operator makes the final choice based on the measurements and a fast computer analysis.

These concepts can be summarised as follows:

- All of these emergency control concepts have only one objective: to preserve the system integrity following a *non-credible* (not foreseen in security plans) contingency. Emergency control costs are therefore of secondary importance.
- Neither the resulting system states nor the necessary containment actions can be determined except in broad terms.

- All of these concepts are based on pre-defined containment actions, which means that extensive planning studies need to be carried out in order to determine in broad terms the best possible set of remedial actions.

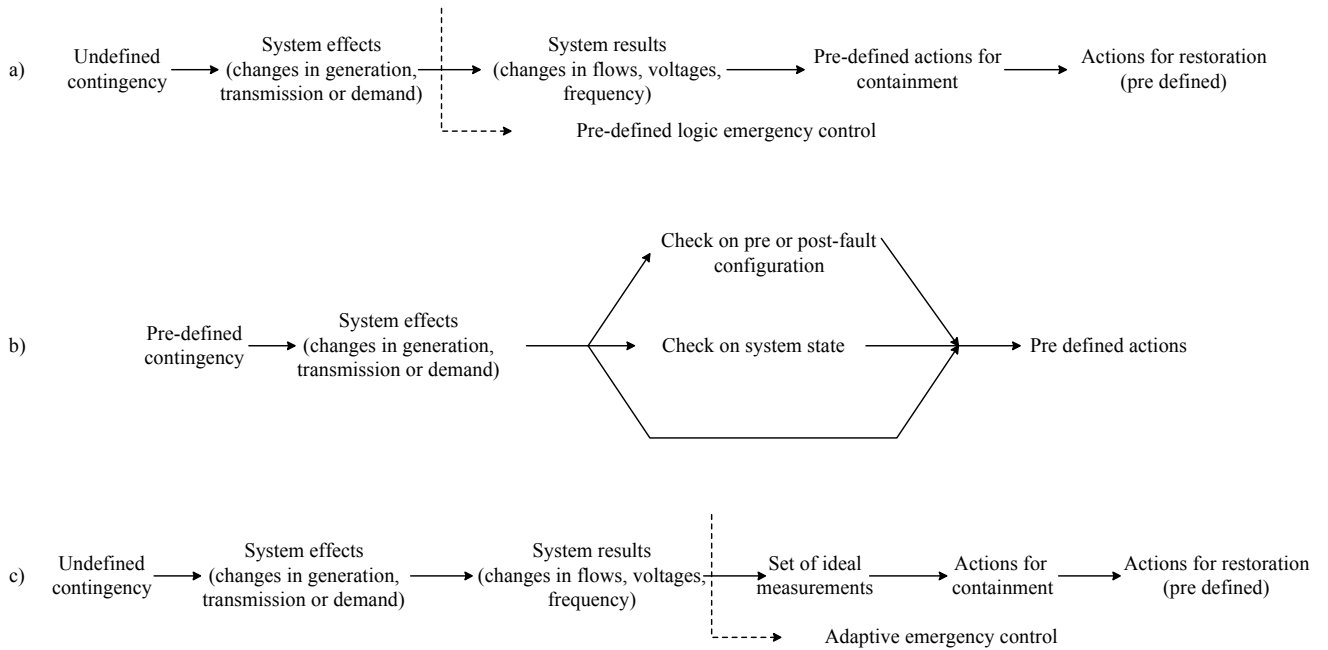


Figure 2.9.: Emergency Control Concepts

2.5. Measures to Minimise the Impact of Disturbances

Preventive measures in management, planning and operation can help reduce both the frequency and the harmful effects of system disturbances. These measures are very important prerequisites for a successful emergency control. In this section, three types of measures are considered: planning measures, operational measures and special protection schemes. These will be discussed separately in the following sections.

2.5.1. Planning Measures

Measures at the planning stage are introduced to minimise the risk of a disturbance. These can be divided into measures focused on generation and measures focused on load. When planning new generation the system planning engineers should provide a certain level of

reserve due to demand forecasting errors, bad weather, delays in commissioning and plant breakdown [Kni01]. This level of reserve should meet some criteria, for instance:

- reserve should cover the sudden loss of the largest generator or the largest import from neighbours in most cases,
- the rate at which this reserve can be marshalled is very important. For instance, it may be decided that 23% of total reserve should be provided by gas turbines

In order to minimise the risk of disturbance, generator characteristics such as minimum load and response rate should be carefully considered when the system planners have to make decision regarding new generation. These characteristic are shown in Table 2.3

Table 2.3 – Unit characteristics [Kni01]

	<i>Minimum load</i>	<i>Response rate</i> (% of maximal load per minute)
Steam units	gas and coal fired 40-50%	gas and oil 2-4%, coal 1.5%
Gas Turbines	30-40% of base load	75-100% of load in about five seconds
Hydro Plant	depends on environmental constraints	10 seconds from no load generation to full load generation for Francis type turbines
Nuclear Units	20% of full power or less	2-5% percent per minute

In contrast to the measures for generator adjustment, load adjustments are relatively cheap to provide but have more impact on customers. Under frequency load shedding is one of the most effective and widely used protective schemes introduced to restore generator demand balance. The main limitations of this scheme are [Kni01]:

- the lack of sensitivity to protect small parts of a power system,
- the difficulties in matching the existing imbalance,
- the impossibility to change the location of the load disconnection

Some utilities use a combination of frequency trend relays and underfrequency relays. Such combination uses two criteria to determine the level of load shedding. These criteria are frequency drop and drop rate. Knight argues that such combination will result in a smaller frequency drop and shorter period of under frequency running [Kni01].

2.5.2. Operational Measures

Three classes of measures are used in the operational time scale: load disconnection and other automatic switching systems, memoranda and procedures adopted throughout the utility and ad hoc measures implemented at short notice often based on equipment overloading [Kni01]. These measures are introduced to minimise the risk and impact of disturbances.

A typical underfrequency load disconnection scheme implemented in operation has several stages. These stages have usually steps of 5%, 7.5% and 10% of load disconnection. Smaller systems will tend to experience bigger frequency drops, which means that more drastic actions might be needed [Kni01]. Underfrequency load disconnection and other mechanisms, manual or automatic, to control frequency deviation should be an integrated package covering a frequency range for example from nominal minus 6 percent to nominal plus 10 percent [Kni01].

Power system operators should be supported by simple and clear rules and guidance. These rules and guidance are provided by different operational groups such as: Grid control, generation, Transmission, Distribution and Principal consumers.

2.5.3. Special Protection Schemes

A Special Protection Scheme (SPS) or Remedial Action Scheme (RAS) is designed to detect abnormal system conditions and take predetermined, corrective action to preserve system integrity and provide acceptable system performance. SPS actions include, among others things, changes in load, generation, or system configuration to maintain system stability and acceptable voltages or power flows. SPS are preferably local equipment co-ordinated by overall system studies [CTF95].

CIGRE report on SPS makes distinction between the protection schemes used to protect power system components from the protection schemes used to preserve system integrity. For example, the overload protection of a power system component is not a SPS. However, if such protection is used to save a system due to high power transfers then it can be classified as a SPS. A special designed protection system is used in Canada to protect a group of generators when the system experiences a separation. Such protection system cannot be classified as a SPS because its intention is to protect generating units [CTF95].

The main characteristics of SPSs are [CTF95]:

- SPSs operate on selected rare contingencies, usually outside the design range. Such operation usually allows control actions which are not used in the secure operating state such as for example load and generation shedding.
- Systems that allow the operators greater operational risk with the likely consequences being outside the capability of conventional protection.
- System wide protection, operating in multiple locations, with co-ordinated control of multiple signals.

The most frequently implemented SPS are [CTF95]:

- *Generation rejection* - This scheme involves the tripping of one or more generating units and most of them are event based (based on direct detection of events such as line trips). The practise of generator tripping is especially used on hydro-generator units. Generator rejection improves transient stability by reducing the accelerating torque on the machines that remain in service after a disturbance. The concept behind the generation rejection is to increase the electrical power output of the remaining generators and thus to reduce their rotor acceleration.
- *Turbine fast valving* –Turbine fast valving is applicable to thermal units and involves closing and reopening of steam valves in order to reduce the accelerating power of generators that remain connected to the network after a severe transmission fault. It is an alternative to generation rejection when a slower reduction in generator output is acceptable. Generation rejection is usually used on hydro turbines because fast valving cannot be used because of the inertia of water.
- *Fast Unit and Pumping Storage Unit Start-Up*- Power support by fast unit (e.g. gas turbine) or pump storage start-up can be used at low frequencies or when there is a high risk of voltage collapse caused by inadequate generation. The latter may result from the tripping of important tie-lines that interconnect regions of high generation to high demand.
- *AGC Setpoint Changes*- For satisfactory operation of a power system, the frequency should remain nearly constant. The main objectives of automatic generation control (AGC) are to regulate frequency to the specified value and to maintain the interchanges between areas at their scheduled values. Due to a lack of generation in a certain area caused by a combination of line trips, setpoint changes on AGC could be used to correct the generation-load mismatch.

- *Underfrequency load shedding* – The most common type of SPS is underfrequency load shedding (UFLS) scheme. Schemes of this type are used to preserve the security of both the generation and transmission systems during disturbances that initiate a major reduction in system frequency. Such schemes are essential if a utility intends to minimise the risk of total system collapse, maximise the reliability of the overall network and protect the system equipment from damage.
- *Undervoltage load shedding*- Undervoltage load shedding (UVLS) is analogous to underfrequency load shedding and provides a low-cost means of preventing voltage collapse. An UVLS scheme uses undervoltage relays to monitor the voltage level in a substation.
- *Remote load shedding* – is similar conceptually to generation rejection but is implemented at the receiving end of the power system. Remote load shedding is designed to operate after extreme contingencies affecting the system's transmission capacity whose severity largely exceeds the robustness of the power system.
- *HVDC fast power change* – HVDC transmission links are highly controllable devices and this unique characteristic may be used to improve the transient stability of the AC power system. The power flow on HVDC links can be modulated by controlling the converters. HVDC modulation can provide powerful stabilisation with active and reactive power injection at each converter.
- *Automatic shunt switching* – SPS are widely used to control the voltage levels in a substation. This is achieved by automatic switching of shunt reactors and capacitor banks. Shunt reactors can be installed at the HV busbar in a substation, or at the tertiary winding of a transformer in an EHV/HV substation. Depending on the measured voltage level, they can be tripped or reconnected. Capacitor banks are installed in many substations to improve the power factor of the consumer load or for feeder voltage control. They are automatically switched in accordance with busbar voltage level.
- *Braking resistor* – Dynamic braking applies an artificial electric load to a portion of the power system. Generally it has been studied and applied as a switching in of shunt resistors. This usually requires a fixed insertion time and occurs immediately after a fault has been cleared on the system.
- *Tap changer blocking and set-point adjustment*- The main goal of on-load-tap-changers (OLTC) is to keep the controlled side of the transformer (normally the lower voltage) within a given voltage range. Typically as load increase the LTC will cause the tap position to be raised in order to maintain the voltage level. However, following a severe disturbance, the voltages will be reduced over a regional area that

may affect many substations. The OLTCs applied to transformer at different voltage levels all operate on local criteria. All of them will independently start the tap changing process designed to re-establish the controlled voltage. If the voltage reduction starts to progress towards a voltage collapse the bulk system voltages will slowly decrease while the OLTCs are trying to restore the distribution system voltages. The transmission system will be further stressed until a new steady state is achieved or a voltage collapse occurs. It is common, at least in Europe, to have controlled OLTCs on both EHV/HV transformers and HV/MV transformers. Tap changers blocking or set point adjustment can be beneficial for preserving system stability in stressed system situations that are close to voltage instability.

- *Quick increase of synchronous condenser voltage set-point*- Synchronous condensers can generate or absorb reactive power depending on the control of their excitation system and are excellent voltage and reactive power control devices. The system voltage does not affect the reactive power production of a synchronous condenser. The automatic voltage regulator (AVR) can automatically adjust this reactive power to maintain constant terminal voltage. While the AVR is controlling the terminal voltage the reactive power output can be increased until a heating limit is reached. The action of the AVR is very fast and quite efficient in the case of voltage collapse if the synchronous condenser is located near the load centre.

2.6. Previous Work

Previous work on large system disturbances can be broadly divided into two groups. The first group contains work related to the description, analysis and summation of large system disturbances. This work was carried out mainly by CIGRE Committee 39 (“Power System operation and Control”), CIGRE Committee 34 (“Optimisation of protection Performances during Major disturbances”) and CIGRE Committee 38 (“Optimisation techniques and analysis of Reactive Power Compensation”). This work is based predominantly on surveys. U. G. Knight made a significant contribution to the work done by CIGRE Committee 39 on system disturbances. Most of his work on this topic was published in his book [Kni01]. The most important facts regarding this work are already described in the previous sections.

The second group contains work related to the simulation of large system disturbances. This work was mainly done at Cornell University and Virginia Tech. In this work, incorrect

protection operations called hidden failures in protection system are seen as the main factors contributing to the spreading of disturbances. Sequences that contain a random fault and unnecessary trips of “healthy” components due to these incorrect protection operations were simulated using a probabilistic approach. It is suggested that the results of such simulation could be used to enhance the protection system of the most vulnerable lines.

The work that belongs to the first group justifies the work that will be presented in this thesis. As it is showed in section 2.1, system disturbances are a real threat for modern power systems. The analysed system disturbances in section 2.2 show that recent power system disturbances often involve an initial non-catastrophic outage that is followed by a malfunction of the protection system. Conventional on-line security analysis does not consider such combinations of events because they are considered as having too low a probability to be included in a predefined list of credible contingencies. However, sections 2.1 and 2.2 confirm that such combinations of events frequently trigger large system disturbances, which means that may not be quite as improbable as one would expect.

The learning order of events is based on the premise that we learn how before we learn why. For example in mathematics, we learn arithmetic before we learn algebra. Practise always comes before theory. However, in the case of system disturbance practise can be particularly dangerous and costly. The challenge is thus to develop a new software tool that can help power system planners and operators learn from a tool before they experienced in practise. To develop such tool was the main objective of this PhD Thesis.

The work done at Virginia tech and Cornell University was a promising first step. This work began with S. Tamronglak PhD thesis [Tam94],[THP96]. In this thesis, failures in protection system were identified as having a key role in spreading the disturbance over the network. Tarmonglak suggests that these failures cannot be revealed during normal system operation. They remain hidden until they are exposed by some abnormal power system state. Tarmonglak analyses all protection schemes used in transmission networks and discusses their possible failure modes. Based on this analysis, he defines the vulnerability region as an area where some of “healthy” power system components might be tripped due to hidden failures. He further introduces four different types of vulnerability regions based on the settings of different protection schemes. Once the vulnerability region for each relay is known, a vulnerability index can be determined for each region in the system. The loss of stability of the power system was used as the criterion for computing this index. Both steady state and stability aspects of the system are investigated. However, only sequences involving two events were considered. The first event is an outage due to a random fault. The second

event is an outage caused by a protection malfunction, which takes place in the vulnerability region.

Tarmonglak's work is further extended in [TPH96] where the number of events in a sequence can be larger than two. The sequences are simulated using a probabilistic simulation based on importance sampling. The simulation determines the probability of a cascading disturbance in terms of individual probabilities of a hidden failure causing an unnecessary trip. If the probability of cascading disturbances is as small as experience indicates, then the simulation can require formidable amounts of computation. One valuable technique that can overcome such an obstacle is importance sampling. Importance sampling alters probabilities in such a way that rare events happen more frequently in the simulation. This technique is a well-known variance reduction technique. Using the results of the simulation Thorp, Phadke, Horowitz and Tarmonglak determine a priority list of relays. The top ranked relays from this list should be checked and monitored more often. They believe that such priority-based inspection and monitoring can greatly reduce the probability of a simple event degenerating into a widespread disturbance.

Bae and Thorp in [BaT97],[BaT02] use a very similar probabilistic simulation to detect weak links in the WSCC power system. The simulation is extended to include similar incorrect protection operation in the generator protection system. The individual probabilities of such incorrect protection operations are calculated using the probability functions shown in Fig. 2.10. The probability of an exposed line tripping incorrectly (Fig 2.10a) is a function of the impedance seen by the relay. Figure 2.10b shows the probability of incorrect generator tripping as a function of the reactive power produced by the generator. Such a probabilistic function suggests that generators close to their capability limits are more susceptible to protection failures.

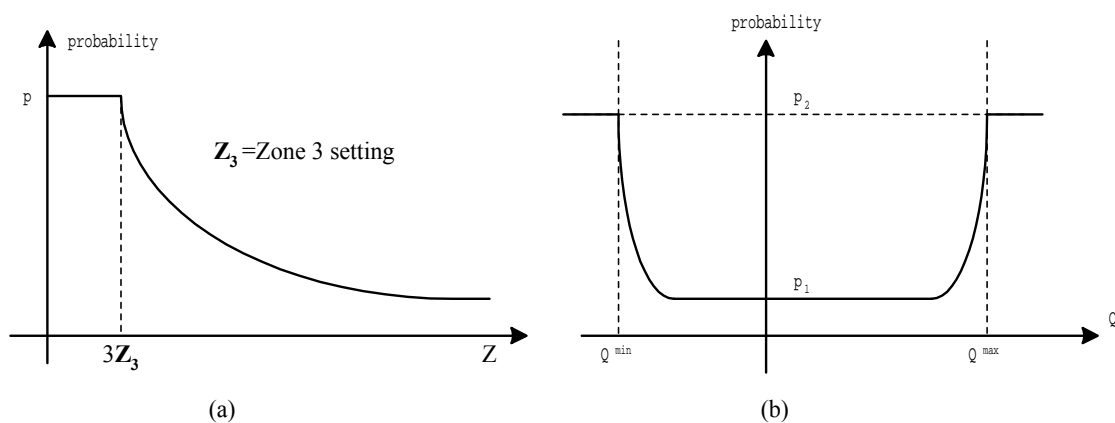


Figure 2.10.: Probabilities of incorrect tripping of (a) lines (b) generator [BaT97]

Chen and Thorp use similar probabilistic simulation based on importance sampling in [ChT02]. Instead of a Newton-Raphson load flow, they used a DC load flow and a linear optimisation to determine the minimum load curtailment when a line is overloaded, or the system breaks into multiple islands. The vulnerability performance index for each line is calculated in order to determine the most vulnerable lines. The index called Expected Energy Lost (EEL) is defined as the product of the amount of load shed and the probability of the sequence of events.

Wang and Thorp in [WaT02] introduce a random search algorithm based on power system heuristics for faster search of important blackout paths. The objective of this search is to locate the most vulnerable locations in a real power system. The search uses a depth first search algorithm. The algorithm starts from the root, which is the “zero” level. This level represents a base case without outages. The next outage is a random fault (the first level), afterwards all subsequent outages are due to either failures in the protection system of the transmission network or failures in the generator protection system or to line overloads. Only one outage is allowed at each level. After a new outage a power flow is performed and the probability of the sequence of outages is updated. If the power flow does not converge, load is shed and the EEL of the sequence is recalculated. Each outage in the blackout path is the last if the EEL becomes larger than a given threshold. Short sequences that have a large amount of load shedding are the most important blackout paths. The search can be completed once the number of important simulated blackout paths is larger than a specified value.

Finally, Elizondo in his MSc thesis expanded the analysis of failures in the protection system previously done by Tarmonglak to failures in the generator protection system and SPS. His thesis is summarised in [ERP01], where it is proved that the recent large system disturbances in the WSCC power system were triggered by such multiple protection failures.

2.7. A New Simulation of Large System Disturbances

The main focus of the work done by Bae, Chen, Horowitz, Padhke, Thorp and Tarmonglak is on potentially weak power system links. They argue that special attention should be paid to the most vulnerable links if enhancement or inspection of the protection system is required. They further believe that enhancement and inspection can greatly reduce the probability of simple events leading to widespread disturbances.

The new simulation of large system disturbances presented in this thesis focuses on the fact that a vast space of disturbance developments causes a lack of knowledge and makes defence plans and emergency actions very restricted. Therefore, instead of focusing on a specific task the following broad objectives are established for the new simulation of large system disturbances:

- to increase the operators' confidence in their ability to weigh up situations under stress,
- to help power system planners develop and implement timely and correct decisions,
- to improve knowledge of the technical characteristics of the system under dynamic or degraded operating conditions and
- to improve knowledge of facilities for handling emergency situations.

These objectives are concentrated on improving power system security. Kirschen in [Kir02] make comparisons between two different measures of security. The first one is based on deterministic security approach, while the second one uses probabilistic techniques. Deterministic approaches use a set of credible contingencies to determine whether a power system is secure or not. Dividing contingencies into credible and non-credible sets implicitly means that large disturbances are definitely outside the scope of deterministic security criteria. Rather than considering a contingency as non-credible because it involves the outage of two components, a probability can be attached to each of them. This makes it possible for "non-credible" contingencies to be simulated using probabilistic approaches. A probabilistic simulation that includes several system phenomena into consideration is presented in [KBN02] and [RKJ02]. In these papers, Kirschen and his associates show that large system disturbances can significantly affect the cost of security. However, these disturbances are very rare events, which may not happen once in 30,000 sampled power system states. Such probabilistic simulations usually represent average system behaviour and therefore cannot be used to simulate large system disturbances. This means that a vast majority of these 30,000 sampled states does not have any component out of service. On the other hand, large disturbances are very rare in these simulations and usually occur due to a busbar fault when the lines connected to the faulted bus have to be tripped.

The probabilistic simulations used in the papers discussed above deal with static power system models such as Newton-Raphson power flow or DC power flow. Such simulations do not consider dynamic phenomena such as transient stability or frequency response or voltage

stability. However, to include all these dynamic models in such simulations would probably result in an almost never-ending computation. Therefore, simplified dynamic models are proposed as part of the new simulation in order to keep the computation time within reason. The new simulation is therefore, a combination of dynamic and static models able to detect a significant amount of system failures that can affect a real power system. Therefore, the interesting search for large system disturbances suggested by Bae, Chen, Horowitz, Padhke, Thorp and Tarmonglak was a promising beginning, but serious modelling effort was needed to develop the new simulation.

One of the objectives of the new Simulation of Large System Disturbances (SLSD) is to detect as many potential system failures modes as possible. These failures modes are described in Chapter 3. To detect these failures different power system models should be used. These models deal with different system phenomena. Three very important dynamic phenomena are considered in the simulation of large system disturbances. These phenomena are:

- transient stability,
- frequency response and
- voltage stability.

Modelling of transient stability and frequency response is described in Chapter 4, while Chapter 6 deals with voltage stability models. Incorrect protection operations still remain the main driving force in the simulation. These operations are discussed in Chapter 5. Instead of the random heuristic search suggested in [BaT97], [WaT02] a new technique based on an event tree is proposed. This technique and the complete algorithm of the simulation of large system disturbances are discussed in Chapter 7.

Another important characteristic of the proposed SLSD is that all these phenomena are considered with respect to their time of response. Thus, transient stability calculation is first carried out after a random fault. Possible outcomes are transient instability, local transient instability when a few generators exhibit unstable behaviour or transient stability. If there is any imbalance between generation and load, frequency response simulation will be run to check whether any of the frequency related failures could take place. If the fault does not cause any transient or frequency related failures, the power flow calculation is run. Otherwise, the sequence is completed. If the power flow does not converge, a load shedding scheme based on a simulation of the logic that an operator might use takes place. The simulation does not continue with new outages if the fault causes power flow divergence or load shedding. If

the power flow converges, a new set of exposed power system components will be determined. These components are only candidates for the next outage in the sequence. However, the set of candidates is large. Taking all these candidates into consideration would trigger a combinatorial explosion. The best candidates are determined using a voltage stability calculation. This calculation favours the components whose outage leads the power system to operating points that are closer to voltage instability. The described procedure is repeated again for the best candidates. Some restrictions are imposed on the simulations in order to avoid a combinatorial explosion. The most important restrictions are that each simulated sequence cannot have more than four outages and that each outage in the sequence cannot have more than three successors. An exception from the last rule is that this number can be larger if more than three successors produce any of the system failures that are used as the stopping criteria.

3

Power System Failures

Power system failures can be defined as unwanted events that should never occur, but might cause catastrophic consequences for a power system. Such events can require emergency corrective actions. These are designed to save the system integrity and protect system components and equipment from damage. The types of failures considered in this work are: transient instability, frequency collapse, voltage collapse, system islanding, load shedding, excessive line overloads and over/under voltages.

They can result from factors external to the system, such as weather or the environment, or internal factors due to plant failures or as a result of operating conditions. System failures can be predictable and unpredictable. The former are due to shortage of: plant capacity, fuel, ancillary supplies, operating or control staff [Kni01]. The latter are usually caused by a combination of external and/or internal factors and outside the scope of most of the security plans.

External factors caused by severe weather are [Kni01]:

- conductor failure on overhead lines due to snow and ice loading,
- conductor sag on overhead line due to conductor heating or by mechanical loading from snow or ice,
- conductors overheating due to a combination of weather conditions such as high ambient temperatures and low wind speed,
- conductor clashing on overhead lines due to wind or loss of snow/ice,

- insulator flashover on overhead lines due to dirty insulator surface caused by industrial pollution, freezing fog,
- flashovers caused by lightning.

External factors caused by the environment are [Kni01]:

- flashover to vegetation from overhead lines,
- falling trees or windblown materials,
- smoke and fire,
- ground excavation or subsidence damaging cables and overhead line towers.

Internal factors can be manifold, some coming from plant failures while others from system effects. System effects can be caused by operating conditions or as a consequence of plant failures. The conditions that may lead to large or small system failures are [Kni01]:

- frequency outside limits,
- instabilities,
- system splitting,
- overloads,
- over/under voltages.

When the system frequency is outside its limits, control or protection actions are required at the system level. Such actions can be produced for example by automatic generator control or underfrequency load shedding. Transient and voltage instability can be either a local or a system-wide phenomenon. While local instabilities can be successfully handled, global system instabilities are a real threat for a power system. System splitting is a system level problem that might cause excessive load shedding, serious imbalance between generation and demand or even instabilities in system islands. Overloads and under/over voltages are more frequently local problems, their existence system wide is rare but gives a warning that the system might experience serious consequences.

The simulation of large system disturbances proposed in this thesis uses different methods and techniques to model as many as possible of these failures. Therefore, system failures such as transient instability, frequency collapse, voltage collapse, underfrequency and system splitting are dominant phenomena in the simulation. However, local phenomena such as overloads, over/under voltages, external factors and especially incorrect protection operation are considered as the main contributory factors. These factors should not produce serious system failures by themselves but can trigger a chain reaction of failures in a power system.

System level failures such as instabilities, frequency collapse, underfrequency and system splitting are discussed in section 3.1. The importance of contributory factors such as overloads, over/under voltages, external factors and incorrect system operation is considered in section 3.2.

3.1. Dangerous System Failures

The more severe disturbances may well affect the ability of the system to remain stable or to continue supplying all its consumers at satisfactory frequency and voltages. The continuity of supply, frequency and voltages are the key characteristics of the system behaviour. When these characteristics are seriously perturbed the system might suffer from frequency collapse, transient or voltage instability, under/over frequency conditions, or system islanding. These dangerous system failures are discussed in this section. For the sake of simplicity and brevity only very simple explanations of these phenomena are offered.

3.1.1. Transient Instability

During normal power system operation, the angles between each pair of generator rotors will change continuously by small amounts as demand, generator outputs and power flows change. However as a result of a sudden large increase in transfer impedances across the network, the relative angles between two or more rotors may increase quickly and significantly. This phenomenon is known as transient instability [Kni01].

A simple illustration of transient stability for a simple system, which connects a generator to an infinite bus via a transmission line, is shown in Fig. 3.1. The illustration uses $P-\delta$ and $\delta-t$ diagrams to show a typical stable and unstable behaviour of this simple system. The intersection between the generator power angle characteristic and the generator mechanical power P_m is the equilibrium point, denoted as 1. For the sake of simplicity and brevity it is assumed that the pre-fault and post fault impedances between the generator and the infinite bus are the same. It is further assumed that a three-phase fault occurs on the transmission line very close to the generator. This last assumption makes the generator electrical output equal to zero and forces the rotor to point 2 on the power angle diagram. Before the fault is cleared the rotor moves from point 2 to point 3 acquiring a kinetic energy proportional to the shaded

area 1-2-3-4. This area is known as the acceleration area. As soon as the fault is cleared (instant t_1 , see $\delta - t$ diagram) the rotor begins to follow the power angle characteristic and moves to point 5. The rotor accelerates until the acquired kinetic energy is not equal to the deceleration area denoted as 4-5-6-7. The rotor again reaches synchronous speed at point 6 where area 1-2-3-4 becomes equal to area 4-5-6-7. After point 6 the rotor starts to decelerate, which is shown on the $\delta - t$ diagram. Point c on this diagram corresponds to point 6 on the $P - \delta$ diagram. If, as shown in Fig.3.1b, the clearing time is longer ($t_2 > t_1$) the kinetic energy acquired during acceleration increases. The system cannot absorb this energy and the rotor continues to accelerate even after point 8 (see $\delta - t$ diagram, trajectory $c-e$), where its mechanical power is equal to its electrical power. Such further acceleration produces transient instability. In order to ensure stability the following criteria should be met:

$$Area_{(1-2-3-4)} \leq Area_{(4-5-8)}$$

The longest possible clearing time for which the generator still remains in synchronism is called the critical clearing time (CCT). CCT can be obtained using the following equation:

$$Area_{(1-2-3-4)} = Area_{(4-5-8)}$$

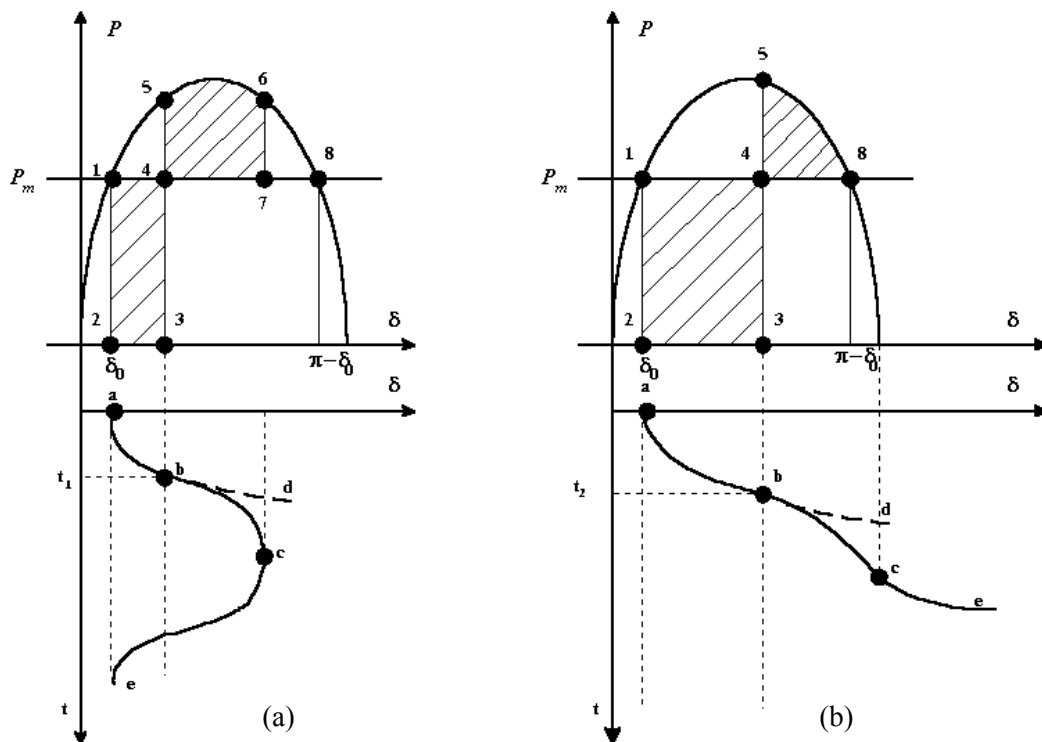


Figure 3.1.: Equal area criterion (a) short clearing time (b) long clearing time

A number of utilities over the past 20-25 years have experienced oscillations in flows between parts of their systems in spite of meeting transient stability criteria. These oscillations are

small in the beginning, often increasing over minutes. They can then trigger out of step and impedance relays. Typical periods of oscillation are in the range between 0.5 and 1.5 Hz. The British power system experienced such oscillations between the Scottish generation and the bulk of the system [Kni01]. It appears that these oscillations tend to occur between discrete generation/demand groups between which there are appreciable power transfers.

Various methods are used by utilities to determine transient stability limits. These methods are discussed in Chapter 4. A simplified transient stability method used in the simulation of large system disturbances is described in the same chapter.

3.1.2. Frequency Variations

System frequency is one of the most important single variables indicating the viability of operating of a power system [Kni01]. Acceptable deviations of frequency set by utilities are different, for instance $\pm 75mHz$ in UCPTE, and $\pm 100mHz$ for the Great Britain and Nordel [Kni01]. The North American standards require that frequency deviations should be corrected within 30 seconds.

Many utilities use automatic generator control (AGC) to maintain frequency at the specified value. AGC is an example of a multi-level control system, which includes primary, secondary and tertiary frequency control. Primary control is decentralised because it is installed in power plants situated at different geographical locations. The purpose of primary control is to halt the frequency drop or increase due to the active power imbalance, eliminate frequency variations and bring frequency to a constant value. Secondary control is a centralised function, which changes the electrical outputs of the generators involved in secondary control in order to bring frequency back to the value it had before the imbalance. Finally, tertiary control is driven by economic dispatch. It is centralised but does not require a response as fast as secondary control.

The response of a power system to a power imbalance can be divided into the following four stages [MBB97]:

1. rotor swings in the generators (first few seconds),
2. frequency drop (a few seconds to several seconds),
3. primary frequency control by the turbine governing system (several seconds),
4. secondary frequency control by the central regulators (several seconds to a minute).

Rotor swings were already described in section 3.1.1. A frequency drop and the primary frequency control are illustrated in Fig 3.2. The equivalent generator and load characteristics before the disturbance are denoted by P_{T-} and P_L , respectively. The equilibrium point 1 before the disturbance is the intersection between these two characteristics. After the loss of the generator that produced the active power P_0 , the equivalent generator characteristic becomes P_{T+} . The new equilibrium point is now the intersection between P_{T+} and P_L . However, this point cannot be reached immediately and the system first moves to point 2, keeping the same value of the frequency. This point is at the new equivalent generator characteristic P_{T+} , but total active power has decreased for ΔP_0 . A large imbalance between the generated power and the load forces the frequency to drop and activates the governors. As the frequency drops the generated power increases while the power taken by the load decreases. However, due to the time delay in the turbine power characteristic, $f(P_T)$ lies below the generator characteristic P_{T+} . This causes the power system to first moves to a quasi equilibrium point denoted as 3. The difference between the load and generation is zero at point 3. Because of the inherent inertia of the governing system, the mechanical power continues to increase after point 3 so that the generated power exceeds the load power and the frequency starts to rise. At point 4 the power balance is again satisfied and corresponds to the maximum value of frequency after the drop. Similar oscillations due to the inertia continue, however with much smaller magnitudes until the frequency finally reaches a steady-state value, that correspond to the intersection of P_{T+} and P_L .

Two very important points are the minimum frequency value (Fig. 3.2b point 3) and the maximum generator output (Fig 3.2c, point 4). The former can be used to determine activation of under frequency load shedding, while the latter indicates the maximum spinning reserve required to stop the frequency drop.

3.1.2.1. Frequency collapse

Fig. 3.2 showed that the power output of turbine is frequency dependent. This might cause a significant frequency drop when the frequency is much lower than the nominal frequency. Sometimes, it might lead a power system to a frequency collapse.

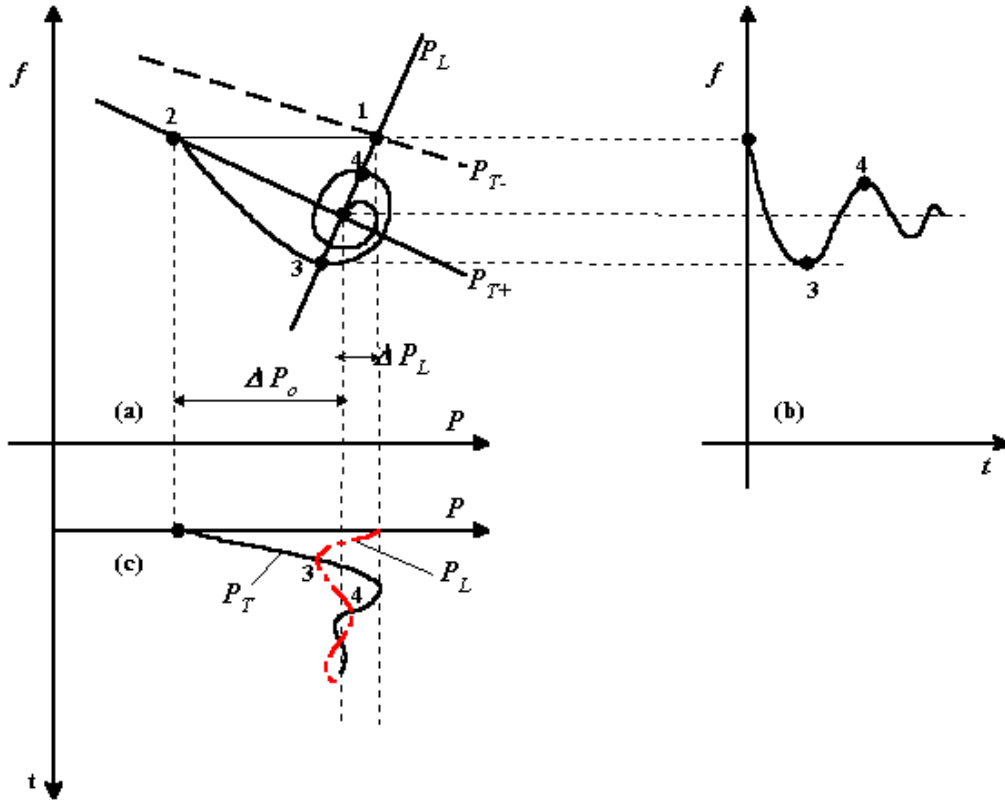


Figure 3.2.: Frequency variation during primary control [MBB97]

The generator characteristics shown in Fig. 3.2 are assumed to be straight lines. In reality the mechanical driving power delivered by turbines depends on the frequency deviation and the lines shown in Fig. 3.2 are not straight. The system generator characteristics are likely to have the shape shown in Fig. 3.3. However, for small frequency deviations the linear assumption is valid. On the other hand, for large frequency deviations this assumption is not valid because the deterioration in the performances of the boiler feed pumps caused by these variations can reduce the mechanical power.

The deterioration effect is shown in Fig3.3. Special attention should be devoted to the lower part of characteristic P_{T+} , which shows how an equivalent generator characteristic can be affected by the deterioration of the performances of the boiler feed pumps. Thus, the intersections of the load characteristic P_L with the generator characteristic P_{T+} are points s and u (see Fig. 3.3). The former is stable, while the latter is an unstable point. Point s is locally stable, as for any disturbance within the vicinity of this point the system returns to point s . The region in which this condition holds is referred to as the area of attraction. The lower point u is locally unstable, as any disturbance within the vicinity of this point will result in the system moving away from the equilibrium point.

As in Fig. 3.2, if a loss of generation occurs the operating point moves from 1 to 2. The significant difference between the generation and load produces an initial rapid drop in frequency. As the difference between load and generation reduces, the frequency drop slows down and the turbine power trajectory $f(P_T)$ approaches the equilibrium point s . However, the trajectory $f(P_T)$ might enter the area of repulsion of point u . In that case it will be forced away and the system will suffer a frequency collapse.

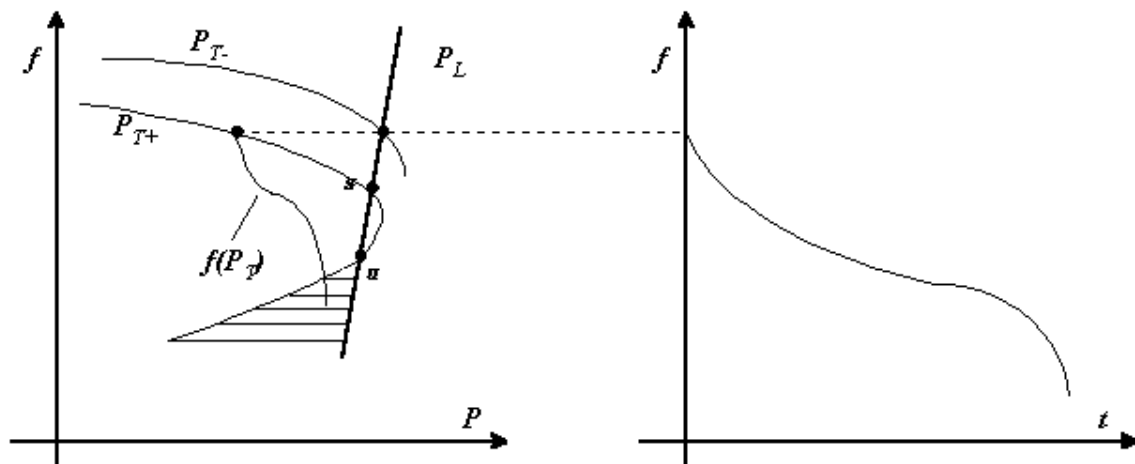


Figure 3.3.: Frequency collapse [MBB97]

3.1.2.2. Underfrequency load shedding

A power system can be protected from frequency collapse either by ensuring a large import of power from neighbouring systems or, when the system is weakly connected or islanded, by implementing automatic load shedding.

Automatic load shedding uses underfrequency relays. These relays detect the onset of decay in the system frequency and shed appropriate amounts of system load until the generation and load are in balance. The relays are usually installed in distribution and transmission substations.

Figure 3.4 shows the effect of load shedding when a power imbalance ΔP_0 appears on a system with a low spinning reserve. Without load shedding the system would suffer a frequency collapse shown by dashed line in Fig. 3.4. The first stage of load shedding is activated at point 3, which shifts the load characteristic P_L to P_{L1} . The frequency drop is smaller now, because the difference between generation and load is smaller. At point 4, another stage of load shedding is activated, further shifting the load characteristic to P_{L2} . At

point 4 the generation becomes larger than load and frequency begins to increase and the system moves towards point s_1 where the generator characteristic P_T and the new load characteristic P_{L2} intersect.

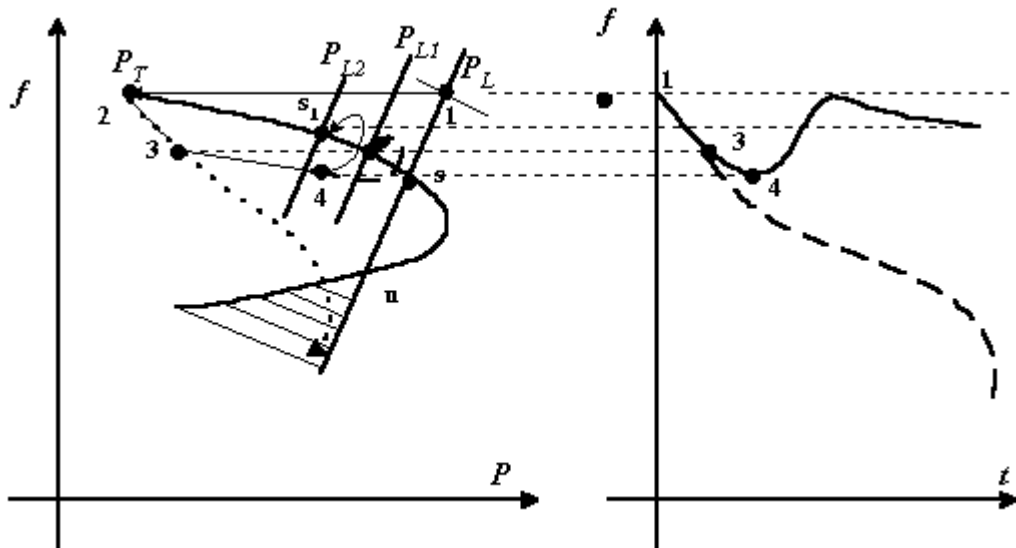


Figure 3.4.: Underfrequency load shedding [MBB97]

3.1.3. Voltage Collapse

Voltage collapse is the process by which voltage instability leads to a loss of voltage in a significant part of the system [Kni01]. There are several pre-indicators of voltage collapse. These are high power transfers, increasing reactive power generation and falling voltages sometimes over a wide area. Moreover, it has been observed that operator actions during such process are less confident than in case of a frequency drop or line overloads [Kni01].

It would be very difficult to simply describe a voltage collapse as was done for transient stability and frequency collapse. Voltage collapse is a very complex phenomenon whose occurrence normally involves the operation of various protection and control devices in a power system. The mechanisms of voltage collapse will be discussed in more details in Chapter 6. However, in this paragraph a simple power system shown in Fig. 3.5a will be used to describe this phenomena. The description is based on system characteristics, which are defined as the relationship between: transmitted power (P_R), receiving end voltage (V_R), and the current (I). These variables are given by the following equations [Kun94]:

$$I = \frac{1}{\sqrt{F}} \frac{E_S}{Z_{LN}}, \quad (3.1)$$

$$V_R = \frac{1}{\sqrt{F}} \frac{Z_{LD}}{Z_{LN}} E_S, \quad (3.2)$$

$$P_R = \frac{Z_{LD}}{F} \left(\frac{E_S}{Z_{LN}} \right)^2 \cos \varphi, \quad (3.3)$$

where

$$F = 1 + \left(\frac{Z_{LD}}{Z_{LN}} \right)^2 + 2 \left(\frac{Z_{LD}}{Z_{LN}} \right) \cos(\theta - \varphi). \quad (3.4)$$

Normalised diagrams of I , V_R and P_R are shown in Fig. 3.5b as a function of load (Z_{LN} / Z_{LD}) when θ, φ are constant values. As the load increases, P_R increases as long as $Z_{LN} / Z_{LD} \leq 1.0$. Therefore, the maximum active power that can be transferred through an impedance Z_{LN} when E_S is constant is obtained when $Z_{LN} / Z_{LD} = 1.0$. The values of V_R and I that correspond to this point are called critical values [Kun94]. Apart from the critical value, any other value P_R has two operating points (see Fig 3.5b where $\frac{P_R}{P_{RMAX}} = 0.8$). The point to

the left from the critical point is the normal operating point. The point to the right corresponds to abnormal operation with much larger current and much smaller voltage. Figure 3.5b shows that for a load larger than the maximum active power, an increase in demand decreases the active power. This is a typical unstable behaviour. Load is often connected to a low voltage busbar which is supplied via an on-load tap changing transformer. In that case the tap changer tries to raise the voltage at the low voltage busbar. This further reduces V_R and it might result in the complete loss of voltage V_R . This loss of voltage is a voltage collapse. This phenomenon will be further discussed in Chapter 6.

However, voltage collapse is a very complex phenomenon involving many factors and does not have an easily recognisable pattern. Machowski, Bialek and Bumby in [MBB97] make the following observations about the voltage collapse mechanisms:

- A very large build up of load followed by low voltages, generators hitting their limits and tap changers moving in order to control voltages in distribution network is a typical voltage collapse scenario described in many references [Cla90],[Tay94],[CV98].

- The network parameters play a vital role in determining the maximum power that can be delivered to the load areas. Tripping one of the lines in the power grid increases the equivalent reactance between the equivalent voltage source and the load, reduces the critical power and increases the probability of voltage collapse.
- A rapid, severe voltage dip can cause a reduction in the induction motor torque and consequent cause the motor to stall. This further increases the demand for reactive power and reduces voltages, which might cause additional motors to stall. Voltage collapse at a few buses might cause a voltage dip at neighbouring nodes leading to voltage collapse at these nodes. The voltage dip can propagate throughout the network and affect the synchronous generators, which can lose their synchronism.

The main results of the analysis made by EDF of 20 major disturbances that lead to a voltage collapse are [CTF87]:

- in many cases the loss of only one more element is sufficient to initiate the disturbance, while in the other cases, successive faults have led to loss of more than one element,
- in several cases the initial fault was a busbar fault,
- in all cases, there is at least one event, “which should never occur”, e.g. human fault or malfunction of equipment. These situations are difficult to forecast because such events have very low probabilities.

3.1.4. System Separation

System separation is a warning that a disaster might happen. However, the system can survive a separation if the generation and demand are well balanced in the islands. Sometimes, controlled separation is used as a preventive measure to minimise the impact of disturbances [Tay99].

System separation however almost always results in an imbalance between demand and generation. If this imbalance is large then an excessive reduction of generation or a disconnection of load can be experienced. As the results of such reduction or disconnection islands can be stabilised. On the other hand, an insufficient or too slow disconnection of load

might cause one or more islands to collapse. In such circumstances, underfrequency load shedding, which is a very fast automatic reduction of load, can play a key role.

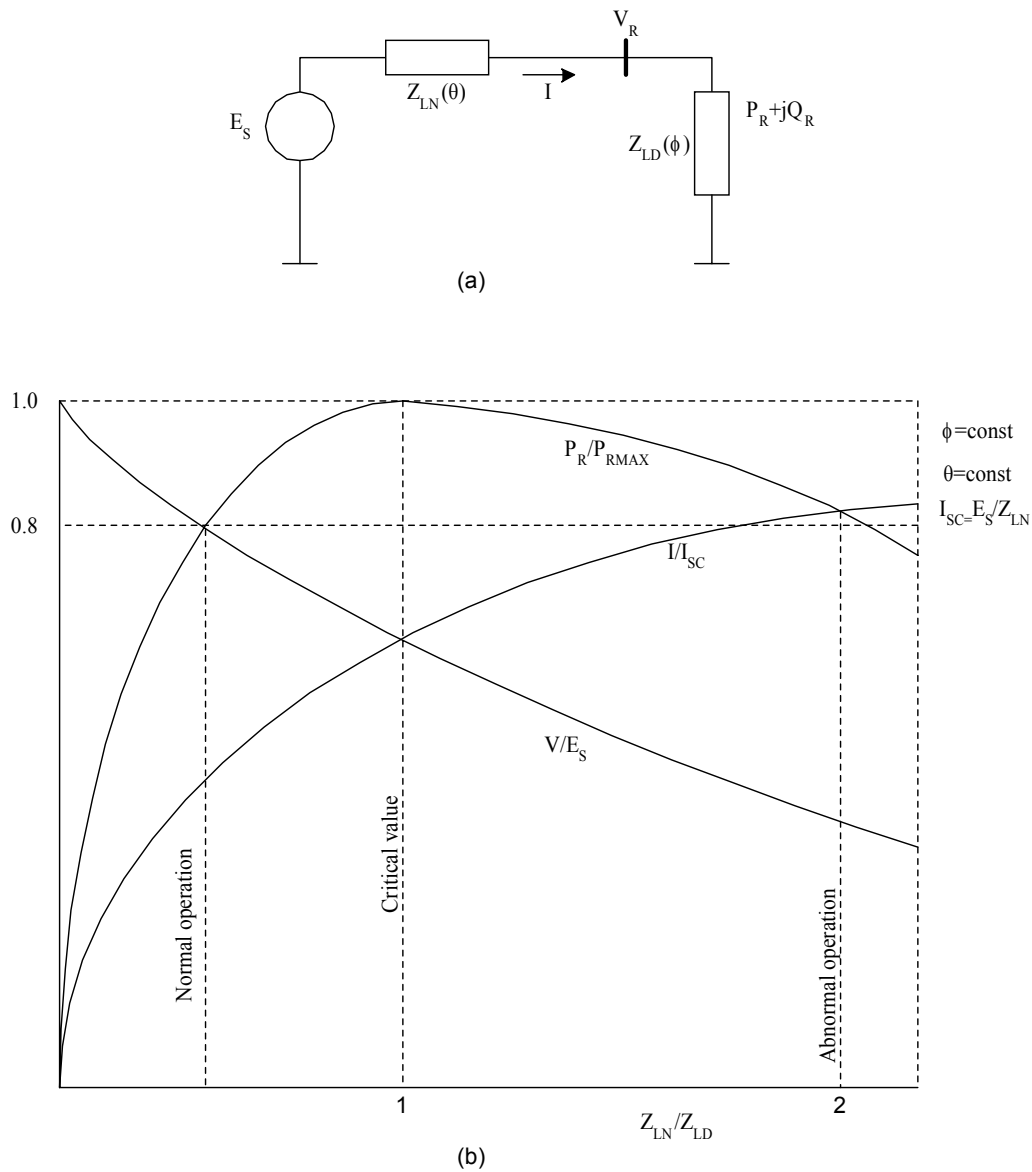


Figure 3.5.: Characteristics of a simple radial system

Several incidents described in section 2.2 ended in a system separation. The most severe separation occurred in the WSCC system during the US020796 and US100896 incidents, when several islands were formed. Apart from these the following incidents resulted in system separation: UK81, Fr77, Fr87, Fr99, Nordel79, Nordel83, Thai85, Au77, US120396, US160496, US250698. Due to such a high number of system separations the power flow used in the simulation of large system disturbances was given the ability of detecting islands and performing separate power calculations for each island.

3.2. Contributory Factors

Contributory factors have the potential of turning routine random outages on an apparently secure power system into major incidents resulting in widespread load disconnections. Failures in the protection system, line outages due to overloads and switching equipment malfunctions are considered as the most important contributory factors in this thesis. These are described in the following paragraphs.

3.2.1. Failures in the Protection System

The analysis of the power system disturbances in Chapter 2 shows that the largest ones often involve an initial non-catastrophic disturbance that is followed by incorrect protection system operations. Incorrect protection operations however, are mainly due to failures that remain hidden in the protection system until they are exposed by a random fault or disturbance. Various terms have been used for such failures, for instance malfunctions and misoperations. These software and hardware failures usually occur in protection schemes involving a relatively complex logic. Such complex logic has often a few alternatives to trip the related circuit breaker. Each alternative usually requires a combination of specific relay operations. If any of these relay operations fails, an unnecessary opening of the circuit breaker may occur. Therefore, failure modes depend on the logic associated with the specific protection scheme. Knowing the logic, it is possible to predefine the failure modes for all protection schemes in the system. Chapter 5 discusses these failure modes.

If the event that triggers a disturbance is a fault on a circuit, the circuits “surrounding” the faulted circuit are more vulnerable to protection failures than all the other circuits [KiN02]. Knowing protection failure modes, a vulnerability region can be predefined for each circuit. A fault on any circuit in the power system can expose protection system defects in its vulnerability region. In other words, it might happen that a multiple outage might arise from a random fault that triggers one or more protection failures in its vulnerability region. Such a situation is certainly unexpected and usually outside the scope of most conventional deterministic security criteria. Conventional on-line security analysis does not consider such combinations of events because they are considered as having too low a probability to be included in a predefined list of probable contingencies. However, the system disturbances analysed in Chapter 2 show that such combinations of events may not be quite as improbable as one might expect.

Tamronglak [Tam94] argues that protection failures were the contributing factors in almost 70% of disturbances in North America Power System between 1984 and 1991. He emphasised the difference between hidden protection failures and other incorrect protection operations. Incorrect protection operations cause immediate effects and they are revealed right away. Therefore, they are not likely to contribute to the development of a large disturbance. On the other hand, Tamronglak suggests that the most critical defects in protection system are those that are not revealed till they are not exposed by some other events.

The CIGRE task force on protection performances during major disturbances summarised the survey carried out in 2000/2001 [CTF01a]. In this survey, questionnaires on the behaviour of protection and control system were collected for over 60 disturbances in 17 countries covering the period from 1986 to 1997. Protection malfunctions together with primary plant failures were the primary causes of many of these disturbances. In terms of escalating the disturbance, incorrect protection operations, inadequate relay settings, failure of load shedding relays and cascade tripping played a key role.

The analysis of system disturbances in Chapter 2 indicates that more than 10 unexpected incorrect protection system operations were recorded in 20 incidents. These incidents are: Nordel79, Nordel83, Thai87, Au77, US160496, US100896, US020796, and US100699. The most severe incidents, such as those that happened in the WSCC system (US100896, US020796), involved more than one hidden failure in the sequence of events.

3.2.2. Line Outages

The analysis of the incidents in Chapter 2 clearly shows that line outages are dominant events in all these incidents. Line outages can be caused by several reasons:

- random faults,
- external factors caused by the weather or the environment,
- low voltages and high currents,
- line overloads.
- power oscillations

External factors related to weather were dominant in all French incidents (Fr77, Fr89, Fr99) and the incident that happened in the UK in 1987 (UK87). However, external factors caused by the weather and the environment significantly contributed to several other incidents (UK81 and almost all the US incidents).

Low voltages and high currents can trigger impedance relays. A significant number of such operations can be observed in almost all the incidents described in Chapter 2. Special attention has to be paid to impedance relays and out of step protection schemes. Out of step relays detect the unstable condition known as out of step condition. Impedance and out of step protection schemes were dominant in the US100896 incident, when power oscillations hit the WSCC system.

Different utilities use different measures to handle overloads on transmission lines. Some of them use over current relays equipped with timers that allow currents to exceed the thermal limits for some time. Other utilities use over current protection for transformers and cables, but do not apply over current protection to overhead lines. In such circumstances only the fault protection can switch off an overloaded line, due to for instance to a flashover to a tree caused by a sag in the conductor. Line outages due to line overloads were very frequently involved in the disturbances analysed in Chapter 2. Outages due to overloads were common events in almost all US incidents. Conductor sag caused flashover to trees on three important transmission lines in the UK incident of August, 1981 (UK81).

3.2.3. Switching Equipment Malfunction

A substation structure consists of switches, busbar sections, breakers and other equipment (see Fig 3.6 (a)). Their status (on/off) can be obtained from the SCADA (Supervisory Control and Data Acquisition). Knowing the status of all the elements in a substation a connectivity diagram can be drawn. This diagram is shown in Fig 3.6b. This diagram can be further simplified eliminating all dummy nodes (hatched nodes). In this process a switch level representation shown in Fig 3.6b converges to a branch and node representation shown in Fig. 3.6c.

Branch and node models have been widely used for steady state calculations such as power flow, contingency analysis and fault analysis. This representation normally has significantly smaller number of buses than switch level representation. However, switch level representation is important for the following reasons:

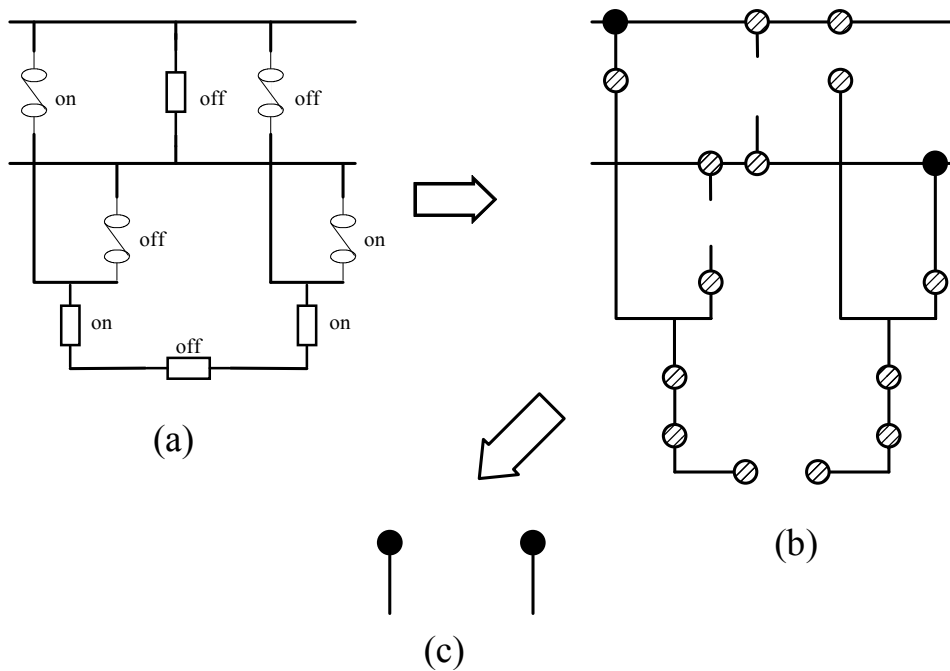


Figure 3.6.: Representations of power system: (a) substation structure (b) switch level representation (c) branch node representation

- the real extent of a fault's impact and the impact of faults on switches can be considered,
- the effect of the optimal substation configuration (running arrangements) can be taken into account.

In a branch and node representation when a fault on a line occurs, the faulted line will be switched off. In an equipment level representation, neighbouring breakers will open to isolate the fault. If these neighbouring breakers are the ones at the sending and receiving node of the faulted line there is no difference between these two representations in terms of tripped lines.

However, it might happen that one of these breakers fails to open, which brings the fault into the substation, to a common bus section. In a branch and node representation such event development would trip all the lines connected to the common bus section. On the other hand, in a switch level representation some of these lines might be saved if there is a possibility to split the section. This is illustrated in Fig. 3.7. Using the branch and node representation, breakers CB1, CB2, CB3 and CB4 will be opened, for the busbar fault F_1 . However, using the switch level representation, only CB1, CB2, and CB5 will be opened. The number of outaged lines for these two different representation makes branch and node representation too pessimistic leading to unnecessary opening of two lines connected via CB3 and CB4. On the

other hand, if a fault occurs on one of the tee point legs, more openings will be represented in the case of the switch level representation. Using the switch level representation all three legs will be opened. However, using the branch and node representation only the faulted leg will be opened.

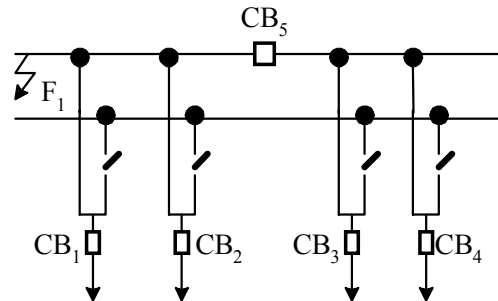


Figure 3.7.: Busbar fault

An operational planning department should always recommend the best running arrangements because the running arrangement at a substation plays a vital role in terms of system security. The purpose of this arrangement is to:

- keep fault level low,
- keep the system as well interconnected as possible, and
- minimise the impact of switch faults and bus section faults.

In order to achieve these requirements certain rules should be introduced. These rules include for example:

- each circuit of a double circuit line should be connected to a different bus section,
- generating units should be divided between the two sides of a double bus substation,
- the sum of flows into each side of a double bus substation should match the sum of the flows out of this side.

These rules are introduced to improve security but under abnormal circumstances they can make the situation even worse. One of these events happened during the US120396 incident (see Chapter 2), when power system operators tried to split a bus to decrease power flows. This had the opposite effect and split the whole system.

A switch level representation has not been considered in the simulation of large system disturbances carried out in this thesis. The amount of information required to develop such representation is very large. On the other hand, for most utilities such information is of a highly confidential nature.

However, protection and control system operations depend on the reliability of switching equipment. The disturbance reports and incidents that are analysed in Chapter 2 show that a switch level representation would help analyse and simulate the mechanisms involving switching equipment. On the other hand, such representation would require significant changes in the simulation logic and a considerable larger amount of information. Therefore, a branch and node representation was adopted as a less risky and demanding. A few important issues discussed in this subsection are seen as useful thoughts for the future work on this topic.

4

Modelling of Failure Modes in the Simulation of Large System Disturbances

The simulation of large system disturbances intends to consider as many as possible of the failure modes discussed in Chapter 3. However, no single model can be used to detect all these failure modes. Instead, a group of simplified models is used for each failure form separately. These simplified models are generally derived from complete models using various assumptions.

In this Chapter the focus is on the models of transient stability, frequency response and line overload. Using these models the simulation of large system disturbances is able to detect the following forms of system failures:

- transient instability,
- frequency collapse, the activation of under-frequency load shedding protection and
- line outages caused dominantly by line overloads.

The first section of this chapter deals with transient stability models, the second section describes frequency response models, while the last section deals with a line overload model.

4.1. Transient Stability

Power system stability may be defined as a property that enables a power system to remain in a stable equilibrium state under normal operating conditions and to regain an acceptable equilibrium state after being subjected to a disturbance [Kun94]. The transient stability phenomenon has been studied since the beginning of modern power systems. A classical definition, proposed by Kimbarck at that time is as follows [Pav98]:

“Power system stability is a term applied to alternating current electric power systems, denoting a condition in which the various synchronous machines of the system remain in “synchronism”, or “in step” with each other. Conversely, instability denotes a condition involving “loss of synchronism”, or falling “out of step”.

Various definitions of transient stability can be found in [Pai79],[BeV86], [PaM94],[SaP98], [MBB97], [Pav98]. All of these assume that that under normal operating conditions all the system machines run at synchronous speed until a large disturbance occurs. After the disturbance the machines start “swinging” with respect to each other. Their motion is governed by non-linear differential equations.

There are two measures of transient stability commonly used: critical clearing time (CCT) and the power limits. The former is defined as the maximum time duration for which the disturbance may act without the system losing its capability to recover a steady state (i.e., stable) operation [PaM94]. The latter is defined as the largest power (generation or transfer) sustainable without loss of synchronism, given the occurrence of a large system disturbance and its clearing scenario (pre-fault, during fault and post-fault) [Pav98].

A variety of methods have been proposed to measure transient stability. These can be compared using different evaluating criteria, which are discussed in section 4.1.1. The transient stability model that best suits the requirements of the simulation of large system disturbances is suggested in 4.1.2. Two different solution techniques for this model are suggested in 4.1.3 and 4.1.4.

4.1.1. Methods for Transient Stability Assessment

Pavella in [Pav98] compares different transient stability methods in terms of four evaluating criteria:

1. type of information required,
2. off-line preparation tasks,
3. computational requirements and
4. type of information provided.

Based on these criteria three classes of methods were compared in [Pav98]:

1. time domain or step by step methods,
2. direct methods and
3. automatic learning methods.

Time domain methods deal simultaneously with the differential equations of all machines, turbines, control devices and the algebraic network equations. The number of state variables for such system can be lower bounded by twice the number of all machines in a system or upper bounded by an order of magnitude larger. The simulation period is split into: pre-fault, during fault and post-fault with different network configurations. The system of differential algebraic equations is solved numerically, step by step for each period. At the end of the simulation period a swing curve that represents the evolution of the rotor angle of each machine is known. These curves are further compared with each other in order to determine whether the rotor angular difference of any two machines exceeds some predefined value (Pavella in [Pav98] and Kundur in [Kun94] suggest 180°). If any angular difference is larger than some predefined value then transient instability is encountered. However, Pai in [Pai79], Bergen and Vittal in [BeV86], Pavella and Murphy in [PaM94] and Kundur in [Kun94] determine stability by detecting a particular shape of this swing curve rather than using one of these predefined values. A similar unstable curve shape, which is found in all these references, demonstrates unstable behaviour from an educational point of view. However, a general approach able to identify transient instability based on the swing curves is not clearly demonstrated in these references.

Direct (Lyapunov) and automatic learning methods belong to the so-called non-conventional methods. The advantages of the Lyapunov methods are: a very small computation time in comparisons with time domain simulations and the possibility to obtain a sound measure of the stability margin [Pav98]. The main advantages of the automatic learning methods are: an

interpretability of the phenomena, an extraordinary on-line computational efficiency and the management of uncertainties.

Direct methods are based on Lyapunov criterion that states that a system is transiently stable if the values of a Lyapunov function are smaller than a predefined transient stability limit. This function is calculated using a value of the system state vector at the instant when the disturbance is cleared. The state vector values are computed using time domain simulations up to this instant. A sound measure of the stability margin is provided as the difference between the value of Lyapunov function and the predefined stability limit. Lyapunov methods suffer from two main difficulties. The first one is related to the impossibility of designing a good Lyapunov function for a multi-machine system. The other one is the determination of good limit values [Pav98]. Many interesting methods have been introduced to circumvent these difficulties. Thus, pseudo-Lyapunov approaches, which combine time domain models together with pseudo-Lyapunov function, have been used to bridge the first difficulty. Nevertheless, various approaches that have been suggested to overcome the second difficulty have generally failed [Pav98].

Automatic learning techniques used to assess transient stability are mostly based on supervised learning. Decision trees (DTs), artificial neural networks (ANNs) and k nearest neighbours (kNNs) are the well-known families of approaches that have been used for those purposes. DTs and ANNs compress the information into synthetic rules, while kNNs learns in a case by case fashion.

DTs and ANNs need a database that contains representatives of all foreseen situations in a power system. Pavela in [Pav98] confirms that the quality of information contained in such database seriously depends on the human knowledge. Once such database is made, DTs and ANNs can start with a building/learning process, extracting information from different representatives. In the case of DTs, the building process starts at the tree's top node scanning all candidate attributes and all the values that it assumes in the learning process [Pav98]. The purpose is to identify an attribute and its threshold value in order to make a decomposition of stable/unstable cases into two learning subsets that are as distinct as possible. These two subsets will be the successors of the top node. This procedure is repeatedly applied to each node until further splitting is statistically meaningless [Pav98].

On the other hand, ANN-based methods treat learning as on a non-linear optimisation problem without constraints. They are able to provide a continuous margin. The objective process minimises the square of the differences between the real outputs (database) and

outputs obtained through ANNs by adjusting weighting factors of hidden neurons. The relationship between hidden neurones in neighbouring layers is non-linear and depends on these weighting factors. As soon as weighting factors have been adjusted the learning process is completed.

The ability to provide detailed information about a state by comparison with other, pre-analysed situations is an important asset of kNN [Pav98]. A kNN classifies an unseen state in the majority class of its k nearest neighbours in the learning set. This method has been widely used to discover outliers [Pav98].

A good database is certainly the crucial point for automatic learning methods. It is also their potential weakness. The main advantage of these methods is that they are computationally fast, they facilitate the interpretation of the phenomena and can manage uncertainties.

The selection of an appropriate transient stability model to be used in the simulation of large system disturbances was a difficult choice. The decision was based on the evaluating criteria and requirements of the simulation of large system disturbances. The simulation of large system disturbances requires a robust, fast and accurate method. The next very important requirement is related to the analysed bulk power system. It was known that such system might rather experience local transient instability when only a few generators are transiently unstable rather than global transient instability. So, apart from robustness and computational efficiency the simulation should provide a tool able to recognise local transient instability.

Regarding these requirements automatic learning methods would take certainly the biggest risk, taking into account that each simulated sequence in the simulation of large system disturbances is a new case, and most likely significantly different from any other already generated. This further means that the creation of a good database for a bulk power system in this case, without any knowledge about the bulk power system itself, would be an extremely difficult task. These methods require very detailed information, tremendous efforts to generate and validate the database. On the other hand, the amount of computational resources required to analyse new cases is almost negligible compared with other methods. The information that they provide is detailed and synthetic. However, the identification of local transient instability is not possible by using these methods.

The choices of a Lyapunov function and of predefined stability limits are the main difficulties with direct methods. These methods do not require fully detailed information about the power system, a minor off-line validation is necessary, computational requirements are lower than

for time domain simulations. Finally, they provide detailed information about the nature of the problem.

Time domain methods require a very detailed model of the power system but do not require off line preparation or validation. They provide fully detailed information about both global and local instability. On the other hand, they are time-consuming.

If these various methods are evaluated in terms of the requirements for the simulation of large-scale disturbances, the following conclusions are reached. Automatic learning techniques are the least favourable option. Direct methods are computationally much more efficient than time domain methods, but the choice of a Lyapunov function involves a significant risk. Time domain methods would be the best option if the computation time could be reduced.

In order to avoid the risks associated with automatic learning techniques and direct methods, a compromise was found in the use of simplified time domain simulations. These simplified simulations use different assumptions to reduce the number of differential equations associated with each machine. The simplest method, which uses only two first order differential equations for each machine, was chosen for the simulation of large system disturbances. This method uses the motion equation for each machine and algebraic network equations. It can thus be described as a classical method.

4.1.2. Complete Time Domain Model and Modelling Assumptions Used for the Classical Model

Analysis of transient stability of power systems involves the computation of their non-linear dynamic response to large disturbances, usually a transmission network fault, followed by the isolation of the faulted element by protective relaying [Kun94]

Figure 4.1 depicts the general structure of the power system model applicable to transient stability analysis [Kun94]. Each machine model is expressed in its own $d-q$ reference frame, which rotates with its rotor, while the network variables are in the common real-imaginary ($R-I$) frame [Kun94]. This model contains non-linear algebraic equations (stator, axes transformation and network) and differential equations (rotor, excitation system, prime mover, governor). Usually a reference frame rotating at synchronous speed is used as the

common reference. Axis transformation equations are used to transform between the individual machine ($d-q$) reference frames and the common ($R-I$) reference.

A complete model includes all these differential and non-linear algebraic equations. The model has been extensively used and can be found in many references [Pai79], [BeV86], [Kun94], [MBB97], [SaP98]. Therefore, this complex model will not be discussed in this thesis. However, various simplified models can be derived directly from this complete model using different assumptions. The simulation of large system disturbances considers a much simpler representation of the power system, which is commonly referred as the classical model. The classical model is used to study the transient stability of a power system for a period of time during which the dynamic behavior of the system is dependent largely on the kinetic energy stored in the rotating masses. This is the simplest time domain model used in stability studies.

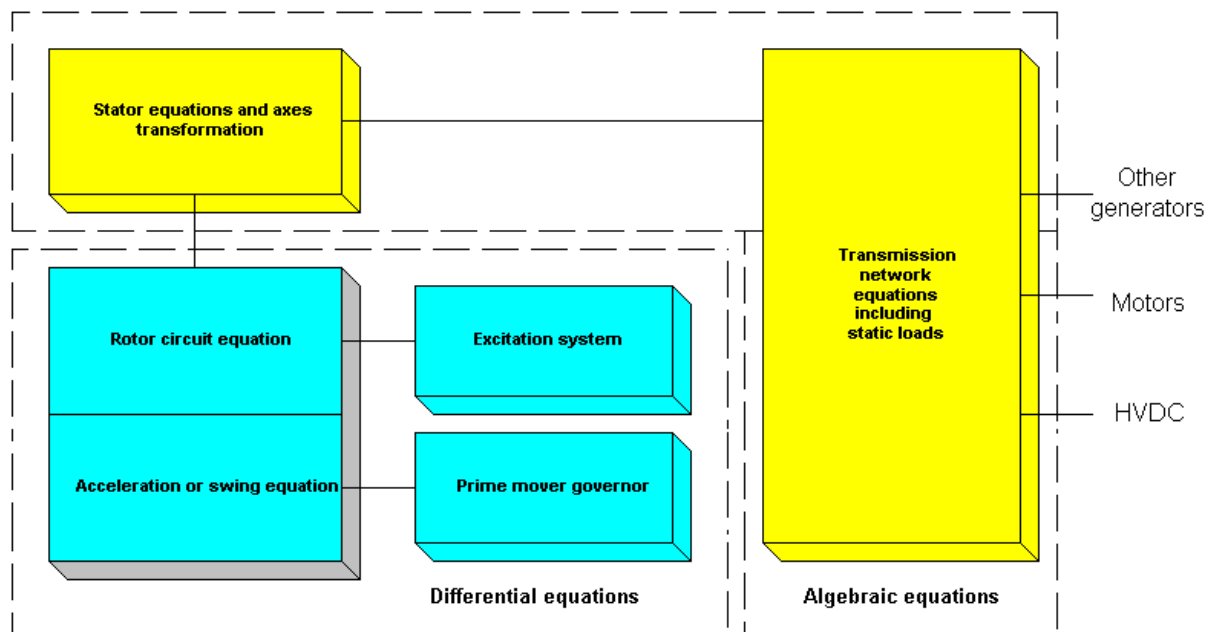


Figure 4.1.: Structure of the complete power system model for transient stability analysis[Kun94]

These are the most important assumptions made in the development of the classical model:

1. The mechanical power input of each synchronous machine is constant.
2. Damping or asynchronous power is negligible.
3. The synchronous machines are represented electrically by a constant voltage behind the transient reactance.

4. The motion of each synchronous machine rotor (relative to a synchronously rotating reference frame) is at a fixed angle relative to the angle of the voltage behind the transient reactance.
5. Loads are represented by constant impedances.

The model is useful for stability analysis but is limited to the study of transient no longer than about two seconds. This type of analysis is usually called first swing analysis. Assumption 2 can be relaxed by assuming a linear damping characteristic where a damping torque is included in the swing equation. In assumption 3, the constant voltage behind the direct axis transient reactance is determined from the initial conditions (i.e. the pre-disturbance power flow conditions). During the transient the magnitude of this voltage is held constant, while the variation in angle is governed by the following second order swing equation:

$$\frac{H_i}{\pi f_0} \frac{d^2 \delta_i}{dt^2} + D_i \frac{d\delta_i}{dt} = P_{Mi} - P_{Gi} \quad i = 1, 2, \dots, m, \quad (4.1)$$

where P_{Mi} is constant and determined from the pre-fault conditions, H_i is the inertia constant, P_{Gi} is the electrical output of the generator and m is the number of synchronous machines. Each of these second order differential equations can be written as a set of two first order differential equations as follows:

$$\begin{aligned} M_i \frac{d\omega_i}{dt} + D_i \omega_i &= P_{Mi} - P_{Gi}, \quad i = 1, 2, \dots, m \\ \frac{d\delta_i}{dt} &= \omega_i, \quad i = 1, 2, \dots, m \end{aligned} \quad (4.2)$$

Assumption 5, dealing with the representation of loads as constant impedance is usually made for simplicity. It is important to have in mind that loads have their own dynamic behavior, which can have a marked effect on stability [SaP98].

4.1.3. Direct Solution

Considering the assumptions in 4.1.2, a multi-machine representation of the swing equations will be derived. The assumptions lead to the representation of the power system shown in Fig. 4.2. Nodes 1', 2', ..., m' are called the internal machine nodes. These are the nodes or buses to which the voltages behind the transient reactances are applied. The transmission network,

together with transformers modeled as impedances, connects the various nodes. The loads, modeled as impedances, also connect the load buses to the reference node.

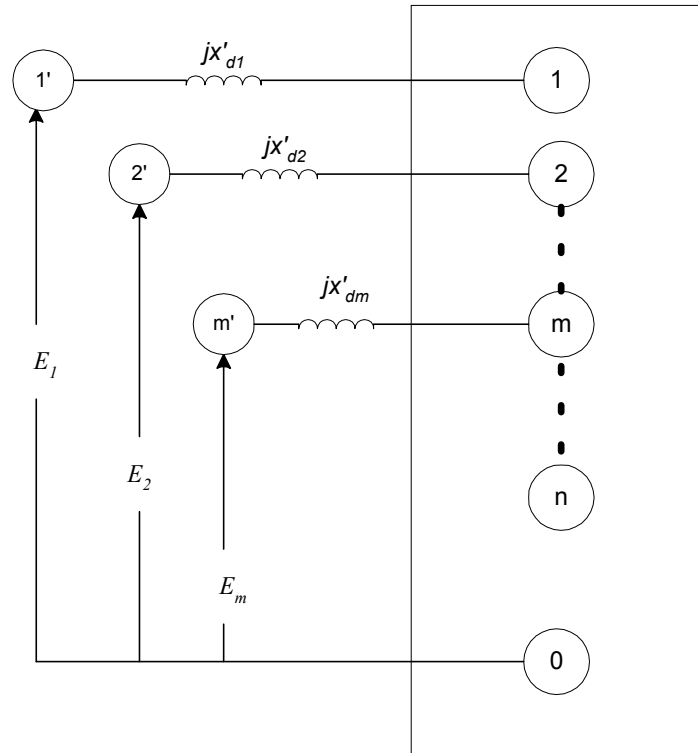


Figure 4.2.: Terminal representation at internal nodes of generators

A direct solution of the classical methods involves the following steps:

Step 1: The system data are converted to a common system base; a system base of 100 MVA is often chosen.

Step 2: The load data from the pre-disturbance power flow are converted to equivalent impedances or admittances. Thus, if a load bus has a voltage V_{Li} , a current I_{Li} and complex power demand $S_{Li} = P_{Li} + jQ_{Li}$ then:

$$y_{Li} = \frac{I_{Li}}{V_{Li}} = \frac{S_{Li}^*}{|V_{Li}|^2} = \frac{P_{Li} - jQ_{Li}}{|V_{Li}|^2}, \quad (4.3)$$

where $y_{Li} = g_{Li} + jb_{Li}$ is the equivalent shunt load admittance.

Step 3: The internal voltages of the generators $|E_i| \angle \delta_i^0$ are calculated from the power flow data using the pre-disturbance terminal voltage $|V_i| \angle \beta_i$. Thus, if the terminal voltage is chosen as a reference, it means that $\beta_i = 0$ and:

$$|E_i| \angle \delta_i = |V_i| + jx_{di} I_i = |V_i| + jx_{di} \frac{(P_{Gi} - jQ_{Gi})}{|V_i|}, \quad (4.4)$$

where δ_i is the angle difference between the internal and terminal voltages while x_{di} represents the direct axis transient reactance, for the i^{th} machine. However, if the actual terminal voltage angle is β_i , one can obtain the initial generator angle δ_i^0 by adding the pre-disturbance voltage angle β_i to δ_i or

$$\delta_i^0 = \delta_i + \beta_i$$

Step 4: The network admittance matrices \mathbf{Y}_{BUS} for pre-fault, faulted and post-fault network conditions are calculated. To obtain these matrices, the following sub-steps are required:

- a. The equivalent load admittances calculated in step 2 are connected between the load buses and the reference node. Additional nodes are provided for the internal generator nodes (node 1', 2', ..., m', see Fig. 4.2) and the appropriate values of admittance corresponding to x_d' are connected between these nodes and the generator terminal nodes.
- b. The network admittance matrix \mathbf{Y}_{BUS} corresponding to the faulted system is calculated assuming that only three-phase to ground faults are considered. Thus, the faulted network admittance matrix \mathbf{Y}_{BUS} is then obtained by adding a large shunt admittance at the faulted node.
- c. The post-fault network admittance matrix \mathbf{Y}_{BUS} is obtained by removing the line that would have been switched by the protective relay at the instant t_c , which is called the fault clearing time.

Step 5: In the final step, apart from the generators internal nodes all the other nodes are eliminated using Kron reduction. The reduced network admittance matrix is denoted by $\hat{\mathbf{Y}}$. This matrix can be derived directly from the following relationship between the node voltages and injected node currents \mathbf{I} :

$$\mathbf{I} = \mathbf{Y}_{BUS} \mathbf{V}, \quad (4.5)$$

In this classical model, injected currents exist only at the m -internal generator buses while all the other currents are zero. This gives equation (4.5) the following form:

$$\begin{bmatrix} \mathbf{I}_m \\ \dots \\ \mathbf{0} \end{bmatrix} = \begin{bmatrix} \mathbf{Y}_{mm} & \vdots & \mathbf{Y}_{ms} \\ \dots & \dots & \dots \\ \mathbf{Y}_{sm} & \vdots & \mathbf{Y}_{ss} \end{bmatrix} \begin{bmatrix} \mathbf{E}_m \\ \dots \\ \mathbf{V}_s \end{bmatrix}. \quad (4.6)$$

Using equation (4.6), the reduced matrix $\hat{\mathbf{Y}}$ can be calculated as:

$$\mathbf{I}_m = (\mathbf{Y}_{mm} - \mathbf{Y}_{ms} \mathbf{Y}_{ss}^{-1} \mathbf{Y}_{sm}) \mathbf{E}_m = \hat{\mathbf{Y}} \mathbf{E}_m. \quad (4.7)$$

From (4.7) one can observe that the reduced admittance matrix provides the relationship between all the injected currents \mathbf{I}_m and the internal generator bus voltages \mathbf{E}_m . Using (4.7) an expression for the electrical power output of each generator can then be derived.

The power injected into the network at node i , which is the electrical power output of machine i , is given by $P_{Gi} = \text{Re}\{E_i I_i^*\}$. The expression for the injected current at each generator bus I_i in terms of the reduced admittance matrix parameters is given by (4.7).

Finally, the electrical power output of machine i is given by:

$$P_{Gi} = |E_i|^2 \hat{G}_{ii} + \sum_{\substack{j=1 \\ j \neq i}}^n |E_i| |E_j| \left[\hat{B}_{ij} \sin(\delta_i - \delta_j) + \hat{G}_{ij} \cos(\delta_i - \delta_j) \right] \quad i = 1, 2, \dots, m \quad (4.8)$$

Substituting the preceding expression for P_{Gi} into the differential equation (4.2) governing the dynamics of the synchronous machine, and neglecting the damping coefficient, the motion equation (4.2) becomes:

$$M_i \ddot{\delta}_i = P_{Mi}^0 - |E_i|^2 \hat{G}_{ii} + \sum_{\substack{j=1 \\ j \neq i}}^n |E_i| |E_j| \left[\hat{B}_{ij} \sin(\delta_i - \delta_j) + \hat{G}_{ij} \cos(\delta_i - \delta_j) \right] \quad i = 1, 2, \dots, m \quad (4.9)$$

In equation (4.9), the value of the mechanical power of each machine is determined from the pre-fault conditions. The mechanical power is set equal to the electrical power output of each generator at the pre-fault conditions. This provides the equilibrium conditions and the initial angles for each generator as given by δ_i^0 calculated in *Step 3*.

In order to perform numerical integration, we can convert each of these second order

differential equations into two first order differential equations as given by equation (4.2). A fourth order Runge-Kutta method is used to numerically solve the set of differential equations.

4.1.4. Alternate Cycle Solution

A very similar solution technique called the alternate cycle solution first solves a system of linear complex equations calculating all the voltages in the network. Afterwards the system of differential equations can be solved. Therefore, the main characteristic of this solution technique is an alternate solution of a system of linear complex equations and a system of differential equations. This technique is very similar to the previous one except that it requires the solution of a system of complex equations. Moreover, the first two steps are identical, while further steps are as follows:

Step 3: The network voltages V_1, \dots, V_n can be obtained solving the following system of complex equations:

$$\begin{array}{rcl}
 (Y_{11} + y_1)V_1 + Y_{12}V_2 & + \dots + Y_{1m}V_m & + \dots + Y_{1n}V_n = y_1E_1 \\
 Y_{12}V_1 & + (Y_{22} + y_2)V_2 + \dots + Y_{2m}V_m & + \dots + Y_{2n}V_n = y_2E_2 \\
 \vdots & & \vdots \\
 Y_{m1}V_1 & + Y_{m2}V_2 & + \dots + (Y_{mm} + y_m)V_m & + \dots + Y_{mn}V_n = y_mE_m, \\
 Y_{m+1,m+1}V_1 & + \dots & + \dots & + \dots + Y_{m+1,n}V_n = 0 \\
 \vdots & & \vdots & \\
 Y_{n1}V_1 & + \dots & & + \dots + Y_{nn}V_n = 0
 \end{array} \tag{4.11}$$

where $y_i = -\frac{j}{x_{di}}$. If three phase to ground fault occurs at p^{th} bus then $V_p = 0$ which is valid during the fault. Besides, a change of network admittance matrix in the post-fault period takes place at instant t_c .

Step 4: The generator currents and electrical outputs can be calculated using the following equations:

$$I_i = (E_i - V_i) * (-j / x_{di}) \tag{4.12}$$

$$P_{ei} = \text{Re}\{E_i I_i^*\}. \tag{4.13}$$

Step 5: Knowing the value of P_{ei} , the system of differential equations (4.2) can be solved and new values of $\delta_i, \dot{\delta}_i$ can be calculated for the next time instant.

Step 6: The voltages E_i behind the transient reactance are updated by keeping their magnitudes constant and changing their phase angle based on the new values of δ_i obtained in the previous step. If the simulation period is not complete, then simulation procedure must be repeated from step 3.

4.2. Frequency control

The complex problem of primary frequency control in power systems has gradually lost the importance that it had in the past, mainly because the interconnection of power systems into synchronous parallel operation has greatly increased the total inertia. In terms of methodology, there are several possible approaches to the analysis of primary frequency control. The rigorous approach combines the complete models of the generating units, turbines, speed governors and network. In engineering practice, however, much greater importance has been given to simpler but still realistic and sufficiently accurate low order models.

In contrast to the transient stability whose complete model is briefly discussed in section 4.1.2, the complete model used for frequency evaluation is rather difficult to find in literature. Therefore, a complete model is discussed in section 4.2.1, while simplified models are described in sections 4.2.2. and 4.2.3.

4.2.1. A Complete Model for System Frequency Evaluation

A complete system frequency evaluation model contains the following components:

1. the network model,
2. the dynamics models of turbo-generators and hydro-generators,
3. the models of control device such as:
 - 3a. voltage regulator model,
 - 3b. hydraulic turbine and governor system model and
 - 3c. steam turbine and governor system model.

These models are discussed in the following paragraphs.

4.2.1.1. Network model

The algebraic network equations have the following form:

$$P_i = \sum_{k=1}^n V_i V_k (G_{ik} \cos \theta_{ik} + B_{ik} \sin \theta_{ik}), \quad i = 1, \dots, n, \quad (4.14a)$$

$$Q_i = \sum_{k=1}^n V_i V_k (G_{ik} \sin \theta_{ik} - B_{ik} \cos \theta_{ik}), \quad i \in \alpha_{PQ}, \quad (4.14b)$$

where P_i, Q_i are the injected active and reactive powers at the i^{th} node, V_i, V_k are the magnitudes of the i^{th} node voltage ($\hat{V}_i = V_i e^{j\theta_i}$) and the k^{th} node voltage ($\hat{V}_k = V_k e^{j\theta_k}$), $\theta_{ik} = \theta_i - \theta_k$, $\hat{Y}_{ik} = G_{ik} + jB_{ik}$ is the bus network admittance element $i-k$, and α_{PQ} is a set of PQ nodes [Kun94].

Equations (4.14a),(4.14b) are algebraic equations where the angles $\theta_i, i = 1, \dots, n$ and voltages $V_i, i \in \alpha_{PQ}$ are unknown. The vector of unknown variables for the algebraic equations (4.14a) and (4.14b) is:

$$\mathbf{y}_{net} = [\boldsymbol{\theta} \quad \mathbf{V}]^T \quad (4.15)$$

4.2.1.2. Dynamic models of turbo/hydro generators

Two-axis models of hydro-generator and turbo-generator are often used for the evaluation of the system frequency. In the two-axis model the transient effects are accounted for, while the subtransient effects are ignored. The transient effects are dominated by the rotor circuits, which are the field circuit in the d axis and an equivalent circuit in the q axis [AnF77].

The assumptions made in the development of the two-axis model are:

- in the stator voltage equations the so-called transformer voltages are negligible compared to the speed voltages [Kun94].
- the stator resistance is negligible compared to the stator reactance.

The block diagram of the two-axis model of the turbo-generator is shown in Fig.4.3. In the case of hydro-generators this model is further simplified taking into account that $x_q = x'_q$.

The block diagram of the two-axis model of the hydro-generator is shown in Fig 4.4.

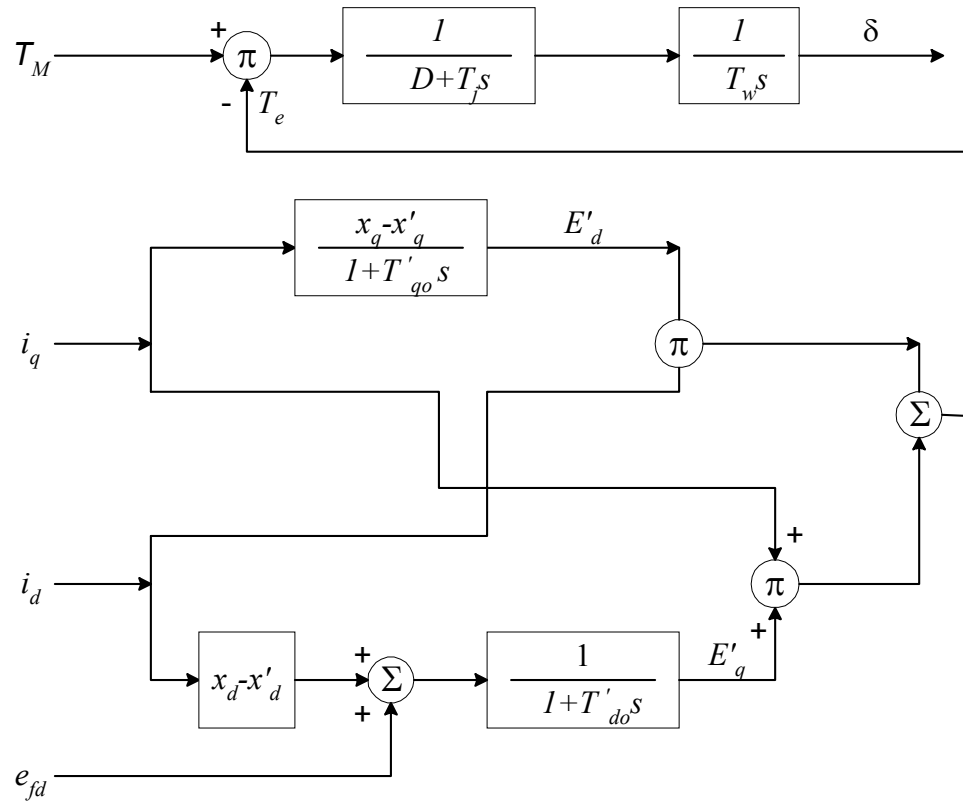


Figure 4.3.: Two axis turbo-generator model

The variables, parameters and constant used in these figures are [AnF77]:

- x_q - quadrature axis synchronous reactance,
- x'_q - direct axis quadrature reactance,
- x_d - direct axis synchronous reactance,
- x'_d - direct axis transient reactance,
- T'_{do} - d axis transient open circuit time constant,
- T'_{qo} - q axis transient open circuit time constant,
- i_q, i_d - q/d axis currents, respectively,
- E'_q - emf proportional to the flux linking the field winding,
- E'_d - emf proportional to the flux linkage of amortisseur winding,

- T_M, T_e - mechanical and electromagnetic torque, respectively,
- δ - rotor angle,
- e_{fd} - voltage proportional to the field voltage,
- D - dumping coefficient
- T_j - time constant,
- $T_w = 1/\omega_s$ and
- ω_s - synchronous angular frequency.

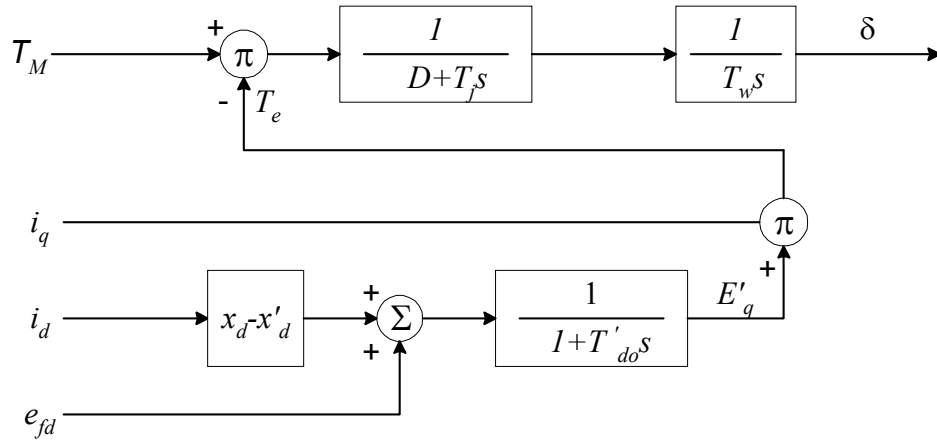


Figure 4.4.: Two-axis hydro-generator model

Dynamic models of turbo and hydro generators are thus determined by differential equations represented by the block diagrams shown in figures 4.3 and 4.4, respectively. The model of turbo-generator uses four differential equations while the hydro-generator model contains only three differential equations. Apart from the differential equations the following algebraic equations are needed for each synchronous machine i :

$$V_i \cos\theta_i - x'_{di} i_{qi} \sin\delta_i + (x'_{di} i_{di} - E'_{qi}) \cos\delta_i = 0, i = 1, \dots, m, \quad (4.16a)$$

$$V_i \sin\theta_i + x'_{di} i_{qi} \cos\delta_i + (x'_{di} i_{di} - E'_{qi}) \sin\delta_i = 0, i = 1, \dots, m. \quad (4.16b)$$

The connection between the network equations given by (4.14a) and (4.14b) and the generator models is based on the expressions for the generator active and reactive power injections:

$$P_{Gi} = V_i \{ i_{di} \sin(\delta_i - \theta_i) + i_{qi} \cos(\delta_i - \theta_i) \}, i = 1, \dots, m, \quad (4.17a)$$

$$Q_{Gi} = V_i \{ i_{di} \cos(\delta_i - \theta_i) - i_{qi} \sin(\delta_i - \theta_i) \}, i = 1, \dots, m \quad (4.17b)$$

The state vector variables for these models can be observed from figures 4.3 and 4.4:

$$\mathbf{x}_{THG} = \begin{bmatrix} \delta^T & \omega^T & \mathbf{E}_q^T & \mathbf{E}_d^T \end{bmatrix}^T, \quad (4.18)$$

where δ is the vector of all rotor angles, ω is the vector of all angular frequencies, while $\mathbf{E}_q, \mathbf{E}_d$ are the vectors of *emf* proportional to flux linkage of field and amortisseur winding, respectively. All these vectors have dimensions equal to the number of turbo/hydro-generators.

The corresponding vector of algebraic equations is:

$$\mathbf{y}_{THG} = \begin{bmatrix} \mathbf{i}_q^T & \mathbf{i}_d^T \end{bmatrix}^T, \quad (4.19)$$

where $\mathbf{i}_q, \mathbf{i}_d$ are m dimensional vectors of q, d axis currents, respectively.

4.2.1.3. Voltage regulator model

Voltage regulators are very important control devices, which sense changes in the output voltage in order to produce corrective actions if necessary. Various regulators have been used in engineering practice. In the late sixties a working group of the IEEE standardized these models. A block diagram of the standard Type 1 regulator is shown in Fig. 4.5. The regulator represents a classical excitation system with a continuously acting voltage regulator.

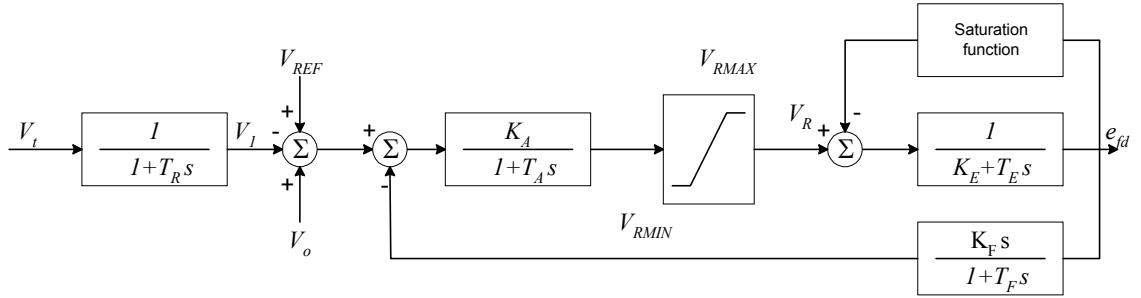


Figure 4.5.: Type 1 excitation system representation for a continuously acting regulator and exciter [AnF77].

Symbols and their typical values used in Fig. 4.5 are listed in Table 4.1.

Table 4.1 – Voltage regulator model symbols

<i>Symbol</i>	<i>Description</i>	<i>Typical values</i>
V_t	generator terminal voltage,	n.a.
T_R	regulator input filter time constant,	0÷0.06
V_{REF}	regulator reference voltage settings,	n.a.
V_o	auxiliary input signals,	n.a.
K_A	regulator gain,	20÷50
T_A	regulator amplifier time constant,	0.06÷2.0
V_R	regulator output voltage,	n.a.
V_{RMAX}, V_{RMIN}	maximum and minimum voltage of V_R ,	1.0,-1.0
K_E	exciter constant related to self excited field,	-0.05÷1.0
T_E	exciter time constant,	0.3÷0.5
K_F	regulator stabilising circuit gain,	0.01÷0.16
T_F	regulator stabilising circuit time constant.	0.35÷1.0

Neglecting the regulator input filter time constant T_R (because it is a few times smaller than the other time constants) and the exciter saturation leads to the simplified block diagram shown in Fig. 4.6. Based on this block diagram the state vector of the voltage regulator can be decomposed into three sub-vectors e_{fd} , V_R , and R_f , whose dimensions are m :

$$\mathbf{x}_{VR} = \begin{bmatrix} e_{fd}^T & V_R^T & R_f^T \end{bmatrix}^T \quad (4.20)$$

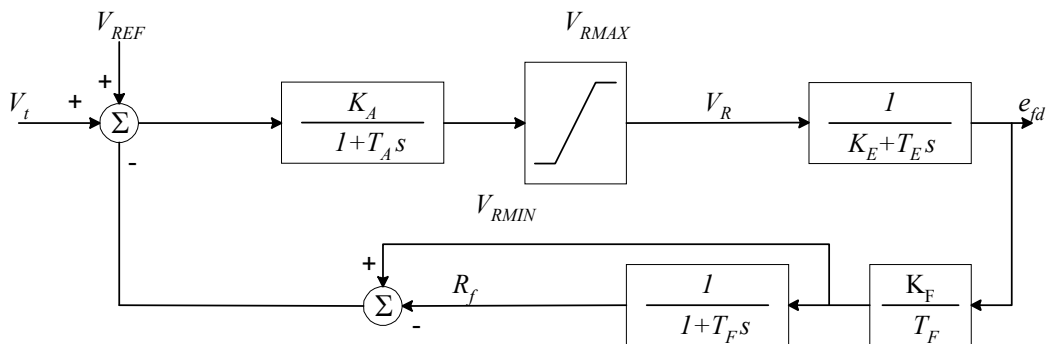


Figure 4.6.: Simplified voltage regulator block diagram

4.2.1.4. Hydraulic turbine and governing system model

The prime sources of electrical energy used by generating plants are the kinetic energy of water and the thermal energy derived from fossil fuels and nuclear fission [Kun94]. These sources are further converted first to mechanical energy by a prime mover and then to electrical energy by generators. The governor of the prime movers controls the generator frequency and power. It is thus an essential component of the Automatic Generator Control (AGC) or load – frequency control. Therefore, prime movers and their governors are very important for system frequency.

The block diagram of a Mechanical-Hydraulic Governor (MHC) is shown in Fig. 4.7. The symbols used in Fig. 4.7 are explained in Table 4.2.

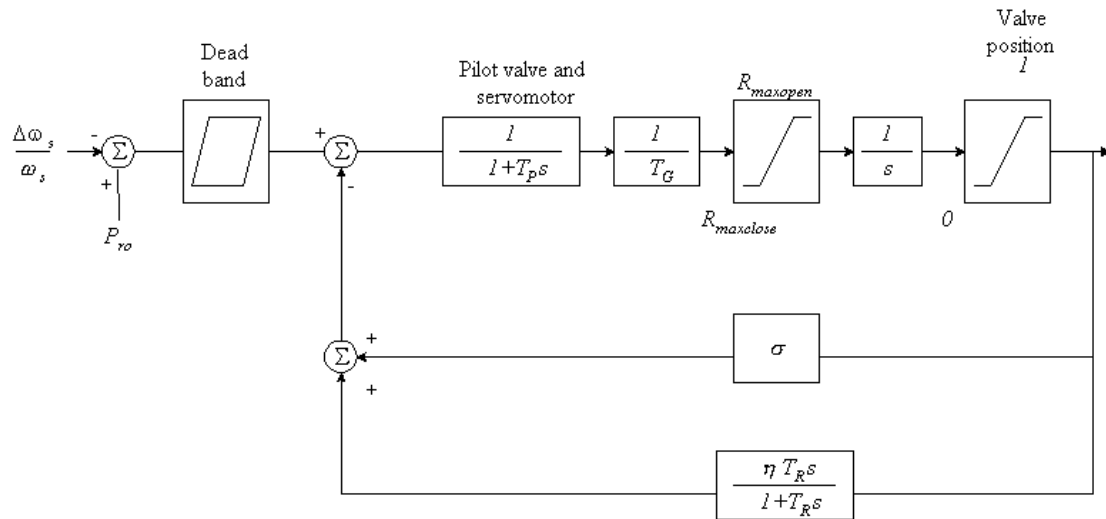


Figure 4.7.: Mechanical-hydraulic governor

Table 4.2 – MHC symbols

<i>Symbol</i>	<i>Description</i>	<i>Typical values</i>
T_P	pilot valve and servomotor time constant,	0.03÷0.05
P_{ro}	active power reference setting,	n.a.
T_G	main servo time constant,	0.2÷0.4
σ	permanent drop,	0.03÷0.06
η	transient drop,	0.2÷1.0
T_R	reset time,	2.5÷25
$R_{max\ open}, R_{max\ close}$	maximum and minimum gate opening rate	0.16

A typical transfer function for a hydraulic turbine shows how the power output of the turbine changes in response to a change in gate opening. A turbine and its governor system can be then represented using the block diagram shown in Fig. 4.8. If the turbine is an ideal then the last block in Fig.4.8 represents its transfer function.

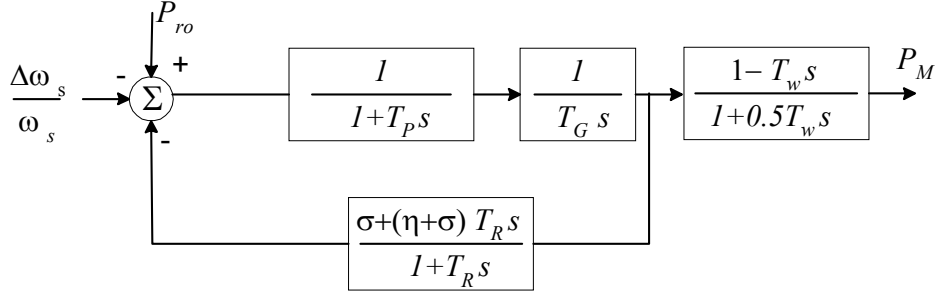


Figure 4.8.: Mechanical-hydraulic governor system and turbine

The block diagram shown in Fig. 4.8. can be further simplified by neglecting the pilot valve and servomotor time constants, which are significantly smaller than all the other time constants. Using these assumptions and introducing the new time constants T_1 and T_2 as

$$T_{1/2} = T_B / 2 \pm \sqrt{\left(\frac{T_B}{2}\right)^2 - T_A},$$

(where $T_B = \frac{(\sigma + \eta)T_R + T_G}{\sigma}$ and $T_A = T_R \frac{T_G}{\sigma}$) leads to the new simplified block diagram

shown in Fig. 4.9. The auxiliary variables P_1, P_2, P_3 are introduced in order to reformulate the complete model using first order differential equations. It appears then from Fig. 4.9 that the complete model of hydraulic turbine and its governor system consists of three differential equations and the following algebraic equations:

$$T_M = P_M = -2\left(\frac{T_R}{T_2} P_1 + P_2\right) + P_3. \quad (4.21)$$

Therefore, the state vector \mathbf{x}_{HTG} contains three sub-vectors of auxiliary variables P_1, P_2, P_3 .

$$\mathbf{x}_{HTG} = \begin{bmatrix} P_1^T & P_2^T & P_3^T \end{bmatrix}^T, \quad (4.22)$$

The dimension of these vectors is $\leq m$, while the vector of algebraic variables \mathbf{y}_{HTG} contains only the vector of mechanical moments of each hydro-generator:

$$\mathbf{y}_{HTG} = \begin{bmatrix} T_M^T \end{bmatrix}^T. \quad (4.23)$$

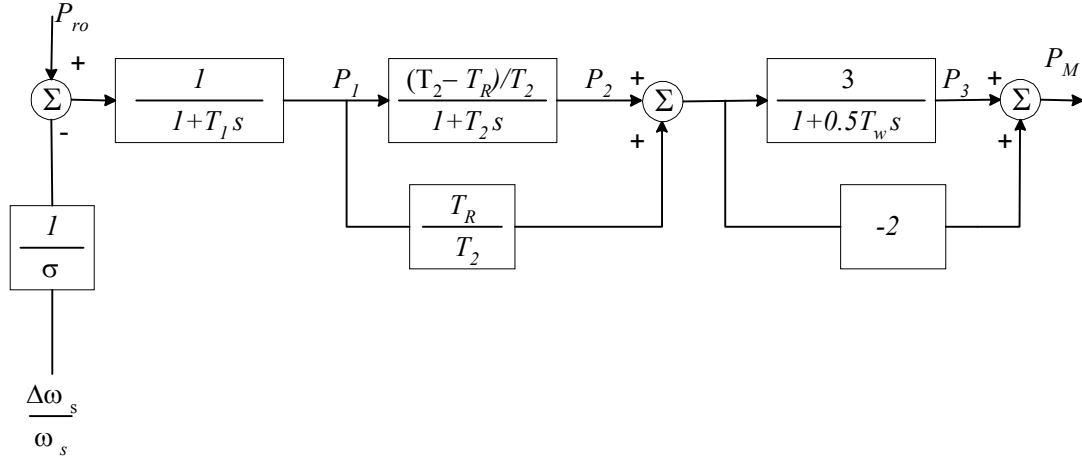


Figure 4.9.: A simplified model of mechanical-hydraulic governing system and turbine

4.2.1.5. Steam turbine and governing system model

A steam turbine converts energy stored in high pressure and high temperature steam into rotating energy, which is in turn converted into electrical energy by the generator. The heat source for the boiler supplying the steam might be a nuclear reactor or a furnace fired by fossil fuel (coal, oil or gas) [Kun94].

A simplified block diagram of a steam turbine and its governing system is shown in Fig. 4.10. The auxiliary variables P_{SM} , P_{CH} , P_{HP} are introduced to help reformulate the steam turbine model using only the first order differential equations. The steam turbine model shown in Fig 4.10. consists of three differential equations and the following algebraic equation:

$$T_M = P_{RH} + F_{HP}P_{CH}. \quad (4.24)$$

The state vector \mathbf{x}_{ST} contains the following three sub-vectors, whose dimensions are $\leq m$:

$$\mathbf{x}_{ST} = \left[\mathbf{P}_{SM}^T \quad \mathbf{P}_{CH}^T \quad \mathbf{P}_{HP}^T \right]^T, \quad (4.25)$$

while the vector of algebraic variables \mathbf{y}_{ST} is:

$$\mathbf{y}_{ST} = \left[\mathbf{T}_M^T \right]. \quad (4.26)$$

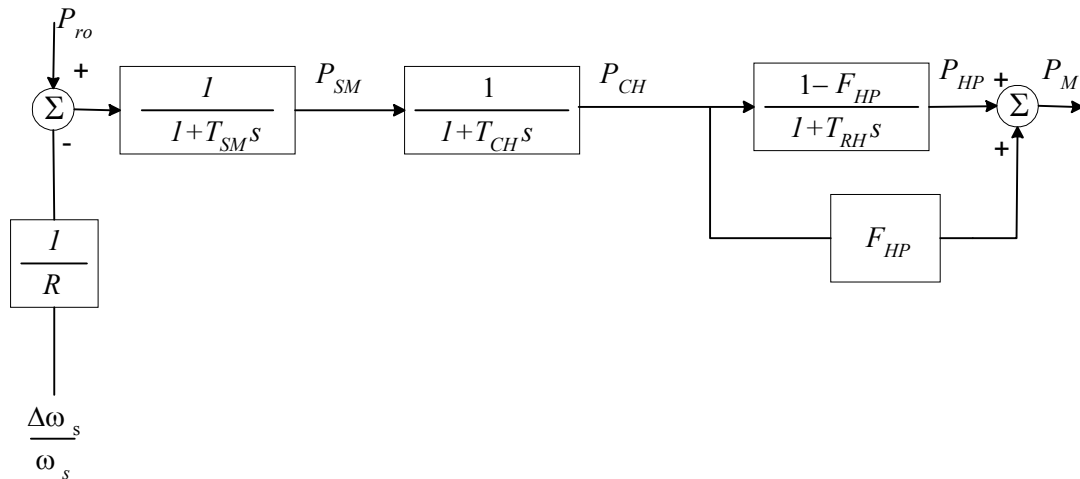


Figure 4.10.: Simplified model of steam turbine and its governing system

Table 4.3 – Symbols used in the steam turbine model

<i>Symbol</i>	<i>Description</i>	<i>Typical values</i>
T_{SM}	servomotor time constant	0.1÷0.3
T_{CH}	time constant of main inlet volumes and steam chest	0.1÷0.5
T_{RH}	time constant of reheater	4.0÷12
F_{HP}	fraction of total turbine power generated by high pressure section	0.3
R	permanent drop	0.05

4.2.1.6. A complete short-term dynamic model

Based on the block diagrams given in 4.2.1.2-4.2.1.5, the algebraic network equations (4.14a) and (4.14b), the algebraic equations (4.16a), (4.16b), (4.17a), (4.17b), (4.21) and (4.24) a complete short-term dynamic model can be obtained. Table 4.4 gives the equations and variables used in this model.

It can be seen from Table 4.4 that there are 10 differential equations for each turbo-generator and 9 for each hydro-generator. On the other hand, the number of algebraic equations for each turbo-generator and hydro-generator is 5. Therefore, the maximal total number of differential equations is $10 * m$, while the maximum number of algebraic equations is $5 * m + 2 * n$, taking into account the network algebraic equations.

Starting from the steady state values, this complete model can be solved alternately implementing the following three steps:

1. find the solution of the network algebraic equations,
2. find the solution of generator algebraic equations,
3. find the solution of generator differential equations.

Table 4.4 –Equations and variables in short-term dynamic model

	<i>Number of differential equations</i>	<i>Number of algebraic equations</i>	<i>State variables</i>	<i>Algebraic variables</i>
	per generator			
turbo-generator (4.2.1.2)	4 (Fig. 4.3)	4 [4.16a-4.17b]	4 [4.18]	4 [4.19]
hydro-generator (4.2.1.2)	3 (Fig 4.4)	4 [4.16a-4.17b]	3 [4.18]	4 [4.19]
voltage regulator (4.2.1.3)	3 (Fig. 4.6)	n.a.	3 [4.20]	n.a.
hydraulic turbine (4.2.1.4)	3 (Fig. 4.9)	1 [4.21]	3 [4.22]	1 [4.23]
steam turbine (4.2.1.5)	3 (Fig. 4.10)	1 [4.24]	3 [4.25]	1 [4.26]
Totals	10 (9)	5 (5)	10 (9)	5 (5)
	10 turbo-generator			
	9 hydro-generator			

4.2.2. Fast Simplified Models for System Frequency Evaluation

The period of time during which this model of the system frequency response should be valid is about 25 s. The detailed models of turbines, generators, governors and voltage regulators were described in section 4.2.1. Using these detailed models, however, is impossible because of the large number of operating regimes that need to be studied. Therefore, it is assumed that the system possesses enough damping to eliminate inter-machine oscillations. In other words, it will be assumed that the system frequency is uniform. Thus, a simple model that gives the system frequency dynamics and the total mechanical power variation during the primary control period can be adopted. Two such models are discussed in the following paragraphs. The first one is based on a motion equation of an equivalent generator and a fictitious inertia

center. It is discussed in section 4.2.2.1. The second simplified model is based on a second order linear model, in which both the motion of the equivalent system generator and the response of the equivalent governor are taken into account. This model is described in section 4.2.2.2.

4.2.2.1. Dynamic model for evaluation of inertia centre frequency

Using the motion equation (4.1) it is possible to estimate the individual generator frequencies if the generator electrical outputs are known. All of these generators have different frequency response characteristics. On the other hand, from a system point of view a unique system frequency is more important than individual generator frequency characteristics. The oscillations of the system frequency should normally be much smaller than the oscillations of individual generator frequencies. The combined inertia constant of all generating units is indeed considerably larger than the inertia constant of an average size generating unit.

The center of inertia of a power system can be obtained by summing the motion equations of each individual generator in the system:

$$\sum_{i=1}^m \frac{H_i}{\pi f_0} \frac{d^2 \delta_i}{d t^2} + \sum_{i=1}^m D_i \frac{d \delta_i}{d t} = \sum_{i=1}^m (P_{Mi} - P_{Gi}) \quad (4.27)$$

If the system inertia constant is $H_{SYS} = \sum_{i=1}^m H_i$ and the system dumping coefficient is

$D_{SYS} = \sum_{i=1}^m D_i$, then equation (4.27) can be brought to the following form:

$$\frac{2H_{SYS}}{\omega_s} \frac{d\omega_{CI}}{d t} + D_{SYS} \omega_{CI} = P_{MSYS} - P_{GSYS} \quad , \quad (4.28)$$

where $\omega_s = 2\pi f_0$, ω_{CI} is the angular frequency of the center of inertia, P_{MSYS} is the total mechanical power of all the generators in the system and P_{GSYS} is the total electrical power of all generators in the system.

4.2.2.2. Dynamic model for evaluation of system frequency

This model is based on a second order linear model, where both the motion of the equivalent system generator and the response of the equivalent governor are taken into account [LNN01]. The differential equations of the model are:

$$\dot{\mathbf{x}} = \mathbf{A}\mathbf{x} + \mathbf{B}\mathbf{u}; \quad \mathbf{x}(t_0) = \mathbf{x}_0, \quad (4.29)$$

where the vectors and matrices are defined as [LNN01]:

$$\mathbf{x}^T = [\Delta f, \Delta P_{me}]; \quad \mathbf{u} = \Delta P_0; \\ \mathbf{A} = \begin{bmatrix} -k_l P_{l0} / T_e & 1 / T_e \\ -P_{ne} / (s_{ne} T_{se}) & -1 / T_e \end{bmatrix}; \quad \mathbf{B} = \begin{bmatrix} 1 / T_e \\ 0 \end{bmatrix}. \quad (4.30)$$

In equation (4.30), Δf is the change in the system frequency (in p.u.), ΔP_{me} is the change in the mechanical power output of the equivalent unit (p.u.), ΔP_0 is the active power mismatch at instant t_o (p.u.), k_l is the self-regulation coefficient of the total power system demand (pu); P_{l0} is the total active power load at t_o (pu), T_e is the inertia time constant of the equivalent generating unit (s), P_{ne} is the rated active power of the equivalent unit (p.u.), s_{ne} is the governor control droop of the equivalent unit (per unit rated active power), and T_{se} is the servomotor relative time constant of the equivalent unit control system (s). Derivation of the equivalent parameters of the model (4.29)-(4.30) is given in [PoM96]. It should be noted that the parameters of the model (4.29)-(4.30) depend on the analysed disturbance case, which means that they should be recalculated for each new disturbance case.

The advantage of the model (4.29)-(4.30) is that we can explicitly solve it using modal decomposition. The analytical expressions of the model are given in [PoM96], and it is emphasized that the non-zero initial conditions allow the consideration of control and protection actions such as under-frequency load shedding and frequency protection of generators. Three ‘‘critical’’ points during the transient process should be carefully monitored. The first instant is t_{\min} at which the extreme frequency deviation Δf_{\min} is reached. This value is used to check whether under-frequency load shedding is going to take place. Next, the maximum mechanical power output change ΔP_{me}^{\max} occurs at time instant t_{\max} , and it should be compared with the available spinning reserve of unblocked turbine governors. In cases where the available spinning reserve is not sufficient, the model (4.29)-(4.30) reduces to the first order model:

$$\dot{\Delta f} = -k_l P_{l0} / T_e + \Delta P_{me} / T_e + \Delta P_0 / T_e; \quad \Delta f(t_0) = \text{known}, \quad (4.31)$$

where ΔP_{me} is a constant value. Finally, the last point is the steady-state value of the frequency deviation (if any). It can be obtained at the end of the simulation period, and it determines the active power generations in the power flow.

A simple logic based on these critical points is used in the simulation of large system disturbances to determine possible system frequency failures. The simplified flowchart of the logic is shown in Fig. 4.11. The minimal frequency value recorded during this simulation can be used to decide whether under-frequency protection will be activated. Under-frequency protection disconnects increasing amounts of load as the frequency drops:

- 10% of total load at 49.2 Hz
- 20% of total load at 48.8 Hz
- 30% of total load at 48.4 Hz and
- 40% of total load at 48.0 Hz

A frequency collapse incident is described in section 3.2.1.1. This incident can be identified monitoring the frequency over the simulation period (see Fig.3.3)

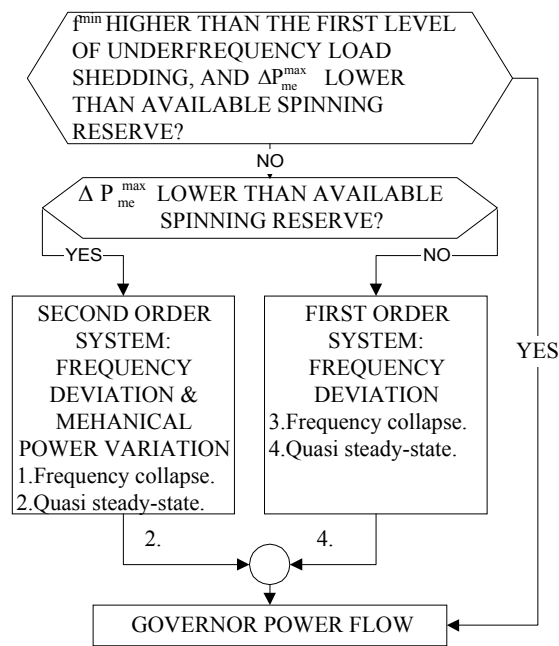


Figure 4.11.: Flowchart of the applied procedure during governor control

4.3. Line Overloading

It appears that line outages due to overload are often the main contributors or the triggering events in large system disturbances. Knight in [Kni01] identifies the line outages of three circuits between the south-east and south-west areas of England and Wales as the triggering events in a disturbance which caused significant load shedding and system islanding. Knight further states that conditions at the time of the incident were foreseen during operational planning work. The outage occurred as a consequence of conductor sag in the hot humid weather due to flashovers to trees. A very similar event occurred in USA in 1996 when a 345 kV line was outaged due to flashover to a tree. As a result of this event, protective malfunctions and insufficient voltage support, about 4750 MW of load was disconnected [Nerc02a]. Cold weather together with high power flows is often seen as a serious treat for the line tripping. The CIGRE report on the storms in France shows that a significant number of 400 and 225 kV lines were tripped due to overload in cold winter conditions in 1978 and 1999 [Mer00]. During a recent severe storm in France, in one day, thirty-eight 400 kV lines were out of operation simultaneously.

These incidents confirm that the sagging of overhead lines is a serious threat to power system stability. This sagging is a direct consequence of high power flows and outdoor conditions. However, a line that begins to sag does not automatically mean that a network failure will occur. Therefore, in this simulation of large system disturbances a very simple but realistic probabilistic approach is used to model possible line outages due to overloads. This approach is based on the following two assumptions:

1. Only if a line is overloaded it can sag beyond the specified limits. Therefore, if a line is not overloaded its probability to be outaged due to sagging is zero.
2. The more a line is overloaded, the larger is its sagging, and hence the larger the probability that it will be tripped.

The very simple probabilistic function shown in Fig. 4.12 was used for this purpose. This function is an exponential when the line flows are larger than thermal limit and smaller than 1.5 times thermal limit. The function has the constant value p_2 when the line flows are larger than 1.5 times thermal limit. Such modelling has the following characteristics:

- the values of probabilities p_1 and p_2 depend on various factors (external factors and maintenance).
- the probabilities of outaged lines due to overload can be calculated off-line, based on recorded system variables during the simulation period. Values that are used for p_1 are taken from [BGF95], while p_2 is varied from two to several times larger. These values are further discussed in Chapter 8.

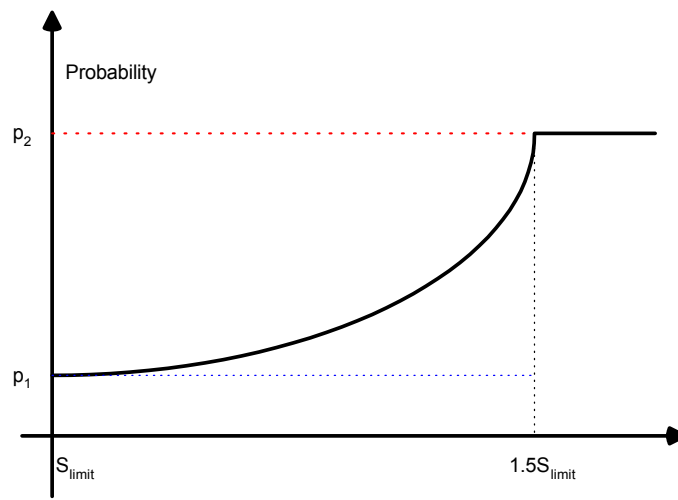


Figure 4.12.: Line overload modelling in the simulation procedure

5

Hidden Failures In A Protection System

Protective relaying is a vital part of any electric power system: quite unnecessary during normal operation, but very important during trouble, faults and abnormal disturbances. Properly applied protective relaying initiates the disconnection of the trouble area while operation and service in the rest of the system continues. Correct operation of the protection system requires that (1) at least one of the primary relays operated correctly, (2) none of the backup relays operated to trip the fault and (3) the trouble area was properly isolated in the time expected [Bla98]. A large majority of all relay operations are correct and wanted. On the other hand, unwanted protection operations might trigger large system disturbances that begin with a random fault followed by one or more other trips caused by unwanted protection operations. Such multiple outages are usually considered to be non-credible contingencies, which are often not foreseen in security plans. Bearing in mind that in last twenty years a significant percentage of large system disturbances have been caused by non-credible contingencies [CWG01], it appears that unwanted protection operations represent a real threat for power systems. The simulation of large system disturbances is therefore focused on the most vulnerable protection schemes covering the most important power system components. Different utilities use different criteria to determine the most vulnerable protection schemes. The criterion used in this work is based on the following principles:

- the vulnerability of protection scheme logic increases with its complexity
- the protection schemes that have already contributed to the analysed world wide system disturbances (see Chapter 2), deserve special attention.

Based on these principles, hidden failures in protection systems are seen as the most important factor in unwanted protection operations. The first section of this chapter defines hidden failures, emphasising the difference between hidden failures and other incorrect protection operations. The second and third sections deal with transmission and generator protection schemes and their hidden failure modes. Finally, the last section introduces the concept of vulnerability region, which is seen as the major generator of outages in the simulation of large system disturbances.

5.1. Definition and Modes of Hidden Failures

The operation of a protection system can be classified into a few categories and subcategories as suggested in [Bla98]:

1. correct operation
 - 1.a. as planned
 - 1.b. not as planned or expected
2. incorrect, either failure to trip or false tripping
 - 2.a. not as planned
 - 2.b. acceptable for the particular situation
3. no conclusions.

The characteristics of correct operations have already been described in the introduction of this chapter. A vast majority of relay operations belong to subcategory (1.a.). Correct operations belonging to (1.b.) are very rare and normally happen when a significant number of operations and events are involved. Such operation was described in section 2.2.4 (see Jap87 incident). This incident was triggered by the impedance protection caused by low system voltages and high currents in the system. However, such operation was unwanted because it caused many other overloads and outages.

Incorrect operations result from a failure, a malfunction, or unanticipated or unplanned operation of the protective system [Bla98]. The reasons for incorrect operations are: application of relays (R1), incorrect settings and human errors (R2), equipment problems and failures (R3) or any combination of these three. All of these belong to subcategory (2.a.). The

incorrect operations that belong to (2.b.) are very rare and represent the inability of the protection system to provide “infinity” protection [Bla98].

The last category refers to circumstances during which one or more relays have or appear to have operated, such as circuit breakers tripping with no cause. A lack of evidence of a power system fault or trouble or not apparent equipment failure can cause a frustrating situation and may result in a long post-mortem investigation [Bla98].

Tamnronglak in [Tam94] defines a hidden failure as a permanent defect that will cause a relay or a relay system to incorrectly and inappropriately remove one or more circuit elements as a direct consequence of another switching event. Hidden failures cause incorrect protection operations, whose consequences are false trippings. However, according to Tamnronglak’s definition failure to trip is not a hidden failure.

Apart from reason (R1) any other reason can cause a hidden failure. In this work the hidden failure caused by a permanent defect (R3) is a Hardware Hidden Failures (HHF), while a hidden failure caused by reason (R2) is called a Non Hardware Hidden Failure (NHHF). Hardware hidden failure modes are analysed for the most vulnerable protection schemes related to transmission lines, generators and transformers. These protection schemes and their hidden failure modes are discussed in 5.2 and 5.3. Based on these hidden failure modes a vulnerability region can be defined. A vulnerability region is thus a set of power system components whose protection might cause unwanted protection operations due to HHFs. Probability of such unwanted operation due to a HHF is a constant value. On the other hand, incorrect settings and human errors are more likely to cause unnecessary trip of a power system component when the protected component is under stressed system conditions. Therefore, the total probability of hidden failure combines the constant probability of a HHF and the probability of a NHHF, which is not constant and depends on system conditions.

It should be noted that the definition of hidden failures found in [Tam94] emphasises the fact that a hidden failure has to be revealed by another switching event. In this work, it is assumed that apart from a switching event, a sudden change in system conditions might reveal a hidden failure as well. For example, a sudden increase in excitation of a generator might activate the overexcitation limiter and trip the field circuit breaker (see 5.2.2.). However, one should keep in mind that hidden failures cannot produce an immediate action by themselves, and they will

remain undetected until they are revealed by another event or sudden changes in system conditions.

Two characteristics of hidden failures are very important. The first one is that hidden failures appear when the system is under stressed conditions. In this thesis it was assumed that stressed conditions are provoked by an initial fault. The first outage is therefore caused by the initial fault, while all other outages in a disturbance sequence are caused by hidden failures or the phenomena discussed in Chapter 3. It means that multiple outages might arise from a benign initial fault. Such outages are usually not foreseen in security plans, which is the second important characteristic.

In order to illustrate some of these ideas, a simple logic diagram of a three zone step distance relay is given in Fig. 5.1. If a HHF affects contacts T_3 , it will result in a hidden failure mode. On the other hand, a HHF on relay Z_1 will not result in a hidden failure mode.

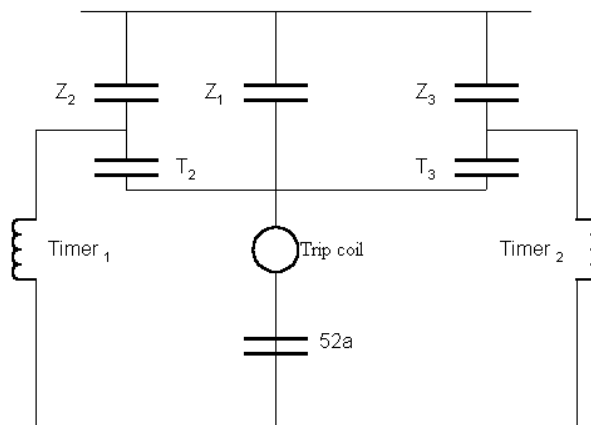


Figure 5.1.: Illustration of hidden failure modes [ERP01]

If a HHF occurs in T_3 , causing the closing of its contact permanently, the three zone distance logic shown in Fig. 5.1 will allow this HHF to remain unrevealed. Thus at the instant when T_3 closes its contact the line protected by third zone protection will remain in operation assuming that contacts Z_3 are still open (see Fig. 5.1, both Z_3 and T_3 are required to close before tripping the line). However, if a fault occurs within the second zone the line protected by the second zone will be switched instantaneously. However after a time delay determined by T_2 the line protected by the third zone will be tripped as well because contact T_3 is closed and Z_3 can see the fault. Therefore, the HHF is revealed by a fault in the second zone and the permanent defect is the closed contacts of T_3 .

On the other hand, if the contact of Z_1 was permanently closed this would instantaneously open circuit breaker of the protected line and the defect would be immediately revealed. Therefore, such HHF cannot result in a hidden failure mode.

5.2. Protection of Transmission Lines

Various protection schemes have been used for transmission lines. These schemes are usually divided into pilot and non –pilot protection schemes. Overcurrent and distance protection are well-known non-pilot protection schemes. In these schemes, the relays based their decisions solely on the measurement of electrical quantities at the relay end of the protected line sections. The main disadvantage of such schemes is the inability to instantaneously clear a fault from both ends of the protected line. On the other hand, pilot protection uses a communication channel between two or more ends of a transmission line to provide instantaneous clearing over 100% of the line [HoP95].

The first principle suggested in the introduction of this chapter suggests that a protection scheme is more vulnerable if its logic is more complex. A pilot protection scheme such as directional comparison blocking, directional comparison unblocking, permissive overreaching transfer trip , permissive underreaching transfer trip , phase comparison is certainly more complex than the logic involved in non-pilot schemes. These schemes and their hidden failure modes are discussed in 5.2.1. – 5.2.5. It is shown in section 5.1 that third zone distance protection can have HHFs that can result in hidden failure modes. These modes are considered in section 5.2.6. Finally, the hidden failure modes of the differential protection of transformer are described in section 5.2.7.

5.2.1. Directional Comparison Blocking Scheme

The directional comparison blocking relay scheme, first used in the 1930s, belongs to the class of pilot protection schemes. The term pilot refers to a communication channel that provides instantaneous clearing at both ends of the faulted transmission line [Bla98], [HoP95]. Such a scheme can operate in either tripping or blocking mode. The logic of a

directional comparison blocking scheme is shown in Fig. 5.2a and a contact logic diagram is shown in Fig. 5.2b. Both ends of the line are equipped with Fault Detector relays (FD_A and FD_B) and Directional relays (D_A and D_B). FD relays can be directional or non-directional and the blocking signals are triggered only by these relays. The blocking signal can be stopped by the directional relay D and only this relay can send a triggering signal to the trip coil TC_A and circuit breaker contacts $52a_A$. A blocking signal is transmitted via transmitter T_A and received via receiver R_A . Fig 5.2b shows that its contacts are normally closed.

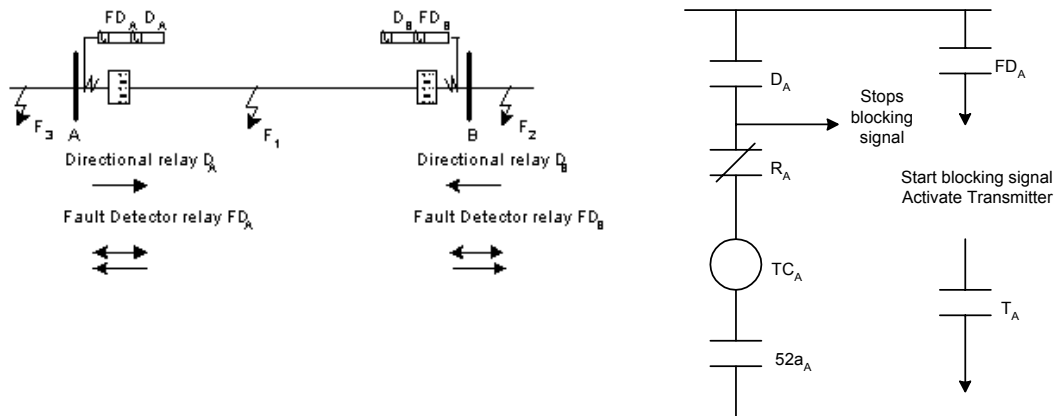


Figure 5.2.: Directional comparison blocking scheme a) One-line diagram b) Logic diagram
[HoP95],[Eli00]

Therefore, if an internal fault F_1 occurs, the directional relays D_A and D_B close their contacts and prevent FD_A and FD_B from sending their blocking signals. At the same time D_A and D_B open the circuit breakers at both ends instantaneously. On the other hand, if an external fault F_2 occurs, the directional relay D_A closes its contacts and prevents FD_A from sending its blocking signal. The directional relay D_B does not operate for fault F_2 and FD_B (either directional or non directional) sends the blocking signal to the receiver on the A-side using its transmitter. The receiver at A prevents the circuit breaker at A from tripping. The circuit breaker at B receives a blocking signal and D_B does not operate because F_2 is behind D_B . Consequently, the line A-B does not trip for the external fault F_2 . On the other hand, the following HHF on the A side could produce unnecessary breaker openings following the external fault F_3 and F_2 , respectively [Bla98][HoP95]:

- FD_A could fail to close, tripping the circuit breaker at B (fault F_3).
- The transmitter T_A may fail to transmit the blocking signal, again tripping the circuit breaker at B (fault F_3).
- The receiver R_A may not receive the blocking signal, tripping the circuit breaker at A (fault F_2).

Similar conclusions can be drawn if the protection system defects are hidden on the B-side and the external fault is on the A-side.

5.2.2. Directional Comparison Unblocking Scheme

This scheme is very similar to the previous one, except that during normal power system states, a continuous blocking signal is transmitted from each terminal to the other over two separate communications channels. A logic diagram of this scheme is shown in Fig 5.3. The directional relay D_A is usually an overreaching unit that can shift transmitted signal from a blocking to an unblocking frequency. Thus for an internal fault F_1 (see Fig. 5.2a) both directional relays D_A and D_B will shift a blocking into an unblocking frequency and the circuit breakers can be tripped. For an external fault F_3/F_2 , the receivers R_B/R_A will receive blocking signals from side A or side B respectively and prevent the directional relays D_B and D_A from closing their contacts.

There are two possible hidden failures modes for this protection scheme at side A:

- D_A contacts are always closed, which will cause an unnecessary tripping of circuit breakers on sides A and B for an external fault F_3 and
- R_A contacts are always closed, which will cause an unnecessary trip of the circuit breaker on side A for an external fault F_2 .

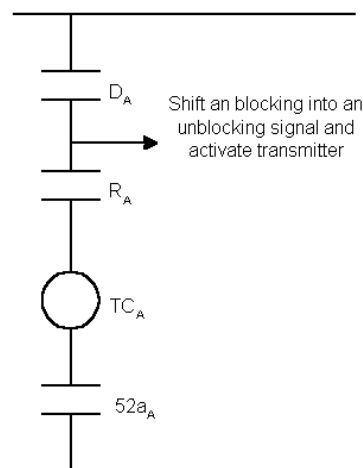


Figure 5.3.: Logic diagram of directional comparison unblocking scheme

5.2.3. Permissive Overreaching Transfer Trip Scheme

Many transfer trip schemes are possible depending upon the application. All schemes, however, use a communication with a frequency shift. If the frequency of the received signal

shifts from the guard state to the trip state, a trip occurs. This scheme is very similar to the directional comparison unblocking scheme described in section 5.2.2, where the directional overreaching relay serves as both the fault detector and a permissive interlock to prevent an inadvertent trip due to noise. The one-line and logic diagrams for such scheme are shown in Fig. 5.4a and Fig. 5.4b, respectively. Thus, if fault F_1 occurs on line A-B both directional overreaching relays D_A and D_B will send a trip signal to the receivers on the opposite side. The circuit breakers on both sides will be opened and the fault will be cleared. If an external fault F_2 occurs, the directional overreaching relay D_A can operate, but the fault is behind D_B and receiver R_A can not operate. A similar situation occurs for an external fault F_3 .

There are two possible hidden failure modes for this scheme on each side. For example, on side A:

- D_A is continuously activated, which leads to an unnecessary trip of both circuit breakers for an external fault F_3 .
- R_A is continuously activated, which leads to an unnecessary trip of the circuit breakers at A for an external fault F_2 .

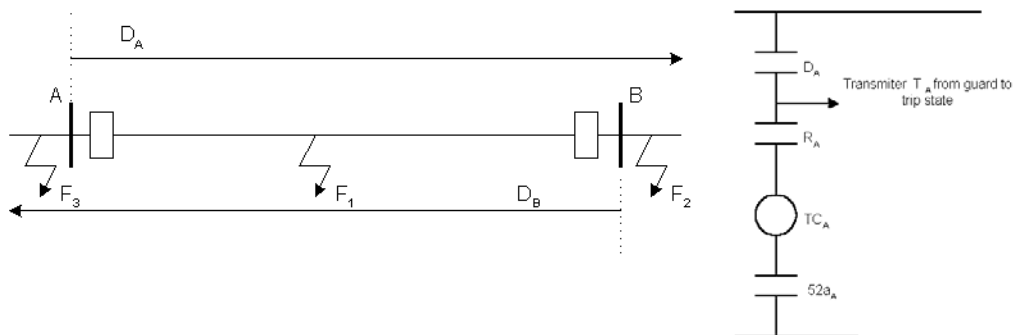


Figure 5.4.: Permissive underreaching transfer trip scheme a) One-line diagram b) Logic diagram

5.2.4. Permissive Underreaching Transfer Trip Scheme

The on-line and logic diagrams of a permissive underreaching scheme are shown in Fig 5.5a and Fig. 5.5b respectively. This scheme can open a circuit breaker if either D_A sees a fault or FD_A and R_A are activated at the same time (see Fig. 5.5b). Therefore, if an external fault F_1 occurs, both directional relays D_A and D_B will pick up and open circuit breakers at both sides. If an external fault F_2 occurs, the fault detector relay FD_A will pick up, but the receiver R_A will

not operate because the directional relay D_B cannot see the fault and the corresponding signal from the opposite side cannot be received.

There are two possible hidden failure modes for this scheme on side A:

- T_A continuously sends a trip signal to R_B , which leads to an unnecessary trip of both circuit breakers for an external fault F_3 .
- R_A continuously receives a trip signal from T_B , which leads to an unnecessary trip of the circuit breaker at A for an external fault F_2 .

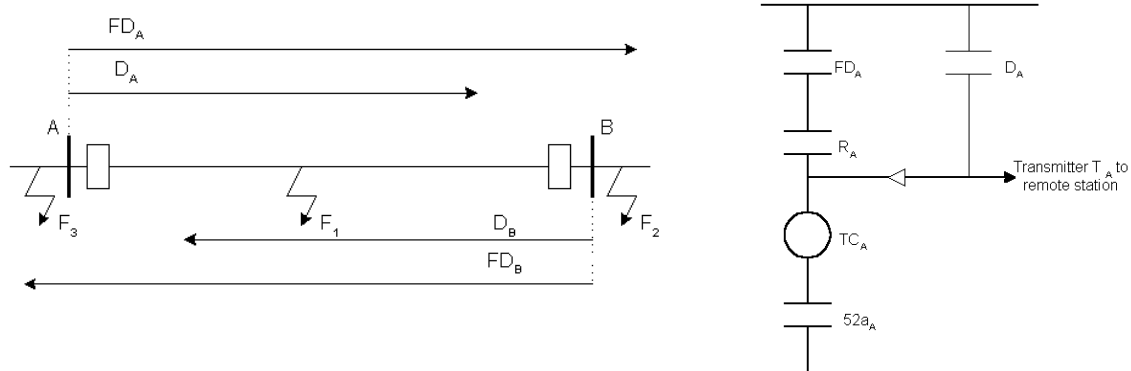


Figure 5.5.: Permissive underreaching transfer trip scheme a) One-line diagram b) Logic diagram

5.2.5. Phase comparison relays

Phase comparison relaying is a differential scheme that compares the phase angle between the currents at the two ends of a line. If the two currents are essentially in phase, there is a fault in the protected section. On the other hand, if these two currents are 180° out of phase, there is no fault within the line section. The basic principles of this scheme are illustrated in Fig 5.6. It can be seen that when external faults (F_3 and F_2) occur, the currents seen by relays at A and B are out of phase. Two comparison schemes are usually applied in practise: single and dual phase comparison schemes. In a single-phase comparison scheme, a signal is transmitted on the positive half of a square wave. If the half of the square wave on the remote end is negative (external faults, see Fig 5.6) the trip of circuit breakers cannot be initiated. In a dual-phase comparison scheme, signals are transmitted on both halves of the square and the comparators on both sides compare received and transmitted signal frequencies. A trip is initiated if these frequencies are the same.

The fault detector relay FD_1 is an overreaching relay, which activates the transmitter and at the same time provides the first input to the comparator. The fault detector relay FD_2 is also an overreaching relay, but a high set relay, which arms the system for tripping. The scheme is such that the positive and negative blocks of square wave of the secondary current are 180°

from the positive and negative half-cycles of the primary current wave and consequently this scheme has a blocking system. A logic diagram of this scheme is shown in Fig. 5.7 [Bla98].

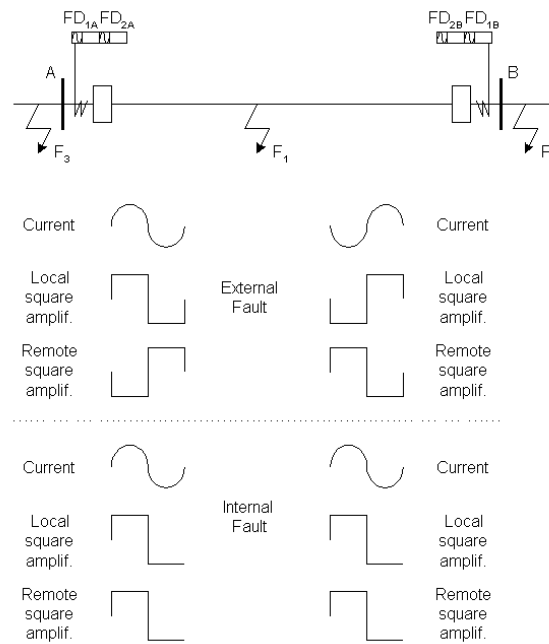


Figure 5.6.: Basic principles of phase comparison scheme

The following hidden failure modes are possible on side A:

- The loss of signal from the remote end will cause both fault detector directional relays on side A to operate as non-directional overcurrent relays.
- FD_{1A} is continuously activated and the relay at side A becomes a non-directional overcurrent relay.
- FD_{1A} cannot pick up and the relay at side B becomes a non-directional overcurrent relay.

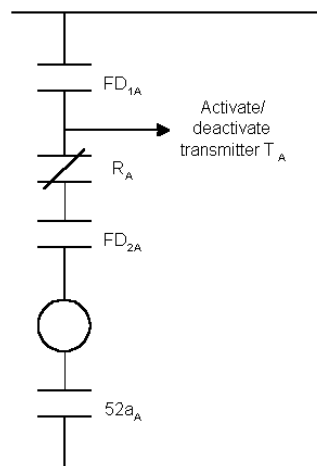


Figure 5.7.: Logic diagram of phase comparison blocking scheme

5.2.6. Back-Up Protection

Hidden failures in back-up protection schemes (such as Zone 2 and Zone 3 distance protection of transmission lines) can also trigger unwanted circuit breaker openings. A simple diagram of such a distance protection scheme is shown in Fig. 5.6. Different zones have different co-ordination delays and different reach settings. The co-ordination delays of zones 2 and 3 are typically and respectively set at about 0.3 and 1 second, while their reach settings are set at 120% to 150% of the line length and 120%-180% of the next line section, respectively. Closed timer contacts for the zone 2 and 3 elements are the types of HHFs that affect this protection. For the simple example shown in Fig. 5.8, such hidden failures will result in the following hidden failure modes:

- If F_1 occurs, the zone 1 element of the relay protecting line C-D instantaneously and correctly trips the circuit breakers at C and D. However, if the timer contacts of the zone 2 element of the relay protecting line A-B are always closed, then this fault will also cause the incorrect trip of line A-B.
- Similarly, if F_2 occurs, the zone 1 element of the relay protecting line E-F instantaneously and correctly trips the circuit breakers at E and F. However, if the timer contacts of the zone 3 element of the relay protecting line A-B are always closed, then this fault will also cause an incorrect trip of line A-B.

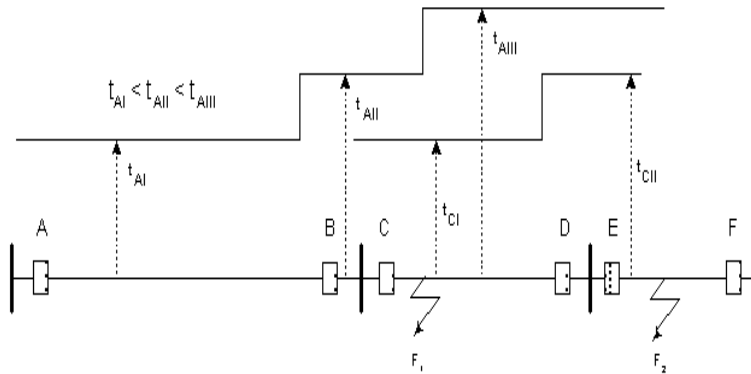


Figure 5.8.: One line diagram of distance protection

5.2.7. Transformer Differential Relay

A transformer differential relay, which consists of operating and restraint coils, is shown in Fig. 5.9. The trip characteristics of the relay can be set as a percentage of the ratio of the operating and restraining forces according to the used current transformer characteristics and ratios, as well as the characteristics of the transformer being protected. The restraining force

may also come from harmonic filters to prevent an incorrect trip due to inrush current. A HHF can occur if the restraining force is missing when the restraint coils are shorted [Eli00]. The HHF can result in a hidden failure mode even for normal loading conditions.

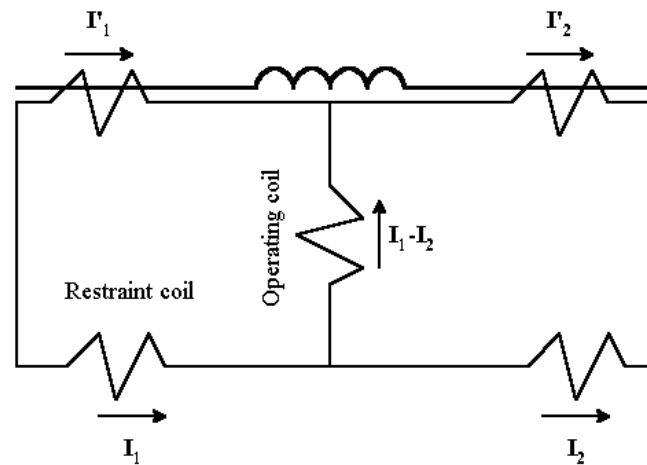


Figure 5.9.: Percentage differential protection

5.3. Generator Hidden Failures

The protection of generators is more complex than the protection of the transmission system because of the variety of possible failures and operating conditions. The frequency of generator failures is higher than the frequency of transmission line failures. However, despite the many failure modes that can affect generators, the generator protection principles are very simple: only differential and overcurrent relays are employed and the complexity of pilot scheme is avoided. The abnormalities and failures which the generation protection has to deal with are listed below along with the corresponding protection schemes (denoted by the numbers in the brackets) [Bla98],[HoP95]:

- winding faults – stator (phase (87),(51v) and ground (51G)), rotor
- overload (49),
- overspeed (85),
- loss of prime mover (32),
- negative sequence (46),
- abnormal voltages (overvoltages(59) and undervoltage(27)) and frequencies (under/over frequency (81)), V/Hz variations (24),
- underexcitation and lost excitation (40),
- inadvertent energization (67).

Some of these protection schemes are shown in Fig. 5.10 for a typical protection of a low impedance grounded generator.

For all generators rated 1MVA or higher, it is standard practise to use differential protection (87) and overcurrent relay (51v) to protect and provide backup for the generator from stator phase faults [HoP95], [Bla98]. This protection and its possible HHF are discussed in section 5.3.1.

Stators are protected from ground faults using either a differential phase relay, if the generator is solidly grounded, or a current transformer and a secondary connected overcurrent relay (51G), if the generator is grounded using neutral impedance. This scheme can fail, but any failure will be revealed as soon as it appears. HHFs for this protection scheme are thus not possible.

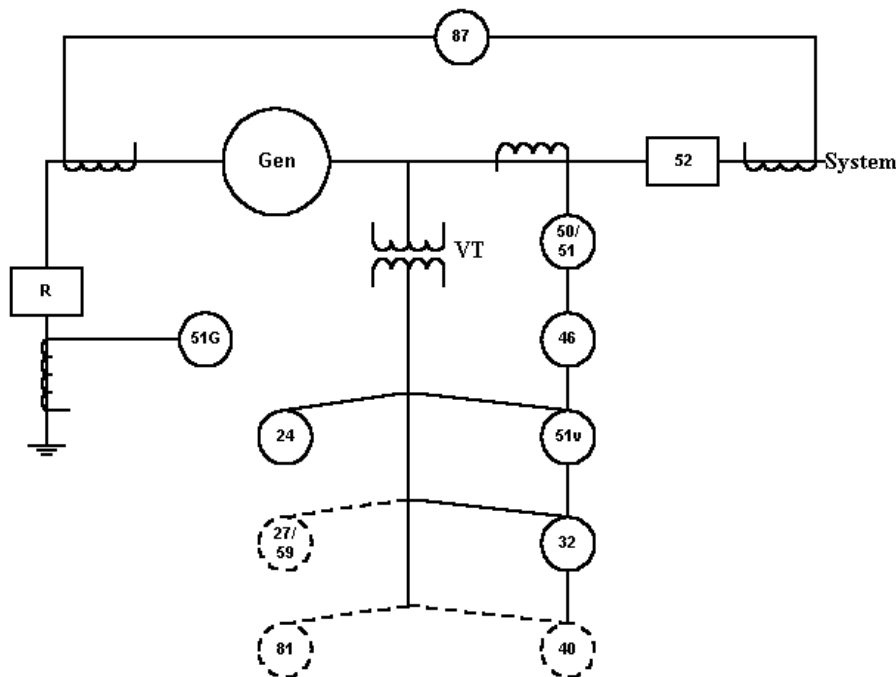


Figure 5.10.: Typical protection for a direct-grounding generator [Bla98]

Overload protection of the generator (49) is primarily used to provide backup protection for bus or feeder faults rather than to protect the generator itself [HoP95]. Therefore, this protection is not considered in the simulation of large system disturbances.

Generator overspeed cannot occur until the generator is disconnected from the network because the system frequency forces the generator to stay close to synchronous speed. The protection (85) is usually provided on the prime mover using electro-hydraulic or electronic

equipment [HoP95]. Such situations when the generator is disconnected from the network are not of interest for the simulation of large system disturbances.

When the prime mover supply is removed while the generator is connected to the power system and the field excited, the power system will drive the unit as a synchronous motor. This situation can be particularly dangerous for steam and hydro units. This abnormality can be detected using various detection techniques but a supplementary reverse power relay (32) is generally recommended [Bla98],[HoP95]. Hidden failures for this protection are not considered in the simulation of large system disturbances for the same reasons as for the overspeed protection

Power systems are not completely symmetrical and loads can be unbalanced so that a small amount of negative sequence is present during normal operation. The protection against negative sequence currents (46) is based on inverse time overcurrent relays using a time characteristic given in [Bla98]. The modelling of unbalanced load is not considered in the simulation of large system disturbances and consequently this protection will not be discussed further here.

Abnormal voltages and frequencies can be further divided into two subcategories. The first category describes abnormalities related to voltages such as over/under voltages, while the second category deals with over/under frequencies.

Overvoltage protection (59) has to protect the generator from the thermal damage to the magnetic caused by excessive flux in the magnetic circuits [HoP95]. Overvoltage might cause overexcitation that can lead the generator to operate beyond its capability limits (see section 6.2.1.1). Overexcitation limiters primarily regulate overexcitation, but if the regulation has no effects, the field breaker will be tripped as the last possible option. Undervoltage protection (27) is designed to protect the generator auxiliary system, which can be seriously damaged by undervoltage conditions and might affect the generator control functions. A combination of a high voltage and a low frequency can cause excessive magnetic flux, which can seriously damage the generator. Therefore, a voltage-frequency quotient known as the V/Hz ratio has been used in V/Hz limiters. Protection scheme (24) prevents excessive variations of this ratio.

Underexcitation, like overexcitation, is regulated by underexcitation limiters. If the regulation has no effect an impedance relay known as a loss of excitation relay (40) can be used to trip the field breaker. The limiters and the loss of excitation relay belong to the excitation control

and protective devices and will be described together with overexcitation limiters in section 5.3.2.

Overfrequency protection prevents abnormal generator speed by using the mechanical overspeed device. It is possible sometime to use an overfrequency relay (81) as backup to the mechanical device. On the other hand, underfrequency protection (81) is focused on mechanical resonant stress, which develop as a result of deviations from synchronous speed and affects the turbine more than the generator [HoP95]. Special protection schemes involving load shedding have been used for underfrequency protection. HHHs related to these special protection schemes are not considered in the simulation of large system disturbances.

A common, catastrophic malfunction that has been reported many times involves the inadvertent closing of high voltage breakers or switches while the unit is on turning gear or at some speed less than synchronous speed [HoP95]. The protection scheme (67) is able to detect inadvertent closing and its HHH is discussed in 5.3.3

5.3.1. Stator Phase – Fault Protection

The fundamental technique of differential protection used to protect the stator from phase faults is shown in Fig.5.10, where this protection is denoted as (87). If both current transformers give the same secondary current for the same primary current, an ideal differential protection would not required restraint coils (see Fig. 5.9). However, the difference in secondary current is often caused by variations in manufacturing tolerances and the unequal length of leads to the relay [HoP95]. The percentage differential relay solves this problem by using restraint coils that enable the relay to operate only if the current through the operating coil is a constant or a variable percentage of the total restraint current. Therefore, the larger the restraint current, the larger the trip current through the operating coil must be. In the case where a restraint coil is shorted, high loading conditions on the generator might cause unnecessary operation of this relay. A HHH can therefore appear for heavy load currents if the restraint coil is shorted, as happens for the transformer differential protection described in section 5.2.7.

5.3.2. Excitation System Control and Protective Devices

A modern excitation control system is much more than a simple voltage regulator [Kun94]. It includes various control, limiting and protective devices, which interface with each other like as shown in Fig. 5.11. These devices include ac and dc regulators, excitation system stabilising circuits, Power System Stabilisers (PSS), load compensators, underexcitation limiters with loss of excitation protection, overexcitation limiters, Volts per Hertz limiters and protection and field shorting circuits.

The basic function of the ac regulator is to maintain the generator stator voltage. The dc regulator holds constant the generator field voltage and is commonly referred as manual control [Kun94]. The dc regulator can be used for testing, start-up and as a back-up for the ac regulator.

The excitation system stabilising system contains either series or feedback compensation, and it is used to improve the dynamic performances of the control system [Kun94].

The PSS uses auxiliary stabilising signals to control the excitation system in order to improve the dynamic performance of the power system. This performance is improved by the damping of system oscillations [Kun94].

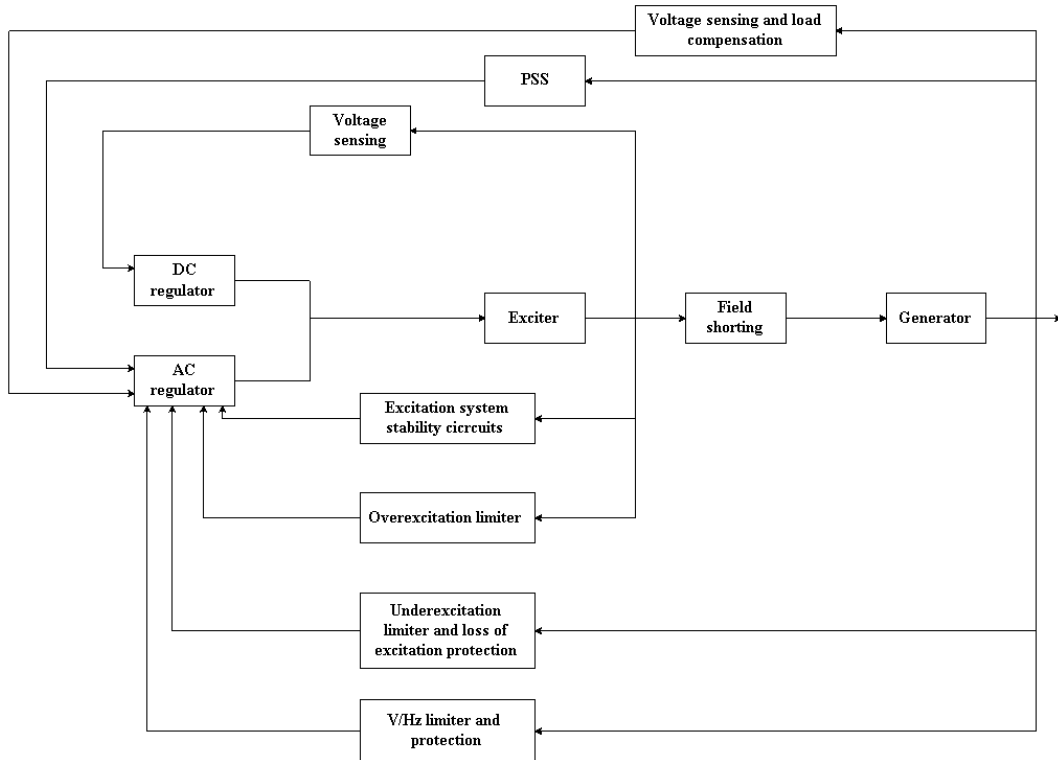


Figure 5.11.: Excitation system control and protective scheme[Kun94]

An Automatic Voltage Regulator (AVR) normally controls the stator voltage of the generator. The controlled voltage can be the voltage behind the step-up transformer if a load compensator provides the value of the voltage drop between the stator terminals and the high voltage terminals of the step-up transformer.

Limiters and devices intended to protect the generator are the parts that are the most important for the work described in this thesis. The UndereXcitation Limiter (UXL) is used to prevent a reduction of generator excitation to a level where the small-signal stability limit or the stator core end region heating limit is exceeded. The control signal from the UXL is derived from a combination of either voltage and current or active and reactive power. These limits are determined by the signal exceeding a reference level [Kun94]. If the UXL is not able to keep the excitation level at a reference level then the loss of excitation relay will be activated. It will first provide an alarm to the plant operator. After a time delay, this alarm is followed by a trip. The logic diagram for the loss of excitation scheme is shown in Fig. 5.12. The scheme uses the distance relay *Z* to measure the distance to the capability curve and the directional relay *D* detects flows *into* the generator. There are two voltage relays *V* that can be *activated* when the voltage drop is *within* predefined limits. The first, whose contacts are normally closed, trips the field breaker while the second, whose contacts are normally open, activates an alarm. If the distance to the capability curve is beyond the tolerance of *Z* and the power system can supply reactive power to the generator (*D* close its contacts), without a significant drop in voltage, an alarm is sounded for possible corrective actions. After a time delay, this is followed by a shutdown trip. However, if the voltage is below a predefined voltage setting (87-80%), tripping is initiated within 0.2-0.3 seconds [Bla98]. The time delay is provided by the timer coil *X*. A typical HHF exists when the voltage relay *V*, whose contacts are normally closed, cannot pick up, and causes an unwanted trip of the generator after 0.2-0.3 seconds.

The OvereXcitation Limiter (OXL) protects the generator from overheating because of a prolonged excess in field current. The OXL is thus able to detect high field current conditions and send a request to the ac regulator to ramp down the excitation. If this is not successful, the OXL trips the ac regulator and transfers its control to the dc regulator. If the dc regulator is still not able to reduce the excitation, the limiter can initiate an exciter field breaker trip and a unit trip [Kun94]. Various permanent defects within the ac and dc regulators can be HHF's. These HHF's can cause an unnecessary unit trip. For the sake of simplicity and brevity these HHF's will not be analysed in details in this section. Special attention in this thesis is paid to the hidden failure modes that were the most important contributing factor in recent system disturbances (see Chapter 2).

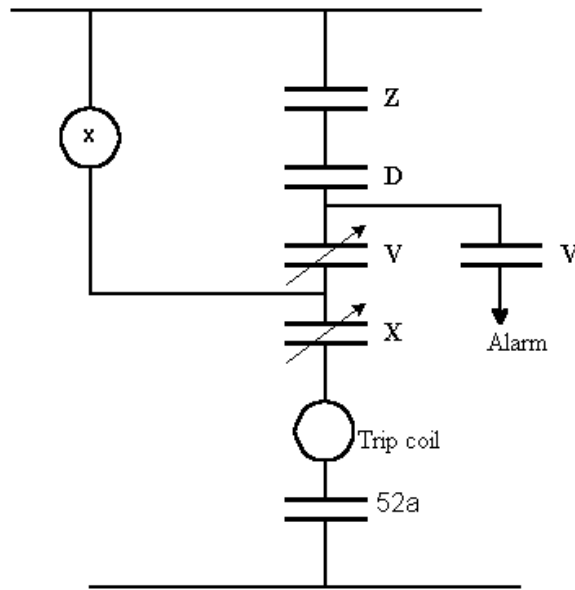


Figure 5.12.: Logic diagram for loss of excitation relay

The Volts per Hertz limiter and the Volts per Hertz protection are used to protect the generator and its step-up transformer from damage due to excessive magnetic flux resulting from a low frequency or an overvoltage. The V/Hz limiter controls the field voltage so as to limits the generator voltage when the measured V/Hz value exceeds a predefined value. The V/Hz protection trips the generator, when the V/Hz value exceeds a predefined value for a specified time. Because of its simple logic, V/Hz protection is unlikely to be responsible for a HHF. However, if the V/Hz limiter does not work properly the V/Hz protection could trip the generator unnecessarily.

5.3.3. Inadvertent Energisation

A common, catastrophic failure that has been reported many times involves the inadvertent closing of high voltage breakers or switches while the unit is on turning gear or at some speed less than synchronous speed [HoP95]. If the generator is energised in this way, it behaves as a synchronous motor or a generator that has been badly synchronised. This can destroy the shaft or another piece of rotating equipment.

The response of the inadvertent energisation protection scheme, as shown in Fig. 5.13 is to trip the generator high-voltage, field and auxiliary breakers [HoP95]. When the frequency decreases, the frequency relay F keeps its contacts closed. During normal and voltage-

balanced conditions, the voltage balance relay VB is closed, which activates timer 81x and its relay after a time delay. The generator high-voltage, field and auxiliary breakers will be tripped only if the O/C relay is energised. Under this scenario, if the O/C relay contacts are always closed the generator breakers might trip unnecessarily. Therefore, a closed O/C contact represents a HHF that might be activated during abnormal system conditions.

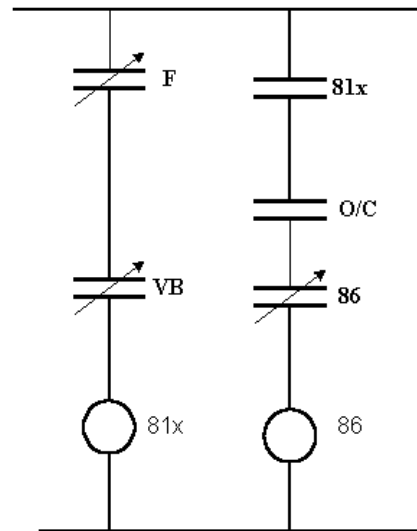


Figure 5.13.: Logic diagram of inadvertent energisation

5.4. Vulnerability Region

The technique presented in this work identifies the most vulnerable protection scheme in terms of HHF, which can be revealed by a random fault or abnormal system conditions. Tamnroglak in [Tam94] suggests that if the event that triggers a disturbance is a fault on a circuit, the circuits “surrounding” the faulted circuit are more vulnerable to hidden failures than all the other circuits. A *vulnerability region* can thus be defined for each circuit based on the possible hidden failure modes of each protection scheme. A vulnerability region in this work is considered as the set of power system circuits that might be incorrectly removed during abnormal power system conditions. These conditions are usually the result of initial events such as a random fault or sudden changes in the system conditions on a nearby circuit. The concept of vulnerability region is based on the following assumptions [KiN02]:

- The initial event is a random fault.
- The protection system of the faulted circuit operates properly and clears the fault.

- Initial events such as faults or sudden changes in system conditions on any circuit in the power system can expose protection system defects in the vulnerability region of the circuit where these ones have occurred.

In other words, it is assumed that a multiple non-credible contingency might arise from a single credible contingency. Such a situation is certainly unexpected and usually outside the scope of most security criteria

The size of the vulnerability region depends on the location of the initial event and the design of the protection system in the area surrounding this event. Various protection system defects can cause a hidden failure and an incorrect (unnecessary) outage following an initial event. Sections 5.2 and 5.3 discuss in detail the possible defects in the protection of generators, transformers and transmission circuits that might occur.

A simple example of vulnerability region is shown in Fig 5.14. The shown vulnerability region encompasses the lines: A-C, A-D, and partially lines C-F, D-E and D-G. Thus, any fault in this vulnerability region might cause some of the hidden failure modes given in 5.2.1-5.2.6. and the unnecessary tripping of the breaker at bus B. The size of the vulnerability region in this case is limited to 1.2 times the longest line behind bus A (line A-C), which is set as the third zone setting of distance protection for relay at the side B.

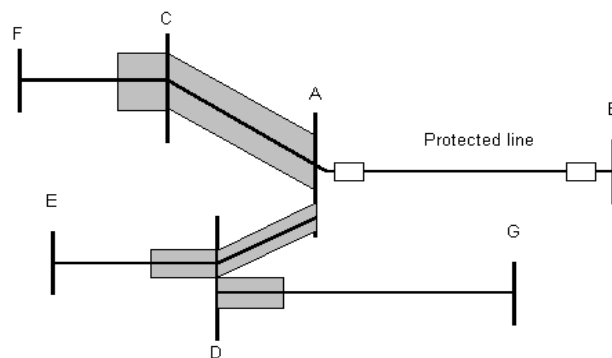


Figure 5.14.: – A simple example of vulnerability region

6

Search for Disturbances Based on the Distance to Voltage Collapse

Voltage collapse has become a serious threat for power systems in the last twenty years. Considerable academic and industry efforts have been taken on analysis and planning in order to prevent catastrophic events caused by voltage instability. Therefore, voltage instability and voltage collapse are very important power system phenomena. A significant amount of time was thus devoted to analysis, development and integration procedures that can correctly represent these phenomena in the simulation of large system disturbances.

Various definitions of voltage in/stability are proposed in the literature. The most frequently used was developed by the IEEE Working Group on Voltage Collapse [CTF94]:

“Voltage stability is the ability of a power system to maintain voltage so that when load admittance is increased, load power will increase, and so both power and voltage are controllable”.

Similarly, Kundur in [Kun94] defines voltage stability as the ability of a power system to maintain steady acceptable voltages at all buses in the system under normal operating conditions and after being subjected to a disturbance. Consequently, when a disturbance, an increase in load demand or a change in system conditions causes a progressive and uncontrollable voltage drop a power system enters a state of voltage instability. Kundur suggests in [Kun94] that voltage instability is a local phenomenon whose consequences might have widespread effects. Van Cutsem and Vournas confirm that that voltage instability might lead to voltage collapse [CV98].

Various definition of voltage collapse can be found in the literature The definition suggested by the IEEE Working Group on Voltage Collapse [CTF94] is:

“Voltage Collapse is the process by which voltage instability leads to loss of voltage in a significant part of a power system”

Another definition given in [Tay94] is slightly different emphasising the difference between blackout and partial voltage collapse:

“A power system at a given operating state and subject to a given disturbance undergoes voltage collapse if post disturbance equilibrium voltages are below acceptable limits. Voltage collapse may be total(blackout) or partial”

Loss of voltage or voltages below acceptable limits increase the reactive system requirements, force reactive devices on their Q limits and initiate a mutual interaction between different control and protective devices in a power system. The outcomes of such mechanism might be catastrophic: generating units can be tripped and a significant amount of load can be lost. Therefore, such outcomes can be treated as large system disturbances. The simulation of large system disturbances is not really focused on repeating already seen mechanisms of voltage collapse. Instead, voltage stability is seen as the driving force, in the sense that the next event to occur in the sequence of events that lead to a large system disturbance is selected because it is foreseen as the worst event to happen from the voltage stability point of view. Therefore, a voltage stability procedure as a part of the simulation of large system disturbances should be able to choose the most dangerous event from a set of possible events. Any of these possible events will be measured using the procedure, which means that the events will be compared based on this measure. The procedure should be able to assess the “size” of both local and global voltage problems and select the worst possible event.

In order to develop such procedure the following issues related to voltage stability were investigated:

- Different voltage instability mechanisms were studied.
- The mathematical models used in voltage stability studies were reviewed in order to find the model that best suit the requirements of the simulation of large system disturbances.

- Once the general model was selected, various methods were studied in order to find the most appropriate one.
- Some of these methods were developed and tested on both a small and a large system.

6.1. Voltage Instability Mechanisms

According to various papers and books on voltage stability, the driving force of voltage instability is load. On the other hand, different authors suggest different time scales and different classification of voltage instability. The following classification of voltage stability with respect to time-scale is suggested in [Kun94]:

- Short-term or transient: 0 to 10 seconds
- Mid-term: 10 seconds to a few minutes
- Long-term: a few minutes to tens of minutes.

Taylor [Tay94] suggests the same classification, while Van Cutsem and Vournas merge the mid-term and long-term categories [CV98].

Short-term response is within a few seconds and is often called transient dynamic response. The mid-term response represents the transition between short-term and long-term responses. In mid-term stability studies the focus is on the synchronising power oscillations between machines, including the effects of some of the slower phenomena. The distinction between mid-term and long-term stability is primarily based on the phenomena being analysed and the power system representation rather than the time scale [Kun94]. Long-term stability analysis assumes that inter-machine synchronising power oscillations have been damped resulting in a uniform system frequency [Kun94].

According to the suggested time scale classification, the following voltage instability mechanisms are possible [Tay94]:

1. The same time frame of a few seconds is for short-term voltage stability and transient angle stability. The distinction between voltage instability and rotor angle instability has not yet been clarified [Tay94] and it is difficult to judge whether voltage collapse causes loss of synchronism or loss of synchronism causes voltage collapse. The South Florida blackout on May 17, 1985 showed that voltage decayed faster than frequency, which delayed

underfrequency load shedding and caused a significant voltage drop in just a few seconds [Tay94]. The three major instability mechanisms related to this period are identified in [CV98]. Stalling of induction motors either after a disturbance that increases the total transmission impedance or short-circuits are the first two mechanisms, while the third mechanism is called oscillatory voltage instability.

2. Mid-term voltage instability might occur when a large system disturbance hits a power system that has high power flow between its sink and source area. Voltages decrease due to a disturbance (line, transformer, generator or capacitor bank trip near the sink area), but the voltage drop is limited because low voltages reduce the system load [Cla90]. On-load-tap-changing transformers try to restore voltages in the sink area, and thereby restore the load power levels. Consequently, the rising load increases transmission line currents and reactive losses, while low voltages reduce the reactive power produced by the transmission line capacitances and capacitor bank. Therefore, voltages decrease further and a fast reactive support is needed. Nearby generators respond by increasing their reactive output, but quickly hit their reactive limits causing the activation of protective devices in order to prevent excessive field or armature currents. This shifts the reactive burden to more remote plants, increasing reactive losses and further decreasing voltages, worsening the reactive shortage and pushing even remote generation to their reactive limits. When the tap changers in the sink area hit their limits voltages in the sink area finally drop, which stabilise the system voltages. If there is enough drop in the sink load, catastrophe might be avoided. On the other hand, if the sink area contain much industry, motors begin stalling and consequently drop from the system. Van Cutsem and Vournas in [CV98] suggest some variations of the mechanism given by Taylor. Thus, instead of one they propose three sub-mechanisms, where the first one is the consequence of load trying to restore their pre-disturbance power through the action of On-Load-Tap-Changing transformers. The second is practically similar to the first one, except that a delayed corrective action is applied. The third sub-mechanism leading a power system to voltage instability through slowly growing oscillations, has not been observed in an actual power system.
3. Long-term voltage instability is primarily driven by a very large and rapid load build-up. Operator actions such as the timely activation of appropriate reactive devices and load shedding are required to save the system [Tay94]. Van Cutsem and Vournas [CV98] suggest the three sub-mechanisms based on the short-term instability induced by long-term dynamics.

It should be noted that many power system components play a role in voltage stability, but only some of them will significantly participate in a particular instability mechanism. These components are classified in Table 6.1

Table 6.1 -Power system components response

Short-Term Dynamics	1. Automatic Voltage Regulator (AVR)
	2. Induction Motors
	3. HVDC component
	4. Static VAR Compensator (SVC)
	5. Undervoltage Load Shedding
	6. Protection System Operation
	7. Overexcitation Limiters (OXL)
Long-Term Dynamics	1. On Load Tap Changing Transformer(OLTC)
	2. Automatic Generator Control (AGC)
	3. Overexcitation Limiter (OXL)
	4. Boiler Dynamics

6.2. Dynamic Versus Static Models

There is considerable debate between researchers on whether voltage stability should be assessed through static or dynamic models. The former means that voltage instability can be analysed using only algebraic network equations and the Jacobian matrix of power flow equations. The latter deals with the machine differential equations and algebraic network equations simultaneously. Therefore, the dynamic model is more complex and more computationally demanding and requires additional engineering work for the analysis of the results. Moreover, dynamic analysis does not readily provide information regarding the sensitivity or degree of instability [GMK96]. Static analysis involves only the solution of algebraic equations and is suitable for studies where voltage stability limits have to be determined for many cases [GMK96]. It should be emphasised that voltage stability is dynamic by nature but static tools can be acceptable for simpler and faster analysis [CV98].

It has been mentioned already that the simulation of large system disturbances requires a procedure able to identify the worst foreseen outages. The worst foreseen outages generate states of power system closer to voltage collapse. Therefore, such procedure has to be able to compare different outages using the distance to voltage collapse. It is clear then that the procedure has to be based on a very fast and robust calculation of the distance to voltage collapse. This was the main motivation for choosing a calculation based on a purely static model and power flow Jacobian. Therefore, in this thesis, the focus will be on the static models and methods based on the power flow Jacobian. For the sake of generality and simplicity, dynamic models will be briefly discussed in section 6.2.1. The static model based on power flow equations is discussed in section 6.2.2.

6.2.1. Dynamic Model

Table 6.1 classifies the important power system components with respect to their time response. All important power system components should be included in the complete dynamic model. Different authors have different criteria to assess the importance of each component, but all of them agree that modelling all components would be an extremely difficult and time-consuming task.

A general dynamic model encompasses algebraic network equations, differential equations for short-term dynamics and a combination of differential and discrete time equations for long-term dynamics. These equations are given by the following equations, respectively [CV98]:

$$\mathbf{0} = \mathbf{g}(\mathbf{x}, \mathbf{y}, \mathbf{z}_c, \mathbf{z}_d), \quad (6.1a)$$

$$\dot{\mathbf{x}} = \mathbf{f}(\mathbf{x}, \mathbf{y}, \mathbf{z}_c, \mathbf{z}_d), \quad (6.1b)$$

$$\mathbf{z}_c = \mathbf{h}_c(\mathbf{x}, \mathbf{y}, \mathbf{z}_c, \mathbf{z}_d), \quad (6.1c)$$

$$\mathbf{z}_d(k+1) = \mathbf{h}_d(\mathbf{x}, \mathbf{y}, \mathbf{z}_c, \mathbf{z}_d(k)), \quad (6.1d)$$

where \mathbf{y} represents the vector of bus voltages, \mathbf{x} is the short-term state vector, \mathbf{z}_c and \mathbf{z}_d are the continuous and discrete long-term state vectors, respectively.

The model given by equations (6.1a - 6.1d) is further extended in Table 6.2 using differential and auxiliary equations for many of the components given in Table 6.1. The main characteristics of the model given in Table 6.2 can be summarised as follows:

- The network equations (6.1a) are complex equations, where the bus voltage vector V is unknown and can be expressed in terms of the current injection vector (I) and the network bus admittance matrix Y .
- Short-term differential equations encompass generators, AVRs, induction motor and only one equation of the OXL model given in Fig. 6.2. All models contain differential equations written in the form given by (6.1b) and auxiliary equations (algebraic equations, $\dot{x} = \theta$). The description of the used variables is given in the last column of Table 6.2 and in Fig. 6.1 and Fig. 6.2. For the sake of simplicity the dimensions of the state vectors (column 2) are omitted. The simple generator model given in Table 6.2 relies on the following assumptions [CV98]:

- the transformer voltages are neglected,
- the speed deviations are negligible compared with the nominal angular frequency,
- the armature resistance is neglected,
- magnetic saturation is neglected.

These equations assume a very simple block model for the AVR, whose inputs are magnitude of the terminal voltage (V_i), the reference voltage V_{io} and the output of the OXL (x_{oxli}). Load modelling in voltage stability studies requires the identification of load composition in order to form a complete load model. Van Cutsem and Vournas in [CV98] aggregate load using an exponential load characteristic, induction motor and shunt compensation. In Table 6.2, only the model of induction motor is given, all other models are undemanding and can be found in various books. It should be pointed out that only one of the two OXL state variable are considered such as continuous long term variable x_t , while the second is short-term variable x_{oxli} (see Table 6.2 and Fig. 6.2).

Table 6.2 – General Dynamic Model

Type	Variable	Equations	Description
$\theta = g(x, y, z_c, z_d)$	$y = \begin{bmatrix} \vdots \\ v_{xi} \\ \vdots \\ v_{yi} \\ \vdots \end{bmatrix}$	$\theta = I - VY;$ $V_i = v_{xi} + jv_{yi};$ $I_i = i_{xi} + ji_{yi};$	V - the vector of bus voltages Y -the network bus admittance matrix I - the vector of injected current
$\dot{x} = f(x, y, z_c, z_d)$	$x = \begin{bmatrix} \vdots \\ \delta_i \\ \dot{\delta}_i = \omega_i \\ E'_{qi} \\ v_{fdi} \\ x_{oxli} \\ s_j \\ \vdots \end{bmatrix}$	<p>i^{th} Generator:</p> <p>1.The motion equation:</p> $\frac{2H_i}{\omega_0} \ddot{\delta}_i = T_{mi} - T_{ei}$ <p>2.Field flux decay equations:</p> $\dot{E}'_{qi} = \frac{-E'_{qi} + E_{fi} - (X_{di} - X'_{di})i_{di}}{T'_{doi}}$ <p>3.Auxillary equations:</p> $E_{fi} = v_{fdi}$ $E_{qi} = i_{fdi}$ $i_{di} = i_{xi} \sin \delta_i - i_{yi} \cos \delta_i$ $i_{xi}, i_{yi} = f(\delta_i, X_{qi}, X'_{di}, v_{xi}, v_{yi})$	H_i - the inertia constant T_{mi} -the mechanical torque T_{ei} -the electrical torque ω_0 - the nominal angular frequency δ_i - the rotor angle E'_{q} -the <i>emf</i> behind transient reactance E_{fi} -the <i>emf</i> proportional to field voltage X_{di}, X'_{di} -direct normal and transient reactance i_{di} -the armature current T'_{doi} -the open circuit transient time constant E_{qi} -the no load <i>emf</i>
		<p>AVR of the i^{th} generator:</p> $\dot{v}_{fdi} = \begin{cases} 0, \text{ if } v_{fdi} = v_{fdi}^{\max} \\ 0, \text{ if } v_{fdi} = v_{fdi}^{\min} \\ \frac{-v_{fdi} + G_i(V_{io} - V_i - x_{oxli})}{T_i} \end{cases}$	<p>Figure 6.1.: AVR model [CV98]</p>
		<p>Induction motor:</p> <p>1.The motion equation</p> $\dot{s}_j = \frac{1}{2H_j} (T_{Mj} - P_{Mej})$ <p>2.Auxiliary equation</p> $P_{Me} = f(v_{xj}, v_{yj}, R_{rj}, X_{rj}, X_{sj}, s_j)$	s_j -the motor slip, T_{Mj} -the mechanical torque P_{Mej} - the electrical power R_{rj}, X_{rj}, X_{sj} -induction motor parameters,

Table 6.2 – General Dynamic Model

$z_c = h_c(x, y, z_c, z_d)$	$z_c = \begin{bmatrix} \vdots \\ x_t \\ \vdots \end{bmatrix}$	<p style="text-align: center;">OXL of the i^{th} generator:</p> <p>1.The non-windup limited integrator</p> $\dot{x}_t = \begin{cases} 0, & \text{if } x_t = K_2, x_2 \geq 0 \\ 0, & \text{if } x_t = -K_1, x_2 < 0 \\ x_2, & \text{otherwise} \end{cases}$ <p>2.The output integrator</p> $x_{oxli} = \begin{cases} 0, & \text{if } x_{oxli} = 0 \text{ and } x_3 < 0 \\ K_i x_3, & \text{otherwise} \end{cases}$ <p>1.Auxillary equations</p> $x_2 = \begin{cases} S_1(E_{qi} - I_{fdi}^{lim}) \text{ if } E_{qi} > I_{fdi}^{lim} \\ S_2(E_{qi} - I_{fdi}^{lim}), & \text{otherwise} \end{cases}$ $x_3 = \begin{cases} E_{qi} - I_{fdi}^{lim}, & \text{if } x_t \geq 0 \\ -K_r, & \text{otherwise} \end{cases}$ $E_{qi} = E'_{qi} + (X_{di} - X'_{di})i_{di}$	<p style="text-align: center;">See Figure 6.2</p>
$z_d(k+1) = h_d(x, y, z_c, z_d(k))$	$z_d = \begin{bmatrix} \vdots \\ r \\ \vdots \end{bmatrix}$	<p style="text-align: center;">OLTC transformer:</p> <p>1.OLTC logic</p> $r_{k+1} = \begin{cases} r_k + \Delta r, & \text{if } V_l > V_{lbase} + d, r_k < r^{\max} \\ r_k - \Delta r, & \text{if } V_l < V_{lbase} - d, r_k > r^{\min} \\ r_k, & \text{otherwise} \end{cases}$	<p>r -the tap changer value, k –time instant d -one half of the OLTC dead-band, V_{lbase} - reference voltage, V_l - the magnitude of controlled voltage, r^{\min}, r^{\max} -the lower and upper changer limits</p>

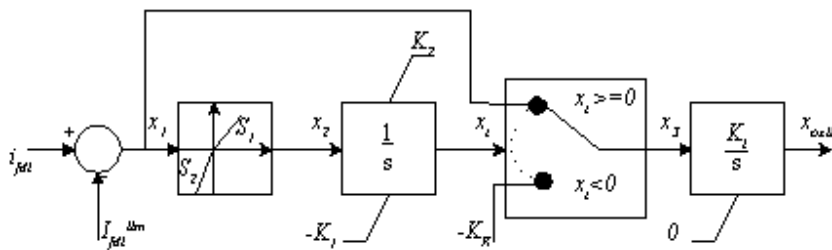


Figure 6.2.: OXL block model [CV98]

- The state vector of long-term dynamics that represents continuous variable z_c contains only one type of variable x_t , associated with OXL. It should be noted that the other power system components (boiler dynamics and AGC) are not considered in this general model. The form given by (6.1c) can be used to represent the thermostatic and aggregate load recovery model [CV98]. The state vector of long-term dynamic that represents discrete variables contains in this case only the tap changer discrete values. This vector can be extended with shunt susceptances, or with variables associated with secondary voltage and frequency controllers if these are digital.

6.2.2. Static Model

The static model based only on the network equation (6.1a) has been widely used in the research on voltage stability. Various techniques and indicators based on the network equation have been derived to estimate the distance from the current operating point of a power system to the voltage collapse point. These techniques and indicators will be discussed in more details in the following paragraphs.

The power flow calculation methods can be directly derived from the network equation given in Table 6.2:

$$\mathbf{I} = \mathbf{YV}, \quad (6.2)$$

where \mathbf{I} is the vector of injected node current, \mathbf{Y} is the network bus admittance matrix and \mathbf{V} is the vector of node voltages. Two methods can be used to solve the system of complex equations given by (6.2). The first one based on an iterative approach proposed by Seidel deals with complex variables and uses the new values of unknown complex voltages on the right hand side as soon as they are computed [SEA68],[GS94],[Kun94]. The second one is based on the Newton-Raphson (N-R) iterative technique for solving a set of non-linear equations. This set can be obtained as follows.

Equation (6.2) for node p is:

$$I_p = \sum_{q=1}^n Y_{pq} V_q, \quad (6.3)$$

where n is the total number of nodes. The equation (6.3) can be brought to the following form using elementary algebraic operations:

$$V_p I_p^* = S_p = P_p + jQ_p = V_p \sum_{q=1}^n Y_{pq}^* V_q^* . \quad (6.4)$$

The last equation can be separated into real and imaginary parts:

$$P_p = \text{Re} \left\{ V_p \sum_{q=1}^n Y_{pq}^* V_q^* \right\}, \quad p=1,2,\dots,n \quad (6.5)$$

$$Q_p = \text{Im} \left\{ V_p \sum_{q=1}^n Y_{pq}^* V_q^* \right\}, \quad p=1,2,\dots,n. \quad (6.6)$$

In terms of polar co-ordinates these equations can be expressed as:

$$P_p - |V_p| \sum_{q=1}^n \left(|V_q| (G_{pq} \cos \theta_{pq} + B_{pq} \sin \theta_{pq}) \right) = 0, \quad p=1,2,\dots,n \quad (6.7a)$$

$$Q_p - |V_p| \sum_{q=1}^n \left(|V_q| (G_{pq} \sin \theta_{pq} - B_{pq} \cos \theta_{pq}) \right) = 0, \quad p=1,2,\dots,n \quad (6.7b)$$

where $V_p = |V_p| e^{j\theta_p}$, $\theta_{pq} = \theta_p - \theta_q$ and $Y_{pq} = G_{pq} + jB_{pq}$. Similarly, using the rectangular co-ordinates:

$$P_p - \sum_{q=1}^n (e_p (G_{pq} e_q - B_{pq} f_p) + f_p (f_q G_{pq} + e_q B_{pq})) = 0, \quad p=1,2,\dots,n \quad (6.8a)$$

$$Q_p - \sum_{q=1}^n (f_p (G_{pq} e_q - B_{pq} f_q) - e_p (f_q G_{pq} + e_q B_{pq})) = 0, \quad p=1,2,\dots,n \quad (6.8b)$$

where $V_p = e_p + jf_p$.

Both version (6.7) and (6.8) of the power flow equations have been extensively used by various researchers for voltage stability assessment. The authors in [ISE90],[TMI83],[Ove94] use the polar co-ordinate version of the power flow in order to determine the maximal loadability points [CV98]. On the other hand, the authors in ([CCC95], [AC92], [GMK92], [LSA92], [LAH93], [CSQ95]) use the rectangular version of the power flow equations to estimate the distance to voltage collapse. The author of this thesis has not observed any significant differences between their convergence characteristics while testing them on different power system models. On the

other hand, the authors in [ISE90] state that the polar version has better convergence characteristics.

If \mathbf{P} and \mathbf{Q} represent equations (6.7a) and (6.7b), respectively, the iterative N-R process in polar version yields the following form at iteration k :

$$\begin{bmatrix} \Delta \mathbf{P} \\ \Delta \mathbf{Q} \end{bmatrix}_k = \begin{bmatrix} \frac{\partial \mathbf{P}}{\partial \theta} \Big|_k & \frac{\partial \mathbf{P}}{\partial \mathbf{V}} \Big|_k \\ \frac{\partial \mathbf{Q}}{\partial \theta} \Big|_k & \frac{\partial \mathbf{Q}}{\partial \mathbf{V}} \Big|_k \end{bmatrix} \begin{bmatrix} \Delta \theta \\ \Delta \mathbf{V} \end{bmatrix}_k = \mathbf{J}^k \begin{bmatrix} \Delta \theta \\ \Delta \mathbf{V} \end{bmatrix}_k, \quad (6.9)$$

where $\Delta \mathbf{P}$ and $\Delta \mathbf{Q}$ are the vectors of active and reactive power changes, \mathbf{J} is the Jacobian matrix, and $\Delta \theta$ and $\Delta \mathbf{V}$ are the vectors of incremental angle and voltage changes.

Similarly, using rectangular co-ordinates and equations (6.8a) and (6.8b) becomes:

$$\begin{bmatrix} \Delta \mathbf{P} \\ \Delta \mathbf{Q} \end{bmatrix}_k = \begin{bmatrix} \frac{\partial \mathbf{P}}{\partial \mathbf{e}} \Big|_k & \frac{\partial \mathbf{P}}{\partial \mathbf{f}} \Big|_k \\ \frac{\partial \mathbf{Q}}{\partial \mathbf{e}} \Big|_k & \frac{\partial \mathbf{Q}}{\partial \mathbf{f}} \Big|_k \end{bmatrix} \begin{bmatrix} \Delta \mathbf{e} \\ \Delta \mathbf{f} \end{bmatrix}_k = \mathbf{J}^k \begin{bmatrix} \Delta \mathbf{e} \\ \Delta \mathbf{f} \end{bmatrix}_k. \quad (6.10)$$

The partial derivatives of the Jacobian matrix \mathbf{J} in (6.9) and (6.10) can be obtained by making the first derivative of the equations (6.7) and (6.8) with respect to the rectangular and polar variables, respectively. The full expressions can be found in [SEA68],[GS94],[Kun94].

Instead of the full Jacobian given in (6.9), Kundur in [Kun94] uses the so-called reduced Jacobian matrix for static voltage stability assessment, which can be obtained by assuming that the vector of active power changes is equal to zero ($\Delta \mathbf{P} = \mathbf{0}$):

$$\mathbf{J}_R^k = \left(\frac{\partial \mathbf{Q}}{\partial \mathbf{V}} \right)_k - \left(\frac{\partial \mathbf{Q}}{\partial \theta} \right)_k \left(\frac{\partial \mathbf{P}}{\partial \theta} \right)_k^{-1} \left(\frac{\partial \mathbf{P}}{\partial \mathbf{V}} \right)_k = \mathbf{J}_4 - \mathbf{J}_3 \mathbf{J}_1^{-1} \mathbf{J}_2. \quad (6.11)$$

Assuming that $\Delta \mathbf{P} = \mathbf{0}$ and introducing the reduced Jacobian matrix \mathbf{J}_R one can obtain the linear relationship between the vector of reactive power and voltage changes:

$$\Delta \mathbf{Q} = \mathbf{J}_R \Delta \mathbf{V} \quad (6.12)$$

These equations (6.12) are essential for the so-called V-Q sensitivity analysis. In contrast with normally used Q-V curves traditionally used in engineering practise, the V-Q sensitivity analysis based on (6.12) analyses voltage stability from a system wide perspective.

The left hand side vectors in (6.9), (6.10) are known, while the vector composed of angles and voltage changes on the right hand side of (6.9) and the vector composed of the real and imaginary parts of the complex node voltages on the right hand side in (6.10) are unknown. The total number of unknown variables depends on the number of PQ (N_{pq}) and PV (N_{pv}) buses. If the total number of buses n is:

$$n = N_{pv} + N_{pq} + 1, \quad (6.13)$$

then the known and unknown variables in (6.9) and (6.10) are summarised in Table 6.3.

According to Table 6.3 the total number of equations for the polar version is equal to the total number of unknowns, which is not the case with the rectangular version. Therefore, the equations given in (6.8) must be extended with the following N_{pv} equations:

$$f_V = |V_p|^2 - e_p^2 - f_p^2 = 0, \quad (6.14)$$

which causes the following change in equation (6.10):

$$\begin{bmatrix} \Delta P \\ \Delta Q \\ \Delta |V|^2 \end{bmatrix}_k = \begin{bmatrix} \frac{\partial P}{\partial e} \Big|_k & \frac{\partial P}{\partial f} \Big|_k \\ \frac{\partial Q}{\partial e} \Big|_k & \frac{\partial Q}{\partial f} \Big|_k \\ -\frac{\partial f_V}{\partial e} \Big|_k & -\frac{\partial f_V}{\partial f} \Big|_k \end{bmatrix} \begin{bmatrix} \Delta e \\ \Delta f \end{bmatrix}_k = \mathbf{J}^k \begin{bmatrix} \Delta e \\ \Delta f \end{bmatrix}_k \quad (6.15)$$

Table 6.3 – Known and unknown variables in a power flow calculation

	<i>Known</i>	<i>Unknown</i>	<i>Total number of equations</i>
Polar	1. V_s, θ_s for slack bus	1. $ V_p , \theta_p$ for each PQ node	$2 * N_{pq} + N_{pv}$
	2. P_p, Q_p for each PQ node	2. θ_p for each PV node	1. $N_{pq} + N_{pv}$ equations of type (6.7a)
	3. $P_p, V_p $ for each PV node	$2 * N_{pq} + N_{pv}$	2. N_{pq} equations of type (6.7b)
Rectangular	1. e_s, f_s for slack bus	1. e_p, f_p for each PQ and PV node	$2 * N_{pq} + N_{pv}$
	2. P_p, Q_p for each PQ node	$2 * (N_{pq} + N_{pv})$	1. $N_{pq} + N_{pv}$ equations of type (6.8a)
	3. $P_p, V_p $ for each PV node		2. N_{pq} equations of type (6.8b)

6.2.1.1. Modelling requirements for the static model

The modelling of power system components that have a significant impact on voltage stability is included in the static model using the following consideration:

- Load characteristics are very important in voltage stability analysis. In this work, voltage dependent loads can be added to constant loads using the following equations:

$$P_p = P_p^0 (1 + k) + P_p^V \left(\frac{|V_p|}{V_p^0} \right)^\alpha, \quad (6.16)$$

$$Q_p = Q_p^0 (1 + k) + Q_p^V \left(\frac{|V_p|}{V_p^0} \right)^\beta, \quad (6.17)$$

where $P_p^0, k, P_p^V, V_p^0, \alpha, Q_p^0, Q_p^V, \beta$ are parameters that make composite load given by (6.16) and (6.17) [CSQ95].

- OLTC transformers also play a key role in mid-term voltage stability mechanism described in section in 6.1. Several approaches for the modelling of automatic tap adjustments have been found in [AlA82],[CB88],[PM71],[Sto74]. These can be categorised as follows:

- The tap position is modelled as an unknown variable instead of the controlled voltage. When the tap position hit its limits it must be fixed and replaced by the controlled voltage in the state vector.

- The controlled voltage is an unknown variable that must be kept within the specified limits using tap changers. Obviously, the tap position will be adjusted only when the controlled voltage is not within limits. The adjustment is based on $(\mathbf{B}'')^{-1}$ and the second cycle of the fast -decoupled power flow [CB88].

A serious drawback of the first approach is the variable replacement during the iterative procedure, which seriously perturbs the Jacobian \mathbf{J} , causing the propagation of perturbation to the subsequent iterations and frequently leading the iterative procedure to a solution quite different from the expected one. The second approach is based on a simplified sensitivity analysis and works reasonably well as a integral part of the fast-decoupled power flow as long as there are no interactions between tap changers or between tap changers and other power system elements [CB88],[CB88].

In order to avoid the drawbacks of both approaches, a new approach based on a full sensitivity analysis has been developed. It calculates the tap movements based on the inverse Jacobian matrix. However, only a few rows of the inverse Jacobian have to be calculated for each transformer whose controlled voltage is not within the limits, which makes this approach as fast as the one described in [CB88]. In order to avoid the interactions related to control adjustments, a special self-adjustment procedure is suggested. The detailed explanation of this approach can be found in [Ned02].

- When an SVC is operating within the normal voltage control range, it maintains bus voltage with a slight drop characteristic. However, when the SVC's voltage is not within the control range the SVC behaves like a capacitor or a reactor. The conventional way of modelling the behaviour of the SVC in the power flow is by a PQ node and an auxiliary PV node [Eri86],[HH92]. Modelling of SVCs in this thesis is based on the implicit model suggested in [You95] and [Bel97]. This model treats the SVC by means of one PQ node at which the reactive injection is a function of the voltage at the node [Bel97].
- The generator current limits dictate the generator reactive limits, and they are very important for the mid-term voltage instability mechanism described in 6.1. A generator capability diagram is shown in Fig. 6.3. One can see that reactive limits depends on the field heating limits represented in Fig. 6.3 by the constant excitation circle ("Constant E"), the armature current limits represented by the constant armature current circle ("Constant I_a "). Therefore,

6.3. Static Voltage Stability Indices

The estimation of the proximity to voltage collapse for all possible events is the main objective of voltage stability calculations in the simulation of large system disturbances. Based on this estimation, the worst foreseen event is the one whose estimated proximity is the smallest one. However, giving advantage to some events or omitting some of them should be based on a certain criterion. Such criterion is the driving force of the simulation because it gives directions to the simulation by worsening the system conditions as much as it is possible.

The chosen criterion in the simulation of large system disturbances is the distance to voltage collapse. Various voltage stability indices have been used to measure the distance to voltage collapse. Some of these were developed and compared in this work in order to find one that suits the requirements for both the accuracy of distance prediction and computational efficiency.

Various methods have been used to determine indices of voltage stability. A classification of these methods is shown in Fig. 6.4. This classification combines similar proposals given in [CFY90] and [CV98]. In general, all the steady state methods used for this purpose can be divided into two categories. The first one is concerned with the maximum power transfer capacity of the network or the existence of solved power flow case [CFY90]. The second category contains different methods, which test for the existence of a stable equilibrium point [CFY90].

This first category encompasses two types of the methods: based on multiple power flow solutions and load flow convergence. The former are related to the work done by Tamura and his associates, and in essence confirm that the existence of a pair of solutions of a power flow is related with voltage instability [IwT81],[TMI83],[TST89],[ISE90]. The indication of the existence is not a typical voltage stability indicator, but it is a very important warning that a system is approaching a voltage collapse. Thus, Iwamoto and Tamura introduce the so called “optimal multiplier” in order to prevent divergence of power flow for ill conditioned and

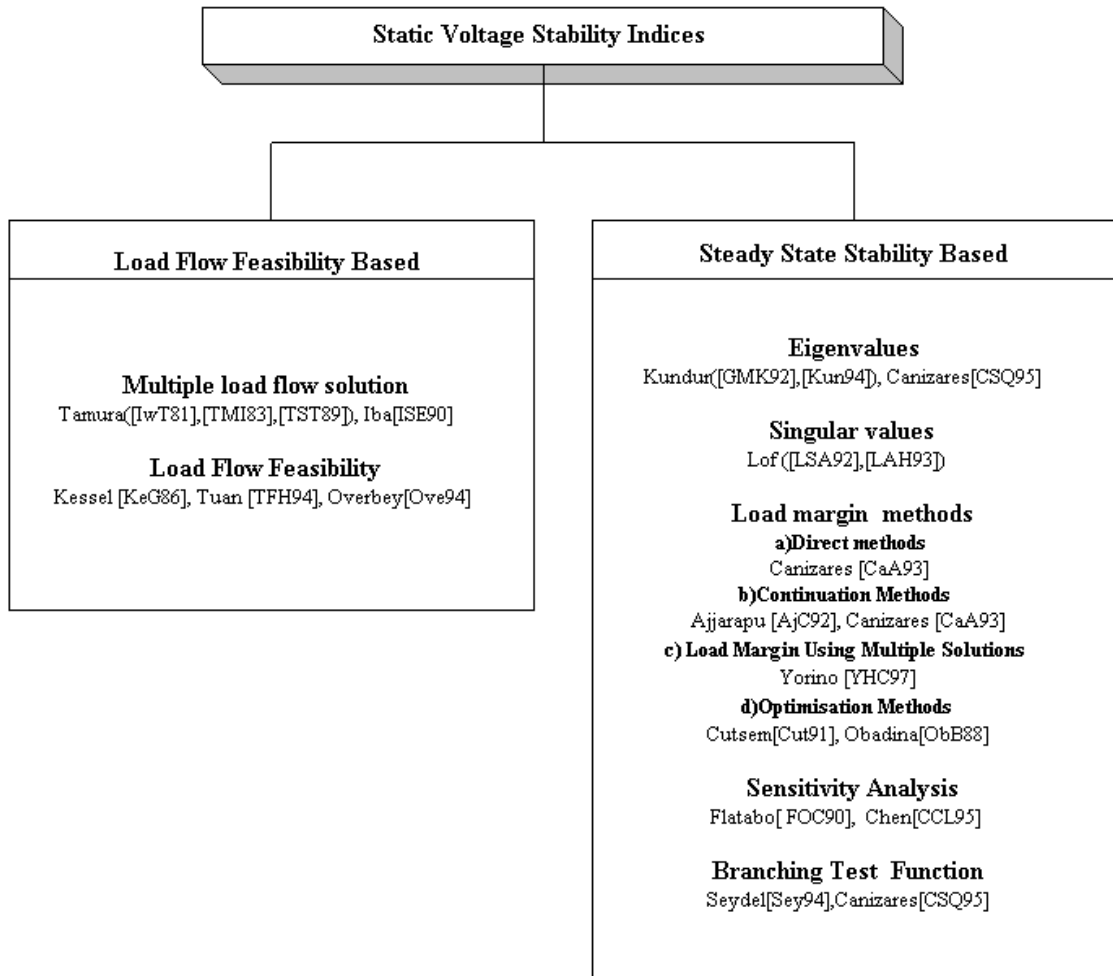


Figure 6.4.: Classification of Methods used for Static Voltage Stability Indices

heavily loaded systems. They minimise a cost function, which is equal to one half of the norm of the power flow mismatch vector. The authors in [TMI83] further investigate the relationship between voltage instability and multiple load flow solutions by introducing a multilevel criterion. Such criterion consists of three criteria, which can recognise voltage instability but they cannot be used separately to determine whether a system is stable. Therefore, a system is seen as voltage stable if all three criteria indicate voltage stability, otherwise if any of these criteria indicate voltage instability a system is unstable. The work presented in [ISE90] is the extension of the work done in [IwT81], where the analytical expression for the optimal multiplier is derived from a cubic equation. A significant conclusion is that the cubic equation has three real roots if the system has a pair of close solutions. Tamura in [TST89] uses a pair of load flow solution to calculate a Voltage Instability Proximity Index (VIPI). The main obstacle in all these methods is

the computation of the low voltage solution. Even though various methods to compute low voltage solutions have been proposed, difficulties still exist especially for lightly loaded systems.

Methods based on load flow feasibility are discussed in the three papers: [KeG86] , [TMI83], [Ove94]. The L indicator proposed by the authors in [KeG86] is a computationally tractable measure of the proximity of a load flow solution to a voltage stability limit. The characteristics of the indicator will be given in more details in the next section. The authors in [TMI83] use some assumptions related to the network bus admittance matrix \mathbf{Y} in order to simplify the calculation of the L indicator given in [KeG86]. The paper [Ove94] deals with the power flow unsolvable cases trying to determine the measure of unsolvability, which is really a rare and very interesting attempt in the research related to voltage stability.

References related to eigenvalue and singular value decomposition are in the author's opinion dominant in the second category. Special attention will be paid to the work done in [GMK92], [Kun94], [CSQ95], [LSA92], [LAH93].

For a particular operating point, the amount of additional load in a specific pattern of load increase that would cause a voltage collapse is called the loading margin to voltage collapse. Load margin has been extensively used and is a well-accepted index of proximity to voltage collapse. The load margin is obtainable through different methods such as: direct methods, continuation methods, methods based on multiple power flow solutions and optimisation methods. The computational cost is the most serious disadvantage of the load margin as is proved in [CaA93]. The method called Point of Collapse calculates the load margin directly as a solution of non-linear equations (6.1a) for which Jacobian \mathbf{J} is singular [CaA93]. The singularity condition is ensured by requiring that the right or left eigenvector is a nonzero vector. The general idea behind the continuation power flow is rather simple [AjC92]. It employs a predictor-corrector iterative scheme, where the predictor is used to obtain the tangent vector and estimate a subsequent solution corresponding to a different value of the load parameter. This estimate is then corrected by the corrector, which is a slightly modified power flow [AjC92]. It was shown that the load margin can also be obtained using a pair of multiple power flow solutions [YHC97]. The load margin in this work is defined as the point on the loadability boundary within the minimum Euclidean distance of the node injection changes [YHC97]. Finally, the load margin can be calculated using optimisation methods. Optimisation is a fairly logical choice when a margin is required. Thus, Van Cutsem in [Cut91], defines an optimisation problem where the objective

function is the maximal load increase, while the balance equations and generator reactive limits are equality and inequality constraints. The optimisation problem is non-linear, while the balance equations are based on the CRIC model. Obadina and Berg in [ObB88] maximise the total MVA demand, considering various equality and non-equality constraints.

The methods based on sensitivity analysis were developed in [FOC90] and [CCC95] to estimate distance to voltage collapse. The Voltage Collapse Proximity Indicator (VCPI) proposed in [CCC95] uses the sensitivity of generator reactive power injections with respect to angles and voltages to calculate the voltage collapse proximity indices for each PQ node. The VCPI was tested in this work and will be further discussed in the following sections.

The last method shown in Fig.6.4 is called branching test function as it was originally proposed in [Sey94] and implemented on a power system in [CSQ95]. This interesting method will be discussed in a subsequent section as well.

6.3.1. L Indicator

The L indicator proposed by P.Kessel and H. Glavitsch in [KeG86] varies in the range between zero (no load) and one (voltage collapse). Load flow solutions with a stability index L close to 1 are also close to singularities of the Jacobian. The calculation of the L indicator is based on the network equation (6.2) and the network bus admittance matrix \mathbf{Y} , where the vector of complex currents \mathbf{I} and voltages \mathbf{V} are further subdivided into the sub-vectors of generators complex current /voltages $\mathbf{I}^G/\mathbf{V}^G$ and the sub-vectors of load complex currents/voltages $\mathbf{I}^L/\mathbf{V}^L$, (see (6.18)). Using these four sub-vectors $\mathbf{I}^G, \mathbf{V}^G, \mathbf{I}^L, \mathbf{V}^L$ and the corresponding admittance sub-matrices $\mathbf{Y}_{GG}, \mathbf{Y}_{GL}, \mathbf{Y}_{LG}, \mathbf{Y}_{LL}$ the equation (6.2) can be reformulated as:

$$\begin{bmatrix} \mathbf{I}^G \\ \mathbf{I}^L \end{bmatrix} = \begin{bmatrix} \mathbf{Y}_{GG} & \mathbf{Y}_{GL} \\ \mathbf{Y}_{LG} & \mathbf{Y}_{LL} \end{bmatrix} \begin{bmatrix} \mathbf{V}^G \\ \mathbf{V}^L \end{bmatrix} \text{ or } \begin{bmatrix} \mathbf{V}^L \\ \mathbf{I}^G \end{bmatrix} = \begin{bmatrix} \mathbf{Z}^{LL} & \mathbf{F}^{LG} \\ \mathbf{K}^{GL} & \mathbf{Y}^{GG} \end{bmatrix} \begin{bmatrix} \mathbf{I}^L \\ \mathbf{V}^G \end{bmatrix} = \mathbf{H} \begin{bmatrix} \mathbf{I}^L \\ \mathbf{V}^G \end{bmatrix}, \quad (6.18)$$

where \mathbf{H} is the hybrid matrix. The L indicator then can be calculated using the following equation [KeG86]:

$$L = \max_{j \in \alpha_L} \left| 1 - \frac{\sum_{i \in \alpha_G} F_{ji} V_i}{V_j} \right|, \quad (6.19)$$

where α_L is the set of all load buses and α_G is the set of all generator buses. A similar approach for the calculation of the L indicator was proposed in [TFH94]. Instead of using complex matrices $\mathbf{Y}_{LL}, \mathbf{Y}_{LG}$ in equation (6.18) these authors suggested that only the imaginary part of $\mathbf{Y}_{LL}, \mathbf{Y}_{LG}$ should be taken into account. A new simplified voltage stability indicator with these assumptions is then obtained using the following equation:

$$B = \max_{j \in \alpha_L} \left| 1 - \frac{\sum_{i \in \alpha_G} C_{ji} V_i}{V_j} \right|, \quad (6.20)$$

where $\mathbf{C} = -\mathbf{B}_{LL}^{-1} \mathbf{B}_{LG}$ and \mathbf{B}_{LL} and \mathbf{B}_{LG} refer to the imaginary parts of $\mathbf{Y}_{LL}, \mathbf{Y}_{LG}$, respectively. It should be noted that this simplified approach requires the inversion of the real matrix \mathbf{B}_{LL} , that is more computationally efficient than the inversion of a complex matrix in the case of the original approach.

Let us find a simple explanation of the L indicator using a simple example. A simple two node system shown in Fig. 6.5 will be used for this explanation. The values for all elements of the network bus admittance matrix for the simple system are given in Fig.6.5. Equation (6.18) in this case is:

$$\begin{bmatrix} V_2 \\ I_1 \end{bmatrix} = \begin{bmatrix} Y_{22}^{-1} & -Y_{22}^{-1}Y_{21} \\ Y_{12}Y_{22}^{-1} & Y_{11} - Y_{12}Y_{22}^{-1}Y_{21} \end{bmatrix} \begin{bmatrix} I_2 \\ V_1 \end{bmatrix} = \begin{bmatrix} -jB_{22}^{-1} & -B_{22}^{-1}B_{21} \\ B_{12}B_{22}^{-1} & jB_{11} - jB_{12}B_{22}^{-1}B_{21} \end{bmatrix} \begin{bmatrix} I_2 \\ V_1 \end{bmatrix}. \quad (6.21)$$

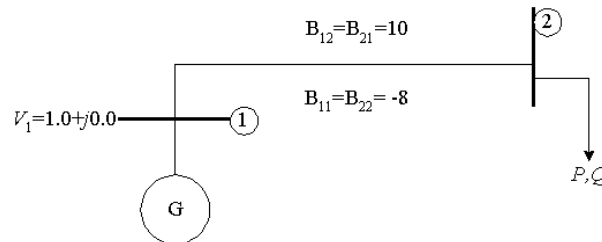


Figure 6.5.: A simple two node system

Using (6.21) and (6.19) the L indicator for this simple example can be calculated as:

$$L = \left| 1 + \frac{B_{21}}{B_{22}} \frac{1}{e_2 + jf_2} \right| \quad (6.22)$$

If the indicator takes $L=1.0$ for a voltage collapse point, then equation (6.2) gives:

$$\left\{ 1 + \operatorname{Re} \left\{ \frac{B_{21}}{B_{22}} \frac{1}{e_2 + jf_2} \right\} \right\}^2 + \left\{ \operatorname{Im} \left\{ \frac{B_{21}}{B_{22}} \frac{1}{e_2 + jf_2} \right\} \right\}^2 = 1.0 \Rightarrow e_2 = -\frac{B_{21}}{2B_{22}}. \quad (6.23)$$

On the other hand, expression for active P_2 and reactive Q_2 power injection at node 2 in the rectangular forms are:

$$P_2 = -f_2 B_{12} \quad (6.24a)$$

$$Q_2 = e_2 B_{12} + f_2^2 B_{22} + e_2^2 B_{22}, \quad (6.25b)$$

which yields according to (6.10):

$$\mathbf{J} = \begin{bmatrix} 0 & -B_{12} \\ B_{12} + 2e_2 B_{22} & 2f_2 B_{22} \end{bmatrix}. \quad (6.26)$$

For this simple example, the point where the Jacobian \mathbf{J} is singular can be obtained analytically as:

$$\det(\mathbf{J}) = 0 \Rightarrow e_2 = -\frac{B_{12}}{2B_{22}}, \quad (6.27)$$

which leads to the same conclusion as (6.23). Therefore, $L=1.0$ coincide with the point where the Jacobian \mathbf{J} of the power flow equations is singular. The behaviour of the L indicator for the simple system and a load $P_2 = 300 \text{ MW}$ is shown in Fig. 6.6. It can be seen that the L indicator exhibits a non-linear behaviour, and the curve is smooth.

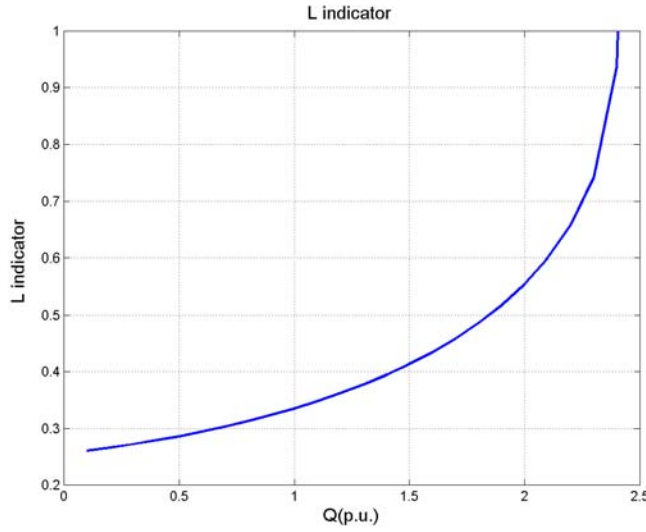


Figure 6.6.: The L indicator for two node system

6.3.2. Eigenvalue Decomposition

Eigenvalue decomposition is a widely accepted method in voltage stability that has been proposed by many authors [GMK92],[Kun94],[CSQ95]. Kundur in [GMK92] and [Kun94] suggests the eigenvalue decomposition of the reduced Jacobian \mathbf{J}_R . Using the decomposition, equation (6.12) gives:

$$\Delta V = \mathbf{J}_R^{-1} \Delta \mathbf{Q} = (\mathbf{R}\mathbf{\Lambda}\mathbf{L})^{-1} \Delta \mathbf{Q} = \mathbf{R}\mathbf{\Lambda}^{-1}\mathbf{L}\Delta \mathbf{Q} = \sum_{i=1}^n \frac{\mathbf{r}_i \mathbf{l}_i^T}{\lambda_i} \Delta \mathbf{Q} \quad (6.28)$$

where \mathbf{R} , \mathbf{L} are the right and left eigenvector matrices of the reduced Jacobian matrix \mathbf{J}_R , $\mathbf{\Lambda}$ is a diagonal matrix of eigenvalues of \mathbf{J}_R , λ_i is the i^{th} eigenvalue and \mathbf{r}_i and \mathbf{l}_i are the associated right and left eigenvectors. It can be seen from equation (6.28) that only a few small eigenvalues (less than 1.0) with corresponding eigenvectors can have a significant impact on the sum in equation (6.28). Therefore, the smallest eigenvalues represent the most dangerous modes in the system. Kundur in [Kun94] confirms that the calculation of all eigenvalues of \mathbf{J}_R can be impractical and unnecessary. Modal analysis is thus a trade off between computation time and validity of conclusions.

The most critical buses can be determined using V-Q sensitivity as:

$$\frac{\partial V_k}{\partial Q_k} = \sum_i \frac{r_{ki} J_{ik}}{\lambda_i} = \sum_i \frac{P_{ki}}{\lambda_i}, \quad (6.29)$$

where P_{ki} is the bus participation factor or the relative participation of bus k in mode i [GMK92],[Kun924]. The value of the participation factor in a given mode represents the effectiveness of remedial action applied at a bus in order to stabilise the mode. Hence, P_{ki} determines the contribution of the mode i to the V-Q sensitivity at bus k .

Let us try to find the eigenvalues of the reduced Jacobian matrix \mathbf{J}_R for the small system given in (6.3.1). Using equations (6.7a), (6.7b), (6.9) and (6.28) the Jacobian and the reduced Jacobian matrices in polar form are:

$$\mathbf{J} = \begin{bmatrix} B_{21}V_2 \cos\theta_2 & B_{21} \sin\theta_2 \\ B_{21}V_2 \sin\theta_2 & -2B_{22}V_2 - B_{21} \cos\theta_2 \end{bmatrix}; \quad \mathbf{J}_R = \frac{(\sqrt{e_2^2 + f_2^2}) \det(\mathbf{J})}{e_2 \times B_{12}} \quad (6.30)$$

For this simple system, \mathbf{J}_R is a 1x1 matrix. The eigenvalue of the matrix is the same as the matrix itself. The V-Q sensitivity given by (6.29) for the second node is equal to the inverse of the eigenvalue. In order to draw the complete V-Q curve and eigenvalue behaviour for both low and high voltage solutions, the analytical solution of equations (6.24) is found:

$$f_2 = -\frac{P_2}{B_{12}}, \quad (6.31a)$$

$$e_{1/2} = -\frac{B_{12}}{2B_{22}} \pm \frac{\sqrt{B_{12}^2 - 4B_{22} \left(\frac{B_{22}}{B_{12}^2} P_2^2 - Q_2 \right)}}{2B_{22}} \quad (6.31b)$$

Equations (6.31b) shows that the point where low(e_1) and high(e_2) voltage solution coalesce is the point where the Jacobian is singular (see(6.27)). The existence of non-complex solutions in (6.31b) requires that:

$$B_{12}^2 - 4B_{22} \left(\frac{B_{22}}{B_{12}^2} P_2^2 - Q_2 \right) > 0, \quad (6.32)$$

which further means that the solvability boundary for this simple system can be obtained analytically as:

$$B_{12}^2 - 4B_{22}\left(\frac{B_{22}}{B_{12}^2}P_2^2 - Q_2\right) = 0 \quad (6.33)$$

This boundary makes a distinction between the regions where the power flow is solvable and the non-solvable as shown in Fig. 6.7.

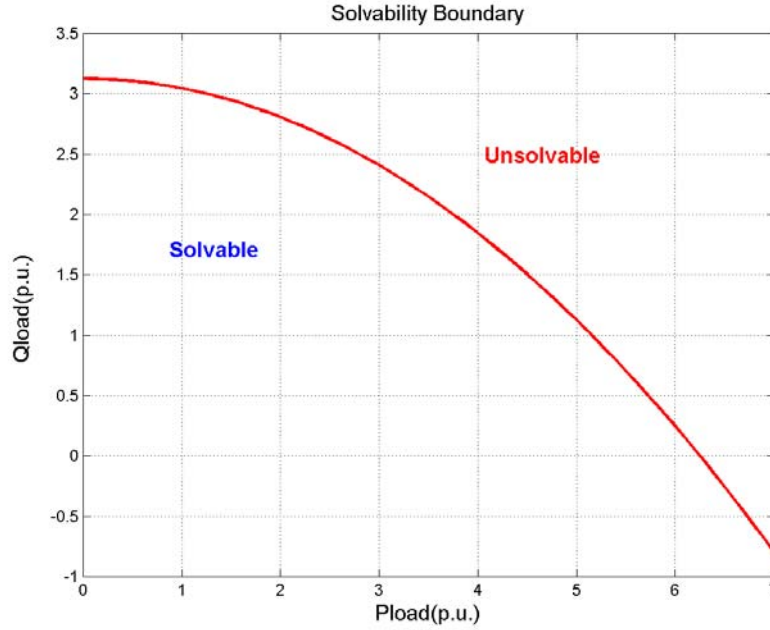


Figure 6.7.: The solvability boundary for two node system

The same expression can be obtained by substituting (6.27) into (6.25b). Once we know the solvability boundary, real e_2 and imaginary parts f_2 of V_2 can be determined using (6.31). Keeping P_2 constant but changing Q_2 , equations (6.31) gives a constant value for f_2 and two possible solutions for e_2 . These two different solutions produce lower and upper branch of V-Q curve. Having found V_2 the reduced Jacobian matrix and its eigenvalue can be determined. If $P_2 = 300 MW$ is the load at node 2, the corresponding V-Q curve and eigenvalues are shown in Fig. 6.8a and Fig. 6.8b, respectively. The upper curve (blue colour) denotes the high voltage solution and its eigenvalues of the reduced Jacobian matrix J_R . Similarly, like the high and low voltage solution, the eigenvalues exhibit a non-linear behaviour as a function of Q_2 , and at the singular point coalesce to zero. It is clear from equation (6.29) that $\frac{\partial V_2}{\partial Q_2} = \frac{P_{21}}{\lambda_1} = \lambda_1^{-1}$, which means that at the point where the Jacobian is singular this sensitivity tends to infinity.

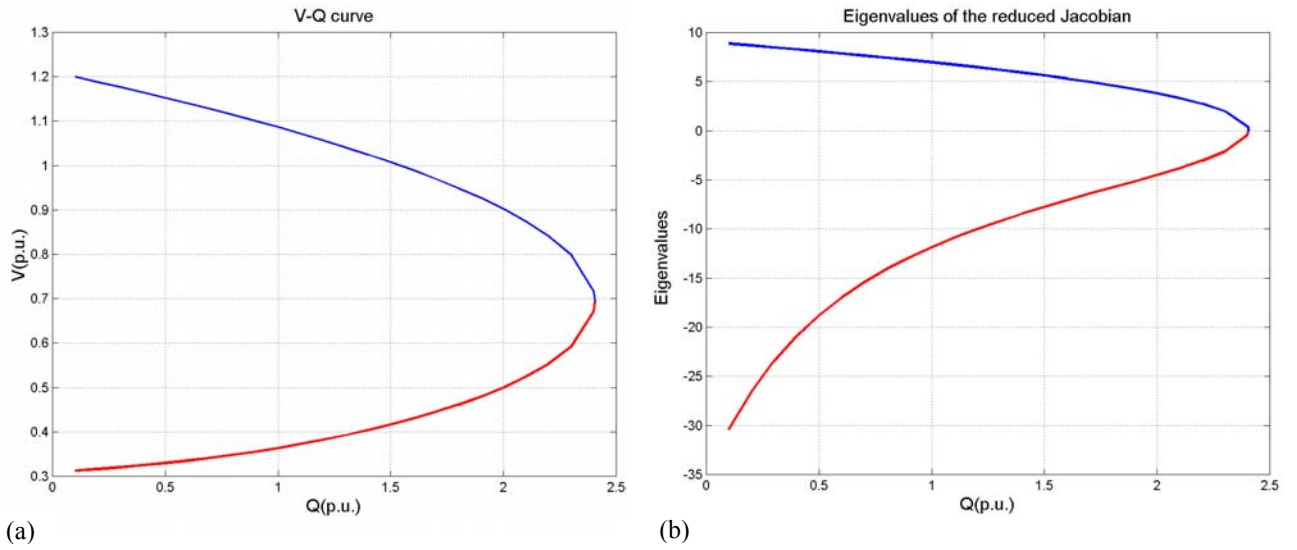


Figure 6.8.: a)V-Q curve b)eigenvalues of \mathbf{J}_R for two node system

6.3.3. Singular Values

The singular value decomposition of the Jacobian matrix \mathbf{J} is based on the following expression [LSA92],[LAH93]:

$$\mathbf{J} = \mathbf{U}\mathbf{\Sigma}\mathbf{V}^T = \sum_{i=1}^n \sigma_i \mathbf{u}_i \mathbf{v}_i^T, \quad (6.34)$$

where n is the order of the Jacobian matrix, \mathbf{U} and \mathbf{V} are n by n orthonormal matrices, σ_i is the i^{th} singular value of matrix \mathbf{J} , \mathbf{u}_i is the i^{th} left singular vector, \mathbf{v}_i is the i^{th} right singular vector and $\mathbf{\Sigma}$ is a diagonal matrix containing singular values. Using equation (6.34), equation (6.9) can be rewritten as:

$$\begin{bmatrix} \Delta\theta \\ \Delta V \end{bmatrix} = \mathbf{J}^{-1} \begin{bmatrix} \Delta\mathbf{P} \\ \Delta\mathbf{Q} \end{bmatrix} = (\mathbf{U}\mathbf{\Sigma}\mathbf{V}^T)^{-1} \begin{bmatrix} \Delta\mathbf{P} \\ \Delta\mathbf{Q} \end{bmatrix} = \sum_{i=1}^n \frac{\mathbf{u}_i^T \mathbf{v}_i}{\sigma_i} \begin{bmatrix} \Delta\mathbf{P} \\ \Delta\mathbf{Q} \end{bmatrix} = \sum_{i=1}^n \frac{P_i^{SV}}{\sigma_i} \begin{bmatrix} \Delta\mathbf{P} \\ \Delta\mathbf{Q} \end{bmatrix}, \quad (6.35)$$

where \mathbf{P}_i^{SV} is a participation vector associated with the i^{th} singular value. The following interpretations can be made of the application of singular value decomposition to the Jacobian matrix [LSA92],[LAH93]:

- The smallest singular value is an indicator of the proximity to voltage collapse.

- P_i^{SV} contains participation factors $P_{ki}^{SV} = u_{ki} v_{ki}$. Apart from the slack bus, these values can be associated with each PQ or PV bus.

It is difficult to judge between eigenvalue and singular value decomposition. According to [LSA92],[LAH93] the singular values of any real matrix A ($n \times n$) of rank is r are the *square roots of the r positive eigenvalues of AA^T* . The singular value decomposition has the advantage of being fairly insensitive to perturbations in the matrix elements, while the eigenvalues of certain unsymmetrical matrices are very sensitive [DaB74].

The analytical expression of the singular values for the two node system is used as an example:

$$s_{vs}(\mathbf{J}) = \begin{bmatrix} f_2 B_{22} + \sqrt{f_2^2 B_{22}^2 - B_{12}^2 - 2B_{12}e_2 B_{22}} \\ -f_2 B_{22} - \sqrt{f_2^2 B_{22}^2 - B_{12}^2 - 2B_{12}e_2 B_{22}} \end{bmatrix}, \quad (6.36)$$

which again shows that both singular values are equal to zero at the point where the Jacobian matrix \mathbf{J} is singular (see (6.27)). The smallest singular value characteristic of \mathbf{J} for the two nodes system is shown in Fig. 6.9. A similar behaviour of the smallest singular value of \mathbf{J}_R is confirmed in [LSA92],[LAH93].

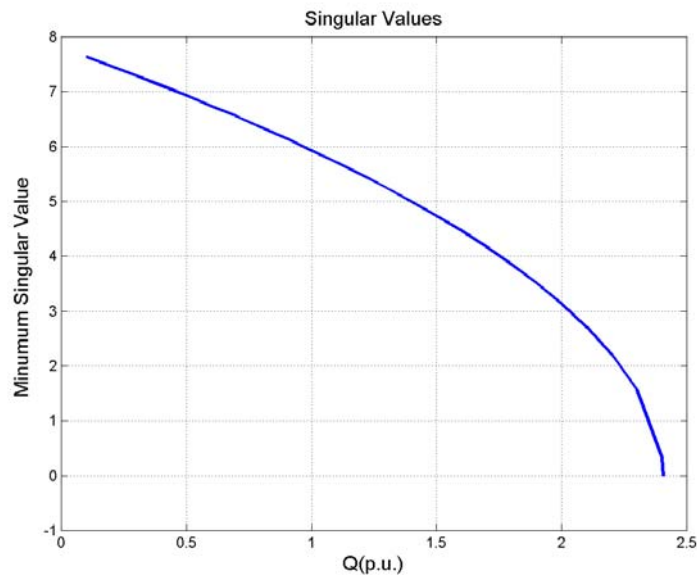


Figure 6.9.: The smallest singular value of \mathbf{J} for two node system

6.3.4. Voltage Collapse Proximity Indicator

The voltage collapse proximity indicator (VCPI) was proposed in [CCC95] for identifying weak nodes and areas in a power system. This indicator can be determined for each load bus using the following equation [CCL95]:

$$VCPI_i = \frac{\sum_{j \in \Omega_G} \Delta Q_{Gj}}{\Delta Q_i} \quad i \in \Omega_L, \quad (6.37)$$

where Ω_G and Ω_L are the sets of generator and load buses, respectively, ΔQ_{Gj} is the change of reactive generation of the j^{th} generator and ΔQ_i is the change of reactive consumption at the i^{th} load bus. It can be shown that these indices take values slightly larger than 1.0 when the state of system is relatively far from voltage collapse [CCC95]. On the other hand, some of these indices take significantly higher values when the power system is approaching voltage collapse. The calculation of these indices can be performed using the following equation [CCC95]:

$$VCPI_i = \sum_{j \in \Omega_G} -\mathbf{B}_{Q_{Gj}} \mathbf{J}^{-1} \mathbf{y}_{Q_i}, \quad (6.38)$$

where $\mathbf{B}_{Q_{Gj}} = \begin{bmatrix} \frac{\partial Q_{Gj}}{\partial \theta} & \frac{\partial Q_{Gj}}{\partial V} \end{bmatrix}$ and \mathbf{y}_{Q_i} is a vector whose dimension is the same as the dimension of the Jacobian matrix \mathbf{J} , and with all its entries equal to zero, except the entry that corresponds to ΔQ_i whose value is equal to 1.

In order to find what is really behind equation (6.38) we can determine $\mathbf{B}_{Q_{Gj}}$ for the two nodes system as:

$$\mathbf{B}_{Q_1} = \begin{bmatrix} \frac{\partial Q_1}{\partial \theta_2} & \frac{\partial Q_1}{\partial V_2} \end{bmatrix} = \begin{bmatrix} B_{12} V_2 \sin \theta_2 & -B_{12} \cos \theta_2 \end{bmatrix} \quad (6.39)$$

The inverse Jacobian matrix can be determined analytically using equation (6.30). Having determined \mathbf{B}_{Q_1} and \mathbf{J}^{-1} VCPI for node 2 is then equal to:

$$VCPI_2 = -\frac{B_{21}}{2B_{22}V_2 \cos \theta_2 + B_{21}} = \frac{B_{21}^2}{\det(\mathbf{J})} \quad (6.40)$$

Equation (6.40) shows why these indices have high values when the system is approaching voltage collapse. The denominator of the expression given in (6.40) is equal to zero at the point where the Jacobian is singular (see (6.27)). This means that for this point VCPI tends to infinity. The VCPI behaviour is shown in Fig 6.10. The index has almost a linear characteristic before it enters the collapse vicinity. Afterwards a rapid change can be observed.

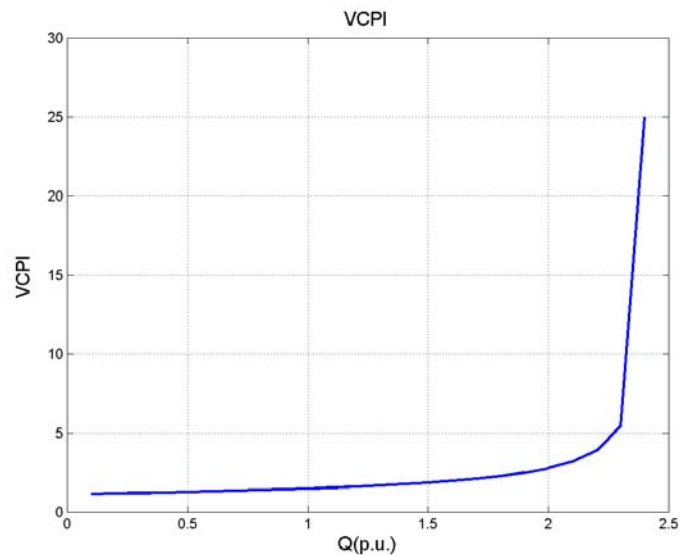


Figure 6.10.: VCPI characteristic for two node system

6.3.5. Branching Test Function

For the purpose of steady state analysis we can assume that the network equations given by (6.1a) can be written as a set of algebraic equations:

$$\mathbf{g}(\mathbf{y}, p) = \mathbf{0}, \quad (6.41)$$

where long-term ($\mathbf{z}_c, \mathbf{z}_d$) and short-term (\mathbf{x}) variables are considered constant, and p is a slow changing parameter that drives the system.

Branching can be simply defined as drawing of a diagram of a non-linear system of equations. Such diagram can be obtained calculating \mathbf{y} for different values of p . A branch point or bifurcation point with respect to p can be defined as a solution (\mathbf{y}_0, p_0) of equation (6.41),

where the number of solutions *changes* when p passes p_0 [Sey94]. For instance, a non-linear equation is $0 = y^2 - p$ has at $p = 0$ only one solution $y = 0$, whereas for $p > 0$ there are two solutions, $y = \pm\sqrt{p}$. The V-Q diagram (curve) shown in Fig 6.8 is a branch diagram where the value of V depends on Q. Therefore, in this case parameter p is Q. The V-Q diagram has a low and a high voltage solution for all its points, except at the point where the Jacobian is singular. The number of solutions on the V-Q diagram changes when p passes the voltage collapse point p_0 . Therefore, the voltage collapse point is a bifurcation point.

In general, there are three procedures that can be used to locate these bifurcation points. A generally accepted method of branch tracing or path following is the continuation method [Sey94], [AjC92], [CaA93]. This method is time demanding because it requires the calculation of a significant number of points on the PV curve and might face convergence problems when the system approaches a bifurcation point.

Instead of calculating unnecessary points, one can be more interested in calculating the bifurcation point indirectly. This can be done using a branching test function that indicates the point where the number of solutions for a non-linear system of equations is changed. This branching test function τ has to satisfy the following condition [Sey94]:

$$\tau(\mathbf{y}_0, p_0) = \mathbf{0} \quad (6.42)$$

Seydel in [Sey94] suggests the following set of test functions τ :

- $\tau = \alpha_k$, where $|\alpha_k| = \min\{|\alpha_1|, |\alpha_2|, \dots, |\alpha_n|\}$, where α represents the real parts of the eigenvalues of the Jacobian ($n \times n$).
- Since, the Jacobian $\mathbf{J} = \mathbf{g}_y(\mathbf{y}, p) = \mathbf{0}$ evaluated at (\mathbf{y}_0, p_0) is singular, the determinant of the Jacobian can be used as a branching test function:

$$\tau(\mathbf{y}, p) := \det \mathbf{g}_y(\mathbf{y}, p) \quad (6.43)$$

A change in the sign of τ for two successive values of p is a useful indication that the bifurcation point has passed. Using the values of the parameter p before and after this function changes sign, the bifurcation point (\mathbf{y}_0, p_0) can be computed using an extrapolation method.

The main weakness of indirect methods is the fact that the PV curve is highly non-linear in the vicinity of bifurcation point.

The third group of methods calculates the bifurcation point directly by formulating a new system of non-linear equations $\mathbf{G}(\mathbf{Y})$ whose solution is a branch point [Sey94]. The non-linear equations $\mathbf{G}(\mathbf{Y})$ represent an enlarged set of the original equations $\mathbf{g}(\mathbf{y}, p) = \mathbf{0}$. Usually, this set of equations is enlarged with the test function:

$$\mathbf{G}(\mathbf{Y}) := \mathbf{G}(\mathbf{y}, p) = \begin{pmatrix} \mathbf{g}(\mathbf{y}, p) \\ \tau(\mathbf{y}, p) \end{pmatrix} = \mathbf{0}. \quad (6.44)$$

The criterion that the Jacobian matrix is singular can be reformulated as existence of a non trivial solution of $\mathbf{g}_y(\mathbf{y}, p)\mathbf{h} = \mathbf{0}$ for the vector \mathbf{h} . This can be illustrated using equation (6.26):

$$\mathbf{g}_y(\mathbf{y}, p)\mathbf{h} = \mathbf{J}\mathbf{h} = \begin{bmatrix} 0 & -B_{12} \\ B_{12} + 2e_2B_{22} & 2f_2B_{22} \end{bmatrix} \begin{bmatrix} h_1 \\ h_2 \end{bmatrix} = \mathbf{0},$$

which gives:

$$\begin{aligned} -B_{12}h_2 &= 0 \\ (B_{12} + 2e_2B_{22})h_1 + 2f_2B_{22}h_2 &= 0 \end{aligned}$$

For this system of equations a trivial ($h_1 = h_2 = 0$) and a non-trivial ($h_2 = 0, h_1 \neq 0, e_2 = -\frac{B_{12}}{2B_{22}}$) solution can be found. The existence of the non-trivial solution

means that the Jacobian matrix is singular ($\det(\mathbf{J}) = 0 \Rightarrow e_2 = -\frac{B_{12}}{2B_{22}}$).

Using this criterion ($\mathbf{g}_y(\mathbf{y}, p)\mathbf{h} = \mathbf{0}$) a direct method can be formulated as [Sey94]:

$$\mathbf{G}(\mathbf{Y}) := \begin{pmatrix} \mathbf{g}(\mathbf{y}, p) \\ \mathbf{g}_y(\mathbf{y}, p)\mathbf{h} \\ h_k - 1 \end{pmatrix} = \mathbf{0}, \mathbf{Y} = \begin{pmatrix} \mathbf{y} \\ p \\ \mathbf{h} \end{pmatrix}, \quad (6.45)$$

which is very similar to Point of Collapse method suggested in [CaA93]. A non-trivial solution for the vector \mathbf{h} can be obtained if for example the k^{th} entry of vector \mathbf{h} takes a certain predefined value. The main weakness of the method is how to find an initial point $(\bar{\mathbf{y}}, \bar{p}, \bar{\mathbf{h}})$

close to the expected solution of equation (6.45). A solution relatively close to the bifurcation point is a good approximation point in terms of $(\bar{\mathbf{y}}, \bar{\mathbf{p}})$, but we still need a good approximation for \mathbf{h} .

A good approximation for \mathbf{h} can be obtained by replacing the l^{th} row of $\mathbf{g}_y(\bar{\mathbf{y}}, \bar{\mathbf{p}})\mathbf{h}$ with \mathbf{e}_l^T ensuring that $h_k = 1$:

$$\bar{\mathbf{J}}_{lk}\bar{\mathbf{h}} = \mathbf{e}_l, \text{ where } \mathbf{J}_{lk} := \mathbf{J}_{lk}(\bar{\mathbf{y}}, \bar{\mathbf{p}}) := (\mathbf{I} - \mathbf{e}_l\mathbf{e}_l^T)\mathbf{J}(\bar{\mathbf{y}}, \bar{\mathbf{p}}) + \mathbf{e}_l\mathbf{e}_k^T. \quad (6.46)$$

Using equations (6.26) and (6.46) $\bar{\mathbf{h}} = \begin{bmatrix} \bar{h}_1 \\ \bar{h}_2 \end{bmatrix}$ can be determined for $l = k = 1$ as follows:

$$\begin{bmatrix} 1 & 0 \\ B_{12} + 2e_2B_{22} & 2f_2B_{22} \end{bmatrix} \begin{bmatrix} \bar{h}_1 \\ \bar{h}_2 \end{bmatrix} = \begin{bmatrix} 1 \\ 0 \end{bmatrix} \Rightarrow \bar{h}_1 = 1, \bar{h}_2 = -\frac{B_{12} + 2e_2B_{22}}{2f_2B_{22}} \quad (6.47)$$

The direct method can be summarised as follows:

- Calculate an initial point $(\bar{\mathbf{y}}, \bar{\mathbf{p}})$ as close to (\mathbf{y}_0, p_0) as possible. This can be done by repeating a standard power flow method for different values of p .
- Calculate $\bar{\mathbf{h}}$ using equation (6.46)
- Solve the set of equations (6.45) starting from $(\bar{\mathbf{y}}, \bar{\mathbf{p}}, \bar{\mathbf{h}})$.

The direct method presented above is more efficient than the indirect methods. Nevertheless, this method requires the solution of the enlarged set of non-linear power flow equations (6.46) and might be computationally time consuming (see [CaA93]). In equation (6.46) the l^{th} equation is removed in order to ensure a non-trivial solution of $\mathbf{g}_y(\bar{\mathbf{y}}, \bar{\mathbf{p}})\mathbf{h}$. The value of removed component can be calculated as:

$$\mathbf{e}_l^T \mathbf{g}_y(\bar{\mathbf{y}}, \bar{\mathbf{p}})\bar{\mathbf{h}}, \quad (6.48a)$$

which is in essence a measure of the distance to the bifurcation point (\mathbf{y}_0, p_0) . Therefore, a new test function can be defined as:

$$\tau_{lk}(\mathbf{y}, \mathbf{p}) = \mathbf{e}_l^T \mathbf{g}_y(\bar{\mathbf{y}}, \bar{\mathbf{p}})\bar{\mathbf{h}} = \mathbf{e}_l^T \mathbf{J}\mathbf{J}_{lk}^{-1} \mathbf{e}_l. \quad (6.48b)$$

Using equations (6.48a) and (6.47) the test function for two node system is:

$$\mathbf{e}_l^T \mathbf{g}_y(\bar{\mathbf{y}}, \bar{\mathbf{p}}) \bar{\mathbf{h}} = \begin{bmatrix} 1 & 0 \end{bmatrix} \begin{bmatrix} 0 & -B_{12} \\ B_{12} + 2e_2 B_{22} & 2f_2 B_{22} \end{bmatrix} \begin{bmatrix} \bar{h}_1 \\ \bar{h}_2 \end{bmatrix} = -B_{12} \bar{h}_2 = B_{12} \frac{B_{12} + 2e_2 B_{22}}{2f_2 B_{22}} \quad (6.48c)$$

The test function given by (6.48b) can be calculated using the following steps [Sey94]:

$$1. \quad \mathbf{g}_y(\bar{\mathbf{y}}, \bar{\mathbf{p}}) \mathbf{v} = \mathbf{e}_l \quad (6.49a)$$

$$2. \quad \tau = \frac{1}{v_k}. \quad (6.49b)$$

Using this version of τ one can benefit from the LU decomposition already available from the calculation of (\mathbf{y}, \mathbf{p}) . The value of the test function depends on choice of l and k . Cañizares [CSQ95] suggests an entry with the largest value of the tangent vector, while Seydel [Sey94] states that an arbitrarily chosen pair of indices works well.

Let us see how the direct method given by (6.44) can be implemented on the simple two-bus example. Equation (6.41) implemented on the two node system is given by (6.24). Substituting these equations directly in (6.44) one can obtain the following set of equations:

$$P_2 = -f_2 B_{12}, \quad (6.50a)$$

$$Q_2 = e_2 B_{12} + f_2^2 B_{22} + e_2^2 B_{22}, \quad (6.50b)$$

$$B_{12}(B_{12} + 2e_2 B_{22}) = 0, \quad (6.50c)$$

which gives exactly the same solution as (6.33). Therefore, all bifurcation points for different values of P and Q must lie on the solvability boundary defined by (6.33). The same conclusion can be made if one substitute (6.24) and (6.26) into (6.45):

$$P_2 = -f_2 B_{12}, \quad (6.51a)$$

$$Q_2 = e_2 B_{12} + f_2^2 B_{22} + e_2^2 B_{22}, \quad (6.51b)$$

$$B_{12} h_2 = 0, \quad (6.51c)$$

$$(B_{12} + 2e_2 B_{22}) h_1 + 2f_2 B_{22} h_2 = 0, \quad (6.51d),$$

Taking into account that $B_{12} \neq 0$ in (6.51c) leads to:

$$h_2 = 0, \quad (6.51e)$$

which according to (6.45) means that $k=1$.

The system of equations (6.51) has the same solution as the system of equations (6.47).

The value of the test function given by (6.48c) for the two node system, with $l = k = 1$ is:

$$t_{11} = \frac{B_{12}(B_{12} + 2e_2 B_{22})}{2f_2 B_{22}} = \frac{\det \mathbf{J}}{2f_2 B_{22}}, \quad (6.52)$$

which shows that the test function is directly proportional to the Jacobian determinant $\det \mathbf{J}$. As such, the test function is equal to zero at the point where the Jacobian matrix \mathbf{J} is singular. The test function characteristic for the two nodes example is shown in Fig.6.11.

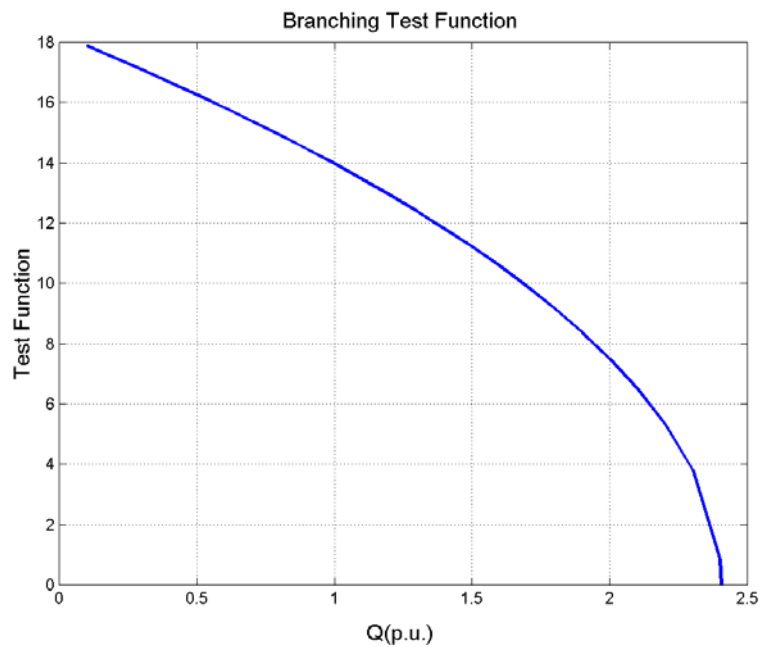


Figure 6.11.: Test function for two node system

6.4. Test Results

Summarising the voltage stability indices discussed in (6.3.1 – 6.3.3), one can observe that these can be divided into two groups: the system-wide indicators and the node-based indices. The L indicator, the smallest eigenvalue and the smallest singular value belong to the first group, while test functions, VCPI and bus participation factors (based on eigenvalues or singular values) belong to the second group. It should be emphasised that the indices from the first group measure the distance to voltage collapse based on only one value. On the other hand, node-based indices give a value for each node or each entry in the state vector of the power flow equations (6.9).

All the static voltage stability indices discussed in (6.3.1 – 6.3.3) have been tested on both a small IEEE 14 node system and a National Grid Company (NGC) power system model with 1078 buses. Results are discussed separately for both groups of indices in the following sections.

6.4.1. Results for the System-Wide Indicators

The L indicator, the smallest eigenvalue of the reduced Jacobian \mathbf{J}_R and the smallest singular value of the Jacobian \mathbf{J} are calculated at each load point along the PV curve for the IEEE 14 node system and a National Grid power system model. These PV curves were produced by repeating the standard power flow calculation for different load points until the power flow diverges. Such power flow calculation is often called a “quasi” continuation power flow. The load is increased by 1% between successive load points, while the generation was changed proportionally with the MW generated for the base case (load increase 0%). The load margin is defined as the maximal percentage load increase, which is the percentage increase for the last load point where the power flow still converges.

These system-wide indicators are shown for both system in Fig. 6.12 and Fig. 6.13, respectively. The following conclusions can be drawn from the figures:

- The load margin for the IEEE 14 nodes example is 15%, while the load margin for the National Grid power system model is 8%.

- The L indicator gradually increases, while the smallest eigenvalue of \mathbf{J}_R and the smallest singular value of \mathbf{J} gradually decrease.
- The L indicator characteristics are very similar to the L indicator characteristic for the two node system, shown in Fig. 6.6, except that at the maximal load point, the L indicator values are smaller than 1.0. It should be pointed out that the load margin obtained for both the IEEE 14 node system and the National Grid power system model is not the Jacobian singularity point. This point cannot be reached by using a “quasi” continuation power flow due to divergence problem in the vicinity of the Jacobian singularity point.
- The smallest eigenvalue characteristic is larger than the smallest singular value characteristic for both systems.
- The smallest eigenvalue and singular value characteristics exhibit some discontinuities between the last two load points for the IEEE 14 node system. These discontinuities are a direct consequence of the quasi continuation power flow. It appears that the power flow solutions obtained for different load points are on the high solution voltage branch until the last point, as shown in Fig 6.14. For the last point (15, see Fig. 6.14), the solution switches to the low voltage branch and the next load increase leads to a power flow divergence. This behaviour of the quasi continuation power flow used in this work is confirmed by the test function calculation of the last two points. A change of sign in the test function (6.47) was observed for the last point.
- The L indicator and the smallest singular value characteristics drawn for the National Grid power system model are almost linear, while the smallest eigenvalue characteristic is linear but has some discontinuities for the last three load points. These discontinuities are sometimes a good indication that a system is approaching the point of voltage collapse.
- The calculation of the system wide indicators for the large system requires fast and robust routines for the calculation of an inverse matrix, a few smallest eigenvalues or the smallest singular value. The author developed some of these routines, while the others were taken from famous libraries such as Harwell [Har94], IMSL [Ims99], or NAG [Nag99]. The author’s experience with the implementation of these routines on the National Grid power system model system is summarised in Table 6.4. The results

obtained by these routines were compared with the results obtained using similar Matlab procedures and their accuracy was confirmed.

The most important routine in this work is one, which provides the solution of a system of sparse linear equations (a linear solver based on a LU decomposition and a forward-backward substitution). The best routines come from Harwell and are called MA48AD and MA50AD. They are written in F77 code, and can be successfully compiled and used on both Unix and Windows operating systems. Similar routines made by IMSL and NAG are not as good in the author's opinion, if the computation time is important. The total CPU time that the routines take to calculate the inverse matrix \mathbf{Y}_{LL} all together with the full-sparse matrix multiplication $\mathbf{Y}_{LL}^{-1}\mathbf{Y}_{LG}$ (see (6.18)) is about 0.7s (see Table 6.4).

The author spent a significant amount of time developing or finding the best routines to calculate the smallest eigenvalues of a real matrix. The routines from Harwell or NAG libraries are extremely computationally demanding. The routine based on lopsided simultaneous iteration (LOPSI), developed by Kundur in [Kun94] is faster, but might have difficulties with complex conjugate eigenvalues. It should be pointed out that the network bus admittance matrix with phase-shifting transformers is not symmetrical and consequently the reduced Jacobian matrix \mathbf{J}_R is unsymmetrical. This further means that that some eigenvalue might be complex conjugate values. The author's experience confirms this possibility. Without a technique able to avoid the occurrence of complex conjugate values, the LOPSI based methods can fail. The best routine is thus found in the IMSL library. The routine called EVLRG calculates **all** eigenvalues of a real general matrix. It is very fast and takes approximately 19s to calculate all the eigenvalues of the reduced Jacobian matrix for the National Grid power system model.

The routine suggested by Lof, Shmed and Anderson in [LSA92],[LAH93] is quite fast routine and calculates the smallest singular value and its associated singular vectors. This routine was modified by the author as suggested in [HPL97]. Moreover, sparse techniques were used for the forward and backward substitutions. The routine takes less than 1s to calculate the smallest singular value and its associated singular vectors for the National Grid power system model.

Table 6.4- Methods, routines and libraries used for the calculation of system wide indicators
(the PC used to perform calculations: Intel Pentium 4, 2.0 GHz, 512 MB RAM)

<i>Method</i>	<i>Chosen procedure</i>	<i>Procedures compared with</i>	<i>CPU time [s]</i>
Matrix Inversion	MA48AD, MA50AD Harwell	1.NAG, IMSL	Takes about 0.7s to calculate L indices.
Smallest eigenvalue	EVLRG IMSL	1.Harwell, NAG 2.LOPSI –the author	Takes about 19s to calculate all the eigenvalues of \mathbf{J}_R
Smallest singular value	Developed by the author	n.a.	Takes less than 1s to calculate the smallest singular value of \mathbf{J} and its associated singular vectors.

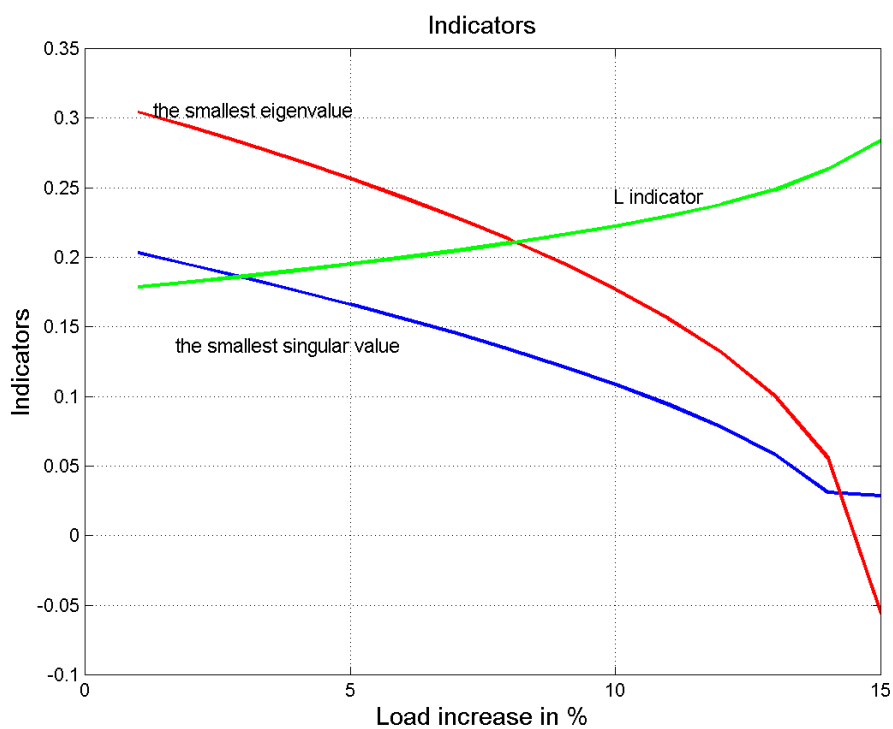


Figure 6.12.: The system-wide indicators for the IEEE 14 node system

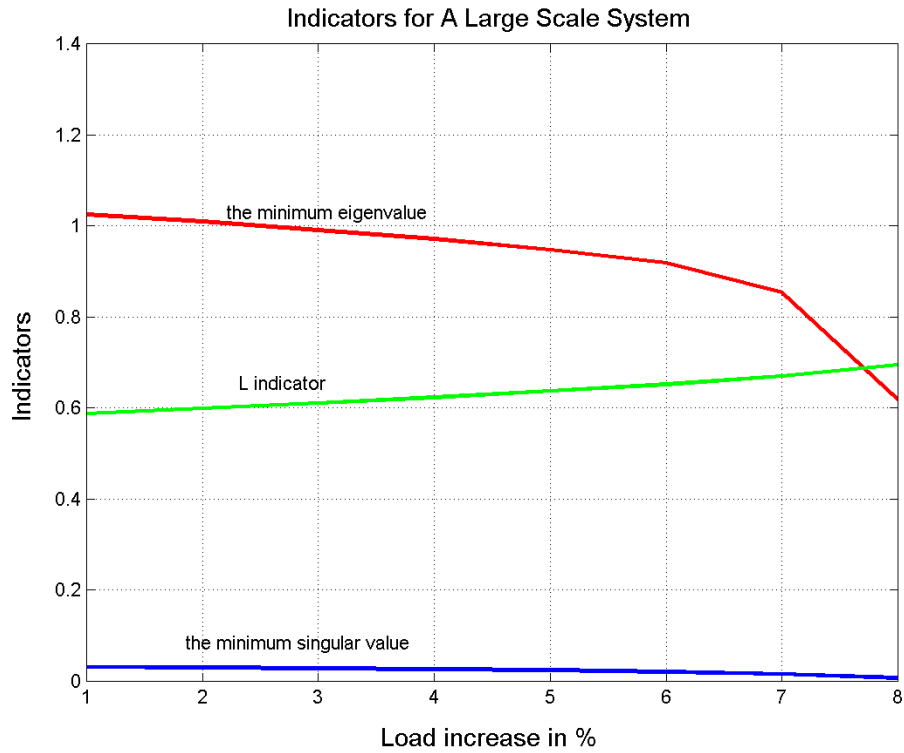


Figure 6.13.: The system-wide indicators for the NGC power system model

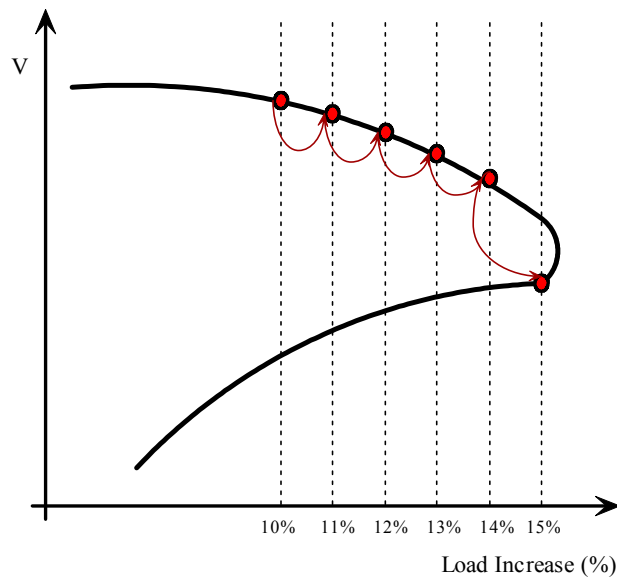


Figure 6.14.: Branch tracing for the IEEE 14 node system

6.4.2. Results for Node-Based Indices

The test function and VCPI indices are voltage stability indices that can be calculated for each node in a system. Therefore, these indices can be used to indicate the existence of local voltage problems. This could be their main advantage because large systems suffer more often from local voltage problems than from global ones. The fact that these indices can be calculated for each node separately makes them very efficient from a computation point of view. Therefore, the node-based indices:

1. are not time consuming and
2. can be used to recognise difference between global and local voltage problems.

These indices were again tested for the IEEE 14 bus system and the National Grid power system model. The normalised test functions and VCPI indices for the IEEE 14 node system are shown in Fig. 6.15 and 6.16, respectively. These indices are shown only for the three weakest nodes: 12, 13 and 14. These nodes are the weakest nodes with respect to their participation factors P_i^{SV} (see equation (6.35)). The test functions $\tau_{12,12}$, $\tau_{13,13}$ and $\tau_{14,14}$ shown in Fig. 6.15 have a similar shape as the test function for two node system shown in Fig.6.11. The change of sign between the last two load points show that the last load point is on the low voltage branch.

The characteristics of $VCPI_{12}$, $VCPI_{13}$ and $VCPI_{14}$ (see (6.48)) are almost identical, and only one is shown in Fig. 6.16. It can be seen that the characteristic is very similar to the characteristic of the two bus system shown in Fig. 6.10. Similarly, like the test function shown in Fig. 6.15 the characteristic becomes negative when the power flow solution switches from the high voltage to the low voltage branch.

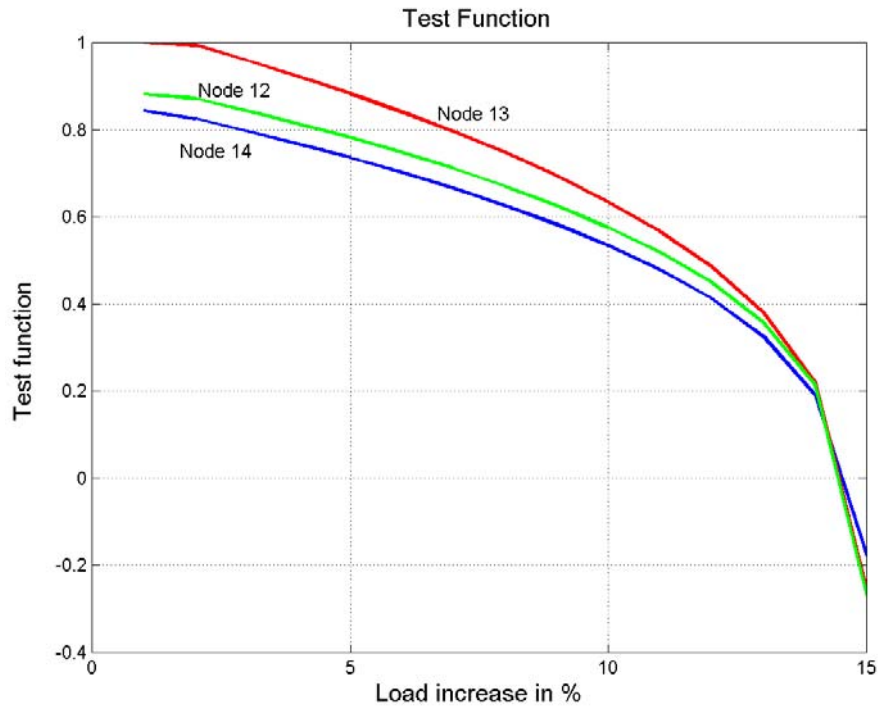


Figure 6.15.: The test functions for $k = l = 12, 13$ and 14 (IEEE 14 node system)

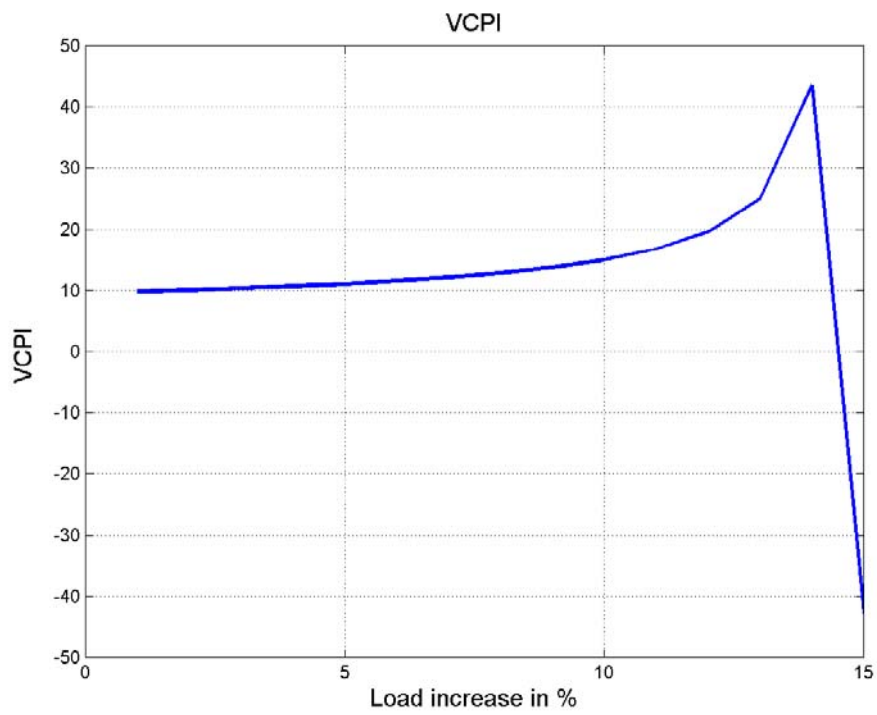


Figure 6.16.: The VCPI indices (nodes 12,13 and 14) for the IEEE 14 node system

The test results of the node based indices for the IEEE 14 node system show that the characteristics $\tau_{12,12}$, $\tau_{13,13}$, $\tau_{14,14}$, $VCPI_{12}$, $VCPI_{13}$ and $VCPI_{14}$ shown in Fig.6.15 have similar shape as the characteristics shown in Fig. 6.12.

For the NGC power system model node-based indicators might respond to local changes (outage, local load increase, etc) even when the system-wide indicators are almost insensitive to these changes. Such situation is shown in Table 6.5, where $VCPI_p$, the test function τ_p and the L indicator are given for all load points for the base case and an outage close to node P . It can be seen that the L indicator values for the base case and with an outage close to node P are almost the same. On the other hand, the test function values are almost 50% smaller, while the VCPI values are about 10% larger. This could be:

- an advantage considering that the system-wide indicators might ignore locally caused changes or voltage problems and end up in an unproductive search in the simulation of large system disturbances.
- an disadvantage considering that the node-based indices favour some non-important local changes and mislead the search for disturbances in the simulation of large system disturbances.

Table 6.5- Node based indices for two different power system states

<i>Load inc. (%)</i>	<i>VCPI_p</i>	<i>τ_p</i>	<i>L indicator</i>	<i>VCPI_p</i>	<i>τ_p</i>	<i>L indicator</i>
	<i>Base Case</i>			<i>Outage close to the node P</i>		
1	1.02891	21.89345	0.58788	1.12767	10.98567	0.58799
2	1.04789	21.68963	0.59891	1.15094	10.76396	0.59904
3	1.07124	21.50514	0.61066	1.17965	10.65170	0.61080
4	1.10070	21.29318	0.62325	1.21605	10.52343	0.62342
5	1.14349	20.74955	0.63691	1.26881	10.34526	0.63710
6	1.19970	20.23478	0.65198	1.33924	10.19747	0.65221
7	1.39603	19.78963	0.66949	1.57815	9.983474	0.66979
8	2.36238	19.123	0.69507	2.78463	9.87234	0.69570

Comparing the results obtained for two node system with the results obtained for larger systems the following conclusions can be drawn:

- The singularity point for two nodes system was obtained by solving $det(\mathbf{J}) = 0$ explicitly. However, this was not possible for larger power systems.

- Having found the singularity point, the exact distance to voltage collapse were determined for two-node system. On the other hand, for larger power systems only a point close to the singularity point was determined. Therefore, the distance that can be determined using such point is an approximation of the exact one.
- Larger systems experienced a change in sign when the system was approaching voltage collapse. Such change led to sudden discontinuities. For two node system the distinction was made between the high and low voltage solutions. Therefore, these discontinuities were not experienced for that system.
- The smaller a system the more sensitive it is to the load change. Some of the characteristics drawn for larger systems are almost linear up to the point of the maximum loading, while the characteristics shown for the two node system are more smoother.

In the simulation of large system disturbances these indicator and indices are used to make comparisons between system states in order to find which states are closer to voltage collapse. Therefore, the simulation does not really need the exact measure of the distance to voltage collapse. An approximation of such distance is rather acceptable from a comparison point of view.

In order to find an indicator that gives the best comparison results the simulation of large system disturbances has been run using different indicators. It was confirmed that all these indicators give similar results. The states selected as closer to voltage collapse are the same in a big majority of comparisons. Therefore, the L indicator is chosen to be used by the simulation, because its computation time is the smallest one.

7

Simulation of Large System Disturbances

This chapter describes the principles of the simulation procedure that has been developed. A large system disturbance is a process where transitional states are created by the outage of components. The representation of this process using an event tree is discussed in section 7.1. The transitional states in this event tree are derived from the base case, which is the root of the event tree. Any transitional state can be obtained from the root by applying a unique set of system component outages. These outages are the branches of the event tree. Therefore, between the root and any other node in the event tree there is a unique path, which is a collection of nodes and branches.

All system component outages are caused by protection system operations. These operations can be broadly categorised into expected and unexpected outages. The former can be activated by transient instability, a large variation in system frequency or violations of the thermal limits. Modelling of these phenomena is described in Chapter 4. The latter are caused by hidden failures in the generator and transmission protection system. These failures are discussed in Chapter 5.

The size of event tree is the main difficulty in the simulation of large system disturbances. This size depends on the number of paths that are considered. The effective exploration of the vast space of possible paths requires the application of the heuristic search techniques that will be discussed in section 7.2. These heuristics focus the search on the worst possible disturbance developments. The voltage stability indicators discussed in Chapter 6 form the basis of these heuristics.

The algorithm of simulation of large system disturbances is described in section 7.3, while the analysis of the simulation outputs is summarised in section 7.4.

7.1 Event Tree

The set of possible disturbance developments in a power system can be represented by an event tree such as the one shown in Fig. 7.1. The following observations can be made about this representation:

- *The root node* (i.e. the node at the top of the tree) represents the base case that is the state of the power system before the disturbance.
- Each *branch* represents the outage of a component.
- Each *node* represents a unique power system state that can be derived from the base case by applying the outages represented by the branches linking this node to the root node.
- All nodes that belong to the same layer (see Figure 3) have the same number of outaged components. Thus, a power flow analysis for each node from the same layer represents a N-1 contingency analysis at *Layer I*, N-2 contingency analysis at *Layer II*,..., N-x contingency analysis at *Layer x*. The number associated with a layer is the layer depth (for example, the layer depth of *Layer IV* is 4)
- The nodes that have no children are called *terminal* nodes. It is reasonable to specify a threshold depth $N_{LayerMax}$ so that $x \leq N_{LayerMax}$, because a disturbance that requires the outage of more than $N_{LayerMax}$ components has a negligible probability. For instance, assuming that the probability of any component outage in a sequence is 0.001, makes $N - 2$ sequences 10^9 times more probable than $N - 5$ sequences

- Each node can have a very large number of *children nodes or successors*. All these children nodes or successors have a unique *parent node or predecessor*. The number of successors must be limited to avoid a combinatorial explosion. This can be done by choosing the worst possible successors of each predecessor. A method to choose the worst possible successors will be described in the following section.
- Using an event tree helps keep track of each simulated sequence. These sequences are unique paths in the event tree, which begin with the root node and finish with a terminal node.

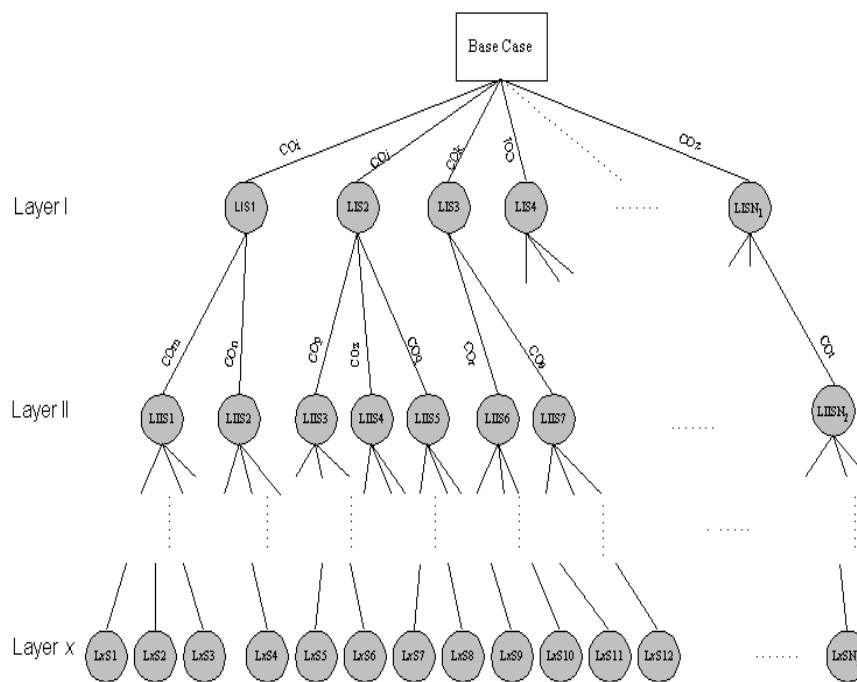


Figure 7.1.: Event tree

7.2. Creation of an Event Tree

To create an event tree the simulation of large system disturbances starts from the root node, which is the base case. Layer I contains initial faults selected at random, which should be specified at the beginning of the simulation. Most of these faults become successors or children nodes of the root node. It was assumed that all of these faults selected at random are line faults. It was further assumed that these line faults are cleared by the protection system.

The simulation first checks whether each of the system states caused by these line faults is secure. This means that certain calculations will be run for each of these faults. Only, faults that do not produce any of the system failures discussed in Chapter 3 become successors of the nodes from Layer I. Taking into account that power systems are normally N-1 secure, Layer I should always contain most of the faults selected at random.

Having completed Layer I, the search through the event three paths can proceed in two different ways. The first way is a depth first search, while the second one is breadth first search. These are illustrated in Fig. 7.2. Depth first search (shown in Fig. 7.2a), starts from the root node looking downward for terminal nodes. The search proceeds from the left to the right. The sequence of the search is A-B-A-C-E-C-F-G-A-D. The lists of open nodes which contain successors at each stage of the search are shown for a few stages of the search. Thus, the open nodes list at the beginning of the search contains three nodes: B, C, and D. At the stage A-B-A-C the open nodes list contains three nodes: E, F and D, while at the stage A-B-A-C-E-C-F the list contains only two nodes: G and D. These lists show that new nodes are always placed at the beginning of a list. Breadth first search is shown in Fig. 7.2b. Downward motion proceeds layer by layer. The sequence of breadth first search is A-B-C-D-C-E-F-G. The open nodes lists that correspond to the stages: A, A-B-C, A-B-C-D-C-E-F show that new nodes are always placed at the end of an open node list.

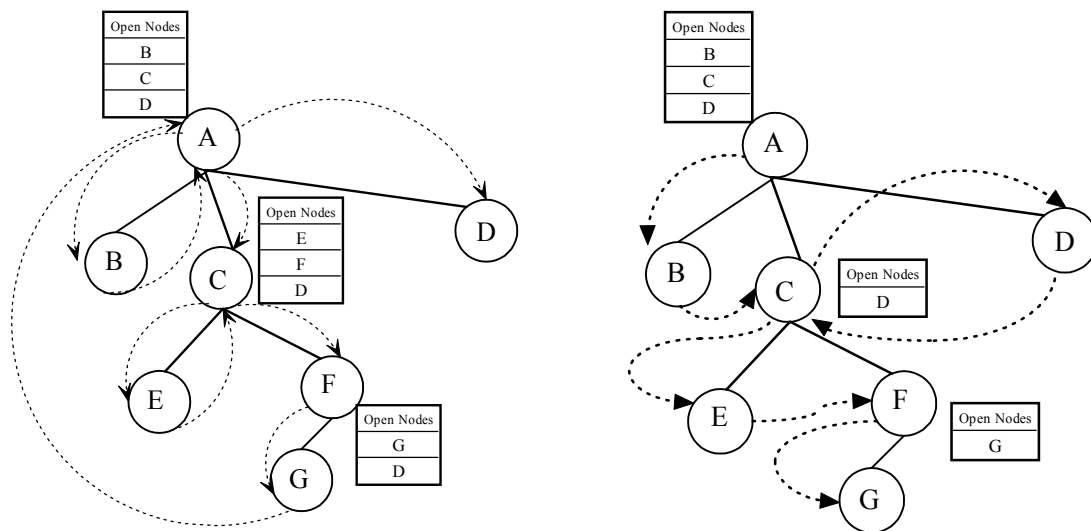


Figure 7.2.: (a) Depth first search (b) Breadth first search

The procedure for a depth first search is:

1. All search paths begin with the component outages between the root node and Layer I. Therefore, the first node in a tree path is a node from Layer I (see Fig. 7.1) only if the node is secure. This node becomes the current predecessor.

2. Determine all possible outages (branches) of the current predecessor. These are *candidates*. The simple event tree shown in Fig. 7.3 will be used to further illustrate some steps of this search. For instance, when S_0 is the current predecessor its candidates are the branches encircled by the dashed line (see Fig. 7.3).
3. Using the calculation of voltage stability indices, rank all these candidates and determine not more than N_{SUCC} candidates. N_{SUCC} is specified at the beginning of the simulation. Three out of five candidates are chosen in Fig. 7.3 as the best possible candidates. These candidates lead to the following nodes: NS_1 , NS_2 , NS_3 and $N_{SUCC} = 3$.
4. Delete the first node (S_0 see Fig. 7.3) from the open nodes list *ONL*. The list contains nodes that can be successors or terminal nodes. Extend the open nodes list *ONL* with the new successors (NS_1 , NS_2 , NS_3). If the *ONL* is not empty, first make entries for the new successors shifting the existing nodes from left to right by N_{SUCC} . This process is shown in Fig.7.3.
5. Continue the search in either of the following two ways, depending on whether *ONL* is empty or not.
 - a)If **yes**
 - Check whether all nodes in Layer I have already been explored
 - a1) If **yes** stop the search.
 - a2) If **no** take the next secure node from Layer I and continue from Step 2,
 - b)If **no** select the first node from *ONL* and continue with the following step.
6. Check whether the layer depth of the node selected in the previous step is larger than the threshold depth N_{LayMax} .
7. a)If **yes** the selected node is a terminal node.
 - b)If **no** run the simulations to detect the system failures discussed in Chapter 3. If any system failure occurs, the node is a terminal one. Otherwise, the node is not terminal and can have its own successors.

8. If the node is terminal, complete the search path, delete the node from *ONL* and continue with Step 5. Otherwise, this node becomes the current predecessor and the simulation continues from Step 2.

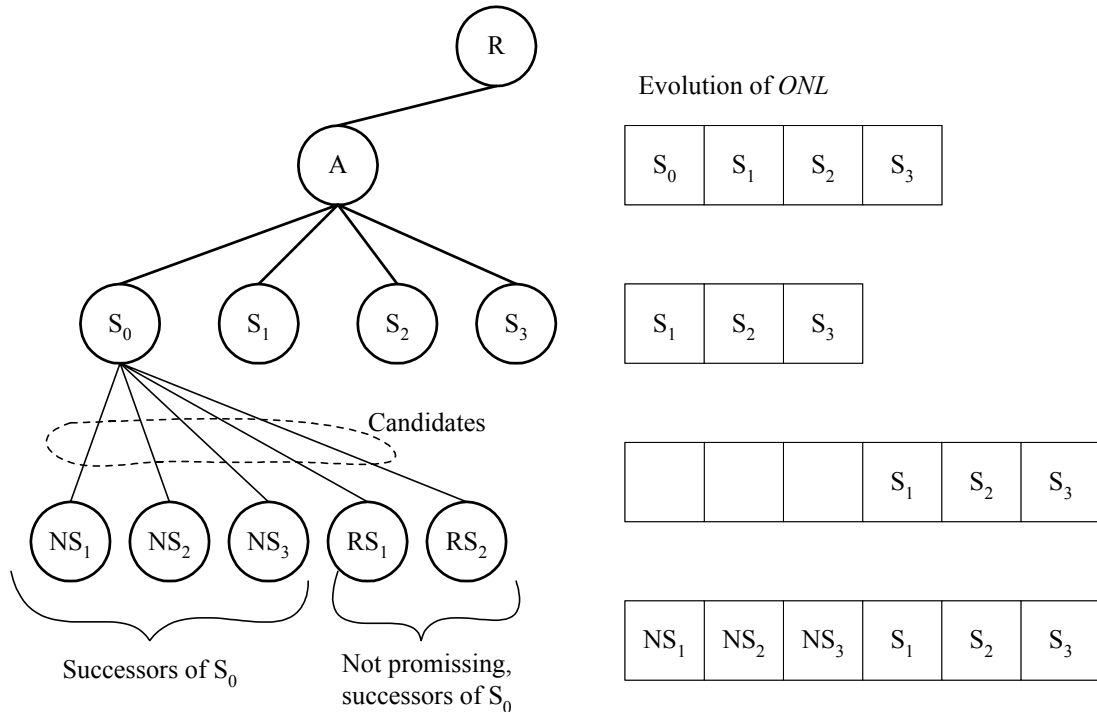


Figure 7.3.: Depth search and *ONL* evolution for a simple example

7.3. Simulation of Large System Disturbances

This section discusses the modelling side of the simulation procedure. For the sake of simplicity and brevity the simplified algorithm shown in Fig. 7.4 will be used to explain the basic concepts and modelling used in the simulation of large system disturbances. The simulation procedure is divided into two stages. The purpose of the first stage is to determine whether the system state caused by an initial fault is secure. It would be pointless to continue with further outages if the initial fault makes the state of system insecure. The second stage is the search procedure given in 7.2. This procedure produces the dangerous sequences of events.

The simulation procedure must start with a predefined list of initial faults (nodes from Layer 1). If the initial fault is recognised as dangerous in terms of transient stability then a transient stability simulation has to be performed. There are three possible outcomes for this simulation. The system can be transiently stable, transiently unstable in the case when several generator exhibit an unstable behaviour, and locally unstable when only a few generators

show unstable behaviour. If the system is transiently stable, a power flow calculation will be run to check whether load shedding is needed to achieve convergence. If the system is transiently unstable, any further outages are not allowed and the state of the system is considered as not secure. In this case a new initial fault will be taken from the predefined list and the process will be repeated. The last outcome (the system is locally unstable) will produce an active power imbalance in the system. The frequency response simulation must therefore be activated. There are three possible outcomes for the frequency response simulation. The system is frequency stable, the system experiences frequency collapse or a predefined limit of under-frequency protection is violated, which causes the activation of the corresponding level of load shedding. The last two outcomes mean that the current sequence is completed, the state of system caused by the initial fault is not secure and a new initial fault from the predefined list should be triggered. Therefore, it is only when the system is both transiently and frequency stable that the next step (a power flow calculation) takes place. If the power system after the initial fault is transiently and frequency stable and no load shedding is needed to achieve convergence of the power flow, the state of the system after the fault is secure. This means that the next outage level can be generated. This is the end of the first stage, which is shown in Fig 7.4a. The next stage of the simulation procedure is shown in Fig. 7.4b.

The most promising candidates should be selected from the vulnerability region discussed in Chapter 5. The size of the vulnerability region depends on the initial fault location and on the protection system design in the area surrounding the outaged components in the sequence. The more lines get involved in the sequence, the larger is the vulnerability region. The vulnerability region can be extended with overloaded lines if this phenomenon is considered.

Some generators close to the faulted area can be added to the vulnerability region as well (see Fig. 7.4b). However, rigorous criteria were used in the simulation of large system disturbances to determine the generators that are most prone to such failures. The criteria used in the simulation of large system disturbances to select the generators most prone to failures in their protection schemes are:

- the generator has to be electrically close to the disturbance,
- the generator has to operate close to its capability limits.

If more than one generator meet these criteria, an additional criterion is used to make a final decision about which generator will be selected. This criterion is based on the increase in reactive power output following the outage. This increase is defined as the quotient of the

generator reactive power output after and before the disturbance. The generator whose quotient is the largest is selected as the most prone to a failure in its protection system.

For each other candidate from the vulnerability region, a power flow calculation is performed. The power flow converges for the majority of these cases. Unfortunately, all these cases cannot be successors and they must be ranked on the basis of some appropriate criterion. A measure of voltage instability is chosen as this criterion. This measure of voltage instability is based on the static voltage stability indicators discussed in Chapter 6. Therefore, all components from the vulnerability region whose outage produce normal power flows convergence are ranked using the values of the voltage stability indicator. Only the best-ranked candidates become members of the *ONL*. Therefore, only these candidates are allowed to have successors, while the nodes associated with transient instability, frequency collapse and load shedding are terminal nodes, which are not allowed to have successors (see Fig 7.4b). The first node from the *ONL* is used to update the current sequence and the whole procedure defined in this section is repeated if the selected node is not terminal. If this node is terminal, a sequence initiated by the initial fault from the first stage is completed. When the *ONL* is empty, a new initial fault is taken from the predefined list if this list is not yet empty. In that case the simulation restarts from the first stage. When all initial faults are already considered the simulation stops.

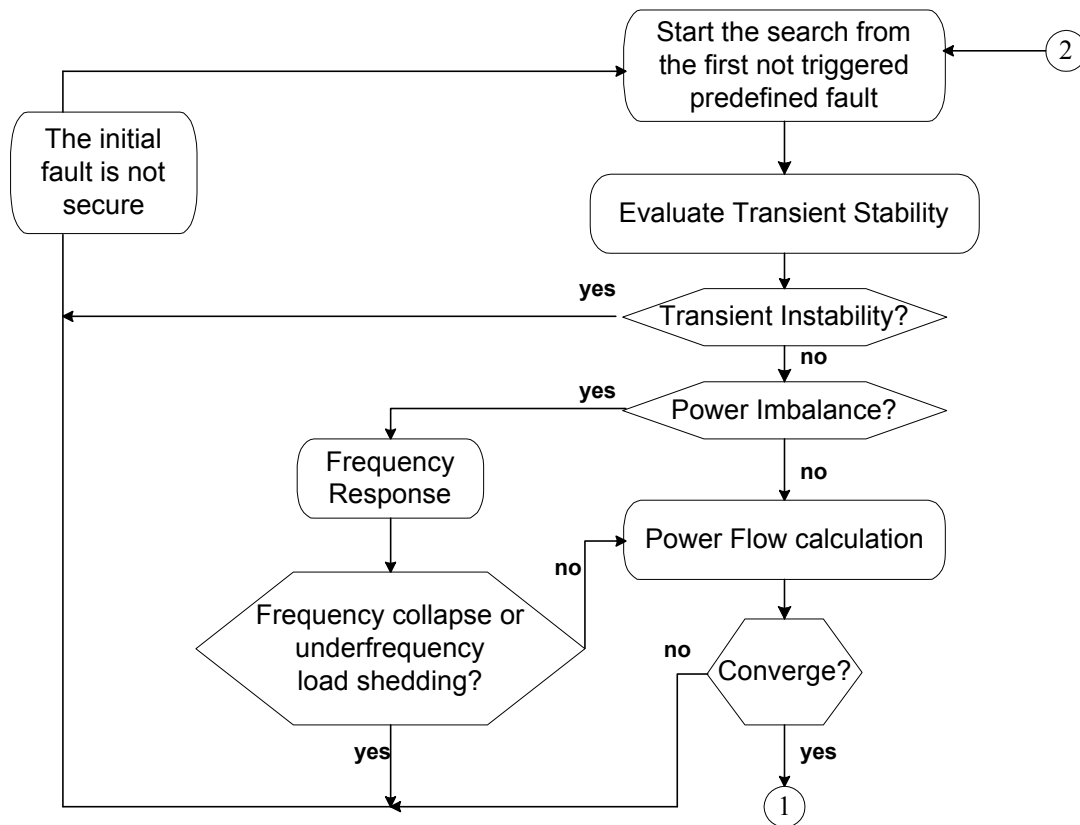


Figure 7.4a.: The first stage of the simulation procedure

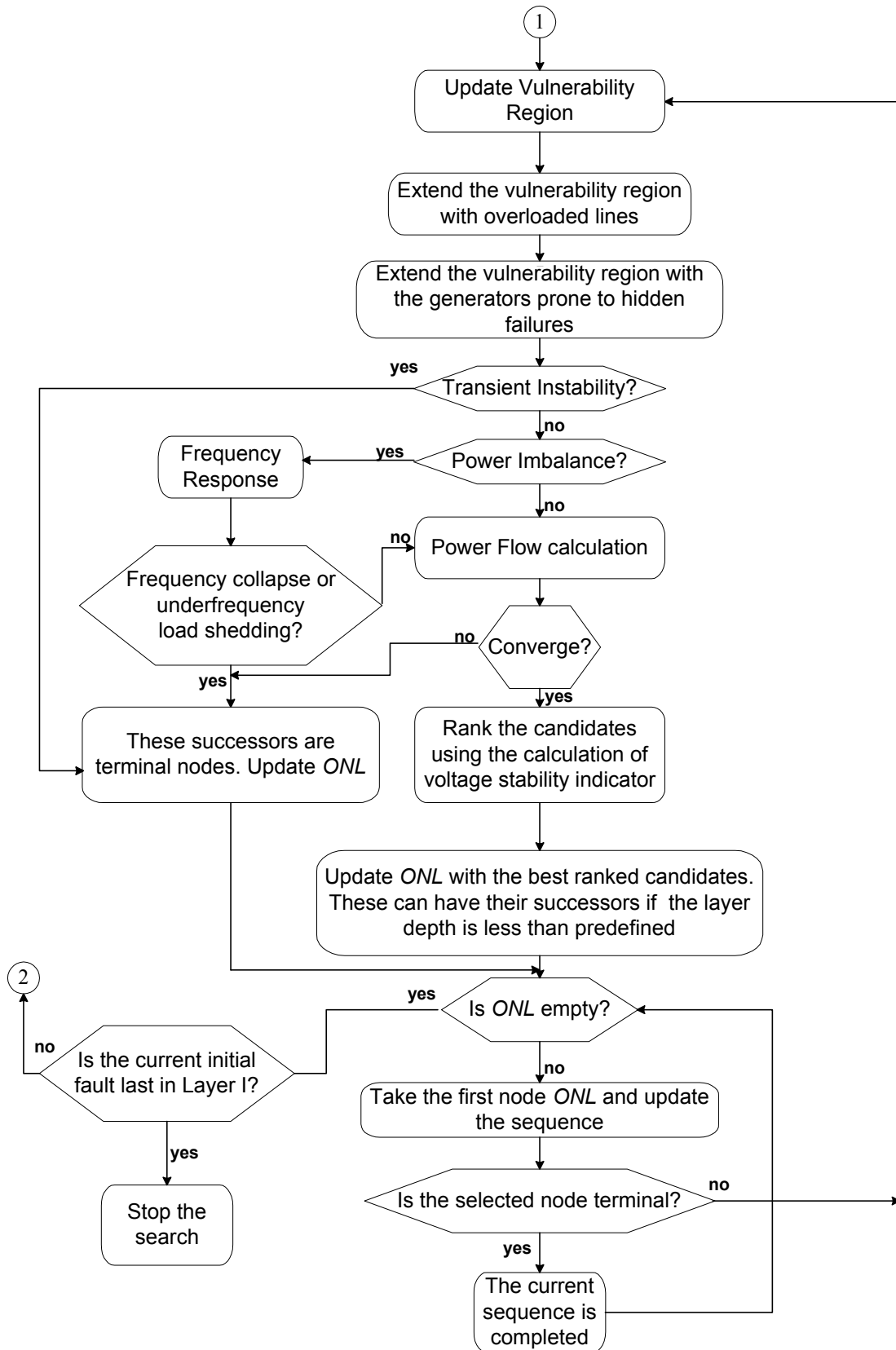


Figure 7.4b.: The second stage of the simulation procedure

7.4. Simulation Outputs

The simulation of large system disturbances can produce various outputs that are discussed in this section.

Among the large number of sequences generated by the simulation, only the interesting ones should be extracted and analysed. Analysing these sequences can help power system planners observe some unexpected event developments, which are usually outside the scope of most security studies. However, out of thousands sequences only a few produce useful information in that sense. Such sequences are normally triggered by a random fault and a hidden failure, but can produce serious line overloads or significantly increase reactive power output of some generators. This can further lead to new outages and end up into transient instability, underfrequency load shedding or even collapse. Some of these sequences will be discussed in the next chapter.

Another important aspect of this simulation is its ability to calculate the probability and cost of each sequence. The calculation of probability is straightforward if the probability of outage for each component of a sequence is known. Unfortunately, the lack of failure statistics that can be used to determine the probability of a hidden failure forced the author to make assumptions regarding their probability. This calculation is described in the following section. On the other hand, the approach used by Kirschen and his associates in [KBN03] is adopted to calculate the cost of each sequence. This approach is summarised in section 7.4.2. A sequence is deemed to have a cost only if load is shed because of component outages. Modelling of load shedding in the simulation is described in section 7.4.3.

The severity of a sequence in this work is represented by its cost. However, the sequences cannot be compared only on the basis of cost simply because they are not equally probable. Therefore, the cost of each sequence is multiplied by the sequence probability in order to estimate the risk of the sequence. Therefore, risk as a measure of both severity and probability is used for various comparisons of the simulation results. This risk calculation is described in the last section of this chapter.

7.4.1. Probability Calculation

Probability calculation of any system relies on failures rates of the system components. To produce these failure rates is a demanding job, which requires information on components behaviour over a long period of time and appropriate techniques to calibrate this information [Bro03].

The probability of any sequence can be calculated as follows if the individual probabilities of the events that make up the sequence are known:

$$P_k = \prod_{j=1}^{N_k} p_j \quad (7.1)$$

where N_k is the number of events in sequence k and p_j is the individual probability of event j in sequence k . Equation (7.1) is based on the assumption that all the events in a sequence are independent. The individual probability of a line being outaged due to line overload can be calculated as described in section 4.3. If a component is outaged due to a hidden failure then the following probability functions are used to calculate the individual probabilities:

1. *CA* – The individual probabilities are constant values and the probability of each hidden failure has been calculated as equal to the standard component unavailability p_{nU} that has been calculated on the basis of published reliability data [BGF95] and [CAS95].
2. *SA* – The individual probabilities are calculated from the step function shown in Fig. 7.5(a), where S_n is nominal power in MVA, p_2 is equal to p_{nU} , while p_3, p_4, p_2 are chosen to be 3, 6 and 10 ten times larger than p_2 , respectively.
3. *EA* – The individual probabilities are calculated from the exponential function shown in Fig. 7.5(b), where coefficients a, b are calculated using the values of exponential functions at the following points $y = p_1, S = 1.5S_n$ and $y = p_2, S = S_n$.
4. *LA* – The individual probabilities are calculated from the linear function shown in Fig. 7.5(c).

Therefore it was assumed that the individual probabilities of component outages due to hidden failures are equal to the standard component unavailability in normal circumstances

but they can increase up to ten times in abnormal circumstances ($S > 1.5 * S_n$). Changing the suggested probability functions and the values of their parameters (p_1, p_2, p_3, p_4) one can carry out a simple sensitivity analysis. This sensitivity analysis shows how the probability of sequences changes with respect to different probability functions and their parameters. A lack of any statistic regarding hidden failures was the main reason to carry out such sensitivity analysis. Chapter 8 shows that different probability functions do not necessarily lead to different conclusions.

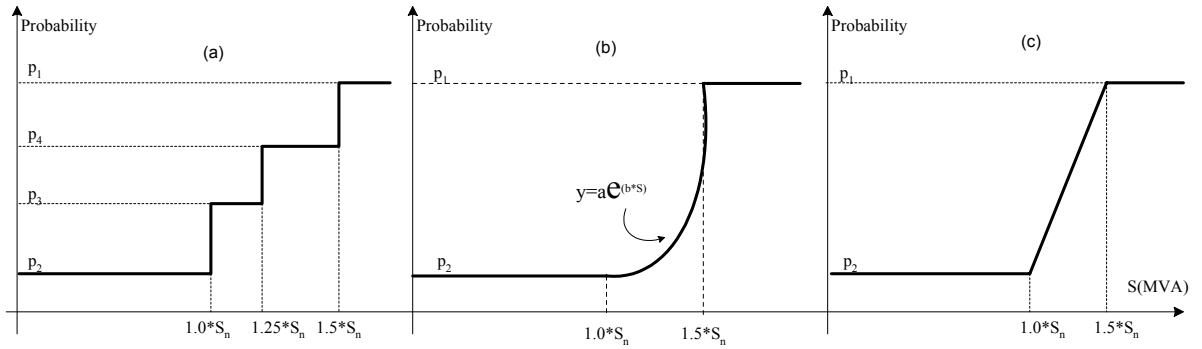


Figure 7.5: Probability functions

7.4.2. Cost of Interruption Supply

Several approaches can be used to determine the value that customers place on energy supply and the cost they associate with interruptions of this supply. One of the most established and accepted methods is based on surveys of customers that attempt to estimate the outage costs they would experience if their supply were interrupted. One such set of studies [KaA96] has been conducted in the UK and these results are used as the basis for the present studies. This UK study, and others conducted elsewhere, shows that the costs of interruption are a function of load interruption duration. These outage costs can be transformed into a parameter known as the “Value Of Lost Load” (VOLL) expressed in £/kWh not served. Since the outage costs are a function of duration, VOLL is also a function of the interruption duration.

Therefore, if the simulation indicates that load shedding is required to save the system, we assume that the shed load will be restored in a predefined number of segments n . The load restoration rates are given in Table 7.1. If the component outages that belong to a sequence cause load shedding, the cost C_k associated with the sequence is given by [KBN03]:

$$C_k = \sum_{j=1}^n (voll(t_j) t_j P_R(j)) \quad (7.2)$$

where t_j is the reconnection time for load segment j computed from the load restoration process, $P_R(j)$ is the reconnected load corresponding to segment j and $voll(t_j)$ is the value of lost load (VOLL). A VOLL function is computed by taking into account the type and distribution of customers using the approach described in [KaA96]. Table 7.2 shows the values of VOLL as a function of the duration of interruption for different sectors.

The total costs can be determined by summing the costs for all simulated sequences:

$$TC = \sum_{k=1}^{N_s} C_k \quad (7.3)$$

where N_s is the number of sequences.

Table 7.1- Load Restoration Rates [KBN03]

Time Period [min]	Restoration Rate [MW/min]
0 – 30	10.0
30 – 60	33.3
60 – 90	66.6
> 90	83.3

Table 7.2 - VOLL as a function of the duration of interruption for different sectors

Sector	VOLL [£/kWh] for duration of interruption of					
	1 min	20 mins	1 hr	4 hrs	8 hrs	24 hrs
Residential	-	1.35	1.62	2.79	2.99	3.12
Commercial	153.0	29.17	26.63	24.40	24.58	10.41
Industrial	776.4	85.62	50.52	36.11	30.03	12.53
Large users	606.6	30.87	10.77	3.32	1.82	0.83

7.4.3 Modelling of Load Shedding

A well-trained operator will shed load only when he or she believes that there is no other way to save the system. In other words, when he or she believes that it is better to disconnect a limited number of consumers rather than risk a large-scale collapse of the system that might leave much larger numbers of consumers without electricity supply. In this work the following two techniques are used to determine the amount of load shedding when it is required to save the system:

- a technique based on a simple logic that is based on the power flow calculation [KBN03] and
- an optimal power flow (OPF) [LeN01].

A simple logic based on the power flow calculation is a way to model the reactions of the operators. It assumes that operators have a reasonably good intuitive understanding of the state of the system and are reasonably good at estimating how much load should be shed to prevent a collapse. The ability of the power flow to converge has thus been taken as an indication of the operator's perception of the state of the system. If the generation equals the load in an island but the power flow fails to converge, it is assumed that this island would suffer a voltage collapse if the operator did not take action. It is further assumed that the operator's response to impending collapse would be to shed load in 5% blocks in the area of greatest mismatch until convergence is achieved. Generation is reduced by equal amounts. This load shedding is repeated until convergence of the power flow is achieved. If convergence cannot be achieved by shedding load in the worst affected area, the load disconnections are extended to neighboring areas where they proceed again in blocks of 5% of the area load. If a significant amount of load had been shed and convergence has not been achieved then the system is deemed to have collapsed.

One could argue that the ability of the power flow to converge is influenced not only by the proximity to a voltage collapse but also by the numerical properties of the power flow algorithm. Modern power flow algorithms, however, are able to converge for states that are quite close to the point of collapse.

The single state OPF developed by the author and described in [LeN01] can be used to determine the minimal amount of load shedding that is required to achieve convergence. This OPF is used only when the power flow calculation diverges. The OPF software was developed for educational purposes and can be used only for a relatively small system models.

The amount of load shedding determined by the first technique is in the big majority of cases larger than the minimum load shedding determined by the OPF. It is more likely that an operator that has made the difficult decision to shed load do not want to shed an amount of load that is insufficient to save the system. Therefore, the first technique may result in larger load shedding than is strictly necessary. However, in a small number of cases due to imposed voltage constraints in the OPF, the first technique can be more efficient.

7.4.4 Risk Calculation

Using equations (7.1) and (7.2) the risk associated with any sequence k can be calculated as follows:

$$R_k = C_k P_k \quad (7.4)$$

The risk associated with initial event j can be obtained as:

$$R_j = \sum_{k \in \alpha_j} [C_k P_k], \quad (7.5)$$

where α_j is the set of all sequences triggered by the initial event j . The total risk can be determined by summing the risks for all simulated sequences:

$$TR = \sum_{k=1}^{N_s} C_k P_k \quad (7.6)$$

8

Simulation

Results

This chapter discusses the results obtained by testing the simulation of large system disturbances on the IEEE 39 buses example.

The main focus of these results is to prove that the simulation achieves the objectives set in Chapter 2. These objectives can be simply stated as an attempt to reverse the traditional learning order and first learn **why** before we learn **how**. Utilities response to large system disturbances is often based on a principle that can be stated as “lesson learned, actions taken”. Unfortunately, quite often these lessons are learned from experience (we learn **how it happened**) rather than from a simulation tool or an analysis (we learn **why it could happen**). Any lesson from such experience might be very expensive. The tool for simulating large system disturbances cannot predict all the possible disturbances that could hit a power system. On the other hand, it can help power system operators and engineers learn more from the simulation results instead of waiting for disasters to happen. Therefore, the main focus of the simulation results is on the following three points:

- identification of the power system components whose outages can trigger sequences that could represent a serious threat to a power system,
- identification of the most vulnerable areas,
- identification of interesting sequences that can help engineers in operation and planning departments discover unsuspected mechanisms of dangerous event developments.

At the beginning of the first section a simple example of a vulnerability region is given and discussed. Various totals related to the simulated sequences are summarised in the second subsection. The simulation results related to the points raised above are given in 8.1.3, 8.1.4. and 8.1.5.

8.1. Simulation Results for the IEEE 39 Buses System

8.1.1 Vulnerability Region

The size of the vulnerability region depends on the location of the initial fault and the design of the protection system in the area surrounding this fault. Various protection system defects described in Chapter 5 can cause a hidden failure and an incorrect (unnecessary) outage following a fault. For the sake of simplicity and brevity, this section concentrates on hidden failures in the protection of transmission lines such as those that caused recent system disturbances (see Chapter 2). The extent of the vulnerability region will be discussed for a fault on the line between Bus-1 and Bus-2, shown in Fig. 8.1.

In Fig. 8.1 the faulted line is thickened and the dashed and dotted lines denote the vulnerability region of this line. The following details should be pointed out:

- The vulnerability region contains 7 lines. Among these lines or candidates we are looking for the protection failures that are most likely to start a chain reaction and lead a power system to catastrophic consequences.
- The dashed lines are lines that might be switched off due to hidden failures in directional comparison blocking scheme. The dotted lines represent lines whose relays might have a hidden failure in the distance protection scheme (Zone II and Zone III).
- It should be noted that the generator step up transformers are not considered in the vulnerability regions. All the generators connected to the network have their own busbar and step up transformer. These step up transformers are normally very

reliable, and it would be too pessimistic to consider their outages due to hidden failures. Therefore, the step up transformer between Bus-2 and Bus-30, is not considered as being in the vulnerability region.

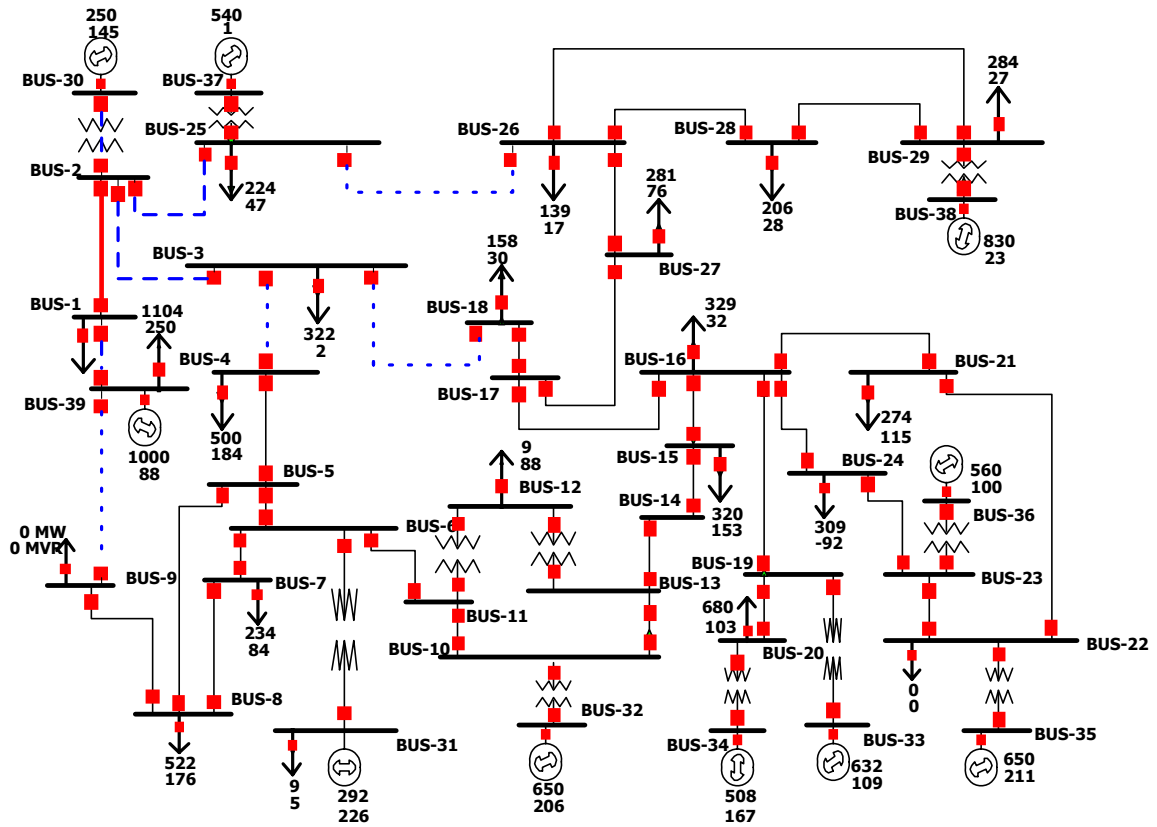


Figure 8.1.: The vulnerability region of line 1-2

8.1.2. Totals

The total number of the simulated sequences, the number of sequences where load shedding is required and the number of divergence cases are shown in Fig. 8.2. It can be seen that the total number of “bad” cases (shedding and divergence) is about 70%. Such a high number of bad cases is caused mainly by two factors:

- the size of the system and the proposed concept of vulnerability regions enable component outages to spread and affect the most vulnerable areas in the system, and
- the maximal number of outages allowed in a sequence is 4, which is a quite big number for such small power system

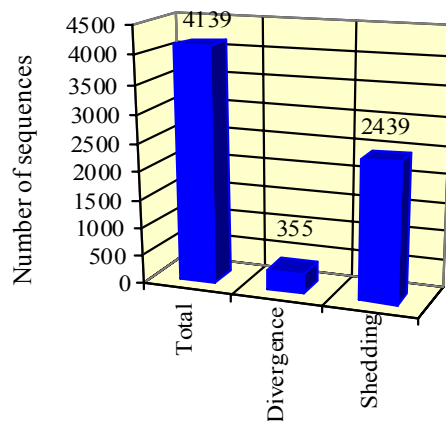


Figure 8.2.: Simulation Totals

Each sequence has a certain number of component outages. The first component outage in any sequence must be triggered by an initial fault (see Chapter 7). Therefore, the total number of initial faults is equal to the total number of simulated sequences, which is 4139. Apart from the first component outage a sequence can have one additional component outage ($x=2$), two additional component outages ($x=3$) or three additional component outages ($x=4$). All other component outages in these sequences are caused by the following events (see Fig. 8.3):

- line hidden failures (8816 events),
- transmission line outages caused by line overloads (2380 events),
- hidden failures in generator protection system followed by underfrequency load shedding (GHF+UFLS, 336 events),
- hidden failures in generator protection system (24 events),
- local transient (angle) instability and underfrequency load shedding (23 +30=53 events), and
- transient (angle) instability (2 events).

The average number of component outages per sequence is 3.80. It should be noted that some initial component outages are recognized as non-secure (see Chapter 7). These component outages were not used in the simulation as the initial component outages.

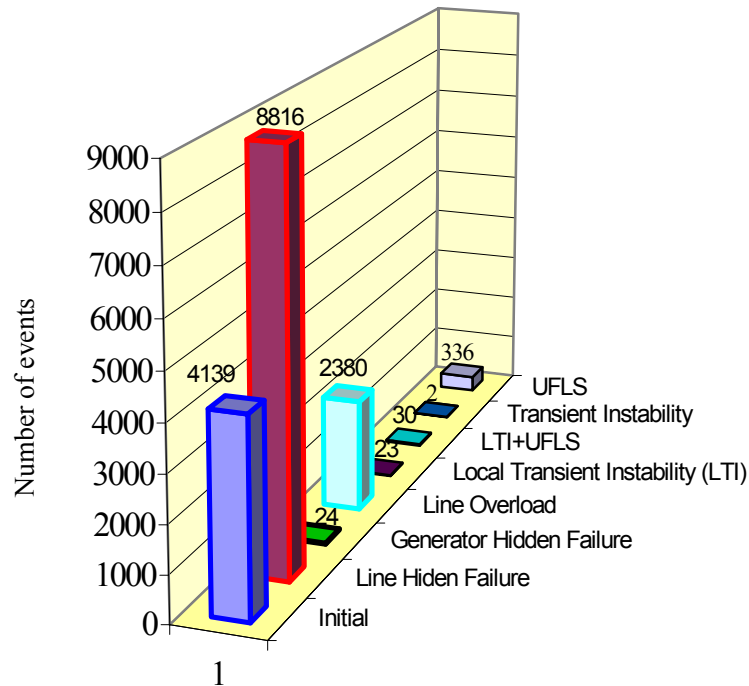


Figure 8.3.: Participation of different events in the simulated sequences

Generator hidden failures are not very frequent (24 + 336) due to the rigorous criteria adopted in section 7.3. In a big majority of the sequences that undergo such failures underfrequency load shedding was activated.

The simulation assumes that the system is transiently unstable if more than two generators show unstable behavior. If only one generator is transiently unstable then the system is locally unstable (23 situations). It means that the generator must be turned off and the frequency drop due to generator loss has to be calculated. Therefore, apart from generator outages due to hidden failures, underfrequency load shedding can be caused by a fault on a line, which causes a local instability. The total number of such cases was 30 (LTI+UFLS). On the other hand, the total number of situations where the system was unstable is 2.

Such a high percentage of underfrequency load shedding situations is in congruence with the fact that only a few of the 10 generators met the criteria required to be triggered due to hidden failure. These generators were mainly large generators. If any of these large generators is turned off the system frequency falls below 48.8 Hz and activates at least the first step of underfrequency load shedding.

Apart from an initial fault each sequence contains one, two or three additional component outages (see Fig 8.4). Therefore, the simulated sequences have different lengths. The largest number of sequences has four component outages $x=4$ (3451 out of 4139). About 15% (570) of the simulated sequences contain three component outages $x=3$, while only 116 out of 4086 is completed with two component outages $x=2$.

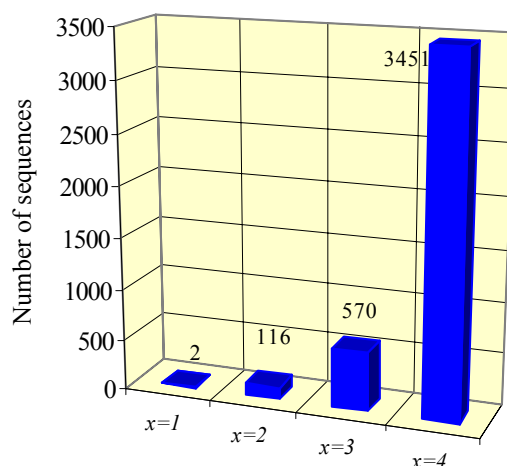


Figure 8.4.: Length of sequences

8.1.3. Ranking and Vulnerable Areas

Tamronglak suggests in [Tam94] that the components “surrounding” the faulted component are more vulnerable to hidden failures than all other components. This means that components that belong to a vulnerability region are more likely to be outaged by a hidden failure than components that do not belong to the vulnerability region. From a security point of view, the concept of vulnerability region assumes that the outage of any component from a vulnerability region is a credible contingency, while the outages component outside of the vulnerability region is much less probable or non-credible.

When applying deterministic security criteria, different utilities use different criteria to select credible contingencies. The $N - 1$ security criterion has been widely accepted among utilities. Using this criterion, power system conditions can be classified as secure if the system voltages and currents are within the specified limits for all possible single contingencies. Utilities often tend to extend this criteria to some selected multiple contingencies. However,

the choice of multiple contingencies differs from one utility to another. On the other hand, classifying system condition as secure based on voltage and current limits can be a serious drawback of deterministic security approaches [Kir02].

It was shown in 7.1 that the sequences produced by the simulation of large system disturbances represent a $N - x$ contingency analysis. The main characteristics of such a contingency analysis are:

- it takes into account all contingencies as $N - 1$ security criteria,
- it is not a complete $N - x$ contingency analysis, because it does not consider all possible combinations of x multiple contingencies.
- it selects multiple contingencies ($x > 1$) using the concept of vulnerability region and the calculation of voltage stability indicators.
- it can calculate the risk associated with each initial contingency (see equation (7.5)).

Considering the above characteristics one can say that $N - x$ contingency analysis:

- extends $N - 1$ security analysis,
- consistently selects multiple contingencies,
- ranks the initial contingency by using risk.

Therefore, instead of using voltage and current limits to rank all initial contingencies this ranking can be based on risk as was proposed in 7.4.3. Using equation (7.5), a measure of risk can be associated with each initial contingency. The measure of risk takes different values depending which probability function is used to calculate the probability of a sequence. These functions are discussed in section 7.4.1 and denoted as: CA , SA , EA and LA . The top ten initial contingencies ranked on risk basis are given in Table 8.1 for all probability functions. It can be seen that the list obtained by using different functions are almost the same. However, when the parameters p_1, p_2, p_3, p_4 of these functions are changed this list of the top ten ranked contingencies is completely different. This is shown in the last column (EAI) of Table 8.1, where the initial contingencies are ranked using the exponential function shown in Fig 7.5(b). Therefore, two identical exponential functions in terms of their shape are used to make the ranking given by columns EA and EAI in Table 8.1. However, parameter p_2 used by the first exponential function EA is chosen 10 times smaller than the same

parameter used by the second exponential function *EAI*. It can be seen that six initial contingencies (grey shaded) remains in the top ten, but the ranking order and risk value are quite different than in the first four columns. Considering that costs are not affected by the choice of probability functions, it appears that the probability calculation can play a key role in this risk-based ranking. Changing the shape of a probability function and its parameters has the following consequences:

- the shape of the probability function does not significantly change the ranking but can change the risk,
- the parameters of the probability functions can significantly change the risk and the order.

The three vulnerable areas highlighted by dotted lines in Fig. 8.4 have been identified using the ranking given in Table 8.1. These lines are very important transmission corridors, which enable power transfer from the generation connected at buses 32,33,34,35 and 38 to load areas.

Table 8.1.: Ranking of initial contingencies

<i>CA</i>				<i>SA</i>		<i>EA</i>		<i>LA</i>		<i>EAI</i>			
<i>Line ID</i>	<i>Bus₁</i>	<i>Bus₂</i>	<i>Risk (p.u.)</i>	<i>Line ID</i>	<i>Bus₁</i>	<i>Bus₂</i>	<i>Risk (p.u.)</i>						
27	19	16	1.00	27	1.00	27	1.00	27	1.00	20	10	32	1.00
44	29	26	0.69	44	0.85	44	0.75	44	0.83	29	24	16	0.78
28	21	16	0.67	28	0.67	28	0.68	28	0.65	38	24	23	0.74
45	29	28	0.44	45	0.60	45	0.55	45	0.58	19	13	10	0.63
38	24	23	0.42	38	0.59	38	0.52	38	0.57	44	29	26	0.59
29	24	16	0.36	29	0.55	29	0.45	29	0.53	6	4	3	0.55
13	11	6	0.34	13	0.35	18	0.36	13	0.36	45	29	28	0.53
18	11	10	0.34	18	0.34	13	0.34	13	0.36	18	11	10	0.53
23	14	13	0.34	19	0.34	23	0.34	23	0.36	40	26	25	0.50
19	13	10	0.34	23	0.34	19	0.34	19	0.36	30	18	17	0.46

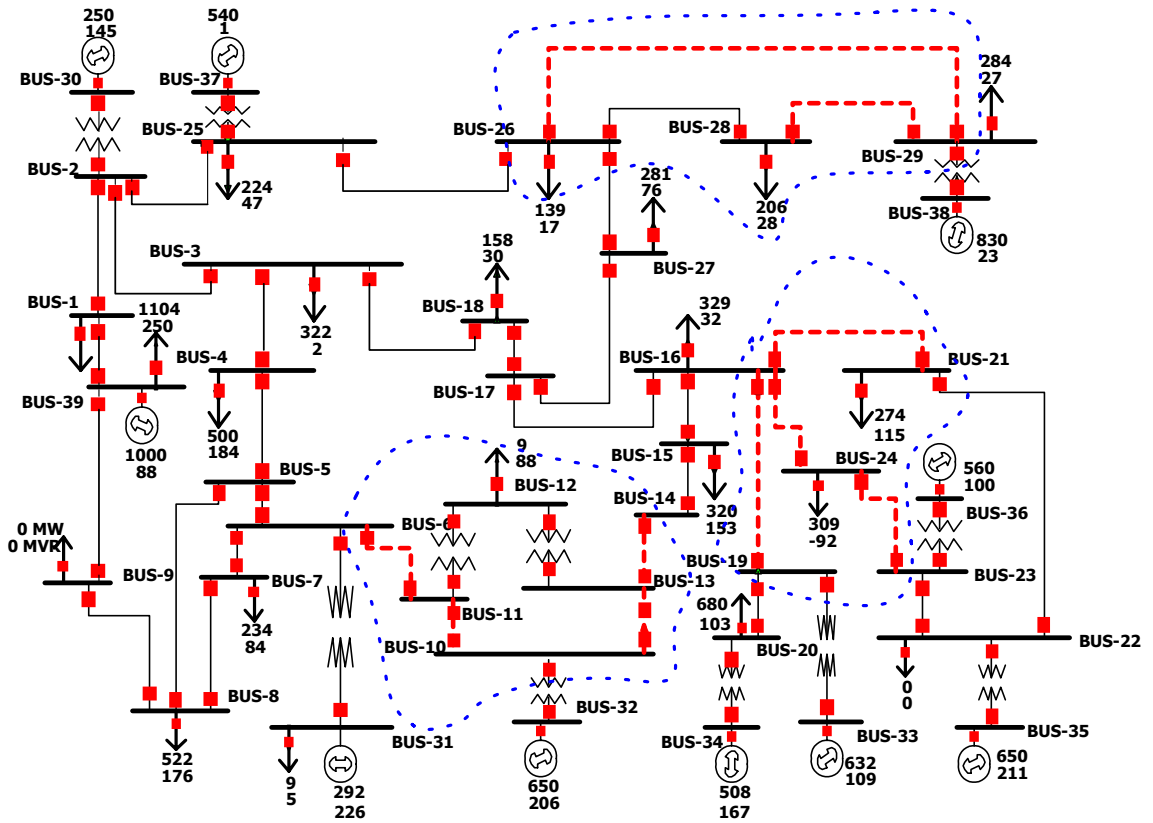


Figure 8.5.: Vulnerable areas

8.1.4. Risk and Costs versus Load Increase

The main focus of this section is to investigate the impact of load increase on the total risk and costs. In order to carry out this investigation the simulation was performed for several load levels. These load levels are obtained by increasing the load from 100% to 108% in steps of 1%. The total costs and risk are calculated using equation (7.3) and (7.6), respectively. The total risk and costs are shown in Fig. 8.6. The changes in the total number of simulated sequences, the number of divergence and load shedding cases are depicted in Fig. 8.7. According to equation (7.1) the length of a sequence dictates the value of the sequence probability. Bearing in mind that the individual probabilities are smaller than 1.0 makes shorter sequences more probable. The length of a sequence is denoted by the number of component outages x . The number of sequences when $x = 1, x = 2$ and $x = 3$ for all load points are shown in Fig. 8.8. In the legend of this figure, the numbers given in the brackets represent the total number of occurrences for each sequence length.

The following conclusion can be made derived from figures 8.6, 8.7 and 8.8:

- the total cost shows a steady increase up to 2% of load increase. Between 2% and 6% these costs are mainly dependent on the number of divergence cases. At 7% of load increase there is a small increase in costs caused by a rapid increase in the number of sequences and the number of load shedding cases,
- The total risk has a steady increase up to 2% of load increase. At 4% of load increase there is a significant increase in the number of sequences where $x = 2$, which caused a significant increase in the sequence probability and consequently an increase in the risk. The risk continues to decrease between 4% and 6% and shows a steady behavior for the last two load points.
- The characteristics that describe the change in the total number of simulated sequences and load shedding cases have a very similar shape. It appears that the number of load shedding cases is almost proportional to the total number of simulated sequences.
- Except for a 2% load increase, the number of divergence cases decreases constantly with load increase. It should be pointed out that its rate of decrease is almost equal to the cost decrease in the interval between 2% and 6% of load increase. This means that costs in this interval are driven mainly on the costs caused by these divergence cases.
- The number of insecure cases $x = 1$ (see Fig. 8.8) increase as the load increases. It can be seen that for an 8% load increase, 17 initial contingencies out of 46 have become insecure. The increase in the number of insecure cases decreases the total number of simulated sequences.

The following conclusions can be drawn from above counter-intuitive analysis:

- the number of simulated sequences decrease when load increases. This decrease produces that the total costs and risk decrease,
- the number of load shedding cases follows almost proportionally the changes in the number of simulated sequences,
- the number of divergence cases make a significant contribution to the total costs and risk.

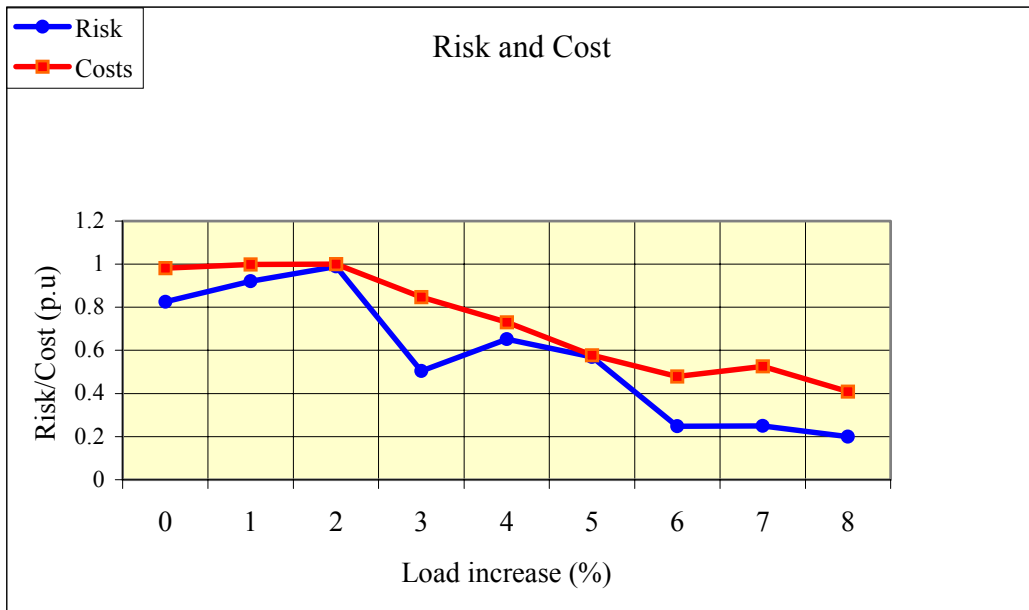


Figure 8.6.: Risk and Cost versus load increase

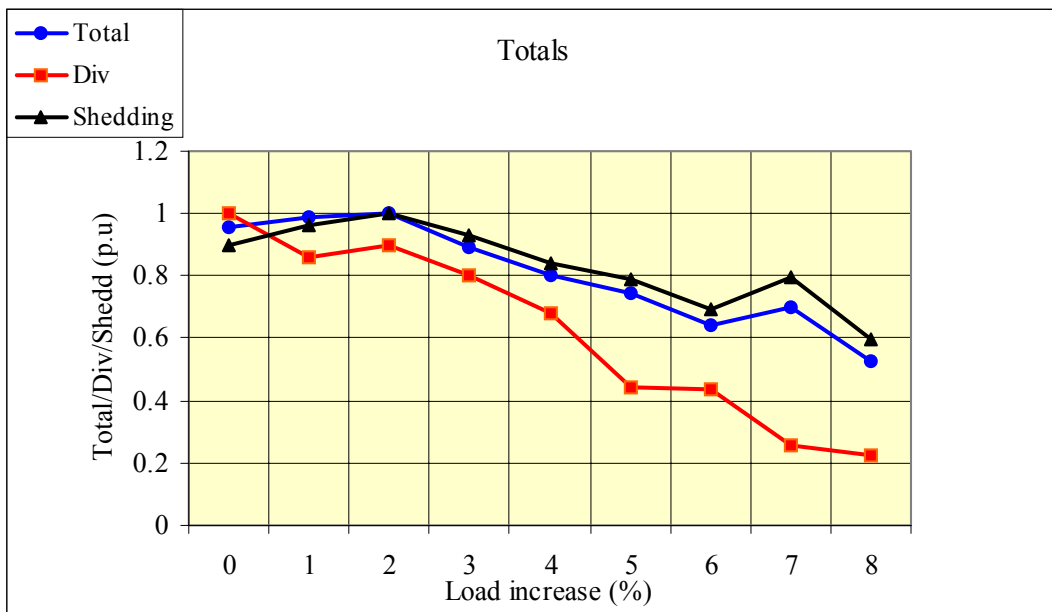


Figure 8.7.: Totals versus load increase

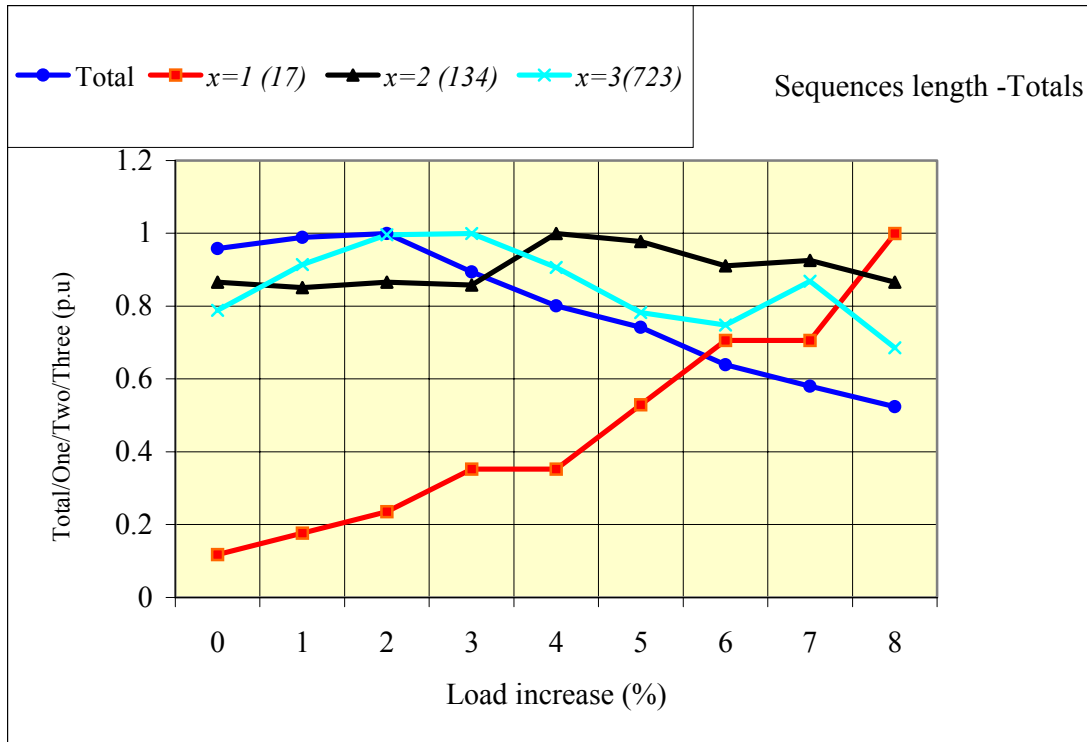


Figure 8.8.: Sequence length versus load increase

8.1.5 Interesting Sequences

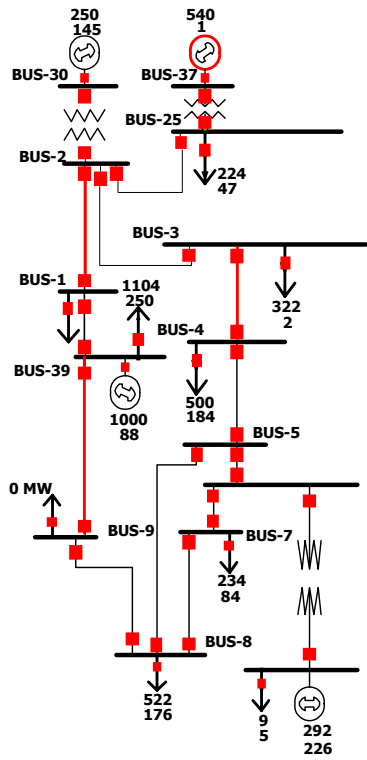
Special techniques based on data mining and artificial intelligence could be used to extract useful information from the simulated sequences. Instead, simple search procedures have been used instead to extract interesting event developments. A few sequences obtained through this search will be explained.

The development of the first interesting sequence is shown in Fig. 8.9a. After the initial fault on the line between buses 1 and 2, this line is switched off by its protection system. However, this fault exposes some other lines in its surrounding. Zone III of the distance protection on line 9-39 sees the same fault but its timer should prevent the line opening for 1.2 seconds after the fault. However, a hidden failure in the Zone III timer might cause the timer to malfunction. This causes the distance protection scheme to unnecessarily open the line straightaway. With these two lines open, power flows have to be shifted to other lines. This significantly overloads line 3-4. The line sags and after some time flashes over to some object beneath it. After these three outages the system becomes more vulnerable and weak, desperately requiring reactive power support. The support comes first from the nearest

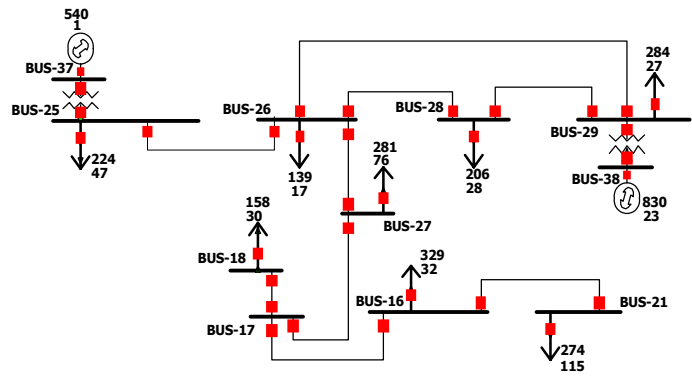
generator at bus 37, which rapidly increases its reactive power output. However, the protection system of the generator excitation system identifies this rapid increase as excessive and turns off the generator. After three line outages and a power shortage due to a generator outage, the system frequency starts to fall. After a short time, the frequency drops below 49.2 Hz, which activates the first step of the underfrequency protection. This protection sheds 10% of the system load.

The development of the second interesting sequence is shown in Fig. 8.9b. It is triggered by an initial fault on the line between the buses 29 and 26. After the protection system disconnects the line, a large amount of active generation produced by the generator connected at bus 38 is redirected to the lines between buses 29-28 and 28-26. At first glance, power system operators would focus their corrective actions on these lines in order to secure the generation at bus 38 and the demand at buses 29,28,26,27 and 18. This demand is a few hundreds MW larger than the generation at bus 38, which means that some support is required from other generators. A part of this support comes from the generator connected at bus 37 via line 25-26. The protection system of this line sees the initial fault through a directional comparison blocking scheme, which is the primary protection scheme of this line. However, the blocking mechanism of this protection might have a hidden failure, which can disconnect this healthy line unnecessarily. Even with this line out of service the power system can survive if it can reach steady state. However, the system becomes transiently unstable after such an unexpected double contingency and the generator connected at bus 38 is disconnected. This further leads to a power flow divergence due to a large concentration of demand in the area shown in Fig. 8.9b. This explanation shows why the line between buses 29 and 26 (line 44) is highly ranked by all approaches.

The last interesting example is related to the line between buses 8 and 5 (see Fig. 8.9a). A careful investigation of one of the sequences triggered by a fault on this line leads to the conclusion that a significant number of sequences contain line overloads. This line outage by itself does not produce any line overload but in combination with some other outages, load shedding or even blackouts can be experienced. After the initial fault on this line the most dangerous hidden failure is the hidden failure in the Zone III distance protection of line 11-6. This failure creates a very dangerous double contingency from a benign single contingency. Such double contingency causes serious overloads on the neighbouring lines. These overloaded lines are a serious threat because their outages can cause serious load shedding.



(a)



(b)

Figure 8.9.: Interesting sequence developments

9

Conclusions

Large system disturbances represent a serious threat for power systems. That is the main reason why huge engineering and research efforts have been devoted to these events. Many of these analyses have been used to improve defence mechanisms and prevent similar disasters. It seems that the policy of utilities regarding large disturbances is based on a principle that can be summarised as “lessons learned, actions taken”. This is an expected response taking into account that large system disturbances are very rare events and unique in terms of their development. However, the introduction of competition in the electricity supply industry, market rules and change in the structure of the generation capacity (e.g. the EU target that 10% of total energy should come from renewable sources), will put more pressure on the security of power systems. Large system disturbances therefore might become more frequent and more severe. Considering all these circumstances it would be difficult to justify the existing policy of utilities regarding the prevention of such disturbances.

The fact that such disasters have occurred on average once in tens of years for large power system does not mean that they will not happen tomorrow or that their frequency will not increase. The fact that their development is unique does not mean that research aimed at predicting them does not have any chance of success. The work done in this thesis is focused on a completely different direction from utility practice regarding these disturbances. This thesis argues that simulation might help discover potential disturbance scenarios. The proposed simulation is not an ideal tool that is able to predict all possible disturbances, but it can help power system planners and operators get some confidence in preventing these disturbances. One might be sceptical and argue that such simulation

cannot be good enough, because using the existing knowledge about disturbances, we are not able to model all possible reasons, common and contributing factors that cause disturbances. That is true, but some of these reasons, common and contributing factors have already been recognised in the work that has been done in the last 30 years. The information and conclusions obtained through that work are used in the proposed simulation. Therefore, the simulation is not able to give answers beyond the knowledge collected through the previous work, but it is capable of discovering scenarios for large disturbances using the reasons, common and contributing factors that were identified previously.

A significant amount of work in this thesis was devoted to modelling various power system phenomena. Both static and dynamic models were used to assess transient stability, frequency response, voltage stability and steady state system conditions. Some of these models such as the dynamic models for transient stability and frequency response are simple but, as suggested in the thesis, they can be replaced easily by more complex models. The main novelty of the simulation is the search for dangerous event developments based on the concept of vulnerability region and on voltage stability indicators. The concept of vulnerability region required a detailed model of the protection system. Various voltage stability indicators were compared in order to choose the one that best suits the simulation requirements.

The simulation creates a set of sequences, assuming that each sequence is triggered by an initial outage caused by a random fault. A measure of risk (probability times severity) is calculated and associated with each sequence. Several probability functions and parameters are used to calculate the probability of a sequence, while the cost of the outages caused by the sequence is used as a measure of its severity. This cost calculation is based on the amount of load shedding required to achieve convergence of the power flow. An optimal power flow and a simple logic that uses the power flow calculation are used to determine the required amount of load shedding.

Considerable efforts have been put in linking all these methods and models into an effective simulation procedure. It should be noted that all developed methods have been tested on difficult system conditions when a power system is affected by more outages.

The simulation is able to identify interesting sequences and to rank initial outages based on risk. These interesting sequences are a combination of a few interlinked events that are beyond the scope of most conventional security criteria. The test results obtained on the

small system example confirm that the simulation is able to create disturbances similar to some that have taken place in real power systems. Initial outages that trigger all these sequences can be ranked and vulnerable areas in a power system can be identified.

9.1. Recommendations for Further Research

The suggestions for further research can be divided into two groups: general suggestions and suggestions related to the simulation method. The former is focused on the new directions for research in power system security, while the latter suggestions deal with possible improvements to the proposed simulation of large system disturbances.

The first group of suggestions results from a comparison between deterministic and probabilistic approaches that have been used to assess power system security. The time horizons of operation and operational planning are considered. The suggestions can be summarised as follows:

- if a deterministic approach is the preferred option, then the set of credible contingencies has to be better defined. This set can be chosen in many different ways. The computing requirements were the only objective for different contingency screening and ranking procedures proposed 20-30 years ago. In these procedures, the following problems can arise: the set of credible contingencies is either too big or too small, the ranking is based on performance indices calculated using voltage and current limits and all contingencies have the same probability to occur. The performance of modern computers is significantly higher than it was 20-30 years ago. Using multiprocessing and high-speed computers, the existing lists of credible contingencies can be significantly extended. On the other hand, instead of focusing only on computing requirements contingency screening and ranking procedures can be changed to take into account some other phenomena such as: dynamic phenomena (stability and frequency), possible protection system “dependent contingencies” and different probabilities for different contingencies. The new performance indices should be based on risk as a measure of both severity and probability.
- if a probabilistic approach is the preferred option, then an approach similar to the one suggested by J. McCalley and his associates in [MMcV03] can be used. This approach is an on-line risk security assessment, which condenses contingency likelihood and severity into indices that reflect probabilistic risk. What can be its

advantage with respect to widely accepted deterministic approaches? The decision making process in a control room requires a significant amount of subjective assessment regarding questions like: How many overloads or voltage violations are there and how severe are they? How close to voltage instability? How close to transient instability? Is cascading due to protection failures possible? What is the likelihood of occurrence for each contingency? The authors in [MMcV03] argue that risk indices may be used to more efficiently address these types of questions. The work done in [MMcV03] describes such indices and the computations required to obtain them online. However, there is still a lot of room for improvements, especially regarding severity functions and the questions raised above.

The second group of suggestions is related to possible improvement of the simulation of large system disturbances. These suggestions are as follows:

- Further knowledge about disturbances can be obtained through additional communication with utilities,
- The models used in this work can be improved. Dynamic models for transient stability and frequency response can be replaced with the more detailed models suggested in this thesis,
- Modelling of switching equipment can be included in the simulation as suggested in Chapter 3,
- Further investigation could be carried out on the probability of hidden failures,
- Different scenarios could be compared based on their associated risk. These scenarios can be created for different network configurations, generation schedules, the number and location of reactive support devices, as well as import/export levels,
- Improvements related to the optimal power flow. These can help improve the accuracy of the cost calculation in the simulation of large system disturbances.

References:

- [AjC92] V. Ajjarapu and C. Christy, "***The continuation power flow: A tool for steady state voltage stability analysis***," IEEE Transaction on Power Systems, Vol. 7, No. 1, February 1992, pp. 416-423.
- [AlA82] R. N. Allan, C. Arruda, "***LTC Transformers and MVAR Violations in the Fast Decoupled Load Flow***", IEEE Transaction on Power Apparatus and Systems, PAS-101, 1982, pp. 3328-3332.
- [AlB00] R. Allan, R. Billinton, "***Probabilistic assessment of Power System***", Proceedings of IEEE, Vol. 88, No. 2, February 2000, pp. 140-162.
- [AnF77] P. M. Anderson, A. A. Fuad, "***Power System Control and Stability***", The Iowa State University Press, Iowa, USA, 1977.
- [BaT02] K. Bae, J. S. Thorp, "***Detecting and Improving the Vulnerable Links in the Power Network: Part I***", www.pserc.wisc.edu/index/, 2002.
- [BGF95] R. Billinton, R. Ghajar, F. Filippeli, R. Del Bianco, "***Transmission Equipment Reliability Using the Canadian Electrical Association Information System***", IEE, 2nd Int. Conference on Reliability of Transmission and Distribution Equipment, 1995, Conf. Pub No. 406, pp. 13-18.
- [BTH92] F. Bourgin, G. Testud, B. Heilbronn, J. Verseille, "***Present Practices and Trends on the French Power System to Prevent Voltage Collapse***" IEEE/PES Summer Meeting, 1992, pp. 1-7.
- [BaT97] K. Bae, J. S. Thorp, "***An Importance Sampling application: 179 Bus WSCC System under Voltage Based Hidden Failures and Relay Malfunctions***", Hawaii International Conference On System Sciences, Kona, Hawaii, 1997.
- [Bel97] K. Bell, "***SVC Modelling in Value of Security Assessor***", Technical Report, UMIST, 1997.
- [BeV86] A. Bergen, V. Vitall, "***Power System Analysis***", Second Edition, Prentice Hall, New Jersey, 1986.
- [BiK92] R. Billinton, M. E. Khan, "***A Security Based Approach to Composite Power System Reliability Evaluation***", IEEE Transaction on Power Systems, Vol. 7, No. 1, February 1992, pp 65-71.
- [Bla98] J. Lewis Blackburn, "***Protective Relaying – Principles and Applications***", Second Edition, Marcel Dekker, New York, 1998.
- [Bro03] R. Brown et al, "***Failure Rate Modelling Using Equipment Inspection Data***", accepted for publication, IEEE Transaction on Power Systems, 2003.

- [CaA93] C. A. Cañizares and F. L. Alvarado, "***Point of collapse and continuation methods for large ac/dc systems***", IEEE Transaction on Power Systems, Vol. 8., 1993, pp. 1-8.
- [CAS95] Canadian Electricity Association, "***Generation Equipment Status***", Annual Report 1995.
- [CB88] S. Chang, V. Brandwajn, "***Adjusted Solutions in Fast Decoupled LoadFlow***", IEEE Transaction on Power Systems, Vol. 6., 1988, pp. 801-805.
- [CB91] S. Chang, V. Brandwajn, "***Solving the Adjustment Interactions in Fast Decoupled Load Flow***", IEEE Transaction on Power Systems, Vol. 3., 1991, pp. 726-732.
- [CCC95] Y. Chen, C. W. Chang, C. C. Liu, "***Efficient Methods for Identifying Weak Nodes in Electrical Power Networks***", IEE Proceeding – Generation, Transmission and Distribution, Vol. 142, 1995, pp. 317-322.
- [CFY90] J. C. Chow, R. Fischl and H. Yan, "***On the Evaluation of Voltage Collapse Criteria***", IEEE Transaction on Power Systems, Vol. 5, 1990, pp. 612-620.
- [Cla90] H. K. Clark: "***New Challenge: Voltage Stability***", IEEE Power Engineering Review, April, 1990, pp. 1-5.
- [CSQ95] C. A. Cañizares, A. Z. de Souza, and V. H. Quintana, "***Comparison of performance indices for detection of proximity to voltage collapse***," IEEE Trans. Power Systems, Vol. 11, No. 3, August 1996, pp. 1441-1450.
- [ChT02] J. Chen J. S. Thorp, "***A Reliability Study of Transmission System Protection via a Hidden Failure Dc Load Flow Model***", Power System Management and Control Conference, 2002, pp. 384-389.
- [CTF87] CIGRE Task force 38-01-03, "***Planning Against Voltage Collapse***", CIGRE Publication 1987
- [CTF94] CIGRE Task force 38-02-10, "***Modelling of Voltage Collapse Including Dynamic Phenomena***", CIGRE Publication 1994
- [CTF95] CIGRE Task force 38-02-19, "***System Protection Schemes in Power Networks***", CIGRE Publication 1995
- [CTF01] CIGRE Task Force 38-06-01, "***Methods to Consider Customer Interruption Costs in Power System Analysis***", CIGRE Publication 2001
- [CTF01a] CIGRE Task Force 34-09-01, "***Summary Report on Survey to Establish Protection Performance during Major Disturbances***", CIGRE Publication 2001

- [Cut91] T. Van Cutsem, "***A method to compute reactive power margins with respect to voltage collapse***" IEEE Trans. Power Systems, Vol. 6, No. 1, February 1991, pp. 145-156.
- [CV98] T. Van Cutsem, C. Vournas, "***Voltage stability of Electric Power System***", Kluwer Academic Publishers, 1998
- [CWG01] CIGRE Working Group 34.09, "***Summary Report on Survey to Establish Protection Performance during Major Disturbances***", M. J. Mackey, Electra, No.196, June 2001 pp. 19-29.
- [CWG93] CIGRE Working Group 38.01, "***Planning Against Voltage Collapse***", by J. Christensen, A. W. Gainger, G. Santagostino, M. Stubbe, J.Verseille, Electra, No. 111, 1993, pp. 55 –75.
- [Eli00] D C Elizondo de la Garza, "***Hidden Failures in Protection Systems and its Impact on Power System Wide-area Disturbances***", MSc thesis, Faculty of the Virginia Polytechnic Institute and State University, 2000
- [Eri86] I. A. Erinmez et al, "***Static VAR compensators***", Technical Rep., CIGRE Task force 38-01, 1986.
- [ERP01] D. C. Elizondo, J. de la Ree, A. G. Phadke, S. H. Horowitz, "***Hidden Failures in Protection Systems and their Impact on Wide-area Disturbances***", IEEE Power Engineering Society Winter Meeting, Columbus, Ohio, USA, 2001.
- [FOC90] N. Flatabo, R. Ognedal, and T. Carslen, "***Voltage Stability Condition in a Power system Calculated by Sensitivity Methods***", IEEE Transaction on Power systems, Vol. 5, 1997,pp. 1286 –1293.
- [GMK92] B. Gao, G. K. Morison, and P. Kundur, "***Voltage Stability Evaluation Using Modal Analysis***", IEEE Transaction on Power Systems, Vol.7, 1992, pp. 1529-1542.
- [GMK96] B. Gao, G. K. Morison, and P. Kundur, "***Towards the development of a systematic Approach for Voltage Stability Assessment***", of Large-Scale Power Systems", IEEE Transaction on Power Systems, Vol.11, 1996,pp. 1314-1324.
- [GS94] J. J. Grainger, W. D. Stevenson,"***Power system analysis*** ", New York, London , McGraw-Hill, 1994.
- [Har95] Harwell Subroutine Library, Vol.1 and Vol.2, December,1995.
- [HH92] I. A. Hiskens and D. J. Hill, "***Incorporation of SVCs into Energy Function Methods***", IEEE Transaction on Power systems, Vol. 7, 1992,pp 133-140.
- [HPL97] *Young-Huei Hong; Ching-Tsai Pan; Wen-Wei Lin,* "***Fast calculation of a voltage stability index of power systems***", IEEE Transactions on Power Systems, Issue 4. , 1997,pp. 1555 -1560

- [HoP95] S. H. Horowitz, A. G. Phadke, "**Power System Relaying**", Second Edition, Research Studies Press Ltd, 1995
- [ISE90] K. Iba, H. Suzuki, M. Egawa, T. Watanabe, "**A Method for Finding a Pair of Multiple Load Flow Solutions in Bulk Power Systems**", IEEE Transaction on Power Systems, Vol. 5, 1990, pp.582-591.
- [Ims99] IMSL Fortran Subroutines for Mathematical Application, Visual Numerics 1999.
- [IwT81] S. Iwamoto and Y. Tamura, "**A load flow calculation method for ill-conditioned power systems**", IEEE Transaction on Power Apparatus and System. , PAS-100, 1981, pp. 1736-1743.
- [KaA96] K. K. Kariuki and R. N. Allan, "**Evaluation of Reliability Worth and Value of Lost Load**", IEE Proc. on Gen., Tran. and Dist., Vol, 143, No. 2, 1996, pp. 171-180.
- [KeG86] P. Kessel, H. Glavitsch, "**Estimating the Voltage Stability of a Power System**", **IEEE Transactions on Power System**, Vol. 1, No. 3, July 1986, pp. 346-354.
- [KBN02] D.S. Kirschen, K.R.W. Bell, D.P. Nedic, D. Jayaweera, R. N. Allan, "**Computing the Value of Security**", Proceedings of Power System Management and Control Conference, London, UK, 2002.
- [KBN03] D.S. Kirschen, K.R.W. Bell, D.P. Nedic, D. Jayaweera, R. N. Allan, "**Computing the Value of Security**", accepted for publication, IEE Proceedings – Generation, Transmission, and Distribution, 2003.
- [KhB92] M. E. Khan, R. Billinton, "**A Hybrid Model for Quantifying Different Operating States of Composite Power System**", IEEE Transaction on Power System, Vol. 7, No. 1, February 1992, pp 187-193.
- [KiN02] Daniel S. Kirschen, Dusko P. Nedic, "**Consideration of Hidden Failures in Security Analysis**", Power System Computation Conference , Sevilla, 2002.
- [Kir02] D. S. Kirschen, "**Power System Security**", Power Engineering Journal [see also Power Engineer], Vol.16 Issue: 5, Oct. 2002.
- [Kni01] U. G. Knight, "**Power System in Emergencies**", John Wiley & Sons, 2001
- [Kun94] P. Kundur, "**Power System Stability and Control**", McGraw-Hill, 1994
- [LAH93] P. A.L. of, G. Andersson, and D.J. Hill, "**Voltage Stability Indices for Stressed Power System**", IEEE Transaction on Power Systems, Vol. 7, 1993, pp. 326-335.
- [LeT92] B.K. Leverend, R.P. Towstego, "**Update On the Disturbance Performance of Bulk Electricity Systems**", Electra, No. 143, August 1992.

- [LNN01] V. Levi, J. Nahman, D.P. Nedic: "**Security Modelling for Power System Reliability Evaluation**", IEEE Transactions on Power System, Vol. 16, 2001, pp. 29-37.
- [LSA92] P. A.L. of, T. Smed, G. Andersson, and D.J. Hill, "**Fast Calculation of a Voltage Stability Index**" IEEE Trans. Power Systems, Vol. 7, No. 1, February 1992, pp. 54-64.
- [LeN01] V.A. Levi, D.P. Nedic, "**Application of the Optimal Power Flow Model in Power System Education**", IEEE Transaction on Power Systems, Vol. 16, No. 4, November 2001.
- [Mer00] Andre Merlin, "**The Storms in France and the Grid**", Electra No. 188, 2000
- [MBB97] J. Machowski, J. Bialek, J. Bumby, "**Power System Dynamics and Stability**", John Willey & Sons, 1997.
- [MMcV03] M Ming., J.D. McCalley, V. Vital, T. Tayiyb, "**Online risk-based security assessment**", Power Systems, IEEE Transactions on, Vol. 18, Feb. 2003, pp. 256 –268.
- [Nag99] Numeric Algorithm Group, <http://www.nag.co.uk>
- [Ned02] D.P. Nedic, "**Tap adjustments in AC Power Flow**", Department of Electrical Engineering UMIST, Manchester, <http://www.umist.ac.uk/>, 2002
- [Nerc] North American Electric Reliability Council, "**Disturbances Analysis Working Group Database**", <http://www.nerc.com/dawg/>.
- [Nerc02a] North American Electric Reliability Council, "**Review of Selected 1996 System Disturbances**", <http://www.nerc.com>, 2002
- [Nerc02b] North American Electric Reliability Council, "**Review of Selected 1998 System Disturbances**", <http://www.nerc.com>, 2002
- [Nerc02c] North American Electric Reliability Council, "**Review of Selected 2000 System Disturbances**", <http://www.nerc.com>, 2002
- [Nerc02d] North American Electric Reliability Council, "**Review of Selected 1999 System Disturbances**", <http://www.nerc.com>, 2002
- [ObB88] O. O. Obadina and G. J. Berg, "**Determination of Voltage Stability Limit in Multimachine Power Systems**", IEEE Transaction on Power Systems, Vol. 3, 1988, pp. 1545-1554.
- [Ove94] T. J. Overbye, "**A Power Flow Solvability Measure for Unsolvable Cases**", IEEE Transaction on Power Systems, Vol. 9, 1993, pp. 1359-1365.
- [Pai79] M.A. Pai, "**Computer Techniques in Power System Analysis**", Tata McGraw-Hill Publishing, New Delhi, 1979

- [PaM94] M.Pavella, P.G.Murthy, "***Transient Stability of Power Systems - Theory and Practice***", John Wiley & Sons, Chichester, UK, 1994.
- [Pav98] M. Pavella, "***Power System Transient Stability Assessment – Traditional vs Modern Methods***", Control Engineering Practise 6, 1233-1246,1998.
- [PM71] N. M. Peterson, W. S. Meyer, "***Automatic Adjustment of Transformer and Phase-Shifter Taps in the Newton Power Flow***", IEEE Transaction on Power Apparatus and Systems, PAS-90, 171, pp.103-108.
- [RKJ02] M.A. Rios, D.S. Kirschen, D. Jayaweera, D.P. Nedic, R. Allan, "***Value of Security: Modelling Time-Dependent Phenomena and weather Conditions***", IEEE Transaction on Power System, Volume 17, August 2002.
- [SaP98] P. W. Sauer, M. A. Pai, "***Power System Dynamics and Stability***", Prentice Hall, Upper Saddle River, New Jersey, 1998.
- [SEA68] G. W. Stagg, A. H. El-Abiad, "***Computer Methods in Power System Analysis***", McGraw-Hill, 1968
- [Sey94] R. Seydel, "***Practical Bifurcation and Stability Analysis From Equilibrium to Chaos***", Springer-Verlag, New York, Second Edition, 1994.
- [TaE97] C. W. Taylor and D. C. Erickson, "***Recording and Analyzing the July 2 Cascading Outage***", IEEE Computer Applications in Power, January 1997, pp. 26-30.
- [Tam94] S.Tamronglak, "***Analysis of Power System Disturbances due to Relay Hidden Failures***", PhD Thesis, Faculty of the Virginia Polytechnic Institute and State University, 1994
- [Tay94] C. W. Taylor, "***Power System Voltage Stability***", EPRI Power System Engineering Series, McGraw Hill, 1994
- [Tay99] C. W. Taylor, "***Improving Grid Behaviour***", Spectrum IEEE, Volume 36, Issue 6, June 1999
- [TFH94] T. Quoc Tuan, J. Fandino, N. Hadjsaid, J.C. Sabonnadiere and H. Wu, "***Emergency Load Shedding to Avoid Risks of Voltage Instability using Indicators***", IEEE Transaction on Power Systems, Vol. 9, 1994,pp. 341-351.
- [THP96] S Tamronglak, S H Horowitz, A G Phadke, J S Thorp, "***Anatomy of Power System Blackouts: Preventive Relaying Strategies***", IEEE Transactions on Power Delivery, Vol. 11, No. 2, 1996,pp. 708-715.
- [TMI83] Y. Tamura, H. Mori, and S. Iwamoto, "***Relationship between voltage instability and multiple load flow solutions in electric power systems,***" IEEE Trans. Power Apparatus and Systems, vol. 102, no. 5, May 1983, pp. 1115-1125.

- [TPH96] J. S. Thorp, A. G. Phadke, S. H. Horowitz, C. Tamronglak, "**Anatomy of Power System Disturbances: Importance Sampling**", 12th Power Systems Computation Conference, Dresden, 1996, pp. 350-357.
- [TST89] Y. Tamura, K. Sakamoto, and Y. Tayama, "**Current issues in the analysis of voltage instability phenomena**", Proc. Bulk Power System Phenomena – Voltage Stability and Security, EPRI January, 1989, pp. 5-39
- [WaT02] H. Wang, J. S. Thorp, "**Optimal Locations for Protection System Enhancement: A Simulation of Cascading Outages**", paper submitted to IEEE Transaction on Power Delivery, 2002.
- [YHC97] N. Yorino, S. Harada, and H. Cheng, "**A Method to Approximate a Closest Loadability Limit Using Multiple Lad Flow Solutions**", IEEE Transaction on Power Systems, vol. 12. No. 1, February 1997, pp. 424-429.
- [You95] R. D. Youssef, "**Implicit Generator and SVC Modelling for Contingency Scheduling of Reactive Power Dispatch**", IEE Proceeding – Generation, Transmission and Distribution, Vol. 142, 1995, pp. 527-534.